TECHNISCHE UNIVERSITÄT WIEN

DISSERTATION

STRATEGIES TO IMPROVE THE MYOGENIC OUTCOME OF SKELETAL MUSCLE TISSUE ENGINEERING APPROACHES THROUGH OPTIMIZATION OF BIOMATERIAL PROPERTIES AND MECHANICAL STIMULI

ausgeführt zum Zwecke der Erlangung des akademischen Grades eines Doktors der technischen Wissenschaften unter der Leitung von

Privatdoz. Dipl.-Ing. Dr.techn. Andreas Herbert Teuschl-Woller
E317
Institut für Leichtbau und Struktur-Biomechanik

eingereicht an der Technischen Universität Wien

Fakultät für Technische Chemie

von

Janine Tomasch, MSc.
01129408

Wien, am 21.11.2022 .....

EIDESSTAATLICHE ERKLÄRUNG

Hiermit erkläre ich an Eides statt, dass ich die vorliegende Dissertation „*Strategies to improve the myogenic outcome of skeletal muscle tissue engineering approaches through optimization of biomaterial properties and mechanical stimuli*“ selbstständig verfasst und keine anderen als die angegebenen Quellen und Hilfsmittel verwendet habe.

Wien, am 21.11.2022 .....

Table of Content

Acknowledgements

First, I want to thank my supervisor Andreas Teuschl for helping me with developing my project ideas and supporting me during their realization. His continuous encouragement and guidance certainly helped me greatly to develop scientifically and to complete this thesis. Additionally, I want to thank Carina Huber-Gries und Veronika Jesenberger from the UAS Technikum Wien and Heinz Redl and the LBI for providing me with the environment to execute my work.

Furthermore, I want to thank all the people that supported me throughout the years and made coming to the lab a lot more pleasant:

- Nane and Babette for both, patiently guiding me through my first days in the lab, but also for their continuous support after that
- Carina, Xavi and Dora for being great officemates, who provided me with plenty opportunities for coffee breaks and distractions, an open ear for worries and countless helpful discussions, ideas and pieces of advice
- Michaela, Anna, Fips, Berni, Dani, Roland, Farzad, Camila, Lilli, Gordin, Bettina, Sophie, Ingrid and Safet, and all the other people in the lab that made this possible
- The former lab youngsters Elias and Sabsi, whose enthusiasm helped to encourage me to give this a shot in the first place

Moreover, I want to thank Feli, Raphi, Nina, Eja, Martin, and Christoph for years (or even decades) of friendship and support, helping me celebrate victories and overcoming hard times, Vivi for always having an open ear and sharing this experience with me, Stelios for accompanying me through many highs and lows of this journey and Xandi, who was the best companion I could have wished for at my side throughout the last years.

Lastly, I am deeply thankful for my family, particularly my mother Ingrid and my sister Carina, without whose seemingly infinite love, encouragement, and trust this would not have been possible!

Kurzfassung

Mit bis zu 40% der Gesamtmasse des menschlichen Körpers ist die Skelettmuskulatur das am häufigsten vorkommende Gewebe und für Fortbewegung, Atmung, Thermogenese und aufrechte Haltung von entscheidender Bedeutung. Außerdem fungiert sie als endokrines Organ, indem sie Zytokine ausschüttet, die sich positiv auf verschiedene, insbesondere altersbedingte, Krankheiten wie Osteoporose, Alzheimer und Diabetes auswirken. Der Verlust der Skelettmuskulatur durch degenerative Muskelerkrankungen, volumetrischen Muskelverlust oder Sarkopenie (Muskelschwund bei älteren Menschen) ist daher einschneidend für die Gesamtfunktion des Körpers. Trotz der gravierenden Auswirkungen auf die Lebensqualität der Patient*innen gibt es immer noch keine wirksamen Behandlungsstrategien für Skelettmuskelpathologien, die von genetischen Defekten (z. B. Muskeldystrophien) und Alterung hervorgerufen werden. Das Gleiche gilt für volumetrischen Muskelschwund, dessen Behandlung entweder mit hohem Maß an Komplikationen oder mit mangelnder Wirksamkeit verbunden ist.

In vitro (Krankheits-) Modelle, die mit den Techniken des Tissue-Engineerings (engl. Gewebekonstruktion) erzeugt wurden, können als alternative präklinische Plattformen dienen, um weitere Erkenntnisse über die molekularen Ursachen und potenziellen Behandlungen von Skelettmuskelpathologien zu gewinnen. Darüber hinaus stellen sie vielversprechende Behandlungsansätze als Implantate für den volumetrischen Muskelverlust dar. Erfolgreiches Erzeugen von Skelettmuskelgewebe hängt vom Zusammenspiel der drei Hauptkomponenten des klassischen Tissue-Engineering-Dreiecks ab: Zellen, Biomaterialien und stimulierende Faktoren. In dieser Arbeit soll die Frage beantwortet werden, wie sich die Auswahl und Herstellung des Biomaterials, sowie die Wahl der Stimulationsstrategien auf die eingesetzten Zellen auswirken. Das übergeordnete Ziel dieser Arbeit ist es, neue Einblicke in die geeignete Gestaltung der Kulturumgebung für ein verbessertes Ergebnis von Skelettmuskel-Tissue-Engineering Strategien zu geben.

In Kapitel 1 werden zwei Studien vorgestellt, die den Einfluss des Elastizitätsmoduls und der Oberflächenstrukturierung von Biomaterialien auf die Entwicklung von Myoblasten aufzeigen. In der ersten Studie wurde festgestellt, dass geringe Veränderungen des Elastizitätsmoduls von Fibringerüsten das Differenzierungspotenzial von Myoblasten stark beeinflussen. Darüber hinaus verglichen wir die Kultivierung in 2D- und 3D-Umgebungen und die Reaktion von murinen und menschlichen Zellen auf die verschiedenen Bedingungen. Dabei zeigte sich, dass das Verhalten der Zellen in 2D-Kultur nicht auf komplexere 3D-Strukturen übertragen werden kann. Das Gleiche gilt für den Vergleich der Ergebnisse von murinen Myoblasten auf Zellen menschlichen Ursprungs. Dies unterstreicht, dass diese Faktoren bei der Weiterentwicklung von Tissue-Engineering Ansätzen berücksichtigt werden müssen, wodurch ihre Translation auf *in vivo* Umgebungen erleichtert wird.

In der zweiten Studie setzten wir Femtosekundenlaser ein, um mikrostrukturelle Veränderungen auf Seidenfibroinsubstraten vorzunehmen. Es wurden parallele Rillen vom Biomaterial abgetragen, wodurch sich dessen Eignung als Gerüst für die myogene Entwicklung erheblich verbesserte.

Kapitel 2 enthält eine umfassende Literaturübersicht über die Entwicklung dynamischer Skelettmuskelmodelle. Unser Ziel war es, biophysikalische und biochemische Stimuli zu identifizieren, die die *in vivo* Umgebung genau nachbilden und folglich die funktionellen und strukturellen Eigenschaften des erzeugten Gewebes verbessern. Darüber hinaus gehen wir auf das Potenzial dieser Plattformen als Krankheitsmodelle ein und stellen einen analytischen Arbeitsablauf vor, der das Identifizieren erfolgreicher Strategien für die Gewebezüchtung erleichtert.

Im dritten und letzten Kapitel beschäftigt sich diese Arbeit damit, die Anpassung des Skelettmuskels an mechanische Belastungen *in vitro* zu modellieren, da Plastizität und eine hohe Regenerationsfähigkeit nach Verletzungen für die Funktionalität des Skelettmuskels entscheidend sind. Um die Lücke an *in vitro* Modellen, die diese Prozesse untersuchen, zu schließen, haben wir mit Hilfe eines Zug-Bioreaktors ein Tissue-Engineering Modell für die Adaption des Skelettmuskels an mechanischen Stress entwickelt. Die Überstimulation führte zur Aktivierung ruhender Myoblasten und zu überlastungsinduzierter Hypertrophie, was wir sowohl auf morphologischer als auch auf intrazellulärer Ebene charakterisierten.

Zusammenfassend lässt sich sagen, dass diese Arbeit einen Beitrag zum Gebiet des Skelettmuskel-Tissue-Engineering leistet, indem sie die aktuellen Forschungsstrategien kritisch bewertet und neue Erkenntnisse zur Optimierung von Biomaterialien und Stimulationstechniken liefert. Dadurch wird das myogene Potential zukünftiger Skelettmuskel-Tissue-Engineering Ansätze, sowie die Relevanz von *in vitro* Modellen für intrazelluläre Mechanismen in gesundem und pathologischem Skelettmuskel verbessert.

Abstract

Skeletal muscle is the most abundant tissue in the human body, comprising up to 40% of its total mass, and is crucial for locomotion, breathing, thermogenesis and the maintenance of an upright posture. Moreover, it acts as an endocrine organ by secreting cytokines with beneficial effects on various, particularly age-related, diseases, such as osteoporosis, Alzheimer's disease and diabetes. Therefore, loss of skeletal muscle due to degenerative muscle disorders, volumetric muscle loss or sarcopenia (muscle wasting in the elderly) has severe negative implications on the body's overall functionality. Despite the impact on the quality of the patients' lives, there are still no effective treatment strategies for skeletal muscle pathologies caused by genetic disorders (e.g., muscular dystrophies) and aging. The same holds true for volumetric muscle loss, whose treatments entail either great donor site morbidity or a lack of effectiveness.

Tissue-engineered *in vitro* (disease) models can serve as alternative pre-clinical platforms to gain further insights into the molecular causes and potential treatments of skeletal muscle pathologies. Furthermore, they present promising treatment approaches as implants for volumetric muscle loss. Successful generation of tissue-engineered skeletal muscle depends on an interplay between the three main components of the classical tissue engineering triad: cells, biomaterials and stimulating factors. This thesis aims at answering the questions how the choice and manufacturing of the biomaterial, as well as the choice of stimulation strategies affect the applied cells. The overall aim hereby was to provide insights into appropriate designs of the culture environment for an improved myogenic outcome of tissue-engineered skeletal muscle.

In chapter 1, two studies are presented that highlight the influence of elastic modulus and surface patterning of biomaterials on the myogenic development of myoblasts. The first study found that subtle changes of the elastic modulus of fibrin scaffolds greatly impact the differentiation potential of myoblasts. Moreover, we compared cultivation in a 2D and a 3D environment and the response of murine and human cells to the different settings. Hereby, we saw that cellular behavior in 2D setups cannot be translated to more complex 3D structures. The same holds true for translation of findings from murine myoblasts to cells of human origin. This highlights that these factors need to be considered when advancing tissue engineering approaches, which will facilitate their translation to *in vivo* settings. In the second study, we applied femtosecond lasers to introduce microstructural changes onto silk fibroin substrates. Parallel grooves were ablated from the biomaterial, which successfully increased its suitability as a scaffold for myogenic development.

Chapter 2 provides a comprehensive literature review on the design of dynamic skeletal muscle models. We aimed at identifying biophysical and biochemical stimuli that closely recapitulate the *in vivo* environment and consequently improve functional and structural characteristics of the engineered tissue. Further, we elaborate on the potential of these platforms in disease modeling and present an analytical workflow for facilitated identification of successful tissue engineering strategies.

In the third and last chapter, this thesis engages in modeling the adaptation of skeletal muscle to mechanical stress, as plasticity and a high capacity to regenerate after injuries are crucial for skeletal muscle functionality. Since there is a lack of *in vitro* models that study these processes, we aimed to create a tissue-engineered model for skeletal muscle adaptation to mechanical stress using a strain-bioreactor. We triggered myoblast activation and overload-induced hypertrophy and characterized the model on a morphological, as well as on an intracellular level.

In summary, this thesis contributes to the field of skeletal muscle tissue engineering by critically assessing current research strategies and introducing new insights in biomaterial optimization and stimulation techniques. Thereby, the myogenic outcome of future skeletal muscle tissue engineering approaches, as well as the relevance of *in vitro* models of skeletal muscle mechanisms and pathologies will be improved.

General Introduction

Skeletal muscle is the most abundant tissue in the human body, comprising up to 40% of its total mass. It is crucial for several physiological functions, including locomotion, breathing, thermogenesis and the maintenance of an upright posture, resulting in widespread negative implications on the body's overall functionality upon its loss [1]. Furthermore, skeletal muscle acts as an endocrine organ by secreting cytokines (termed myokines) [2] that are known to have beneficial effects in various, particularly age-related, diseases, such as osteoporosis [3], Alzheimer´s disease [4] and diabetes [5], [6]. Moreover, myokines entail great potential in reducing sarcopenia (muscle wasting in the elderly) by maintaining an anti-inflammatory status and thereby reducing fatty tissue infiltration and scar formation [7]. Due to the global increase in life expectancy, the number of patients affected by sarcopenia is growing, which leads to increased demand of treatment strategies [8]. Also progressive muscle diseases of genetic origin, such as muscular dystrophies, still lack effective cures, as it is only possible to treat symptoms and delay the progression of these diseases [9]. Volumetric muscle loss presents a further pathological muscle state that still lacks functional treatment options [10]. Tissue-engineered *in vitro* models for healthy and diseased muscle tissue can serve as an alternative pre-clinical approach to gain further insight into the molecular causes and potential treatments of muscle pathologies, but also as potential treatment solutions for volumetric muscle loss [11].

1. Development and function of skeletal muscle

1.1 Skeletal muscle development

The musculoskeletal system, thus also skeletal muscle, derives from the mesoderm during the nerula stage of embryonic development. In this stage, the mesoderm is divided into four regions, one of them being the paraxial mesoderm, the origin of the skeleton and skeletal muscle. The paraxial mesoderm is the source of different structures, including the cranial mesoderm, where all head and neck muscles and connective tissues originate from, and somites in the limb region that will be divided in a ventral and a dorsal region. Cells from the ventral region form the sclerotome, which gives rise to cartilage and bone of the trunk. The dorsal dermomyotome retains an epithelial outer layer, while forming the underlying myotome. Eventually, the myotome is the source for all skeletal muscle in trunk and limbs [12].

The formation of mature fibers from the myotome involves a complicated network of extra- and intracellular signaling pathways. The starting point of myofiber development is the creation of the somite by condensation of cells of the paraxial mesoderm, which is guided by extracellular signaling cues. A detailed schematic representation of the process is shown in figure 1. Wingless-Int proteins (Wnts), Sonic Hedgehog (Shh) and Bone Morphogenic Proteins (BMPs) are the most crucial signaling molecules for the development of distinct cell compartments. Their

secretion by the surrounding environment underlies a tight spatiotemporal control and varying combinations result in the development of the dermomyotome, the myotome and the sclerotome. Thus, amongst others, myogenic fate is induced by signaling of Wnt1, Wnt3a and Shh secreted from the dorsal neurotube or Wnt7a secreted from the dorsal ectoderm [13], [14].

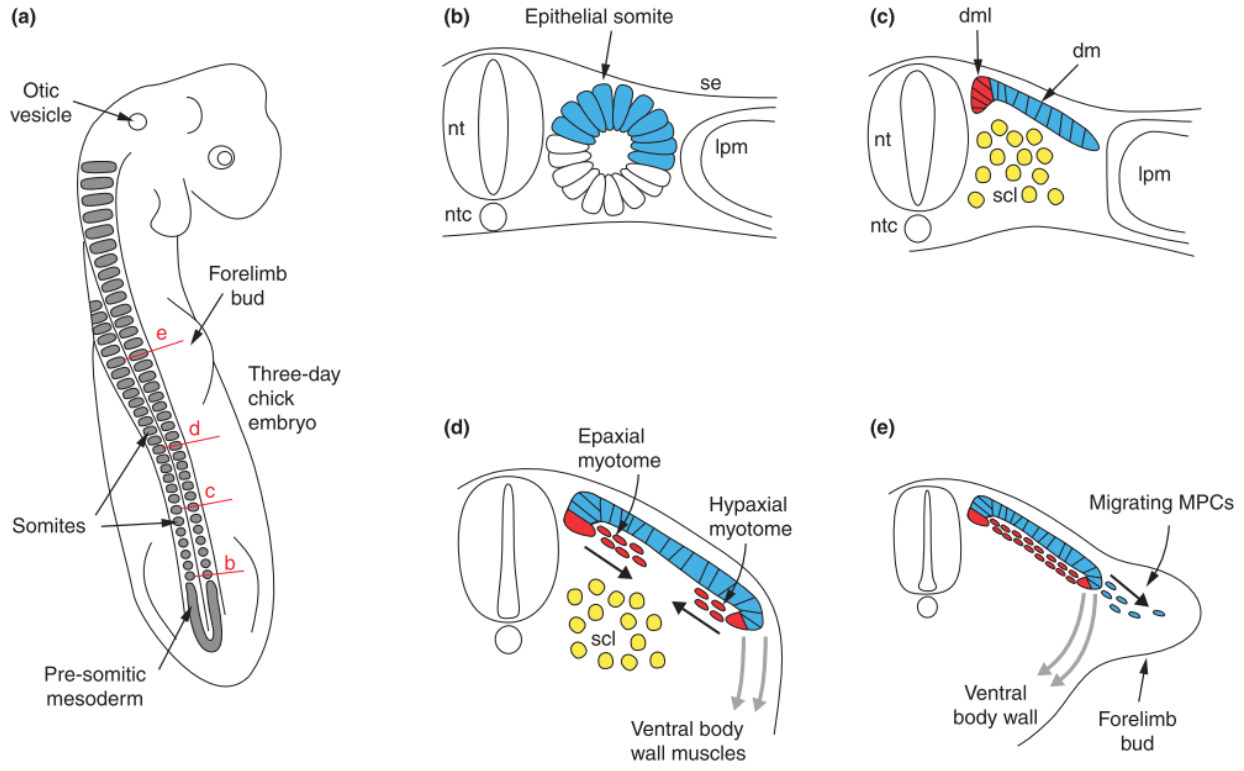

Figure 1: Stages of embryonic myogenesis. (a) Schematic representation of the somites of a chick embryo at day three (shown in gray) with their cross section in **(b-e)**. **(b)** The epithelial somite at level I receives signals from the neural tube (nt), notochord (ntc), surface ectoderm (se), and lateral plate mesoderm (lpm). The dorsal part of the somite will form the dermomyotome (dm) (shown in blue). **(c)** The somite at level VII expresses *Pax3* and *Pax7* (differentiated dm shown in blue). The dorsomedial lip (dml) (shown in red) expresses *MyoD* and high levels of *Myf5*. Yellow circles indicate somites that undergo an epithelial-to-mesenchymal transition forming the sclerotome (scl) (origin of vertebrae and ribs). **(d)** The epaxial and hypaxial myotome is formed in the thoracic/interlimb level somite by migration of cells from the dm. The gray arrows indicate ventro-lateral growth of the lateral lip of the dm (origin of ventral body wall muscles). **(e)** The myotome (shown in red) is forming next to the dm (shown in blue) in the forelimb level somite. Migrating myogenic progenitor cells delaminate and invade the limb bud [13].

Development of muscle cells from the myotome presents the end result of this signaling cascade, which starts with the delamination of myogenic progenitor cells (MPCs) from the dermomyotome. These cells are already committed to the myogenic lineage at this stage of development, which becomes evident by the high expression levels of *Myf5*. Delaminated MPCs either directly differentiate into mononucleated myocytes or stay undifferentiated (yet committed) until they receive further activating signals. Myocytes display a characteristic elongated shape and their intracellular signaling network is prepared to express the required proteins to fuse to form myotubes [16], [17]. Eventually, the newly created myotubes arrange in a highly structured manner and increase in size to form mature muscle [15]. In parallel to activated MPCs, satellite cells also evolve at this stage, which will serve as a pool of resident stem cells in adult muscle. They do not express *Myf5* and therefore do not differentiate into myoblast until they become activated by external factors in case of regeneration of injured muscle is required [18], [19]. An overview of this process is shown in figure 2.

Commitment to myogenic lineage is tightly controlled by a set of transcription factors; the myogenic regulatory factors (MRFs) (figure 3). The cascade of transcription factor expression is initiated by expression of *paired box 3* and *7* (*Pax3* and *Pax7*) that induce the expression of *Myf5* either directly or via other transcription factors [15]. The MRFs *myogenic differentiation 1* (*MyoD*) that is downstream *Myf5*, is the major regulator of myogenic differentiation and presents the hallmark of commitment to this lineage. *MyoD* induces expression of *myogenin* (*MyoG*) and *myogenic regulatory factor 4* (*Mrf4*) that are required for fusion of myocytes to myotubes [12], [14].

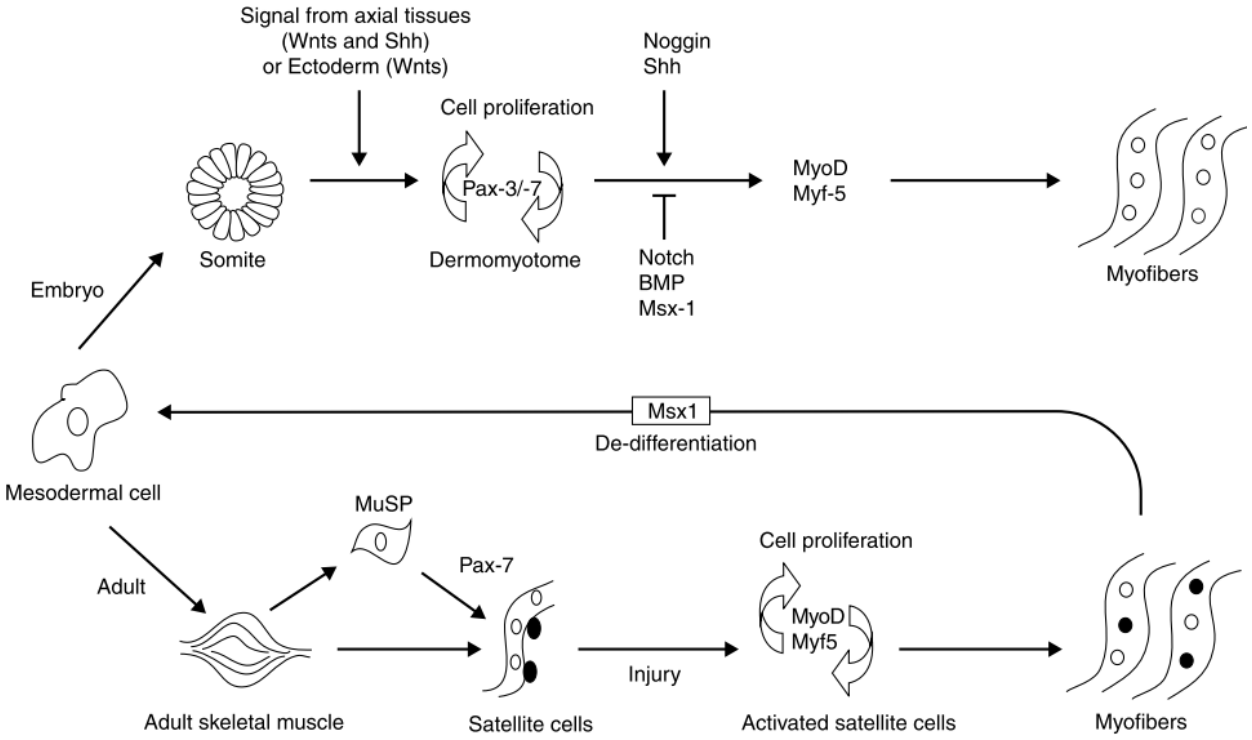

Figure 2: Overview of muscle progenitor cells formation. Cells of the dermomyotome are induced to express *MyoD* and *Myf5* by signals from the axial tissues and ectoderm forming the dorsomedial lip of the myotome. Myogenic progenitor cells on the lateral dermomyotome are *Pax3*$^{+}$ and *Pax7*$^{+}$, but *MyoD*$^{-}$. Therefore, their differentiation is delayed, and their cell number can increase to be sufficient for populating more distant areas. This is mediated by singling from Bone Morphogenic Proteins (BMPs), Notch and Homeobox protein (MSX-1) pathways, while signaling from the BMP antagonists noggin and Sonic Hedgehog (Shh) induce direct myogenesis. In adult muscle, satellite cells are the main myogenic progenitor population. It is speculated that they are derived from muscle-derived side population (MuSP) cells that become determined upon *Pax7* expression. quiescent satellite cells can become activated sue to signaling cues after injury. Thereupon, they express *MyoD* or *Myf5* and re-enter the cell cycle to undergo replication to form a cell pool. A certain number of this pool will develop to myoblasts and eventually create new myotubes or fuse to existing ones. Msx1 expression leads to de- differentiation of myotubes into cells that do not express myogenic markers, which create a cell pool with a high levels of plasticity that can differentiate into cells from the chondrogenic, myogenic, osteogenic or adipogenic lineage [13].

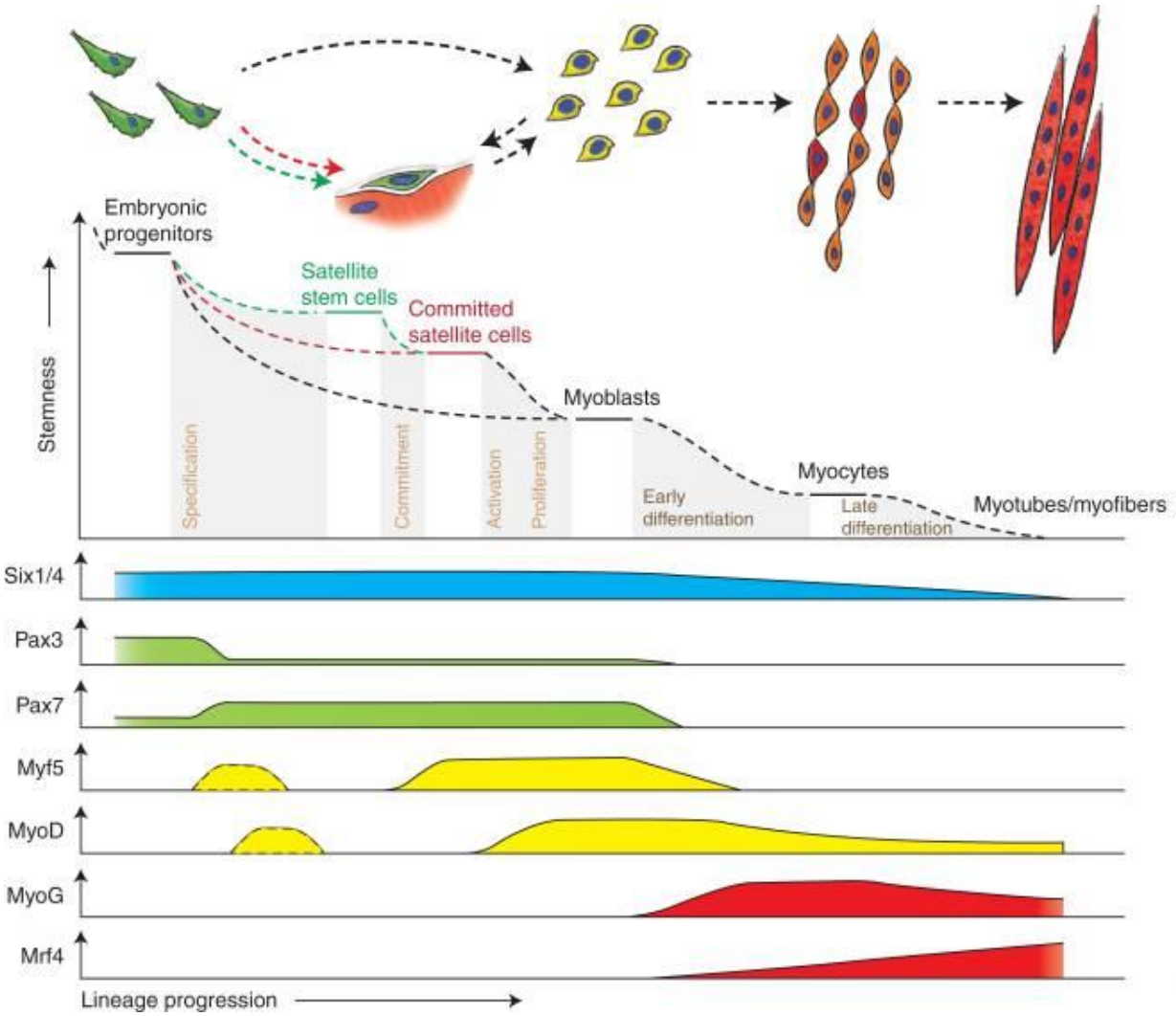

Figure 3: Cascade of expression of transcription factors during myogenic differentiation. Embryonic muscle progenitors develop either into satellite cells or into myoblasts. While some progenitor cells remain quiescent in their stem cell niche underneath the basal lamina (termed satellite cells), others skip this stage and develop into differentiated muscle directly. In rare cases, committed myoblasts can dedifferentiate to the quiescent state. Early lineage specification is controlled by *Six1/4* and *Pax3/7* and *Myf5* and *MyoD* regulate commitment to the myogenic program. Fusion of myocytes to myotubes is regulated by expression of terminal differentiation genes *MyoG* and *Mrf4* [15].

1.2 Skeletal muscle regeneration

Skeletal muscle has remarkable regenerative capacities, mostly attributed to the presence of quiescent satellite cells, the adult stem cell pool of skeletal muscle. These cells have the ability to repopulate injured muscle tissue with myogenic cells in case of stress (trauma, disease, etc.). This process is supported by other interstitial cells, such as pericytes and fibroadipogenic progenitor cells. Therefore, skeletal muscle can successfully cope with slight injuries or early-staged diseases [12]. Nevertheless, in case of chronic pathologies, such as muscular dystrophies and sarcopenia, or severe acute injuries, such as traumatic volumetric muscle loss, the satellite cells become depleted [20]. Consequently, especially elderly people are more susceptible to a diminished muscle regeneration potential [21]. In case of insufficient regeneration, the results are scar formation, fatty tissue infiltration and, subsequently, loss of muscle functionality, which implicates severely reduced quality of patients' lives [22].

1.3 Skeletal muscle structure and force generation

Skeletal muscle tissue consists of muscle cells (also referred to as myofibers) and connective tissue that are arranged parallel to each other and in a hierarchical structure (figure 4 A). This arrangement presents the biomechanical prerequisites required for normal tissue function. A whole muscle is protected by a layer of connective tissue, called the epimysium. Each muscle consists of several bundles of myofibers, which are again covered by another layer of connective tissue, called perimysium. Within these bundles, there are single myofibers surrounded by the endomysium (figure 4 B). These three fibrous layers mostly consist of collagen and laminin [1]. Furthermore, blood vessel run parallel to the bundles of myofibers and eventually penetrate through the endomysium, where they form capillaries in order to reach each myofiber. Motor neurons reach the myofibers through the same path as blood vessels ending at neuromuscular junctions (figure 4 B) [10].

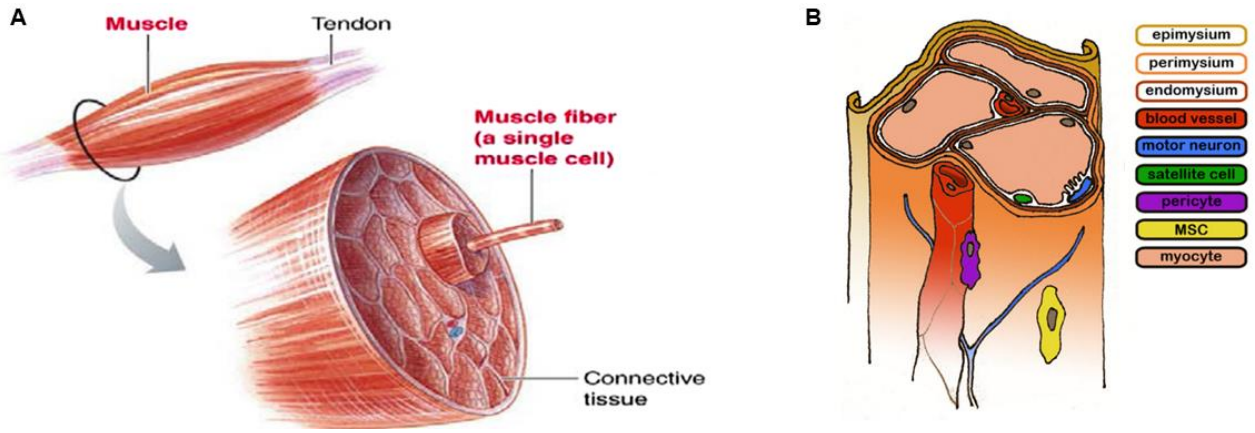

Figure 4: Structure of skeletal muscle. A whole muscle strand that is connected to bone via tendons is wrapped by the epimysium and consists of separate bundles of fascicles. Fascicles are wrapped by the perimysium and consist of single muscle fibers (also known as muscle cells) [1]. **(B)** All three structural levels (*i.e.* the whole muscle, myofiber bundles, and myofibers) are supported by layers of connective tissue, called epimysium, perimysium and endomysium, respectively. Furthermore, functional muscle tissue requires the presence of blood vessel, motor neurons and other cell types apart from myofibers, such as satellite cells, pericytes and mesenchymal stem cells (MSCs) [10].

Each myofiber is surrounded by its cell membrane, the sarcolemma, which is not only essential to protect the cell, but also to carry out muscle function. The sarcolemma is connected to actin filaments through a glycoprotein complex, which is necessary for force generation. Myofibers are composed of highly arranged structural components, called myofibrils, which are themselves made of different fiber types, the two most important ones being thinner actin and thicker myosin filaments [1]. When these filaments are arranged in a highly structured manner, they form the so-called sarcomeres, the contractile units of skeletal muscle (figure 5). Furthermore, there are several other proteins within the sarcomeres, such as troponins, titins and nebulins that enable functional muscle contraction [23]. There are various muscle fiber types that are distinguished by characteristics, such as contractility when electrically stimulated, speed of shortening, metabolic activity, and presence of specific isoforms of the aforementioned muscle proteins (especially myosin). Depending on the physiological function of a specific muscle, it is composed of different fiber types [24]. Skeletal muscle is essential for carrying out several pivotal functions of the human body. Apart from locomotion, it is also necessary for breathing, stabilization of the body, protection of interior organs and many more, which require an interplay static and dynamic action [1].

Force generation in skeletal muscle is initiated after activation by the transmission of a stimulus through motor neurons that is followed by calcium release into the sarcoplasm. Subsequently, calcium binds to troponin C, a regulatory protein on the actin filament, which results in its displacement from the active site of the filament. This enables binding of myosin to the actin filament, followed by adenosine triphosphate (ATP) hydrolysis, which again leads to detaching of the myosin head. Thereby, the so-called power stroke is initiated, which allows a sliding of the two filaments alongside each other. This process is known as the sliding filament model [25].

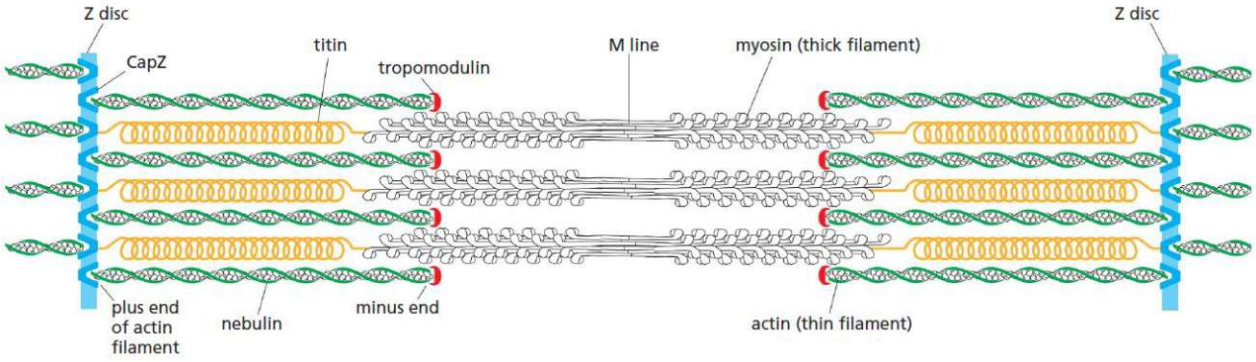

Figure 5: Sarcomere with accessory proteins. Myosin and actin filaments are arranged in a highly structured manner between the M line, where adjacent myosin filaments are attached to each other, and the Z disc, where actin filaments are anchored. Accessory proteins spread over the sarcomere on distinct locations: titin reaches from the Z disc to the myosin filament; nebulin is associated to actin filaments; CapZ is located at the plus end of the actin filament, whilst tropomodulin anchors the minus end [23].

1.4 Response to mechanical stimuli

Cells constantly react to mechanical stimuli that originate from changes in their environment. Neighboring cells and tissues exert mechanical stresses onto them, either directly or via the deformation of the extracellular matrix (ECM). These mechanical stimuli are constantly translated to biochemical signals intracellularly. These stimuli include compression or tension, but also changed stiffness of their substrate [26]. In terms of tissue engineering, this is of relevance for the choice of biomaterials, but also scaffolds structure [27].

The translation of mechanical cues to biochemical signals and eventually to changed cellular behavior is termed “mechanotransduction” and involves a complex network of signaling mechanisms. The key complex of signaling molecules in this process is a cluster of transmembrane and cytosolic proteins called focal adhesions. Through the dynamic assembly and changes in this protein cluster, cells are able to sense their environment and adapt quickly. The transmembrane part of focal adhesions, integrins, directly bind to specific amino acid sequences of the ECM and its clustering changes depending on ECM properties, such as attachment sites. Thereby, they recruit different sets of focal adhesion core proteins. The intracellular proteins are either scaffolding, docking, or signaling proteins that are combined variably. Figure 6 shows a schematic representation of the most important components of the focal adhesion site. The structure of focal adhesions, the number of proteins involved, and the signaling mechanism are highly variable and therefore it is not possible to summarize them as one pathway [26].

Effectors of mechanical stimuli that are transferred either through mechanotransduction via focal adhesions or directly through mechanosensitive channel proteins in skeletal muscle include the mitogen activated protein kinase (MAPK) cascade, the Hippo pathway and phosphatidylinositol-3' kinase (PI3K) signaling [28], [29]. Signaling through PI3K upon mechanical stimulation in skeletal muscle is of particular interest since its downstream target mTOR is majorly involved in protein synthesis. This is relevant, as increased protein synthesis in myotubes is required for adaption to mechanical stress by myofiber growth and increased load-bearing and force-generating abilities [30].

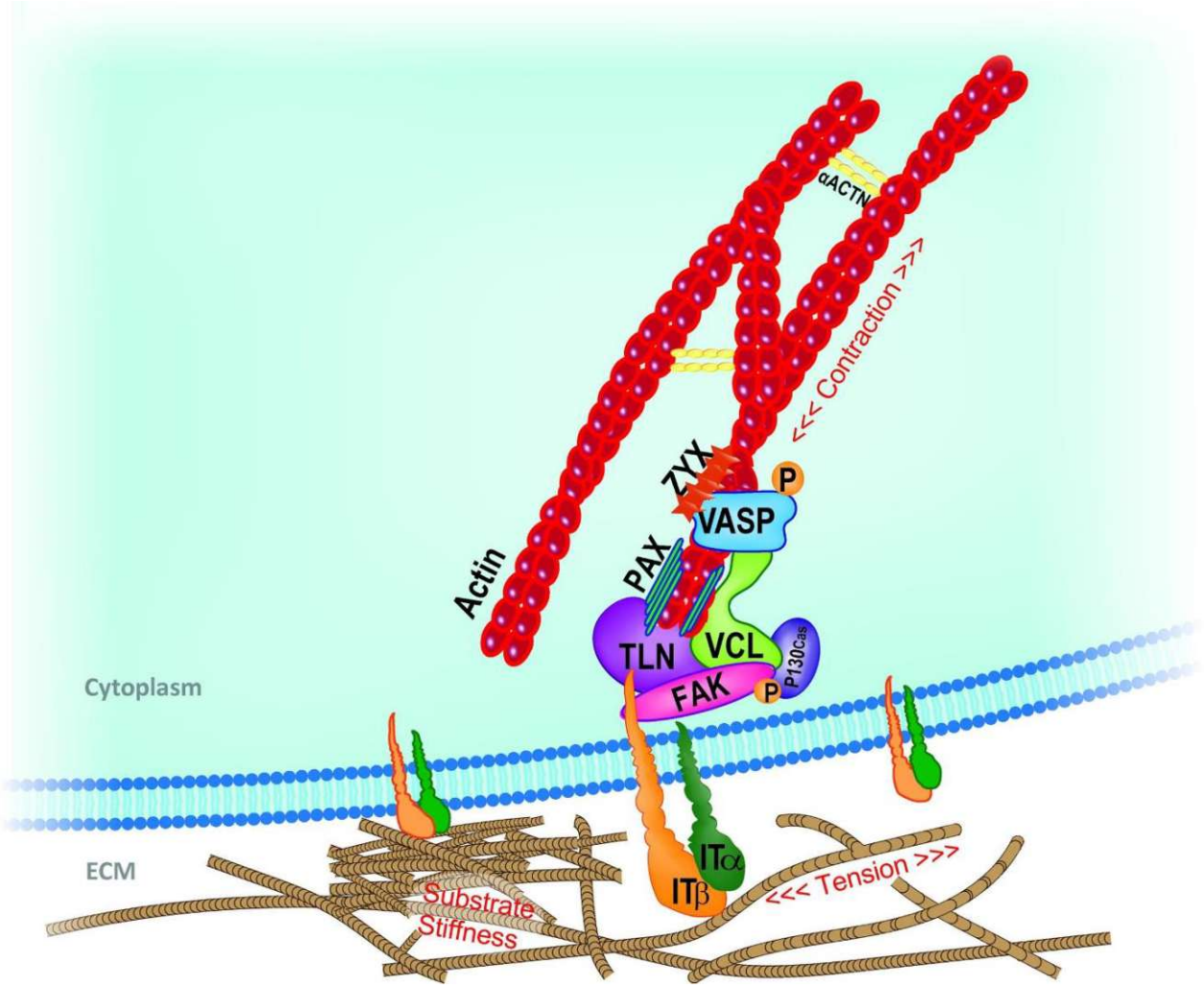

Figure 6: Signaling molecules involved in mechanotransduction at the focal adhesion site. Mechanical changes occurring outside the cell, such as changed substrate stiffness, tension or compression are sensed by integrins (IT) that undergo changes in morphology or special arrangement. This leads to recruitment of focal adhesion kinase (FAK). The complete focal adhesion complex is formed when talin (TLN), vinculin (VCL), paxillin (PAX), and adaptor protein p130Cas assemble as well and transfer the mechanical cue to the actin filaments. Vasodilator-stimulated phosphoprotein (VASP), zyxin (ZYX) and actinins (ACTNs) regulate actin dynamics through direct interaction [26].

2. Modeling of skeletal muscle disease, injury, and regeneration

Apart from greatly compromising the lives of affected people, pathological muscle conditions also entail a great socioeconomic burden. Healthcare costs caused by muscle-related disorders have been rising in past years. This is partly attributed to the rising life expectancy and global population aging in combination with the fact that susceptibility to these injuries and diseases rises with age and is further increased by a still existing lack of effective treatment options [31], [32]. There is an urgent need for models to mimic their initiation, progression, and recovery, in order to study pathological muscle conditions. With adequate organotypic *in vitro* models, it is possible to both, investigate the underlying pathomechanisms of diseases and trauma and their regeneration, and then evaluate novel treatment strategies targeting these mechanisms.

Historically, research that aims to investigate mechanisms underlying muscle pathologies, regeneration and treatment strategies has been based on animal models ranging including invertebrates, non-mammalian vertebrates and mammals [33], [34]. Nevertheless, animal models do not recapitulate the exact course of pathologies and their regeneration as they occur in humans. Thus, they frequently do not correctly predict results from preclinical drug tests that, thereupon, fail in clinical trials [35], [36]. Biomimetic *in vitro* models of skeletal muscle disease, injury, and regeneration present appropriate time- and cost-effective alternatives. When using tissue-specific cell types, they are capable of mimicking human conditions more accurately and therefore have higher predictive power than standard animal models [36]. Moreover, they allow for precise control over single parameters, which enables specific analysis of their impact [37]. Simple 2D cell culture models, however, do not accurately mimic the complex organization of tissues *in vivo*, which also limits their predictive power. Therefore, current research strives to develop 3D cell culture systems that reflect the *in vivo* situation more closely [38]. In these systems, cells can interact with the matrix they are embedded in, which presents a pivotal factor influencing cell development, and form 3D tissue-like structures [37].

While a small number of 3D systems for investigating myogenic diseases have already been published, models for myogenic injuries are still rare. Furthermore, existing approaches are often executed as 2D models, or the simulated injuries are induced as freeze injuries or through addition of venoms, such as cardiotoxin, which both are important aspects decreasing relevance of these models. In the few models simulating mechanical injuries, the focus mostly lies on compression injuries, whereas there is still lack of models for strain-induces injuries [39]–[42]. In this regard, novel tissue engineering techniques are required to create such models of skeletal muscle *in vitro*.

The knowledge of the effects of mechanical stimulation on skeletal muscle fusion, hypertrophy and regeneration *in vivo* is also predominantly based on models using rodents due to the invasive nature of biopsy collection that complicates studies in humans. Surgical synergist ablation is the most common model used to study overload of muscle. Since this model poses a high amount of overload on the muscle, however, it does not allow for discrimination between hypertrophy upon mechanical load and hypertrophy occurring in the course of regeneration [43], [44]. Voluntary wheel running presents a less invasive alternative but does not provoke hypertrophy to the same extent [45]. Currently, weighted wheel running [46] and high intensity interval training [47] are under investigation as intermediate forms of high-impact training that induce hypertrophy without causing tissue damage. Also in this research area, animal models, entail inherent disadvantages, such as the fact that they are costly in terms of time and money and that numerous parameters influence the outcome due to complexity of the organism, in addition to obvious ethical considerations. Therefore, 2D *in vitro* models have contributed immensely to understanding the underlying mechanisms of myotube formation, regeneration, hypertrophy and myonuclear accretion. In the past, various systems were applied to study the impact of stretch on hypertrophy and fusion using, mechanical stimulation e.g. with magnetic beads [48] or various bioreactor systems [49]–[51] including the FlexCell® system [52]–[54]. Moreover, specific targeting of integrins was used to induce hypertrophy [55], [56]. While providing crucial insights into the intricate mechanisms of mechanobiology involved in these processes, only few approaches were successful in inducing significant hypertrophy comparable the outcomes of successful *in vivo* models. Scott *et al.* presented an advancement of their established stretch bioreactor system including exposing myogenic cells to agrin, a proteoglycan required for the development of neuromuscular junctions. Thereby, they induced substantial hypertrophy in 3D tissue engineered muscle constructs [57]. Furthermore, Terrie *et al.* recently reported a drastic increase in hypertrophy in 3D bioartificial muscles upon electromagnetic stimulation [58]. A drawback of these studies, however, is the fact that they focused on the morphological changes in the hypertrophic myotubes and do not provide data on intracellular, molecular effects. This lack of knowledge presents the basis of the study presented in chapter three of this thesis.

3. Skeletal muscle tissue engineering

Despite the high regenerative capacity of skeletal muscle, regeneration cannot be maintained if the pool of available satellite cells is insufficient. Depletion of satellite cells is a natural implication of aging, but also occurs in the course of degenerative diseases resulting in degradation of muscle mass and loss of strength and function. In these cases, as well as upon volumetric muscle loss, the body's capability to rebuild the tissue is insufficient and treatment solutions are required [22]. Currently, state-of-the-art treatment options for muscle loss is the transfer of muscle tissue with functional vessels from another site of the body (free functional transfer). This process, however, entails high donor-site morbidity [59]. Cell therapy and engineering of artificial tissue present promising approaches for these conditions. Furthermore, tissue engineering allows for the development of *in vitro* models for muscle development and diseases. Therefore, extensive research efforts were put into developing skeletal muscle tissue engineering (SMTE) strategies that yield tissue models with high structural and functional similarity to *in vivo* tissue [60]. Successful generation of skeletal muscle constructs relies on three crucial factors that are the basis of classical SMTE approaches, called the tissue engineering triad (figure 7): (1) a suitable scaffold biomaterial that offers adequate micro-architectural and biodegradable properties as well as cues, such as growth factors, that favor the commitment to the myogenic lineage; (2) a cell type with the potential to differentiate along the myogenic lineage; (3) effective stimulation strategies in the form of mechanical, electrical or electromechanical stimuli to induce cellular alignment, fusion, differentiation and maturation [11].

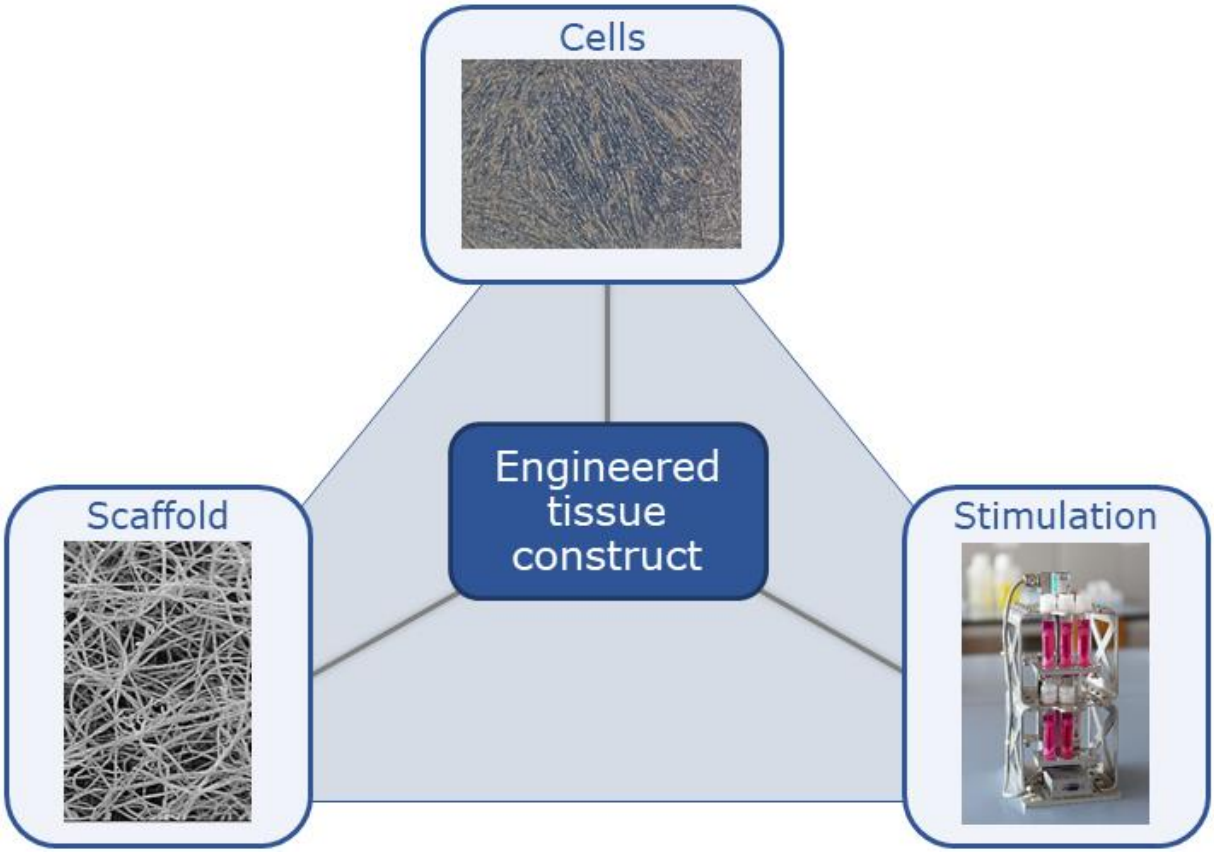

Figure 7: TE triad for skeletal muscle. Successful generation of skeletal muscle constructs relies on three crucial factors: **1.)** a suitable scaffold material (shown: fibrin), **2.)** cells with myogenic potential (shown: the myoblast cell line C2C12), **3.)** effective stimulation strategies (shown: the MagneTissue bioreactor for tensile mechanical stimulation)

2.1. Biomaterial characteristics

Biomaterials in tissue engineering serve as scaffolds for cell attachment and therefore allow formation of three-dimensional tissue constructs. Thereby, they should act like a substitute for the ECM and create a suitable microenvironment for the cells. To achieve this similarity to the native ECM, materials must fulfill a plenitude of specific requirements, such as surface properties that support cell attachment and suitable mechanical properties that differ for each type of tissue. Furthermore, more general requirements include properties, such as biocompatibility and usability for manufacturing [60]. When creating tissue constructs *in vitro*, the goal is to provide the cells with a material they can attach to initially, but that will be degraded with time. Thereby cells are allowed to deposit their own matrix components, which yields tissue constructs that mimic *in vivo* tissue more closely. Therefore, the materials must be biodegradable, however, not be degraded to rapidly to allow for sustained build-up of newly

formed matrix. Furthermore, appropriate porosity needs to be given to ensure sufficient nutrient and oxygen supply and removal of waste products [61].

The used biomaterials can be processed in numerous different ways, yielding various scaffold types, such as sponges, meshes, hydrogels, films, etc. In SMTE, the use of hydrogels has proven most suitable due to their advantageous features. Most importantly, their mechanical properties are easily tunable to resemble native muscle tissue. They can be produced from materials that interact with cells innately and can be functionalized with ligands to enhance cell interaction. This facilitates encapsulation of cells in an optimized 3D microenvironment leading to uniform cell distribution [62]. Another consideration in SMTE is that mature skeletal muscle mainly consists of contracting cells. Therefore, it is essential that the material used as a basis for the generation of functional muscle tissue can withstand the mechanical strength exerted by the contracting cells, but is also pliable enough to allow for the contraction [62], [63].

There are numerous different synthetic or natural biomaterials successfully used for SMTE. The most prominent synthetic ones are polyesters, such as poly glycolic acid (PGA), which are popular for scaffold fabrication, as they can easily be molded in many different shapes, sizes, and scaffold types (e.g., hydrogels, meshes, sponges...). However, their biological similarity (e.g., regarding cell attachment sites that trigger intracellular signaling) to the native tissue is lower than in natural materials. Therefore, they are often combined with natural materials or functionalized with ECM proteins, which leads to increase cell attachment and development. Natural biomaterials, on the other hand, provide these biological cues and thus facilitate cell attachment and proliferation and are furthermore more likely to be biocompatible. Manufacturing these materials, however, is often more complicated and costly. The most prominent natural biomaterials for skeletal muscle TE are collagen, alginate, hyaluronic acid and fibrin [60]. An overview of most common biomaterials in muscle TE is given in table 1.

Table 1: Most common biomaterials for skeletal muscle tissue engineering and their beneficial properties. poly-L-lactic acid (PLLA); poly(lactic-co-glycolic acid) (PLGA); polycaprolactone (PCL); poly(L-lactide-co-ε-caprolactone) (PLCL); polyaniline (PANI); polyethylene glycol (PEG); extracellular matrix (ECM); mesenchymal stromal cell (MSC); stromal cell derived growth factor 1 (SDF-1); vascular endothelial growth factor (VEGF); insulin like growth factor 1 (IGF-1); hepatocyte growth factor (HGF); fibroblast growth factor (FGF); (modified from [60])

Desirable biomaterial property	Materials utilized	Benefits	Key parameters for optimization
Porosity	- Alginate - Collagen	- High surface area resulting from porosity allows seeded cells to proliferate. - Macroporous structure promotes outward migration of transplanted cells and inward migration of host cells. - Migrated cells then interact with cells from native tissue and participate in the regeneration process.	- Pore size and interconnectivity. - Cell adhesive cues (e.g. RGD peptide motifs when using alginate)
2D Topographical cues (Patterned substrates, Electrospun aligned fiber patches)	- PLLA - PLGA - PCL - Collagen - PLCL - PANI - Fibrin - Gelatin	- Potential to combine different materials to form composites of desirable mechanical and physicochemical properties. - Electrically conductive polymers can be incorporated for additional stimuli to seeded cells. - Myoblast differentiation can be enhanced by synergic effects of electroactivity and fiber alignment. - Cell sheets composed of differentiated myotubes can be detached from patterned substrates for direct transplantation. Topographical cues promote: - Cytoskeletal alignment - Myotube assembly and fusion - Myotube striation	For patterned substrates: - Groove width - Groove depth - Ridge width For electrospun fibers: - Polymer composition - Fiber alignment
3D Topographical cues (Grooved scaffolds, Aligned pores)	- Collagen - Chitosan	- Contact guidance for alignment and fusion of myoblasts. - Mechanical properties can be varied without affecting porous structure. - Structural parameters (pore size) can be varied without influencing pore orientation. - Large diameter myotubes (similar to native muscle fiber) can be grown on such scaffolds *in vitro*.	- Continuous channels to facilitate myoblast fusion and formation of long myotubes. - Ensuring no change in structure (due to degradation and/or swelling) takes place during cell culture.
Injectable	Hydrogels including: - Alginate - Collagen - Hyaluronic acid - PEG - Fibrin	- Minimally invasive application of gel. - Encapsulated cells can migrate and interact with cells from injured tissue as gel degrades over time. - Tunable mechanical properties permit optimization of cellular microenvironment. - Encapsulated cells can be protected from direct effects of immune cells in the injury environment. - Encapsulated cell based drug delivery (e.g. paracrine signaling from MSCs).	- Hydrogel concentration optimized to maintain high cell viability. - Final volume of gel should ensure sufficient nutrient diffusion to encapsulated cells.
Native structural and biochemical cues	Decellularized tissues/ECM including: - Tibialis Anterior - Extensor digitorum longus - Abdominal muscles - Porcine bladder - porcine intestinal submucosa	- Pro-myogenic environment. - Intact native ECM structure, basement membrane structural proteins, cytokines and growth factors. - High clinical potential due to utilization of natural tissues (autografts/xenografts). - Maintenance of structural integrity. - Generation of full thickness *in vitro* tissue engineered skeletal muscle tissues. - Potential treatment option for volumetric muscle loss. - Can be formed into an injectable hydrogel without loss of bioactivity.	- Effective removal of all cells and debris. - Minimization of undesirable effects of chemical agents and detergents used during the decellularization process.
Presentation of growth factors	- Alginate (SDF-1) - Alginate (VEGF, IGF-1) - Alginate (HGF, FGF)	- Growth factors can be released locally over a period of time and therefore have a long lasting, localized effect at injury site. - Growth factors can either stimulate transplanted cells, or directly influence injured tissue.	- Growth factor release kinetics.

Fibrin is one of the most prominent natural biomaterials for the creation of skeletal muscle constructs, since it has proven to be highly suitable for SMTE approaches in the past [63]–[66]. Fibrin is a natural polymer created in the body as the end product of the blood clotting cascade. The fibrin network presents the basis for hemostatic plugs that serve as a scaffold for immune cells that are required for repair mechanisms leading to successful wound healing [67]. The fibrin polymer is made from fibrinogen monomers that are cleaved by the protease thrombin. Fibrinogen is abundant in the blood stream and when thrombin is activated upon wound-induced signaling, its enzymatic activity leads to the release of fibrinopeptides. The release of the fibrinopeptides reveals the polymerization sites of fibrinogen that are otherwise not accessible to prevent unwanted clotting. This allows for interaction between specific peptide motifs in the fibrin monomers. So-called “knobs” (Gly-Pro-Arg (GPR) motifs) of one monomer bind to so-called “holes” (the binding pockets for the GPR motifs in the γ-nodule) of another monomer [68]. The knob-hole interaction leads to formation of fibrin oligomers that aggregate laterally to form protofibrils. Protofibrils pack into fibrin fibers that become thicker and elongate and eventually branch into a 3D network. Branching occurs either bilaterally, when a four-stranded fibril separates into two separate protofibrils, or trimolecular, when a monomer binds only one γ-nodule, leaving another γ-nodule available in each protofibril (figure 8 A) [67]. The polymerization conditions, such as thrombin and salt concentration or the pH, determine which type of branching occurs [68], which eventually affects the porosity of the created clot, as shown in figure 8 B.

One of the main advantages concerning the use of fibrin as a scaffold biomaterial for SMTE is its elasticity. Fibrin is a viscoelastic material, demonstrating both, viscous and elastic properties at different stages of polymerization. At a certain moment of network formation, called the gel point, it loses its viscous properties and gains stiffness. The elastic modulus of fibrin clots can vary greatly. It was shown that if small strains are applied over short times (1-100 seconds), fibrin clots are highly elastic and can return to their initial shape when the strain is released. At higher strains or higher frequencies, however, inelastic deformation occurs. The exact magnitude of the parameters at which inelastic formation occurs depends on the specific characteristics of the fibrin clot, such as fiber thickness and network density [69]. Another reason for the popularity of fibrin in SMTE is its tunability. The elastic modulus can easily be manipulated, and it further demonstrates fast polymerization times, which makes it very convenient for the use as a scaffold biomaterial. Moreover, bioactive peptides can easily be incorporated [70]. Nevertheless, it also entails certain disadvantages concerning structural properties, such as shrinkage of the gel or rapid degradation by incorporated cells. This can be overcome by blending it with more stable biomaterials, such as polyurethane or polyethylene glycol and by the addition of the plasmin inhibitor aprotinin to the culture media or the scaffold [71]. Another disadvantage is that fibrin hydrogels fabricated with high fibrinogen concentrations demonstrate high material density, which limits cell migration and nutrient exchange. On the other hand, if low fibrinogen concentrations are used, the resulting hydrogel will lack stability [70]. A way to overcome this is

the incorporation of gelatin beads to obtain sufficient stability while maintaining adequate porosity, which has shown to increase their usability for *in vivo* injection [72].

One of the most important arguments for using fibrin in SMTE is that it contains a high number of attachment sites for myogenic cells, which allows their encapsulation and uniform distribution within fibrin gels. Specifically, developing myotubes express α5β3 integrins that bind to the arg-gly-asp (RGD) 572-574 motif located in the α chain of fibrinogen [73], [74]. This is particularly important, since it has been shown that a high cell density is highly beneficial for skeletal muscle development [75].

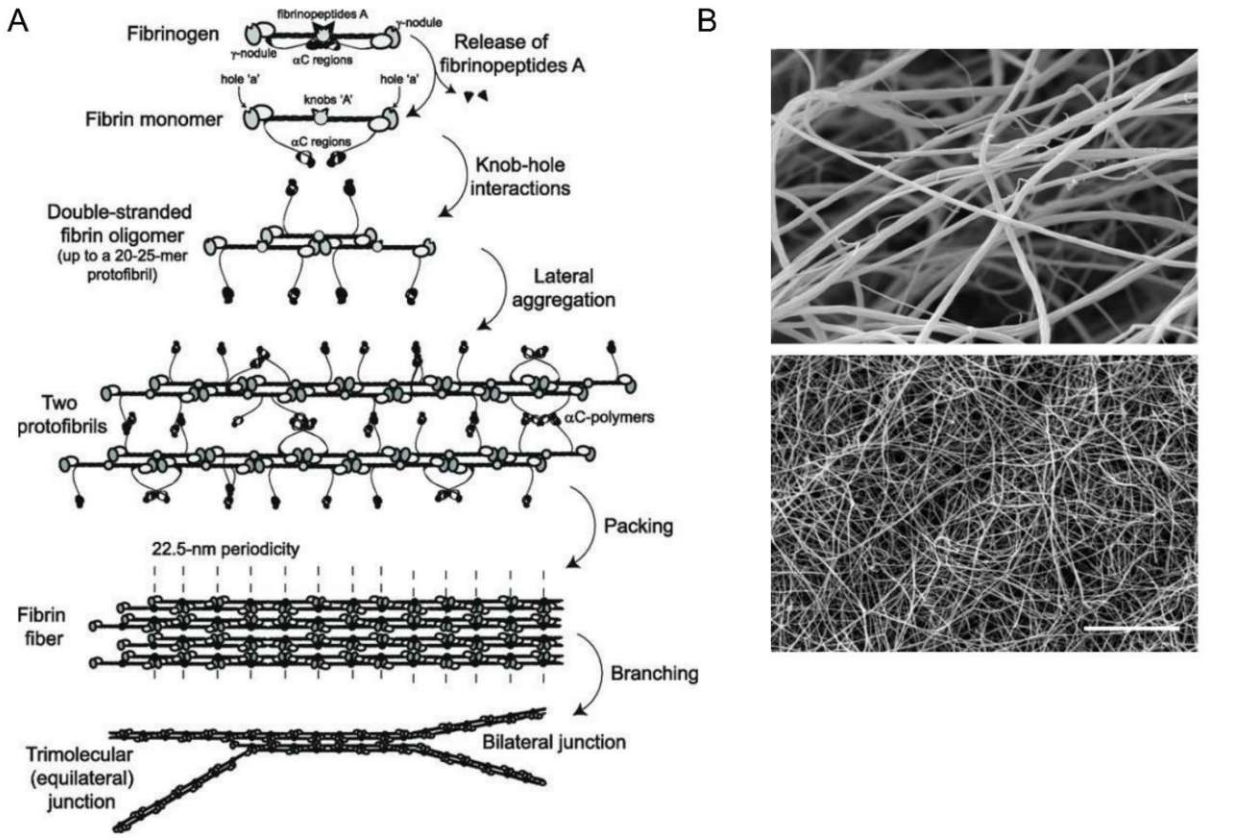

Figure 8: Fibrin polymerization. (A) Thrombin cleavage leads to release of fibrinopeptides and thereby the polymerization sites in the fibrin monomer become revealed. Thus, interaction between so-called "knobs" (Gly-Pro-Arg (GPR) motifs) of one monomer and so-called "holes" (the binding pockets for the GPR motifs in the γ-nodule) of another monomer are possible. This leads to formation of fibrin oligomers that aggregate laterally to form protofibrils. Protofibrils pack into fibrin fibers that become thicker and elongate and eventually branch into a 3D network. Branching occurs either bilaterally, when a four-stranded fibril separates into two separate protofibrils, or trimolecular, when a monomer binds only one γ-nodule, leaving another γ-nodule available in each protofibril [76]. **(B)** The type of branching affects the fibrin fibers and hydrogel porosity. Fibrin clots can have thick fibers with few branch points (upper panel) or thin fibers with few branch points (lower panel). (scanning electron image; scale bar = 5 μm; modified from [69])

Fibrin has been used in various approaches in numerous SMTE studies. Huang *et al.* displayed a prominent example for how the ability of muscle cells to generate force can be exploited to create muscle constructs using fibrin. They developed a system, in which myoblasts were cultured on a fibrin gel that was cast around two anchors. When the myoblasts differentiated, they contracted the gel that eventually rolled up due to the isometric strain created by the anchors (figure 9 A) [63]. Due to the rapid formation of muscle constructs, this approach gained popularity and was used with smooth muscle cells in order to generate a sphincter model [77]. Lam *et al.* used this concept by differentiating myoblasts on micropatterned PDMS plates and adding a layer of fibrin gel on top of the cells. Once the cells migrated into the gel and contracted it, it also rolled up, forming a cylindrical muscle construct (figure 9 B). Long-term cultivation, however, was not possible, as the cells digested the fibrin after a month, which lead to the constructs' degradation [78]. Furthermore, this method was used to study the formation of acetylcholine clusters [79], the influence of culture conditions and choice of cell type on the maturation of engineered muscle construct [80], methods to refine and control the microarchitecture [81], and the effect of ECM composition on tissue maturation [82].

Fibrin-based SMTE approaches were also under investigation for the treatment of muscle defects *in vivo*, by using it as a cell carrier for primary myoblasts or mesoangioblasts. Animal studies showed that cells introduced by fibrin carriers engrafted successfully. Increasing hydrogel stability through the addition of polyethylene glycol to the gels increased their stability in longevity in the body [65], [83].

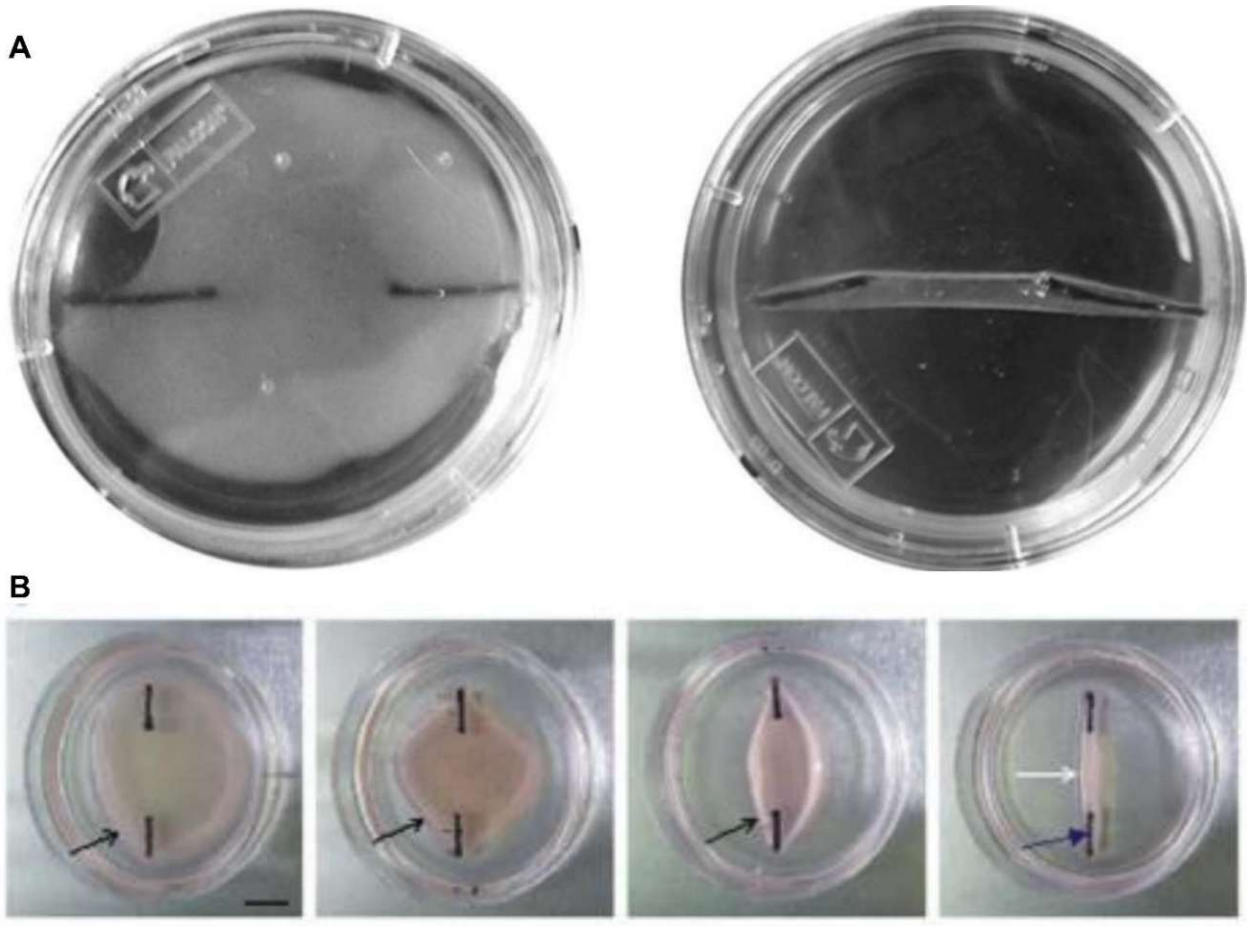

Figure 9: Formation of fibrin-based muscle constructs through self-organization of myogenic cells. **(A)** Myoblasts cultivated on top of a fibrin gel layer contracted upon differentiation (left panel), which eventually lead to formation of a free-standing construct that folded cylindrically around two anchors [63]. **(B)** A fibrin gel layer was added on top of differentiated myotubes that had been cultivated on micropatterned polydimethylsiloxane plates. The contractile forces of the myotubes led to formation of a free-standing construct that folded cylindrically around two anchors over the course of a month (process shown chronologically from left to right) [78].

The stiffness of the biomaterial presents a further crucial factor determining the cell fate and thus the effect of cultivation conditions on cells and the myogenic outcome of SMTE approaches. Myogenic progenitor cells grown on standard cell culture plastic lose their stemness and show a lower engraftment efficiency when implanted *in vivo* [70]. In contrast to that, cultivation on matrices demonstrating a rigidity similar to that of native muscle tissue (*i.e.* a Young´s Modulus of 12 kPa) leads to improved proliferation and maintenance of *Pax7* expression [18], [84]. Differentiation of myogenic cells is also affected by the rigidity of the underlying substrate. The most fundamental studies on the effect of substrate stiffness on fate determination and myogenic differentiation were conducted by Engler *et al.* (figure 10) [85], [86]. They found that cultivation on a substrate with a stiffness in the range of 8–11 kPa generated striated myotubes

in contrast to stiffer substrates [85]. This study was the basis for further research by other groups that concluded that culture on softer matrices is more beneficial for myogenesis compared to stiffer ones [85], [87]–[89]. It must be noted, however, that the range of substrate stiffness analyzed in most studies varies over several orders of magnitude (from 1 kPa to several MPa), reducing their biological relevance, as those variations do not represent the *in vivo* situation. The stiffness of skeletal muscle *in vivo,* indeed does change depending on age and health status, but not to such drastic extents [90]–[92].

Given the structural properties of skeletal muscle tissue, it is evident that cellular alignment during formation of engineered muscle constructs is a crucial factor contributing to tissue maturation and functionality. It has been shown that using patterned substrates is highly beneficial regarding myogenic differentiation of cultivated cells. Longitudinal patterning can be achieved using different methods, such as introducing material alignment through mechanical stress applied with a bioreactor [66], laser ablation [93], electrospinning [94], introducing alignment with glass fibers [95] or molding substrates with PDMS stamps [78], [96].

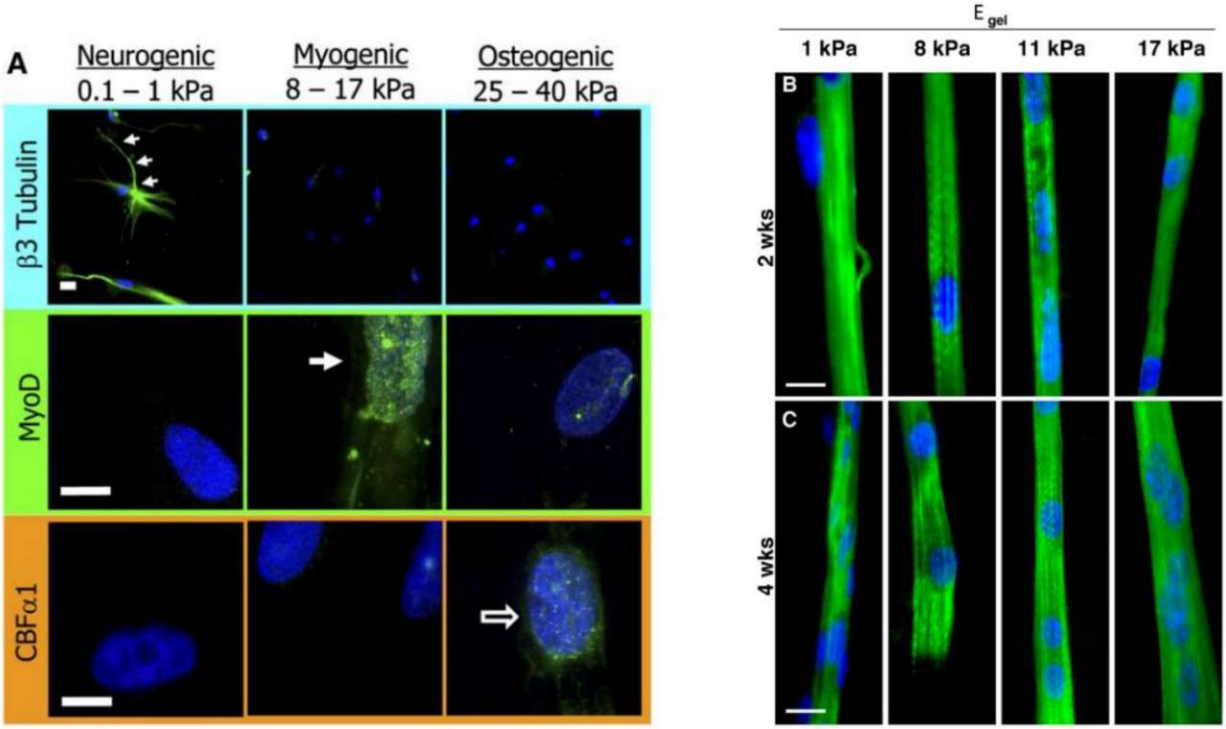

Figure 10: Substrate stiffness affects stem cell fate determination and myogenic differentiation. (A) Mesenchymal stem cells were cultivated on micropatterned gels with Youngs's Moduli representing neurogenic environments (0.1 – 1 kPa), myogenic environments (8 – 17 kPa) or osteogenic environments (25 – 40 kPa). Stainings for marker proteins of the different lineages (β3 tubulin, MyoD and Core-Binding Factor Alpha 1 (CBFα1), respectively) show that cultivation on substrates with varying stiffness leads to fate determination in the respective lineage [86]. **(B** and **C)** Myoblasts were cultivated on micropatterned gels with different Youngs's Moduli (1 kPa, 8 kPa, 11 kPa and 17 kPa). Myosin stainings show that cultivation on substrates Youngs's Moduli between 8 kPa and 11 kPa leads to the development of striated myotubes [85].

2.2. Cells for skeletal muscle tissue engineering

There are numerous cell types with the potential to differentiate along the myogenic lineage. Some of those have been studied extensively regarding their use in SMTE and shown varying results. Immortalized cell lines are mostly used to establish model systems due their easy cultivation. While they present important features also found in primary cells, their differentiation behavior recapitulates *in vivo* processes to a lesser extent than primary cells [97]. The most widely used myogenic cell line are C2C12 myoblasts. They were generated by Yaffe and Saxel from a C3H mouse in 1977 [98] and have been used extensively ever since, as their cultivation is easy and cost-effective, and they differentiate rapidly upon serum deprivation [97]. To increase the relevance of *in vitro* models in terms of translatability to human conditions, human myoblast lines were introduced as well. Thorley *et al.* developed a myoblast cell line, called C25 that displays similar characteristics to primary myoblasts in terms of myogenic development [99]. Regarding primary cells, the most used cell types in SMTE are myoblasts, satellite cells and stem cells from different sources, the most important one being muscle satellite cells (MuSCs). They can be isolated from muscle tissue by plating fibers on protein-coated dishes or by enzymatic digestion [62], [100]. Like *in vivo*, they have the capability to self-renew and differentiate into myotubes upon stimulation [101]. However, their cultivation requires caution since they cannot return to the self-renewing state once they were activated. Thus, exactly as *in vivo*, the pool of proliferating MuSCs can become depleted [102]. Other tissue-resident cells also have been employed in SMTE, such as interstitial skeletal muscle progenitor cells [102], Pw1 interstitial cells [103], fibroadipogenic progenitors, pericytes, and mesoangioblasts [104]–[110].

Multi- and pluripotent stem cells also entail great potential in regenerative medicine and SMTE. In this regard, mesenchymal stem cells (MSCs) in induced pluripotent stem cells (iPSCs) became the most promising cell types in recent years. MSCs were shown to contribute to tissue repair and reduction of inflammation [111]–[113] and enhance muscle fiber formation *in vivo* [111], [113]–[116]. Furthermore, their regenerative potential was shown in *in vivo* injury models [117]. It is widely accepted that one of the ways they promote regeneration is through their capability of paracrine signaling, including release of immunomodulating and promyogenic factors, as well as matrix metalloproteases [113], [118]–[120]. In the field of skeletal muscle research, iPSCs were mostly studied with a focus on disease modeling and drug testing. As they can be derived from patients, they are a promising tool to investigate diseases, such as muscular dystrophies. Tedesco *et al.* performed an important study underlying the potential of iPSCs in dystrophy research. They isolated fibroblasts from patients suffering from limb-girdle muscular dystrophy, reprogrammed them into iPSCs and subsequently corrected their genetic defect and differentiated them into mesoangioblasts. When these cells were grafted into diseased muscle of a humanized limb-girdle muscular dystrophy mouse model, the dystrophic phenotype was ameliorated and the previously depleted MuSC pool was replenished [121]. Moreover, this group used iPSCs for a SMTE model of Duchenne, limb-girdle, and congenital

muscular dystrophies by creating 3D tissue constructs with iPSCs generated from patient-derived cells [122].

2.3. Mechanical stimulation

Given the importance of mechanical stimulation for the development and regeneration of skeletal muscle, it is not surprising that incorporation of such stimuli gained a lot of attention in the field of SMTE. Numerous approaches incorporating mechanical stimulation have been developed to overcome the lack of conventional static cell culture. The results of these attempts were highly successful and included improved morphology and functionality of created muscle constructs improve that became more *in vivo*-like [123]. Depending on the applied regimen, cellular proliferation [64], [124], [125] and differentiation [64], [66], [125]–[128] increased. When *in vivo* studies were performed with the pre-trained constructs, they showed better performances concerning contractile forces and functional recovery of muscle injuries compared to their control counterparts [49], [50], [129].

Vandenburgh *et al.* pioneered in introducing mechanical stretch to 3D muscle constructs by cultivating myoblasts on flexible membranes that could be stretched and thereby exerted mechanical stress onto the cells [130]. In the upcoming decades, they further improved their system to stimulate 3D tissue constructs, with which they had great success in generating engineered muscle [131], [132]. The most advanced development of this system uses actuators that move pins onto which the muscle constructs are fixed to stretch them (figure 11 A) [125]. A similar setup is the addition of sutures to the cell-loaded scaffolds that fix the constructs on one side, while the other end is attached to a stepper motor (figure 11 B) [49], [50], [64], [126], [129], [133]. One of the main advantages of these automated systems that make use of actuators is the fact that various types of strain regimens can be implemented. Therefore, they can be employed for a multitude of research questions regarding mechanical stimulation and mechanotransduction. Auluck *et al.* used a different approach for force transduction and clamped one end of collagen gels with embedded cells to cell culture dishes, while the other end was clamped to a magnet. Thereby, it was possible to stretch the scaffolds by moving the magnets using electromagnetic coils (figure 11 C) [127]. A different approach to apply uniaxial mechanical strain to collagen scaffolds with embedded cells was established by Okano *et al.* in 1998. They molded gels into a ring-like shape, which allowed them to mount the scaffolds between two glass rods in a cell culture flask. One of the rods was fixed to the flask, whereas the other one was connected to a piston, which allowed straining of the rings with a motor (figure 11 D) [124].

The method used in this thesis for application of mechanical stress to cells embedded in scaffolds combines some of the aforementioned ideas. Our research group established a bioreactor system called MagneTissue that takes advantage of electromagnetic force transmission. Myoblasts are embedded in ring-shaped fibrin hydrogels that are mounted on spool-hook systems that are placed in conical tubes. The hooks, onto which the scaffolds are

suspended, contain magnets. Therefore, the scaffolds can be stretched when another magnet that is outside the tube moves vertically. The bioreactor system contains external magnets that are connected to a stepper motor that enables automated movement and therefore stretching of the scaffolds (figure 11 E) [66].

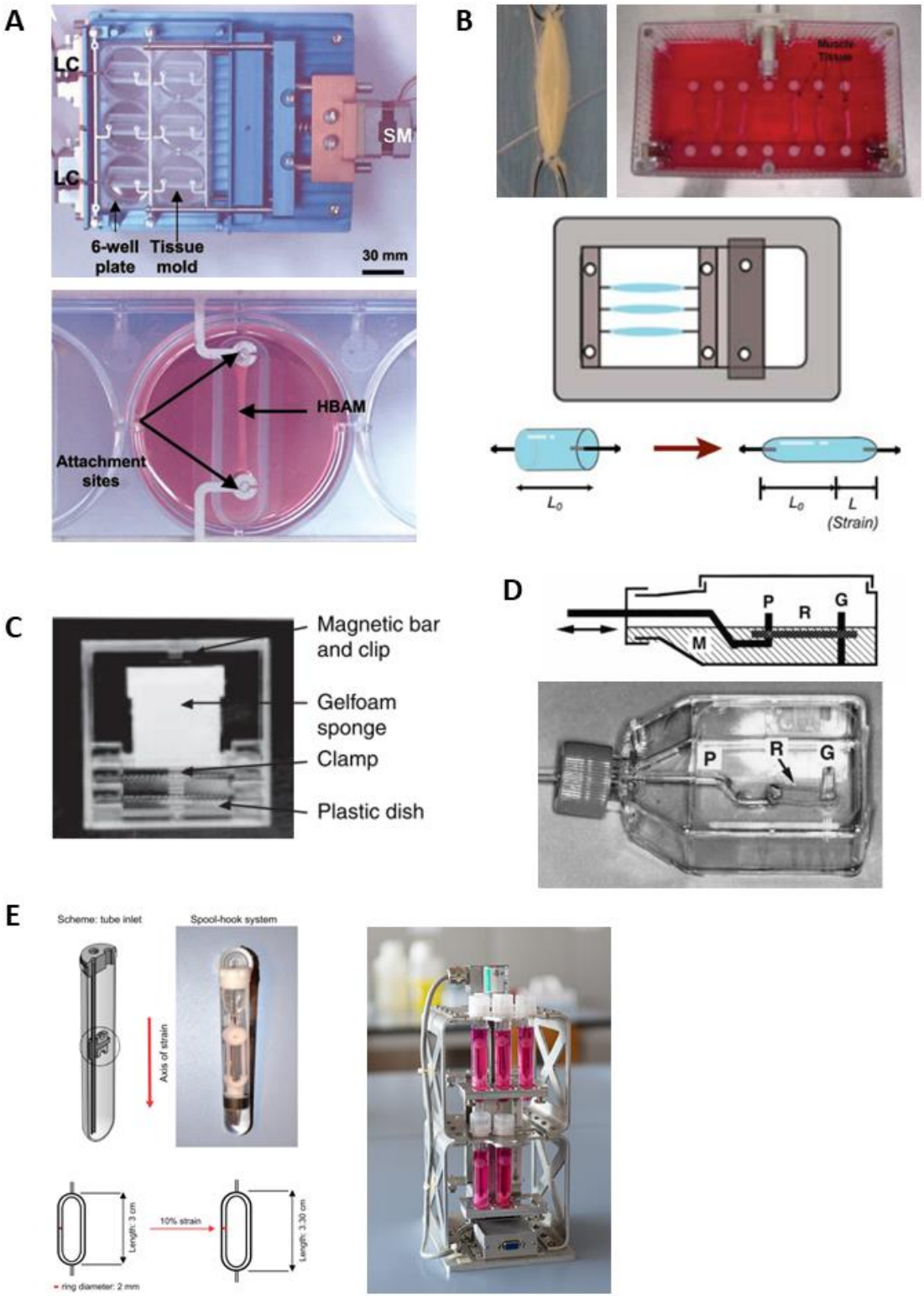

Figure 11: Different bioreactor types for the mechanical stimulation of skeletal muscle constructs. **(A)** Human bioartificial muscles (HBAMs) were attached to pins that can be moved by a stepper motor (SM). The tension was measured by two load cells (LC) [125]. **(B)** Cell-loaded scaffolds were fixed with sutures onto the cell culture flask on one side, while the suture of other side was moved with a stepper motor [49], [64]. **(C)** Collagen scaffolds with embedded cells were clamped onto plastic dishes on one side, while the other side was clamped to a magnet, which enabled stretching of the scaffolds by moving the magnets using electromagnetic coils [127]. **(D)** Cell-containing hydrogels were molded into a ring-shape (R), immersed in medium (M) and fixed onto a glass rod (G) that was fixed on the plastic flask. Stretching of the ring-shaped scaffolds was induced by movement of a piston (P) that was attached to the other side of the ring [124]. **(E)** Ring-shaped scaffolds that contained cells were suspended between a spool and a hook that contains a magnet and placed in conical tubes. Horizontal movement of an external magnet placed outside the tube led to stretching of the scaffolds that was automated by connecting the external magnets to a stepper motor [66].

Hypotheses of the thesis

Successful generation of tissue-engineered skeletal muscle depends on an interplay between the three main components of the classical tissue engineering triad: cells, biomaterials and stimulating factors. This thesis focuses on the questions, how choice and manufacturing of the biomaterial, as well as the stimulation strategies affect the applied cells. The overall aim hereby was to provide insights into appropriate designs of the culture environment for an improved myogenic outcome of tissue-engineered skeletal muscle.

The three main hypotheses of the thesis were:

I) biomaterial elasticity, biomaterial patterning and cultivation in a 3D environment affect proliferation and differentiation of myoblasts

II) choosing appropriate system components, particularly biophysical and biochemical stimuli, allows for the creation of optimized SMTE strategies

III) application of mechanical overload on skeletal muscle-like constructs induces hypertrophy and myonuclear accretion

I) Biomaterial elasticity, biomaterial patterning and cultivation in 3D environments affect proliferation and differentiation of myoblasts

The mechanical properties of the substrate cells are grown on greatly influence their developmental fate. Therefore, we hypothesized that subtle changes of the elastic modulus of fibrin scaffolds will impact myogenic differentiation of myoblasts. Moreover, we addressed the issue of translatability of the results gained in *in vitro* models. Most of the knowledge on cellular behavior is derived from experiments in which cells are cultivated in a two-dimensional environment. This, however, does not reflect the situation *in vivo* and furthermore is insufficient for the creation of artificial tissue constructs. Therefore, we cultivated myoblasts on top of two-dimensional or embedded in three-dimensional hydrogels, expecting that the culture type will influence their development.

Most preliminary studies on SMTE strategies are performed with murine cells due to their availability and well-studied culture conditions. However, results gained from those studies cannot always be translated to human cells, which renders the generation of human tissue-engineered skeletal muscle highly challenging. Anticipating that murine and human myoblasts behave differently, we also assessed their reaction on changed elastic modulus and culture type.

The structural properties of scaffolds used for SMTE approaches presents a further factor influencing their myogenic outcome. It is well known that parallel alignment of the substrate is highly beneficial for the development of aligned myotubes, which is a prerequisite for their functionality. We hypothesized that this also holds true for silk fibroin substrates. Therefore, we applied femtosecond lasers to introduce microstructural changes silk films. Parallel grooves were introduced on the biomaterial, expecting increased suitability as a scaffold for SMTE.

II) Choosing appropriate system components, particularly biophysical and biochemical stimuli, allows for the creation of optimized SMTE strategies

While research on SMTE strategies has achieved great results in modelling the tissue characteristics on a small scale, they still do not reflect the complex environment of *in vivo* tissues. Therefore, we hypothesized that the choice of culture settings in tissue engineering approaches in terms of exerting additional stimulation on cells has great potential to improve their ability to recapitulate the *in vivo* environment and consequently improve functional and structural characteristics of engineered tissue. This was answered by a comprehensive literature review on the design of dynamic skeletal muscle models whose success is based on an effective integration of cells, biomaterials, and biophysical and biochemical stimuli. Further, we elaborate on the potential of these platforms in disease modeling and present an analytical workflow for facilitated identification of successful tissue engineering strategies.

III) Application of mechanical overload on skeletal muscle-like constructs induces hypertrophy and myonuclear accretion

Skeletal muscle is known for its high capacity to adapt to mechanical stress and to regenerate after injuries. This high degree of plasticity is enabled by the activation of dormant satellite cells upon stress, as well as increased metabolism and protein synthesis in myotubes. These stress responses lead to increased hypertrophy and myonuclear accretion in myotubes.

Since there is a lack of *in vitro* models that study these processes, we aimed to create a tissue-engineered model for skeletal muscle adaptation to mechanical stress. We hypothesized that the stress responses observed *in vivo* will be recapitulated by subjecting differentiated 3D skeletal muscle-like constructs to cyclic tensile stress. Therefore, we created tissue constructs using a strain-bioreactor and applied tensile stress to trigger myoblast activation and overload-induced hypertrophy. Besides analyses of morphological changes upon mechanical stress, we examined intracellular signaling pathways during these processes to characterize the model for skeletal muscle hypertrophy and myonuclear accretion.

CHAPTER 1

BIOMATERIAL ELASTICITY, BIOMATERIAL PATTERNING AND CULTIVATION IN A 3D ENVIRONMENT AFFECT PROLIFERATION AND DIFFERENTIATION OF MYOBLASTS

Changes in elastic moduli of fibrin hydrogels within the myogenic range alter behavior of murine C2C12 and human C25 myoblasts differently

Janine Tomasch[1,2], Babette Maleiner[1,2], Philipp Heher[3], Manuel Rufin[2,4], Orestis G. Andriotis[2,4], Philipp J. Thurner[2,4], Heinz Redl[2,5], Christiane Fuchs[2,6,7], Andreas H. Teuschl-Woller[1,2*]

[1]Department Life Science Engineering, University of Applied Sciences Technikum Wien, Vienna, Austria

[2]The Austrian Cluster for Tissue Regeneration, Vienna, Austria

[3]Ludwig Randall Centre for Cell and Molecular Biophysics, King's College London, Guy's Campus, London, UK

[4]Institute of Lightweight Design and Structural Biomechanics, TU Wien, Vienna, Austria

[5]Ludwig Boltzmann Institute for Traumatology, the research center in cooperation with AUVA, Vienna, Austria

[6]Wellman Center for Photomedicine, MGH, Boston, MA, USA

[7]Harvard Medical School, Boston, MA, USA

*Corresponding author: Andreas H. Teuschl-Woller, teuschl@technikum-wien.at

Published in *Frontiers in Bioengineering and Biotechnology* on May 20th, 2022

Abstract

Fibrin hydrogels have proven highly suitable scaffold materials for skeletal muscle tissue engineering in the past. Certain parameters of those types of scaffolds, however, greatly affect cellular mechanobiology and therefore the myogenic outcome. The aim of this study was to identify the influence of apparent elastic properties of fibrin scaffolds in 2D and 3D on myoblasts and evaluate if those effects differ between murine and human cells. Therefore, myoblasts were cultured on fibrin-coated multiwell plates ("2D") or embedded in fibrin hydrogels ("3D") with different elastic moduli.

Firstly, we established an almost linear correlation between hydrogels' fibrinogen concentrations and apparent elastic moduli in the range of 7.5 mg/mL to 30 mg/mL fibrinogen (corresponds to a range of 7.7 kPa to 30.9 kPa). The effects of fibrin hydrogel elastic modulus on myoblast proliferation changed depending on culture type (2D vs. 3D) with an inhibitory effect at higher fibrinogen concentrations in 3D gels and vice versa in 2D. The opposite effect was evident in differentiating myoblasts as shown by gene expression analysis of myogenesis marker genes and altered myotube morphology. Furthermore, culture in a 3D environment slowed down proliferation compared to 2D, with a significantly more pronounced effect on human myoblasts. Differentiation potential was also substantially impaired upon incorporation into 3D gels in human, but not in murine, myoblasts.

With this study, we gained further insight in the influence of apparent elastic modulus and culture type on cellular behavior and myogenic outcome of skeletal muscle tissue engineering approaches. Furthermore, the results highlight the need to adapt parameters of 3D culture setups established for murine cells when applied to human cells.

Keywords: skeletal muscle tissue engineering, fibrin, biomaterials, mechanobiology, myogenesis

1. Introduction

Skeletal muscle not only gives us the ability to move but also has numerous other essential functions in the human body. Although muscle tissue has a high regenerative capacity, when more than 20% of the tissue of a particular muscle is lost, healing of the tissue is substantially hampered [134]. Besides volumetric muscle loss due to trauma or muscular diseases, muscle wasting is a considerable socioeconomical burden affecting 561 million people worldwide. Therefore and since autologous muscle grafts harbor the risk of donor-site morbidity and additional impairment of quality of life, the need for strategies to generate *ex vivo* functional muscle tissue is evident [135], [136].

Shortly after the boom in tissue engineering (TE), a new wave emerged within this field: it became apparent that the mechanical properties of scaffold materials or the cell microenvironment and related mechanotransduction are of utmost importance when trying to engineer tissue. Although the science of mechanotransduction and biomechanics is not new, it gained substantial attention through the TE field. Numerous reviews and publications in top-tier peer-reviewed journals are proof [26], [137]. Biomaterial and TE research not only focuses on the identification of novel biomaterials for TE purposes or their tuneability, but also on how the material properties can influence cellular behavior or tissue formation. In general, most cell types are capable of self-organization into tissues and synthesizing as well as modifying their extracellular environment. This can be achieved by different processes, as reviewed by Sthijns *at al.*, who highlighted the importance of organization in a three dimensional environment for cell fate decisions and maturation [138]. It is well accepted that providing the right microenvironment of biophysical and biochemical cues highly influences the outcome in TE constructs [139].

It has long been known that in skeletal muscle tissue engineering (SMTE) structural and mechanical cues in the respective scaffold biomaterial, such as micro-architecture and stiffness, guide and induce muscle differentiation and are pivotal for the myogenic outcome [82], [84], [85], [88]. To name just one example, culture on micropatterned soft gels with substrate stiffness in the range of 8-11 kPa generated striated myotubes in contrast to stiffer substrates [85]. These findings are in accordance with several other studies that found that culture on softer matrices is more beneficial for myogenesis compared to stiffer ones [85], [87]–[89]. The range of substrate stiffness analyzed in most studies, however, varies over several orders of magnitude (from 1 kPa to several MPa), reducing their biological relevance, as minor changes in biomaterial modulus can already elicit substantial changes in the embedded biological system. The premise of most studies analyzing the effect of substrate stiffness, and SMTE approaches in general, is the use of scaffolds with mechanical properties close to the native tissue. In this regard, however, the stiffness of skeletal muscle depends on age and health status and also species (table 2), and this has to be taken into account for designing patient-specific regenerative approaches. Thus, when translating findings from different studies using murine cells to SMTE approaches with human cells, the same outcomes cannot be expected. Furthermore, the choice

of method for mechanical characterization [e.g. tensile testing or atomic force microscopy (AFM)] may influence the results due to the load case applied and the length-scale at which the method is applied.

Although researchers have looked at different geometries, (bio)-materials and stiffness [66], [78], [140]–[142], there is still no consensus about optimal material properties to foster myogenesis in order to engineer muscle-like tissue in the SMTE field. This stems from the fact that many studies either solely look at 2D differentiation of TE muscle or 3D setups. Few are comparing both and results on the effects on myogenesis from such comparisons are often different. One example is that in 2D, murine myoblasts only aligned in grooves less than 100 µm wide, whereas in 3D constructs, these cells only aligned in larger grooves of 200 µm [143], highlighting the differences of cell responses depending on 2D *vs.* 3D culture.

In a previous study, our group used 3D fibrin scaffolds for the generation of muscle-like structures through application of tensile stress onto myoblasts [66]. We chose fibrin as a cell carrier, since it has proven highly suitable for SMTE approaches in the past [63]–[66], [78], [79], [81] as we further elaborated on in a follow-up review [51]. To the best of our knowledge, despite its popularity, there are no studies directly comparing cellular behavior in 2D *vs.* 3D in fibrin in SMTE. Therefore, this aspect of 2D *vs.* 3D cultures of myoblasts on or within fibrin with varying stiffness will be analyzed within this study.

A further issue tackled in this study is the transferability of the material's influence on myogenesis in murine to human models. The most frequently used myoblast cell line used in SMTE is the murine myoblast cell line C2C12, as it constitutes a fast, reliable and low-cost approach. Without question, the data generated and contributions to the field are essential but, ultimately, the goal is to engineer tissue that is transplantable into humans or serves as a human model of muscle tissue for drug screens, disease modelling or simulating acute pathologies such as trauma. Thus, efforts have been made to engineer skeletal muscle-like tissue using various human cell types, ranging from satellite cells to iPSCs and myoblasts [51], [106], [110], [122], [144]. Successful translation of concepts developed in murine SMTE approaches to the use of human cells requires similar responses of human cells to these specific environments. In order to obtain this information, studies applying cell types with similar myogenic potential derived from different species in the same culture setups are required. We want to achieve this through comparison of the widely used murine myoblast cell line C2C12 to the human myoblast cell line C25 [99], which has gained increasing importance in human skeletal muscle models. Noteworthy, transcriptomic analysis showed that immortalization of C25 myoblasts did not overtly affect their behavior throughout myogenesis [99], which ensures comparability of the line with the murine C2C12 myoblasts.

With this study, we want to shed light on the impact of culture conditions in fibrin hydrogels on a well-established murine myoblast cell line, C2C12, and the human C25 myoblast cell line, by answering the following questions: 1) How do subtle variations in fibrin hydrogel stiffness within a defined range, proposed to be most compatible with myogenesis, affect murine and human myoblasts?; 2) Does the culture type, namely 2D vs. 3D, affect myogenesis differentially in myoblasts from these two species?; and 3) How does the combination of stiffness and culture type influence myogenic differentiation? These are key questions in the SMTE field, and therefore this comparison of species and other essential differentiation cues has potential to contribute to unresolved issues in the SMTE field advancing it a step further.

Table 2: Overview of mechanical properties of skeletal muscle in mice and humans.

Mouse					***Human***				
Source		**Modulus/Stiffness**	**Method**		**Source**		**Modulus/Stiffness**	**Method**	
Single fibers									
	healthy	12 ± 4 kPa	AFM (indentation)	Engler *et al.* 2004					
	dystrophic	18 ± 6 kPa	AFM (indentation)	Engler *et al.* 2004					
adult	intact	0.4 ± 0.1 kPa	AFM (indentation)	Lacraz *et al.* 2015					
	damaged	2.3 ± 0.4 kPa	AFM (indentation)	Lacraz *et al.* 2015		young	~8kPa/µm [Δ]	force transducer (stretch-relax)	Noonan *et al.* 2020
old	intact	1.9 ± 0.3 kPa	AFM (indentation)	Lacraz *et al.* 2015		old	~12kPa/µm [Δ]	force transducer (stretch-relax)	Noonan *et al.* 2020
	damaged	10.4 ± 1.6 kPa	AFM (indentation)	Lacraz *et al.* 2015		healthy	28.2 ± 3.3 MPa	force transducer (stretch-relax)	Lieber *et al.* 2003
	healthy	~7 kPa	force transducer (stretch-relax)	Meyer and Lieber 2011		spastic	55 ± 6.6 MPa	force transducer (stretch-relax)	Lieber *et al.* 2003
Bundles of fibers									
	healthy	~40 kPa	force transducer (stretch-relax)	Meyer and Lieber 2011		healthy	462.5 ± 99.6 MPa	force transducer (stretch-relax)	Lieber *et al.* 2003
						spastic	111.2 ± 35.5 MPa	force transducer (stretch-relax)	Lieber *et al.* 2003
Whole muscle									
					young	male	292 ± 36 N/m *	MyotonPRO (damped natural oscillation)	Agyapong-Badu *et al.* 2016
						female	233 ± 35 N/m *	MyotonPRO (damped natural oscillation)	Agyapong-Badu *et al.* 2016
					old	male	328 ± 29 N/m *	MyotonPRO (damped natural oscillation)	Agyapong-Badu *et al.* 2016
						female	311 ± 42 N/m *	MyotonPRO (damped natural oscillation)	Agyapong-Badu *et al.* 2016

2. Materials and methods

If not indicated otherwise, all chemicals and reagents were purchased from Sigma Aldrich (Vienna, Austria) and were of analytical grade.

2.1. Cell culture

Two different myoblast cell lines were used for this study. The murine line C2C12 (American Type Culture Collection, Manassas, USA) was cultured in Dulbecco's modified Eagle's medium high glucose (DMEM-HG; Life Technologies, Carlsbad, California), supplemented with 10% fetal calf serum (v/v) (GE Healthcare, Buckinghamshire, United Kingdom), 1% penicillin/streptomycin (v/v) (Lonza, Basel, Switzerland) and 1% L-glutamine (v/v) (Lonza, Basel, Switzerland). The human line C25 (kind gift from Peter Zammit, King´s College, London, United Kingdom) was cultured in skeletal muscle cell growth medium (PromoCell, Heidelberg, Germany), supplemented with the skeletal muscle cell growth medium supplement kit (PromoCell, Heidelberg, Germany) with final concentrations of 50 µg/mL bovine fetuin, 10 ng/mL recombinant human epidermal growth factor, 1 ng/mL recombinant human basic fibroblast growth factor, 10 µg/mL recombinant human insulin, 0.4 µg/mL dexamethasone, and 20% fetal calf serum (v/v), 1% penicillin/streptomycin (v/v) and 1% L-glutamine (v/v). Those media will be referred to as growth medium (GM). For expansion, cells were cultured in standard cell culture dishes (37°C, 5% CO_2) and sub-cultured at 70% confluence to avoid induction of differentiation. Differentiation media (DM) consisted of DMEM-HG, supplemented with 3% horse serum (v/v), 1% penicillin/streptomycin (v/v) and 1% L-glutamine (v/v) for C2C12 cells and skeletal muscle cell differentiation medium (PromoCell, Heidelberg, Germany), supplemented with recombinant human insulin (10 µg/mL), 1% penicillin/streptomycin (v/v) and 1% L-glutamine(v/v) for C25 cells.

2.2. Preparation of fibrin hydrogels for cell-based experiments

To investigate the effect of substrate stiffness and architecture on myoblasts, cells were either cultured on fibrin-coated well-plates (referred to as 2D) or encapsulated in fibrin hydrogels (referred to as 3D) using the clinically approved Tissucol Duo 500 5.0 mL Fibrin Sealant (Baxter Healthcare Corp., Deerfield, USA) (figure 12 B).

For the 2D culture setups, fibrin coating was generated by mixing fibrinogen and thrombin in a 1:1 ratio. Different fibrinogen concentrations were used to create hydrogels with different mechanical properties, while the final thrombin concentration was 1 U/mL for all hydrogels. Fibrinogen was diluted from a 78.5 mg/mL stock in the respective GM. A thrombin stock of 500 U/mL was diluted in 40 mM $CaCl_2$ to a working solution of 4 U/mL and further diluted in GM. Polymerization of fibrin coating was achieved after 30 minutes at 37°C prior to cell seeding.

For the 3D culture setups, different fibrinogen concentrations were used with a constant final concentration of 1 U/mL thrombin. To encapsulate cells in the hydrogels, the thrombin working solution was diluted with a cell suspension (in GM). Thrombin+cells and fibrinogen were mixed

in a 1:1 ratio and polymerized in 2 mL syringes, of which the cap had been cut off, for 30 minutes at 37°C.

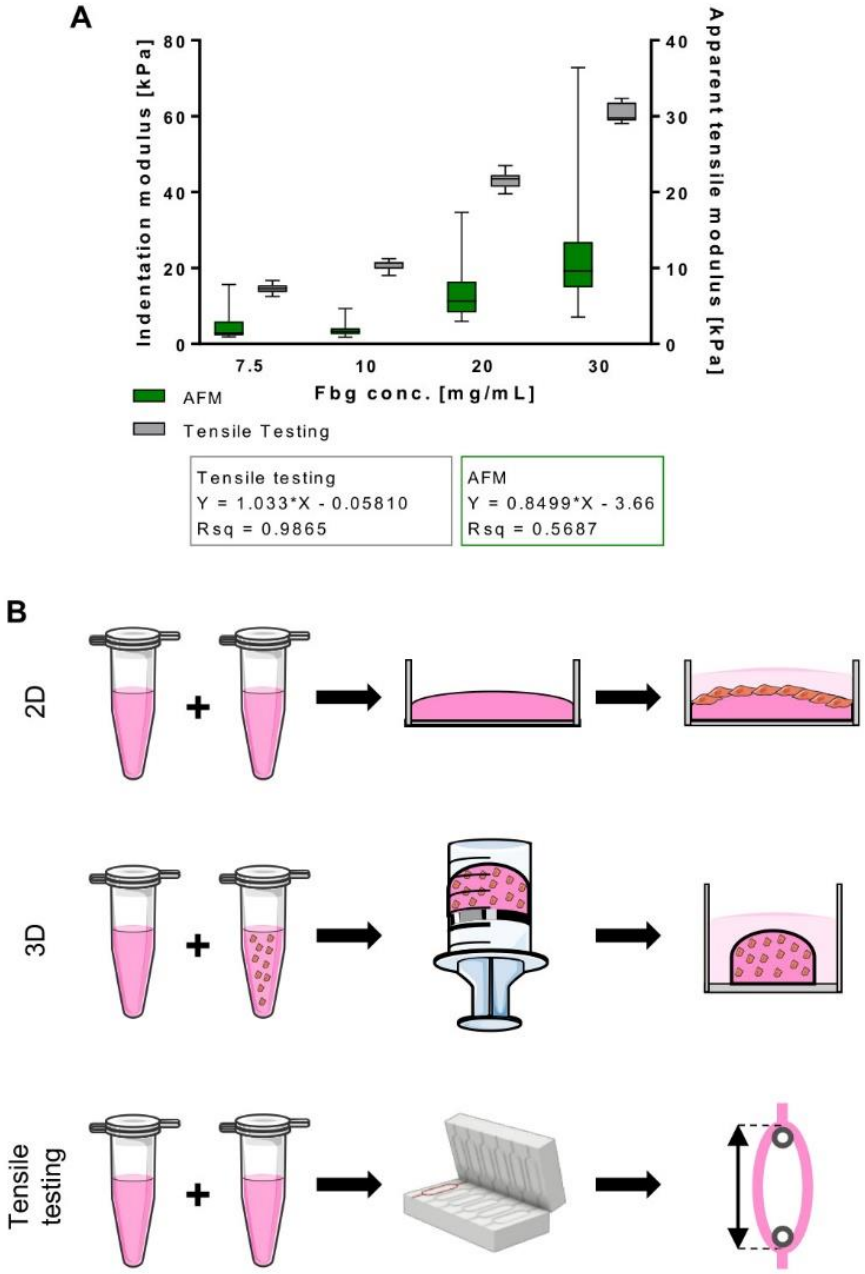

Figure 12: Normalized stiffness of fibrin hydrogels used in this study correlates directly with fibrinogen content. (A) Indentation and apparent tensile modulus [kPa] of fibrin hydrogels with different fibrinogen concentrations [mg/mL] acquired through AFM indentation and tensile testing, respectively. Data is shown as box and whiskers (min to max); N ≥ 2, n ≥ 6 for tensile testing and N = 2, n = 2 AFM. **(B)** Hydrogel types used in this study. 2D: cells were seeded on top of fibrin-coated wells of cell culture well-plates; 3D: cells were incorporated into fibrin hydrogels that were polymerized in 2 mL syringes and transferred to cell culture well-plates afterwards; tensile testing: fibrin hydrogels were cast in a ring shape and mounted onto spools for tensile testing.

2.3. Proliferation assay

For analysis of proliferative behavior, hydrogels were generated as described above. For the 2D setup, fibrin coatings with a final volume of 300 µL in 24-well plates with the different fibrinogen concentrations (5 mg/mL fibrinogen, 10 mg/mL fibrinogen and 20 mg/mL fibrinogen) were created. The hydrogels were seeded with $1x10^5$ cells in their respective GM. Proliferative behavior in a 3D environment was analysed by encapsulating $1x10^5$ cells in fibrin hydrogels. 3D fibrin hydrogels had a final volume of 300 µL at different fibrinogen concentrations (5 mg/mL fibrinogen, 10 mg/mL fibrinogen and 20 mg/mL fibrinogen).

Cells were cultured in their respective GM, supplemented with the fibrinolysis inhibitor aprotinin at 100 KIU/mL (Baxter Healthcare Corp., Deerfield, USA) for 4 days. A medium exchange with GM was performed on day 2 and DNA quantification on day 0 (D0), day 2 (D2) and day 4 (D4).

2.4. Differentiation assay

For analysis of differentiation, hydrogels were generated as described above. For the 2D setup, fibrin coatings with a final volume of 400 µL in 6-well plates with the different fibrinogen concentrations of 7.8 mg/mL fibrinogen, 11.67 mg/mL fibrinogen and 19.42 mg/mL fibrinogen corresponding to apparent tensile moduli of 8 kPa, 12 kPa and 20 kPa, respectively, as assessed by tensile mechanical testing, were created. The hydrogels were seeded with $5x10^5$ cells in their respective GM on D0 of the experiment. Differentiation in a 3D environment was analyzed by encapsulating $2.4x10^6$ cells in fibrin hydrogels on D0. Fibrin hydrogels had a final volume of 300 µL and different fibrinogen concentrations (7.8 mg/mL fibrinogen, 11.67 mg/mL fibrinogen and 19.42 mg/mL fibrinogen (corresponding to tensile moduli of 8 kPa, 12 kPa and 20 kPa, respectively as assessed by tensile mechanical testing). Cells were cultured in media supplemented with 100 KIU/mL aprotinin for a total of 5 days. GM was replaced by DM on day 1 (D1) to induce differentiation and partially (1:1) exchanged with GM on day 3 (D3).

2.5. Preparation of cell-free fibrin hydrogels for mechanical characterization

To assess the effect of fibrinogen content on fibrin hydrogels' apparent tensile moduli, hydrogels were cast in ring-shaped scaffolds, as previously described [66] (figure 12 B). Briefly, scaffolds were cast by mixing 250 µL fibrinogen and 250 µL thrombin to achieve final concentrations of 7.5 mg/mL fibrinogen, 10 mg/mL fibrinogen, 20 mg/mL fibrinogen and 30 mg/mL fibrinogen with a constant concentration of 1 U/mL thrombin. Hydrogels were polymerized in custom-made POM molds for 30 minutes at 37°C and then equilibrated in phosphate-buffered saline (PBS) overnight. Fibrin hydrogels for AFM microindentation experiments were cast according to the procedure for 2D fibrin coatings (figure 12 B) and also stored in PBS overnight.

2.6. Mechanical characterization of fibrin scaffolds

Tensile mechanical testing: cell-free scaffolds were mounted on two spools for tensile testing with a Zwick BZ2.5/TN1S uniaxial material testing machine (Zwick GmbH & Co. KG, Ulm, Germany) (as described in [66]) one day after casting. Briefly, samples were strained to failure at a rate of 20 mm/minute at room temperature and data was recorded after achieving a pre-load of 10 mN. To calculate the apparent tensile modulus, the manually determined linear portion of the stress/strain curve was used.

AFM microindentation: AFM microindentation experiments were performed in PBS on a NanoWizard® ULTRA Speed AFM system (JPK Instruments AG, Berlin) equipped with an inverted optical microscope (Axio Observer.D1, ZEISS) one day after casting. Colloidal probe preparation and characterization by imaging a calibration grating (TGT1, NT-DMT Spectrum Instruments) and microindentation force tests were done as described in Kain *et al.* [145]. Force volume maps were recorded at 2 µm/s indentation speed with an applied load of 2 nN. The maps were done in an evenly spaced 5-by-5 grid covering an area of 20 µm x 20 µm. For each hydrogel of different fibrinogen concentration (7.5 mg/mL, 10 mg/mL, 20 mg/mL and 30 mg/mL), two samples of different fabrication batches were tested with three force volume maps per sample from different locations. This totals to a maximum of 75 force curves per sample, 150 per fibrinogen concentration category, barring bad quality curves that have been disregarded during data analysis. For data analysis, force versus indentation data were analyzed using the Oliver-Pharr method adapted for AFM microindentation tests according to [145] and [146]. Since the elastic modulus of colloidal probes (tenths of GPa) is 5 to 6 orders of magnitude larger than the fibrin hydrogels (tenths of kPa), the apparent indentation modulus E_S of the sample can be approximated as:

$$E_S = \frac{\sqrt{\pi}}{2\beta}(1-\nu_S^2)\frac{S}{\sqrt{A_C(h_C)}}$$

$$h_C = h_{max} - \varepsilon\frac{F_{max}}{S}$$

where $\beta = 1.0226$ and $\varepsilon = 0.75$ are probe-shape-dependent empirical parameters for spherical probes according to [147], $\nu_S = 0.5$ is the Poisson's ratio for incompressible materials (high water content), F_{max} is the maximum indentation force, S the contact stiffness at maximum indentation depth and A_C the projected indentation area dependent on h_C, the indentation depth adjusted for deformation of the surface.

2.7. DNA quantification

At D0, D2 and D4 of culture, cells were harvested from 2D and 3D fibrin hydrogels by digestion in 100 µL nattokinase (Japan Bioscience Lab, California, USA) at a concentration of 100 U/mL in PBS, pH 7.4 supplemented with 15 mmol/L ethylenediaminetetraacetic acid (EDTA) for 1 h at 37°C. To facilitate digestion, samples were constantly agitated at 700 RPM and triturated every 10 minutes. Afterwards, the cells were washed with 0.5 mL PBS once and the cell pellet was resuspended in 1 mL DMEM-HG without any supplements containing 1 µL Hoechst 33342 (Invitrogen, California, USA) (5 mg/mL) yielding a final concentration of 5 µg/mL. After 1 hour of incubation at 37°C in the dark, the cell suspension was resuspended and 200 µL per sample were measured in quadruplicates in black 96-well plates using the GloMax-Multi Detection System (Promega, Madison, USA) at 410-460 nm. Quantified fluorescence signals were normalized to D0 to demonstrate increase of DNA over time.

2.8. Quantitative reverse transcription polymerase chain reaction (RT- qPCR)

On D0, D1, D2 and D5 of differentiation, cells were harvested for RNA isolation and subsequent RT-qPCR. Cell retrieval was performed by digestion with nattokinase (as described above). RNA isolation was performed with the peqGOLD total RNA Kit (VWR International GmbH, Erlangen, Germany), reverse transcription into cDNA with the EasyScript PlusTM Reverse Transcriptase cDNA Synthesis Kit (ABM, Richmond, Canada) according to the manufacturers' protocols. Transcription of 1 µg RNA was performed for 50 minutes at 42°C, followed by an inactivation step at 85°C for 5 minutes.

Quantitative PCR was performed with the KAPA Fast SYBR Fast Universal Kit (VWR International GmbH, Erlangen, Germany) in a Stratagene Mx3005P cycler (Agilent Technologies, Santa Clara, USA). Assays were performed in triplicates with 10 ng input cDNA per reaction. Thermal cycle conditions were 5 minutes at 95°C, followed by 40 cycles of either 10 s at 95°C and 30 s at 60°C ("fast-two-step"), 30 s at 95°C and 1 minute at 60°C ("normal-two-step"), or 15 s at 95°C, 30 s at 55°C and 30 s at 72°C ("fast-three-step"). Target cycle threshold (CT) values were normalized to the housekeeping gene *Ribosomal Protein Lateral Stalk Subunit P0* (*RPLP0*) [known to be stably expressed independent of mechanical stress [148]] and compared to D0 values, as well as to the corresponding 8 kPa value of the respective group using the comparative CT (ΔΔCT) method. Primer sequences, primer concentrations and used thermal profiles are listed in table 3. Two primers for different myosin heavy chain genes were used. The primer referred to as "*MHC I*" is specific for the gene *Myh7* that encodes for slow-twitch myosin heavy chain found in type I fibers. The primer referred to as "*MHC II*" is specific for genes that encode for all different fast-twitch myosin heavy chains found in type II fibers (*i.e. Myh1*, *Myh2 and Myh4*).

Table 3: Primer sequences, primer concentrations and thermal profiles used for qPCR.

Target	Species	Primer Forward	Primer Reverse	Primer Conc.	Thermal Profile
RPLP0	Mouse	CTCCAACAGAGCAGCAGA	ATAGCCTTGCGCATCTGGT	200 nM	fast-2-step
CCND1	Mouse	TCAAGTGTGACCCGGACTG	ATGTCCACATCTCGCACGTC	200 nM	fast-2-step
Myf5	Mouse	TGACGGCATGCCTGAATGTA	GCTCGGATGGCTCTGTAGAC	200 nM	fast-2-step
MyoD	Mouse	ACTACAGTGGCGACTCAGAT	CCGCTGTAATCCATCATGCC	200 nM	normal-2-step
MyoG	Mouse	GGTCCCAACCCAGGAGATCAT	ACGTAAGGGAGTGCAGATTG	200 nM	normal-2-step
Tnnt I	Mouse	AAACCCAGCCGTCCTGTG	CCTCCTCCTTTTTCCGCTGT	200 nM	fast-2-step
MHC I	Mouse	CTCAAGCTGCTCAGCAATCTATTT	GGAGCGCAAGTTTGTCATAAGT	200 nM	fast-3-step
MHC II (all isoforms)	Mouse	GAGGGACAGTTCATCGATAGCAA	GGGCCAACTTGTCATCTCTCAT	200 nM	fast-3-step
RPLP0	Human	GAAATCCTGAGTGATGTGCAGC	TCGAACACCTGCTGGATGAC	200 nM	normal-2-step
CCND1	Human	GTGCCACAGATGTGAAGTTCATT	CTCTGGAGAGGAAGCGTGTG	200 nM	fast-2-step
Myf5	Human	ATGCCATCCGCTACATCGAG	ATTCGGGCATGCCATCAGAG	400 nM	fast-2-step
MyoD	Human	CACGTCGAGCAATCCAAACC	TGTAGTCCATCATGCCGTCG	400 nM	normal-2-step
MyoG	Human	CATCCAGTACATCGAGCGCC	GCAGATGATCCCCTGGGTTGG	200 nM	fast-2-step
Tnnt1	Human	ACCTGGTCAAGGCAGAACAG	CAGGAGGGCTGTGATGGAG	200 nM	fast-3-step
MHC I	Human	ACACACTTGAGTAGCCCAGG	ACGGTCACTGTCTTGCCATA	400 nM	normal-2-step
MHC II (all isoforms)	Human	TACTGCACACCCAGAACACC	TTTTCTTCTGCATTGCGGGC	200 nM	normal-2-step

2.9. Immunofluorescence staining and analysis

On day 5 of differentiation, cells were fixed with 4% paraformaldehyde (PFA; Roth, Karlsruhe, Germany) overnight at 4°C, washed with distilled water and permeabilized with Tris-buffered Saline/0.1% Triton X-100 (TBS/T) (v/v) for 15 minutes at room temperature. Blocking was performed with PBS/T-1% bovine serum albumin (BSA) (w/v) at room temperature for one hour. The primary antibody targeting all MHC isoforms (MF 20, Developmental Studies Hybridoma Bank, Iowa, USA, RRID: AB_2147781) was diluted 1:300 in PBS/T-1% BSA (w/v) and incubated overnight at 4°C. Subsequently, the hydrogels were washed with PBS/T and incubated with the secondary antibody labelled with Alexa Fluor 488 (Life Technologies, Lofer, Austria) diluted 1:400 in PBS/T-1% BSA at 37°C for one hour. Nuclei were by staining with 4´,6-diamidino-2-phenylindole (DAPI) diluted 1:1000 in PBS/T-1% BSA for 10 minutes at room temperature. All stainings were analyzed with a Leica DMI 6000b inverted microscope (Leica Microsystems GmbH, Wetzlar, Germany).

For assessment of myotube maturation, fusion index and myotube alignment of MHC-stained samples were analyzed using the imaging analysis software Fiji. Fusion index was calculated as the ratio of nuclei in fused myotubes (defined as myotubes with a minimum of three nuclei) to the total number of nuclei. Myotube alignment was calculated as the deviation between the axis of orientation of single myotubes from the mean axis of orientation.

2.10. Statistical analyses

All statistical calculations and depiction of data was performed with GraphPad Prism Software (GraphPad Software Inc., SanDiego, USA). Data is presented in box and whisker plots (minimum to maximum) or as time-lines relative to D0 (means are shown), except figure 5C that is presented as mean + standard deviation. All data sets were analyzed for normal distribution with the D'Agostino & Pearson omnibus normality test. Comparison between groups was performed with one-way ANOVA with Tukey's multiple comparison test, Kruskal–Wallis test with Dunn's multiple comparison test or two-way ANOVA with Sidak's multiple comparison test, as indicated in the figure legends with p values ≤ 0.05 considered statistically significant.

3. Results

3.1. Stiffness of fibrin hydrogel scaffolds directly correlates with total fibrinogen content

To ensure optimal conditions to prime cells for developing into muscle-like tissue, providing the right stiffness of the biomaterial is of high relevance. Therefore, we analyzed the effect of varying fibrinogen concentrations on the elastic properties of fibrin hydrogel. Within the tested fibrinogen range (7.5 mg/mL – 30 mg/mL), an almost linear relationship between apparent tensile modulus and fibrinogen concentration was observed (figure 12 A) by tensile mechanical testing of intact ring-shaped constructs and by AFM microindentation measurements. It can be seen that stiffness values from AFM microindentation measurements were significantly lower compared to those measured by test-to failure tensile measurements (figure 12 A).

3.2. Matrix properties affect proliferation of murine and human myoblast differently

Cell cycle progression is one of the cellular processes known to be largely affected by material properties. One of our aims was thus to study the differential effects of substrate stiffness and geometry on cell proliferation. Human and murine myoblasts were cultured either on fibrin-coated well plates (“2D”) or embedded in fibrin hydrogels (“3D”). Fibrinogen concentrations of 5 mg/mL, 10 mg/mL and 20 mg/mL were chosen as they result in apparent tensile moduli in a range relevant for SMTE (5.1 kPa, 10.3 kPa and 20.6 kPa, respectively) (Engler *et al.* 2004). Results of DNA quantification clearly suggest that stiffness, as well as culture type influenced cellular proliferation. When cultured in 2D, increased stiffness resulted in increased proliferation with significant differences in human, but not in murine myoblasts (figure 13 A, left panels). By D4, DNA amounts increased on average 6.4-, 7.1-, and 7.9-fold in murine myoblasts and 5.8-, 6.0-, and 6.6-fold in human myoblasts (compared to D0) when cultured on fibrin hydrogels with ascending apparent elastic moduli. Upon incorporation into fibrin hydrogels, however, the opposite effect was seen with significant differences between the fibrinogen concentrations in both cell lines (figure 13 A, right panels). In this setup, DNA amounts increased on average 3.1-, 2.8-, and 1.6-fold in murine myoblasts and 4.0-, 3.6-, and 2.6-fold in human myoblasts (compared to D0) in fibrin hydrogels with fibrinogen concentrations of 5 mg/mL, 10 mg/mL and 20 mg/mL, respectively. Comparing changes over time, culture in 2D led to a significantly higher increase in DNA content than in 3D in both cell lines and all scaffold rigidities (figure 13 B). Interestingly, the difference between 2D and 3D culture was less pronounced in the softest hydrogel (5 mg/mL fibrinogen), in comparison to the more rigid ones. Furthermore, it is notable that the DNA content of murine myoblasts increased less after D2 of culture than in human myoblasts, particularly in softer hydrogels (figure 13 B).

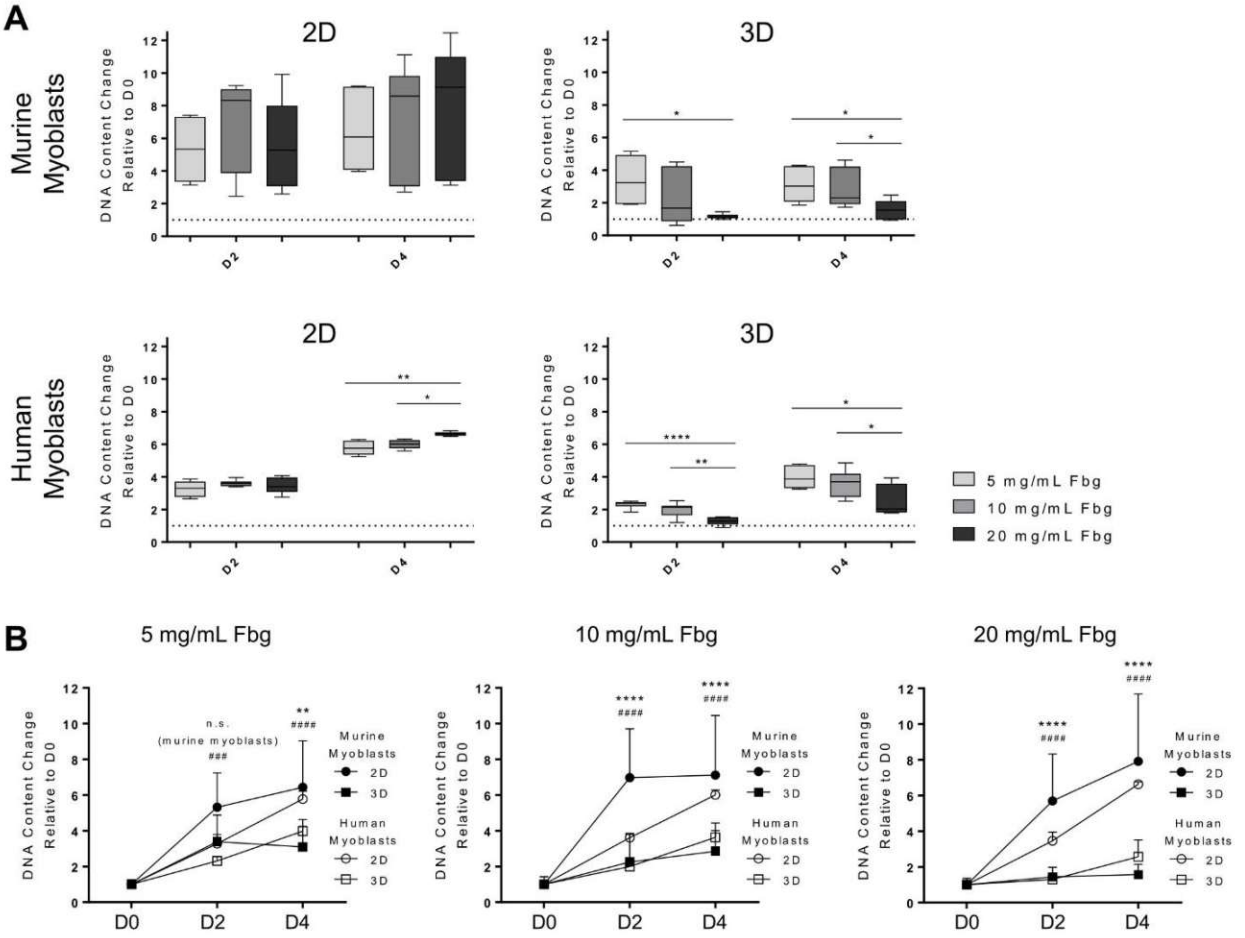

Figure 13: Substrate stiffness and architecture affect myoblast proliferation. Murine and human myoblasts were cultured on fibrin-coated cell culture plates (2D) or encapsulated in fibrin hydrogels (3D) with different fibrinogen (Fbg) concentrations (5 mg/mL, 10 mg/mL and 20 mg/mL) for 4 days under proliferative conditions. DNA content of samples was assessed by Hoechst staining. **(A)** DNA content of each fibrinogen concentration (5 mg/mL, 10 mg/mL and 20 mg/mL), culture set up (2D and 3D) and cell type (murine and human myoblasts) was normalized to their respective D0 values (dotted line indicates D0 level). Data is shown as box and whiskers (min to max); N ≥ 2, n ≥ 6; one-way ANOVA with Tukey's multiple comparison test was performed comparing all fibrinogen concentrations of each day with each other, *p < 0.05, **p < 0.01, ****p < 0.0001. **(B)** DNA content of all fibrinogen concentrations (5 mg/mL, 10 mg/mL and 20 mg/mL) of each culture set up (2D and 3D) and cell type (murine and human myoblasts) was normalized to their respective D0 values. Data is shown as mean ± standard deviation; N ≥ 2, n ≥ 6; two-way ANOVA with Sidak's multiple comparison test was performed comparing culture set ups (2D vs, 3D) of each cell type (* indicates murine myoblasts, # indicates human myoblasts) with each other, ****/####p < 0.0001.

3.3. Scaffold geometry affects early myogenesis in murine and human myoblasts

To gain insight into the effects of material geometry and mechanical properties on myogenesis in human and murine myoblasts, we changed the experimental setup to promote differentiation rather than proliferation. Myoblasts were seeded at a high density ($1x10^5$ cells/cm^2), which is known to promote onset of differentiation [75] and treated with their respective differentiation media one day after transferring them into/onto the biomaterial. Furthermore, fibrinogen concentrations were adapted to reflect rigidities relevant for SMTE. In accordance with Engler *et al.* [86], who defined a range between 8 kPa and 17 kPa as suitable for myogenic specification in 2D, and taking into account the fact that human muscle is characterized by higher rigidities (see table 2), we generated 2D and 3D fibrin clots with apparent tensile moduli of 8 kPa, 12 kPa and 20 kPa (which corresponds to fibrinogen concentrations of 7.8 mg/mL fibrinogen, 11.67 mg/mL fibrinogen and 19.42 mg/mL fibrinogen). Calculation of fibrinogen concentrations for respective apparent tensile moduli was based on the results gained from tensile testing (figure 12 A). To observe the progression of myogenesis in different culture setups, we analyzed the gene expression of a set of early- (*Myf5, MyoD*) and mid-stage (*MyoG*) myogenic markers, as well as a marker for proliferation / active cell cycle (*CCND1*) with RT-qPCR.

Cyclin D1, encoded by the *CCND1* gene, is a member of the highly conserved cyclin family, which, while being expressed in all adult tissue, is subjected to periodic fluctuations in its abundance throughout the cell cycle. Cyclin D1 regulates the activity of the cyclin dependent kinases 4 and 6 that are required for transition from the G1 to the S-phase [149]. One day after transferring myoblasts from cell culture plastic to different biomaterial settings, these fluctuations in *CCND1* transcription depending on cell cycle state became apparent. For both cell lines, embedding into a 3D fibrin matrix, independent of rigidity, led to a drastic drop in *CCND1* gene expression compared to D0 (average 4.7- and 2.8-fold downregulation, respectively) despite culture in GM. Culture on top of fibrin-coated wells, on the other hand, induced significantly higher *CCND1* expression than in the 3D setup, with only a slight decrease in murine and even an average 5.1-fold increase in human myoblasts (figure 14 A). During the course of the experiment, *CCND1* gene expression levels in all cultured murine myoblasts converged to similar levels of an average 2.4-fold decrease compared to D0 (figure 14 A, left panel), whereas it dropped an order of magnitude lower, to less than 0.1 times the expression of D0 in human myoblasts (figure 14 A, right panel). While in all other setups the different material rigidities had no effect on *CCND1* expression levels, culture on the stiffest matrix (20 kPa) did alter its expression rate in human myoblasts. They showed comparatively low fold-change increases 24 hours post-plating (3.2-fold increase in the 20 kPa group *vs*. an average 6-fold increase in the others) and a peak of a 6.3-fold increase on D2 (figure 14 A, right panel).

The major regulators of the onset of myogenesis are a set of transcriptional regulators, the myogenic regulatory factors (MRFs). The MRFs observed in this study, *Myf5*, *MyoD* and *MyoG*, are basic helix loop helix transcription factors that are themselves expressed in hierarchical time-dependent manner and their expression can be used to characterize the differentiation state of

myogenic cells [150], [151]. *Myf5* and *MyoD* are required for myoblast determination from the satellite cells state. *Myf5* expression peaks before and during early phases of differentiation and diminishes completely afterwards; *MyoD* peaks in early differentiation, but is constantly expressed at low levels throughout terminal differentiation [152]. Expression of *MyoG* during differentiation is dependent on prior *MyoD* expression and is required for terminal differentiation [151], [153]. Overall, this time-dependent cascade-like expression pattern was observed in both cell lines, and in all different matrix setups with some alterations in the extent and timing of upregulation of the different transcription factors. Upregulation of *Myf5* was observed 24 hours into differentiation in all setups, except when murine myoblasts were cultured on a 2D fibrin matrix (figure 14 B). In this condition, transcriptional levels of *Myf5* remained constant at all time points throughout the observed culture period (figure 14 B, right panel). The expression levels on D2 compared to D0, however, differed between the two species. A moderate (average 1.8-fold) upregulation was observed in murine myoblasts in the 3D setup, whereas increases in the range from 17.2- to 208-fold upregulation were measured in human myoblasts. Upregulation was observed in a similar range within the different groups independent of substrate rigidity, except for one group, human myoblasts grown on the most rigid substrate (20 kPa). Those showed a more pronounced upregulation on D2 (208-fold increase *vs*. an average of 17.3-fold increase; figure 14 B, right panel). In murine myoblasts, *Myf5* expression remained at similar levels throughout the observed culture time with a significantly higher gene expression in the 3D compared to the 2D setup (figure 14 B, left panel). In human myoblasts, on the other hand, transcription of *Myf5* dropped drastically by D5 to expression between 0.24- to 0.31-fold the D0 levels independent of biomaterial stiffness and architecture (figure 14 B, right panel). In all studied groups, the average *MyoD* transcriptional levels were higher in the 2D setup compared to the 3D setup. Murine myoblasts differentiated on fibrin showed significantly higher *MyoD* expression levels compared to 3D-cultured counterparts, in which even downregulation compared to D0 was measured on the first two days of differentiation (figure 14 C, left panel). *MyoD* levels in human myoblasts did not exceed the basal level prior to transfer to the biomaterial at any of the observed time points with a sharp drop on D1 of an average 10.8-fold decrease. When cultured in a 2D setup, however, expression levels reached the basal levels of *MyoD* expression by the second day of differentiation, but not in the 3D setup (figure 14 C, right panel). The trend concerning differences between substrates of different stiffness was also confirmed in *MyoD* expression: overall, substrate stiffness within the myogenic range did not impact changes in expression levels, except for human myoblasts grown in the most rigid substrate (20 kPa), which showed a downregulation by the end of the differentiation period (0.25-fold change *vs*. an average of 1.4-fold increase) (figure 14 C, right panel). *MyoG* expression increased by the second day of differentiation in all treatment groups. In murine myoblasts, it further proceeded to an average 29-fold increase by D5, independent of scaffold type and stiffness (figure 14 D, left panel). Human myoblasts cultured embedded in 3D fibrin matrices showed comparably moderate fold changes of 126.8 on average, while culture of these

cells on top of biomaterials induced a significantly higher upregulation with fold change increases of 1724 on average compared to D0 (figure 14 D, right panel).

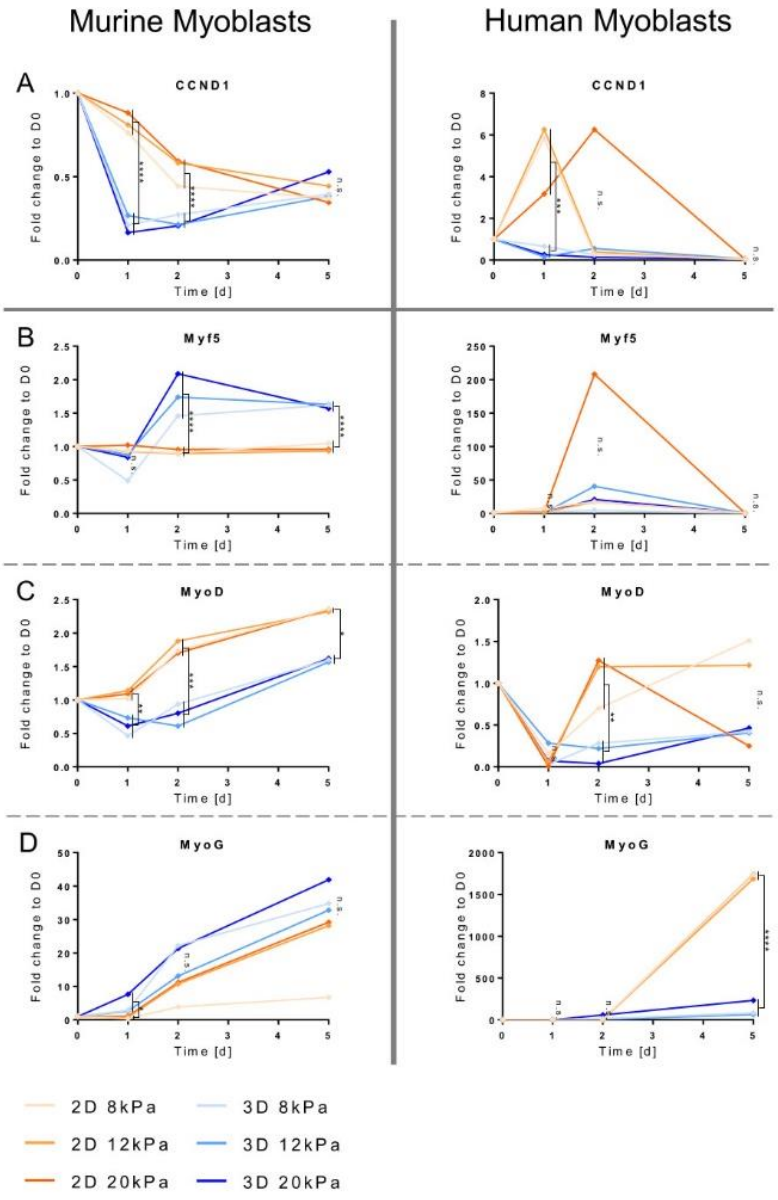

Figure 14: Culture in a 3D environment slows down progression of myogenesis in myoblast cell lines. Murine and human myoblasts were differentiated on fibrin-coated cell culture plates (2D) or encapsulated in fibrin hydrogels (3D) with different stiffness (apparent tensile modulus of 8 kPa, 12 kPa and 20 kPa) for 5 days. They were seeded in growth medium that was replaced by differentiation medium on D1. mRNA expression of marker genes specific for cell cycle progression [*cyclin D 1* (*CCND1*)] **(A)**, early, mid and late stage myogenesis [*Myf5* **(B)**, *MyoD* **(C)** and myogenin (*MyoG*) **(D)**, respectively] was assessed by RT-qPCR. Fold change expression levels were normalized to D0 control samples of each cell line and relative expression over time is shown as a linear curve between means of fold-change values; N = 3, n ≥ 8; two-way ANOVA with Sidak's multiple comparison test was performed comparing all rigidities (8 kPa, 12 kPa and 20 kPa) of the two (culture set ups (2D vs. 3D) with each other, no significant difference (n.s.), *p < 0.05, **p < 0.01, ***p < 0.001, ****p < 0.0001.

3.4. Matrix properties have different effects on terminal differentiation in murine and human myogenic cells

Terminal myogenic differentiation is accompanied by the development of a functional muscular ultrastructure. Successful development of said structure is dependent on production and arrangement of structural and motor proteins [154]. Troponin T and myosin are proteins required for skeletal muscle contraction, thus its functionality. The troponin subtype T1, encoded by the gene *Tnnt I*, is a part of the troponin complex and therefore required for Ca^{2+}-induced striated muscle contraction [155]. Myosin is the most prominent protein required for muscle contraction and consists of several subunits. Its heavy chain [myosin heavy chain (MHC)] appears in different isoforms, whose expression transitions during development and throughout *in vitro* differentiation in a distinct temporal pattern. The isotypes most prominent in slow muscle fibers (MHC I) occur prior to those specific to fast fibers (MHC IIa, MHC IIx, MHC IIb) [156]. Analyzing the expression of the genes encoding for troponin T 1, MHC I and all MHC II isoforms (*Tnnt I, MHC I and MHC II*), it was apparent that culture in a 2D compared to a 3D setup affected terminal differentiation drastically. Furthermore, the influences of scaffold architecture differed in the two cell lines. In murine myoblasts grown in the 2D setup, transcriptional levels of all observed markers significantly decreased with increasing substrate stiffness to an average 2-fold downregulation comparing cells grown in the softest (8 kPa) to the stiffest (20 kPa) material (figure 15 A; upper panels). On the other hand, under these conditions, substrate stiffness did not alter gene expression of *Tnnt I, MHC I* and *MHC II* in human cells (figure 15 A; lower panels). Interestingly, the exact opposite effects were observed in the 3D setup. When incorporated into fibrin hydrogels, terminal differentiation was not affected by different substrate rigidities in murine myoblasts (figure 15 A; upper panels). In human myoblasts, in contrast, incorporation in stiffer hydrogels led to an average 3.3-fold upregulation of the expression of the aforementioned structural genes (figure 15 A; lower panels). Observing the time course, it was evident that human cells were more susceptible to influence by incorporation into 3D hydrogels in terms of terminal differentiation. In murine myoblasts, upregulation of transcriptional levels of late-stage myogenesis marker genes are on a similar level in cells cultured in 2D and 3D. Here, the only variation between the setups was observed in gene expression of *MHC I* that was significantly higher in 3D-cultured cells than their 2D counterpart one day post induction of differentiation (figure 15 B; upper panels). Notably, the differences between 2D and 3D culture were more pronounced in human cells. An average 14-fold higher upregulation of *Tnnt I* was measured one day after induction of differentiation. This effect, however, was not evident by the end of the culture period. In contrast, the expression of the two MHC isoforms, *MHC I* and *MHC II*, at the end of the observed period was on average 11-fold higher in 2D than in 3D environments (figure 15 B; lower panels).

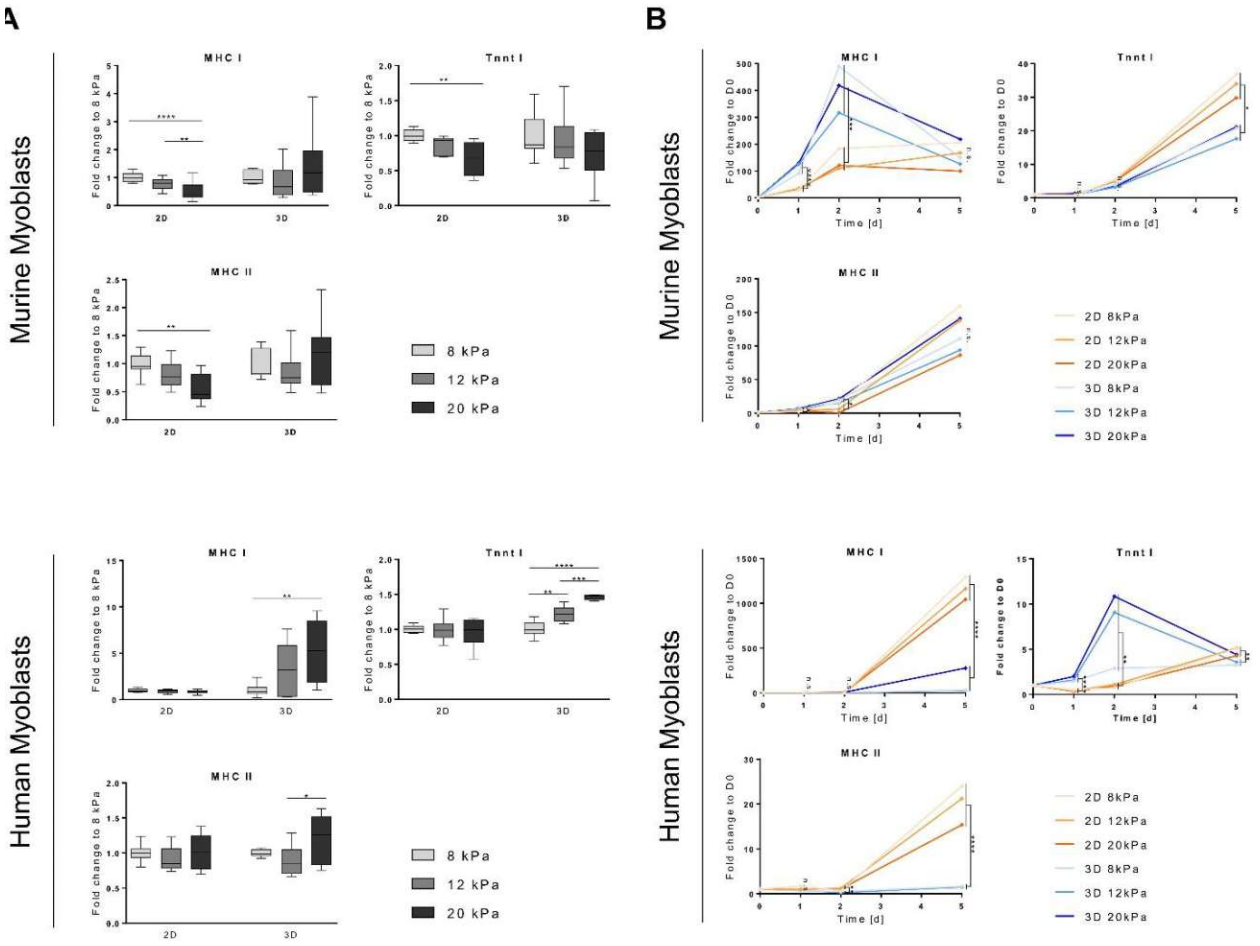

Figure 15: Culture in a 3D setup affects impact of substrate stiffness and myogenic outcome. Murine and human myoblasts were differentiated on fibrin-coated cell culture plates (2D) or encapsulated in fibrin hydrogels (3D) with different stiffness (apparent tensile modulus of 8 kPa, 12 kPa and 20 kPa) for 5 days. mRNA expression of marker genes for terminal differentiation (*troponin T I* (*Tnnt I*), *myosin heavy chain I* (*MHC I*) and *myosin heavy chain II* (*MHC II*) was assessed by RT-qPCR. **(A)** Fold change expression levels on D5 were normalized to the 8 kPa group for each condition. Data is shown as box and whiskers (min to max); N = 3, n ≥ 8; one-way ANOVA with Tukey's multiple comparison test was performed comparing all rigidities for each condition (2D and 3D) with each other, *p < 0.05, **p < 0.01, ***p < 0.001, ****p < 0.0001. **(B)** Fold change expression levels were normalized to D0 control samples of each cell line and relative expression over time is shown as a linear curve between means of fold-change values; N = 3, n ≥ 7 two-way ANOVA with Sidak's multiple comparison test was performed comparing all rigidities (8 kPa, 12 kPa and 20 kPa) of the two (culture set ups (2D *vs*. 3D) with each other; no significant difference (n.s.), , *p < 0.05, **p < 0.01, ****p < 0.0001.

3.5. Matrix stiffness affects morphology and patterns of myotube arrangement

A key aspect of terminal myogenic differentiation is the arrangement of myotubes in a functional way. Thus, we analyzed the effect of substrate stiffness on myotube morphology, particularly alignment and fusion. Myoblasts were cultured on fibrin-coated well-plates and differentiated for 5 days prior to immunofluorescence staining of MHC, which confirmed the findings of the gene expression analysis of late-stage myogenic markers. When differentiated on stiffer substrates, myotubes derived from both myoblast lines showed lower MHC protein expression (figure 16 A), which is in accordance with the corresponding qPCR data (figure 15 A). Quantifications of myotube fusion and alignment showed the same trend of decreased myotube maturation with increasing substrate stiffness. The fusion indices of cells grown on more rigid materials were lower than those grown on softer ones. The ratios of fused nuclei to total number of nuclei were 20.3%, 18.5% and 14.8% in murine and 15.8%, 15.4% and 11.0% in human myotubes grown on 8 kPa, 12 kPa and 20 kPa substrates, respectively (figure 16 B). Myotube alignment was also negatively impacted by culture on stiffer substrates. When grown on the softest substrate (8 kPa), the majority of myotubes showed a 0° - 10° deviation from the main axis of orientation in both species. Culture on the most rigid substrate (20 kPa), on the other hand, led to deviations larger than 20° from the main axis (figure 16 C). Interestingly, human myoblasts differentiated less than murine ones, in terms of MHC expression and myotube fusion (figure 16 A, B). The detrimental effect of culture on stiffer substrates on cell alignment, however, was less severe than in murine cells (figure 16 A, C). Furthermore, images of IF stainings of myotubes differentiated embedded in 3D fibrin hydrogels were taken at different sites of the hydrogel. Evidently, more cells were located at the outer area, whereas almost no cells were found in the centers of the hydrogels. Moreover, differentiation to myocytes only took place in the outer areas, and not in the center (figure 16 D).

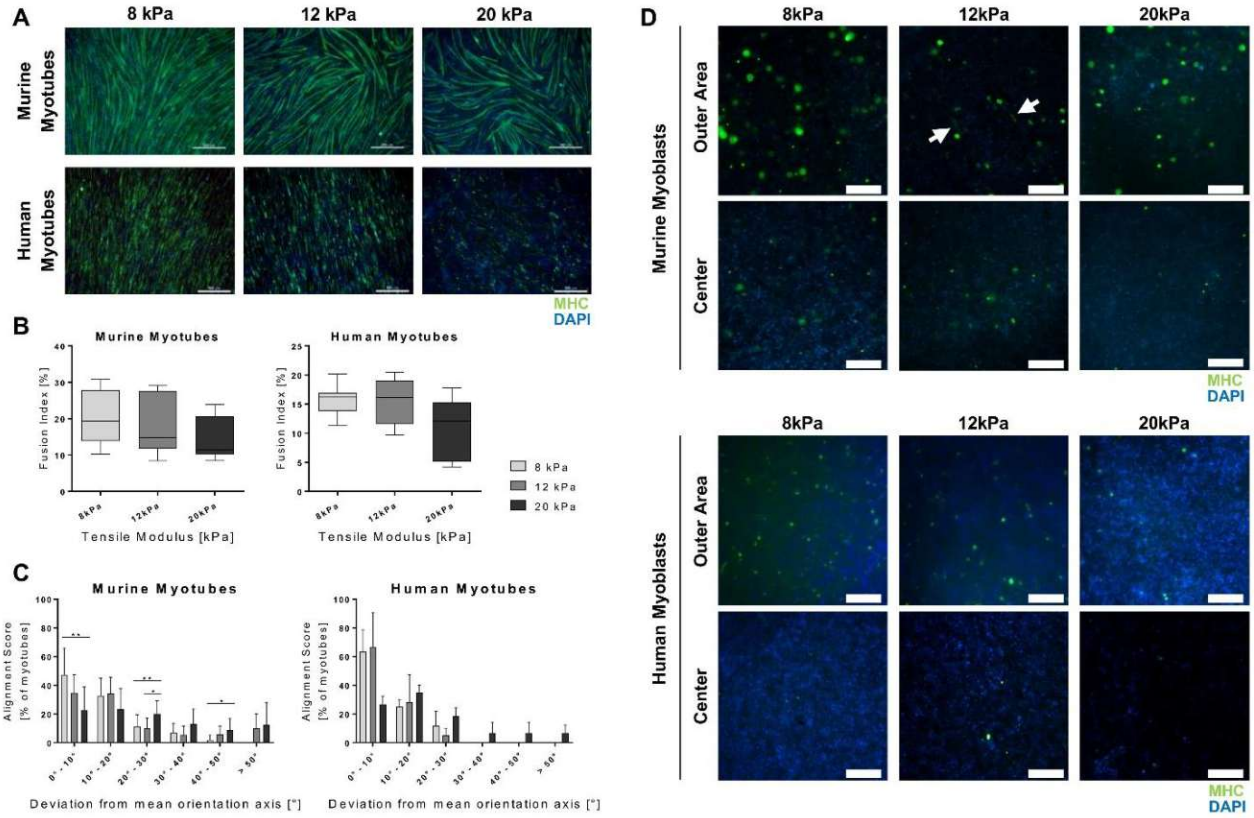

Figure 16: Culture on more rigid substrates interferes with myotube maturation. Murine and human myoblasts were differentiated on fibrin-coated cell culture plates (2D; **A-C**) or embedded in fibrin hydrogels (3D; **D**) with different stiffness (apparent tensile modulus of 8 kPa, 12 kPa and 20 kPa) for 5 days. **(A)** Representative images of immunofluorescence (IF) stainings for MHC (green) with nuclei stained with DAPI (blue). Scale bars represent 500 µm. **(B)** Myotube fusion index of IF stainings (MHC and DAPI); analyzed as the ratio of fused nuclei to total nuclei per visual field (N = 4, n ≥ 10 for murine myoblasts, N = 3, n ≥ 9 for human myoblasts with 4 regions of interest, at least 400 nuclei per sample and 4000 nuclei per experimental group analyzed. Data is shown as box and whiskers (min to max); one-way ANOVA with Tukey's multiple comparison test was performed comparing all rigidities with each other with no significant differences found. **(C)** Myotube alignment score of IF stainings (MHC and DAPI); analyzed as the deviation of single myotubes from the main axis of orientation, represented as a histogram of the percentage of myotubes deviating in the respective interval of 10° angles. (N = 4, n ≥ 10 for murine myoblasts, N = 3, n ≥ 9 for human myoblasts with at least 180 myotubes per experimental group analyzed. Data is shown as mean + standard deviation; one-way ANOVA with Tukey's multiple comparison test was performed comparing all rigidities of each deviation interval, *p < 0.05, **p < 0.01. **(D)** Representative images of IF stainings for MHC (green) with nuclei stained with DAPI (blue) taken either at the edge or in the center of the hydrogels. White arrows indicate myocytes. Scale bars represent 200 µm; N = 2, n = 4.

4. Discussion

The aim of this study was to examine the effect of different scaffold geometries (2D *vs*. 3D culture) and material stiffness on the behavior of myoblasts. Two different myoblasts lines were compared, murine C2C12 cells and human C25 cells. We chose the C2C12 cell line as a basis for this study, since SMTE strategies are often developed and characterized using cell lines. The murine cell line C2C12 is used most frequently due to its easy handling and cost. Moreover, its behavior is well-studied and predictable. Aiming at increased relevance in terms of translatability to humans, human-derived cell lines, such as the C25 line, can be employed [51]. Frequently, applying methodology established in murine lines fails when using human cells due to the murine cells' divergent behavior. To ensure that there are no substantial differences between the two cell lines, we characterized their differentiation behavior on cell culture plastic as a preliminary experiment (supplementary figure 1). Another potential pitfall in the development of TE strategies is that they often rely on 3D cell carrier systems for the creation of tissue constructs. In this regard, one must keep in mind that knowledge gained on cellular behavior in 2D cultures cannot be translated to 3D environments. Given that *in vivo* cells grow in complex structures, it is obvious that 2D setups do not account for the intricate spatial arrangement of tissues. Few studies, however, have addressed the different impacts on cellular behavior triggered by 2D culture [157]. To analyze the impact of 3D culture specifically, we grew cells under otherwise standardized conditions in two different setups (2D and 3D), where fibrinogen content translating to differential stiffness and network density was the only variable (figure 12).

Furthermore, there is strong evidence that the stiffness of the substrates cells are cultured on influences their behavior in many ways. This is of great interest for TE applications, as it also affects the differentiation potential drastically. Moreover, maturity of engineered tissues as well as their engraftment efficiency and functionality when implanted *in vivo* are affected [70], [84], [85], [158], [159]. Data on optimal substrate stiffness for creation of mature muscle constructs differ greatly. Optimal values for myoblasts differentiation found in literature range from a Young's modulus of 11 kPa [85] to 1.72 MPa [159]. Frequently, it is stated that optimal substrate stiffness lies in the range of the stiffness of actual skeletal muscle tissue. As shown in table 2, those values differ significantly as well. In the context of the apparent lack in comparability of different studies, not only the ranges of compared Young's moduli vary. Additionally, the methods for Young's modulus measurements differ as well, as it can be performed through tensile testing [87], [88], [159] or AFM [85], [86], [89]. A review by McKee *et al.* pointed out that elastic modulus values of muscle are ~70 times higher when assessed with tensile testing in comparison to indentation measurements [160]. These variations in measured Young's moduli can affect the comparability of different studies. As a first step to characterize the material used in this study, correlations between increasing fibrinogen concentrations of fibrin hydrogels and tensile and indentation moduli were analyzed (figure 12). AFM microindentation measurements take place at lower length scales compared to the tensile tests performed. Therefore, AFM microindentation measurements are more sensitive to locally heterogeneous properties of the

sample, for example microsized pores, roughness and locally changing stiffness, resulting in higher standard deviations. The fact that our measured microindentation moduli are always lower compared to the tensile moduli from macroscale tests can be due to a number of reasons, including viscoelastic sample properties and different strain rates. Additionally, the stress states are different and more complex in indentation-type loading compared to tensile or compressive tests. Indentation results in compressive, tensile, and shear stresses all taking place at the vicinity of the indentation point. As described, the models used in both the tensile and the indentation experiments are by design purely elastic models. Hydrogels are generally viscoelastic due to their high water content, resulting in material responses that vary with strain rates. As the strain rate increases, the apparent elasticity also increases. Furthermore, the tensile tests were conducted at much higher displacement rates of 300 µm/s compared to the 2 µm/s indentation velocity of the AFM. This may well explain the difference in apparent elasticity (indentation modulus *vs*. tensile elasticity) between the two testing modalities. Although differences exist between the two methods, both experiments result in the same trend of increasing apparent elasticity with concentration of fibrinogen.

Subsequently, we assessed effects of different apparent elastic moduli on human and murine myoblast embedded in or grown on fibrin hydrogels. We compared moduli in a narrow range (from ~5 kPa to ~20 kPa) aiming to identify the impact of the mechanical environment on cellular behavior. The chosen range is based on the findings by Engler *et al.*, who identified an indentation modulus of 12 kPa as optimal for skeletal muscle substrates, reflecting the stiffness of native tissue [85]. Our data on the effects on proliferation demonstrate that culture on gels with higher stiffness increased proliferation (figure 13). It is difficult to establish a relation between the obtained data to what is found in literature, as most studies compare different ranges of elastic moduli. Frequently, the analyzed stiffness is different from native muscle (table 2), such as in a study by Boonen *et al.*, in which substrates with 3 kPa, 21 kPa and 80 kPa were compared [18]; a study by Gilbert *et al.* that compared a gel with 12 kPa to a polymer used for cell culture (~ 3 GPa) [84]; a study by Romanazzo *et al.*, in which only gels with a tensile modulus higher than 0.9 MPa were analyzed [88], or a study by Boontheekul *et al.* that compared gels with elastic moduli of 1 kPa, 13 kPa and 45 kPa [161]. However, the conclusions drawn are similar to this study: while we found that in a range between 5.1 kPa and 20.6 kPa, stiffer hydrogels result in higher cell proliferation, others state that 21 kPa are more advantageous than 3 kPa and 80 kPa [18], 12 kPa than 3 GPa [84], or 45 kPa than 13 and 1 kPa [161], and that when grown on substrates more rigid than 0.9 MPa, no differences were observed [88]. A study by Trensz *et al.* revealed potential reasons underlying the interference of substrate stiffness with myoblast proliferation by establishing a relation between myofiber damage, myofiber stiffness and progenitor cell proliferation. It was shown that damaged myofibers have a 4-fold increased Young's modulus as well as a 15-fold increased number of proliferative cells compared to intact ones. Culture of explanted myogenic progenitor cells on substrates with Young´s moduli representing intact (0.5 kPa) and damaged (2 kPa) myofibers

also came to the result that stiffer hydrogels mimicking damaged myofibers increase proliferation [162].

Furthermore, the fibrin matrix itself influences cellular behavior since it acts pro-proliferative. In our study, the commercially available fibrin sealant Tissucol [163] was used for production of fibrin scaffolds. As the fibrinogen component of the sealant is derived from purified human plasma, it does not only contain fibrinogen, but also small fractions of other proteins [163], [164]. It is stated by the manufacturer that only approximately 90% of the plasma protein fraction are made up of fibrinogen [163]. Thus, the presence of growth and wound healing factors, such as epidermal growth factor, platelet-derived growth factors, IGF, transforming growth factor β, vascular endothelial growth factor potentially contributed to increased proliferation. Besides factors influencing cellular growth and proliferation, fibrin also contains extracellular matrix proteins that enhance cell attachment, such as fibronectin [165], [166]. Moreover, it is known that developing and mature myotubes express α5β3 integrins that specifically bind the Arg-Gly-Asp (RGD) 572-574 motif located in the α chain of fibrinogen, which leads to further cell attachment [73], [74]. These effects could have been further intensified as fibrinogen concentrations used in these experiments are an order of magnitude higher than those found in blood, which range between 1.5 mg/mL and 3.5 mg/mL [167].

In contrast to our observations in myoblasts grown on fibrin hydrogels, embedding them in a 3D environment yielded opposite results. In this setup, proliferation was significantly decreased with increasing fibrin hydrogel stiffness (figure 13) and drastic decrease of cell cycle regulator *CCND1* expression (figure 14). Furthermore, myoblasts could not develop a network and spread out in stiffer hydrogels, but rather had a globular shape (supplementary figure 2). Most likely, this is caused by the increased density of fibrin fibers in the network of gels with higher fibrinogen concentrations [66], [68]. Thus, cellular motility, supply of nutrients and oxygen, as well as waste removal are reduced or impaired in stiffer hydrogels, resulting in decreased proliferation. This can be connected to changes in a plethora of intracellular mechanisms, as reviewed by Birgersdotter *et al.* [157]. These include altered spatial arrangement of receptors (e.g. integrins) and other cytoskeletal components compared to 2D cultures, which changes regulation of signaling molecules (e.g. focal adhesion kinase or PI3K). That, in turn, suppresses cell cycle progression, for example through upregulation of P21 [157]. The crucial impact of high biomaterial density in 3D on cellular behavior can also be seen in the experiments assessing the influence of substrate stiffness on differentiation (figure 16 D). In our setup, the effects of factors such as altered migration potential and nutrient supply cannot be separated from the influence of 3D culture *per se*. This, however, holds true for most 3D approaches. Therefore, we want to point out the importance of accounting for those added stressors when designing TE experiments. Appropriate seeding densities are of particular importance for SMTE since they are directly related to the myogenic outcome [75], [168]. This also presents the rationale for employing different cell densities in proliferation and differentiation experiments in this study. The high cell densities required to promote myogenic development would have potentially

interfered with the cells' proliferative behavior. Therefore, lower seeding densities were chosen for those experiments. Due to the influence of the configuration of the cells in 3D in an appropriate spatial manner, it is advisable to include a resting period after embedding myoblasts in a 3D environment. Thereby to the new surrounding is enabled and sufficient cell density ensured, as employed in other studies [66], [124], [125].

Furthermore, we observed that human myoblasts proliferated to a lower extent than murine myoblasts (figure 13). This inter-species difference has already been reported by several other studies *in vitro* as well as *in vivo* [169]–[171]. It is speculated that the lower proliferation rates of human cells can be attributed to the longer lifetime of humans, which would entail ~10^5 more cell divisions during their whole lifetime and severely increase the risk of accumulating mutations. Thus, it is assumed that the slower proliferation rates in humans serve as a protection mechanism from increased chance of cancer development [171]. This could be connected to another observation we made. CCND1 expression strongly increased in C25 cells but decreased in C2C12 cells (figure 14) when cells were transferred from cell culture plastic to fibrin-coated well plates (2D). This differential behavior could be attributed to the fact that C25 cells, with their generally lower proliferation rates, benefit from the profitable environments of the hydrogel. C2C12 cells, on the other hand, have a high basal level of cell cycle markers and furthermore initiate the onset of myogenesis more readily (see below). Thus, downregulation of cell cycle markers is a logical consequence. These effects, however, were only observed immediately after the change of environment. Throughout the course of differentiation, expression levels converged, indicating that those effects were overruled by advancing differentiation.

Proliferation and differentiation are mutually exclusive processes in muscle cell development. Hence, the fact that, overall, proliferation levels are lower in C2C12 cells compared to C25 cells can be interpreted as a sign of increased differentiation in the former cell type. This is reflected in the concomitant belated decrease of *CCND1* and increase of MRF gene expression in the human muscle cell line (figure 14, right panels). Cells grown on the stiffest matrix (apparent elastic modulus of 20 kPa) stand out particularly. Compared to all other culture setups, those cells showed a delayed peak in *CCND1* expression and still expressed *Myf5* one day after induction of differentiation. *Myf5* is a MRF that is expressed only for a short period of time early in the process of differentiation [150] and had ceased in all other conditions at this time point. Comparing different culture setups, *i.e.* 2D *vs*. 3D culture, gene expression patterns of early MRFs *Myf5* and *MyoD* confirm the observation made concerning the effect on proliferation. While 2D culture led to a rapid decrease of proliferation, differentiation was initiated earlier than in 3D, which is indicated by higher *MyoD* levels and earlier passing of the initial Myf5 peak in 2D culture. Later stages of differentiation did not seem to be impacted in the case of murine myocytes. Human myocytes, however, profited immensely from culture in 2D in contrast to 3D, as shown by the drastically higher increase in *MyoG* expression (figure 14 D). This trend continues throughout the course of myogenic differentiation. Particularly, the observation that human myogenesis is sensitive to culture in a 3D environment is substantiated. We observed

severe impairment of terminal differentiation in human myotubes (figure 16). Increase of expression levels of genes encoding for proteins required for muscle functionality, troponin T 1 and different MHC isoforms, was significantly higher in human myotubes matured in a 2D environment. In murine myotubes, however, these types of culture just showed mild beneficial effects on a transcriptional level (figure 15 B).

Onset of terminal differentiation was not only affected by the type of scaffold (2D or 3D), but also by its stiffness. Culture of murine muscle cells on substrates with an apparent elastic modulus of 8 kPa compared to substrates with 12 kPa or 20 kPa resulted in higher expression levels MHC I and II and Tnnt I (figure 15 A), increased myotube development and alignment and improved myoblast fusion (figure 16). The trend that culture on softer substrates promotes myogenic differentiation is in accordance with several other studies. However, apparent elasticities included in these studies greatly differ from our setups and range from 51 kPa up to the MPa range [87]–[89]. Interestingly, a study by Palchesko *et al.* came to the opposite conclusion, showing that maximum myotube length was reached on PDMS substrates with a Young's modulus of 830 kPa, whereas culture on PDMS with 5 kPa led to lowest myotube length. However, tested substrates had different rigidities than those applied in the present study, with 5 kPa, 50 kPa, 130 kPa, 830 kPa and 1.72 MPa being tested. Furthermore, differences between the groups are only seen in early time points of the experiment (up to 5 days), whereas after 7 days of differentiation no significant difference between the groups were observed. Therefore, it is speculated that these initial results are generated by increased proliferation leading to earlier confluence, which is a major determinant of myoblast fusion [159]. In contrast to that, the first study that pointed out the major impact of substrate stiffness on myogenic differentiation conducted by Engler *et al.* clearly stated that a Young's modulus at the physiological range of native muscle (especially 8 kPa and 11 kPa) is most beneficial for myogenesis [85]. A follow-up study confirmed that substrate stiffness in the myogenic range (*i.e.* 8 – 17 kPa) promotes expression of the myogenic marker *MyoD* in MSCs to a higher extent when compared to much softer (1 kPa) and stiffer (34 kPa) substrates and can even regulate fate decision towards myogenic differentiation [86]. The influence on myoblast differentiation is attributed to the interference of substrate stiffness with myofibrillogenesis from nascent myofibrils. They state that a compliant substrate allows developing myofibers to generate a contractile force that promotes cell alignment and fusion, which is crucial for further maturation. Culture on rigid materials leads to high contractile forces causing development of too many stress fibers and focal adhesions, which eventually inhibits organization of actin and myosin filaments that is required for myotube development. On the other hand, if substrates are too soft, cell adhesion and spreading are impaired, which prevents generation of sufficient contractile forces to induce alignment and functional maturation [85]. Apparently, the range of substrate stiffness considered optimal for force generation is different for human myoblasts compared to murine ones. In the 2D setup, changing rigidities did not affect gene expression of MHC and Tnnt I (figure 15 A), while morphological changes were the same as in murine cells (figure 16). In 3D, however, a clear

trend of stiffer materials being advantageous for onset of terminal myogenic differentiation was observed (figure 15 B).
In the context of observing cellular behavior in 3D, biomaterial density and nutrient supply need to be considered. As mentioned before, increasing substrate stiffness inevitably leads to increased material density due to higher fibrinogen content. This is supported by the observation that 3D culture in the softest hydrogel, while still having a negative effect compared to 2D, is less detrimental compared to culture in stiffer hydrogels. This was observed for proliferative behavior in both species (figure 13) and for progression of myogenesis only in the murine cell line (figure 15 A). In this matter, the cells' ability to degrade the matrix gains relevance. It is known that C2C12 cells have high levels of plasminogen, a fibrinolytic enzyme, that are further upregulated in the process of differentiation [172], [173]. The importance of adequate rates of fibrinolysis regarding myogenic outcome of TE approaches has been shown in the past [174]. Prolonged culture and improved differentiation of C2C12 cells requires balanced rates of material degradation. Excessive degradation, which is the case culturing C2C12 cells in fibrin, leads to insufficient mechanical stability of the engineered constructs, while insufficient degradation hindered differentiation, potentially due to a lack of movement and cell-cell contacts [161], [174]. In contrast to that, the pattern of plasmin activation in the C25 cell line has not been studied yet. This presents another potential key difference in the adaption of these cell lines to 3D environments. In this regard, we speculate that 3D culture could benefit from scaffolds with higher material stiffness and higher porosity.

The cell line C2C12 is known to be very robust in terms of handling in culture, but recapitulates the steps of myogenesis less accurately [51], [61]. This should be kept in mind when comparing the behavior of other cell lines with C2C12 cells. Culturing C2C12 cells in the same TE setup (alginate gel scaffolds) as primary murine myoblasts showed that they react similarly to the different culture methods. The effects of changing environments, such as stiffness and degradability of hydrogels, however, were more pronounced in the primary cells, as shown by Boontheekul *et al.* [161]. Our findings substantiate their observation of limited capability of C2C12 cells to recapitulate the physiological responses in the context of mechanotransduction. Regarding the C25 cell line, it is assumed that their response reflects more closely the situation in non-transformed cells, since transcriptomic analyses have shown that their immortalization did not modifdy any relevant clusters of genes [99].

Overall, we can conclude that the design of an SMTE approach's material properties is of utmost importance for its ability to promote and foster myogenic differentiation. Particularly evident and relevant from a practical perspective is the observation that cellular behavior observed in 2D setups cannot be translated to more complex 3D structures. The same observation was made concerning the translation of findings from the frequently used murine myoblast line C2C12 to other cell types, specifically the human myoblast line C25. Therefore, our findings contribute to answering the questions of comparability of different approaches in SMTE. Solving this issue, however, will require more attention and studies dedicated to this specific problem in the future.

Conflict of interest

The authors declare that the research was conducted in the absence of any commercial or financial relationships that could be construed as a potential conflict of interest.

Author contributions

JT: Performed all cell-based experiments, preparation of the manuscript, design of figures and tables; BM: establishment of methods; PH: tensile mechanical testing, revising the manuscript; MR, OGA: design and execution of AFM experiments, revising the manuscript; CF: development of study design, preparation of manuscript; PJT: design of AFM experiments, revising the manuscript; AT, HR: development of study design, revising manuscript.

Funding

This study was supported by the projects Signal Tissue (MA23#18-08) and FFG COIN Disease Tissue (FFG#845443) projects.

Acknowledgments

We would like to thank Peter Zammit (King´s College, London, United Kingdom) for providing us with the C25 cell line.

Contribution to the field statement

In the field of skeletal muscle tissue engineering, it has long been known that mechanical cues related to the used scaffolds, such as micro-architecture and stiffness, guide and induce muscle differentiation and are pivotal for the myogenic outcome. Although researchers have looked at different scaffold geometries, (bio)-materials and stiffnesses, there is still no consensus in the field about optimal material properties to foster myogenesis in order to engineer muscle-like tissue. Fibrin has proven highly suitable for skeletal muscle tissue engineering approaches in the past. Despite its popularity, there are no studies directly comparing myogenic cell behavior in 2D *vs*. 3D in fibrin. Therefore, the aspect of 2D *vs*. 3D cultures of myoblasts on or within fibrin are analyzed in this study. Moreover, the effect of hydrogels' elastic properties are assessed to contribute to increased comparability amongst different setups. A further issue tackled in this study is the transferability of the material's influence on myogenesis in murine to human models. The questions answered in this study concerning comparison of species and other essential differentiation cues have potential to contribute to unresolved issues in the field and to advance it a step further.

5. Supplemental information

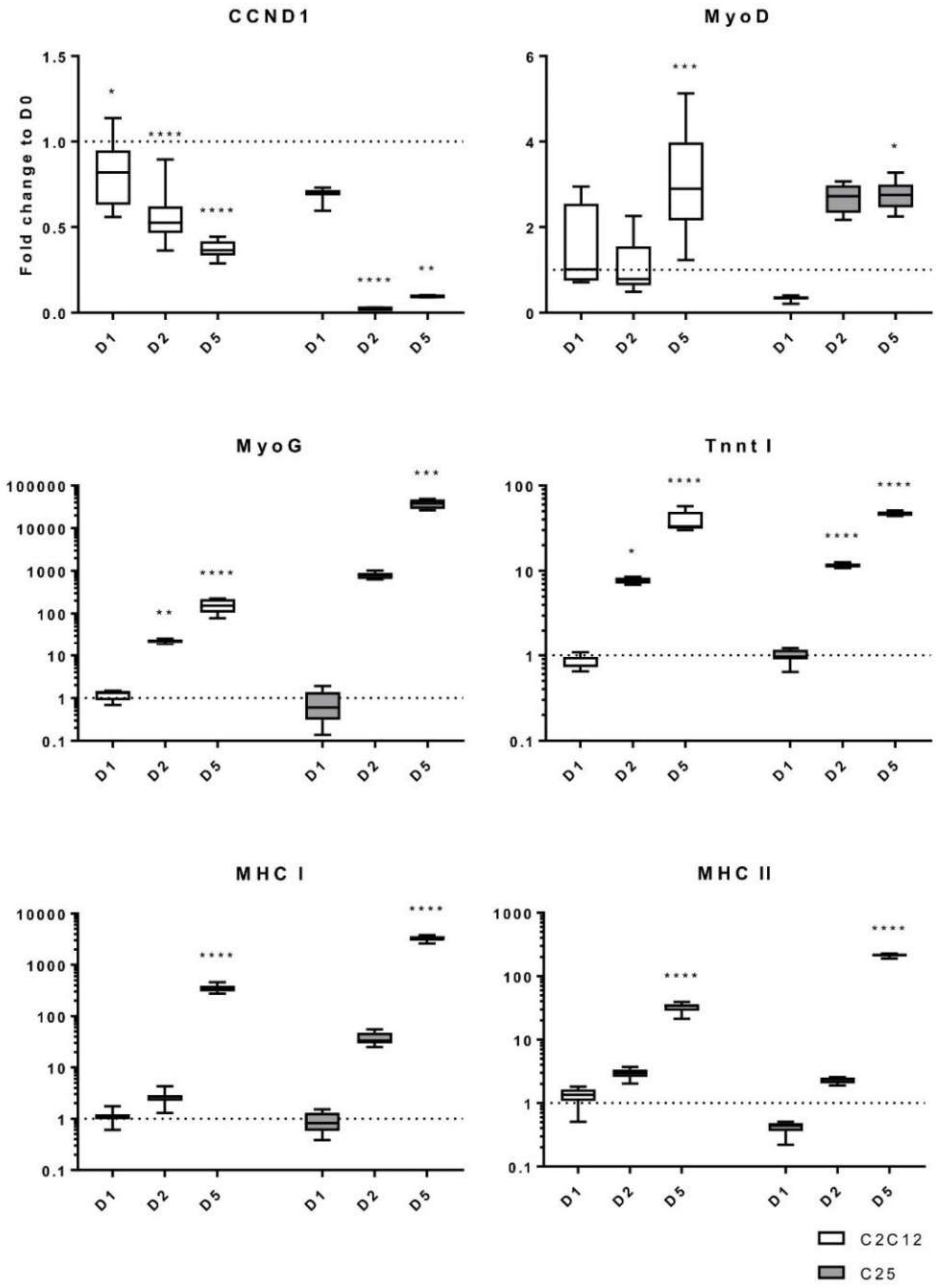

Supplementary figure 1: Myogenic marker gene expression of murine C2C12 and human C25 myoblasts during differentiation. 0.5x10^6 cells were seeded per well of a conventional 6-well plate in growth medium that was replaced by differentiation medium on D1. mRNA expression of marker genes specific for cell cycle progression [cyclin D 1 (CCND1)], early, mid and late stage myogenesis [MyoD, myogenin (MyoG), troponin T I (Tnnt1I), myosin heavy chain I (MHC I) and myosin heavy chain II (MHC II)] was assessed by RT-qPCR. Fold change expression levels were normalized to D0 control samples of each cell line, indicated by the horizontal dotted line; N = 3, n ≥ 7; one-way ANOVA with Sidak's multiple comparison test was performed comparing all time points to D0; *p < 0.05, **p < 0.01, ***p < 0.001, ****p < 0.0001.

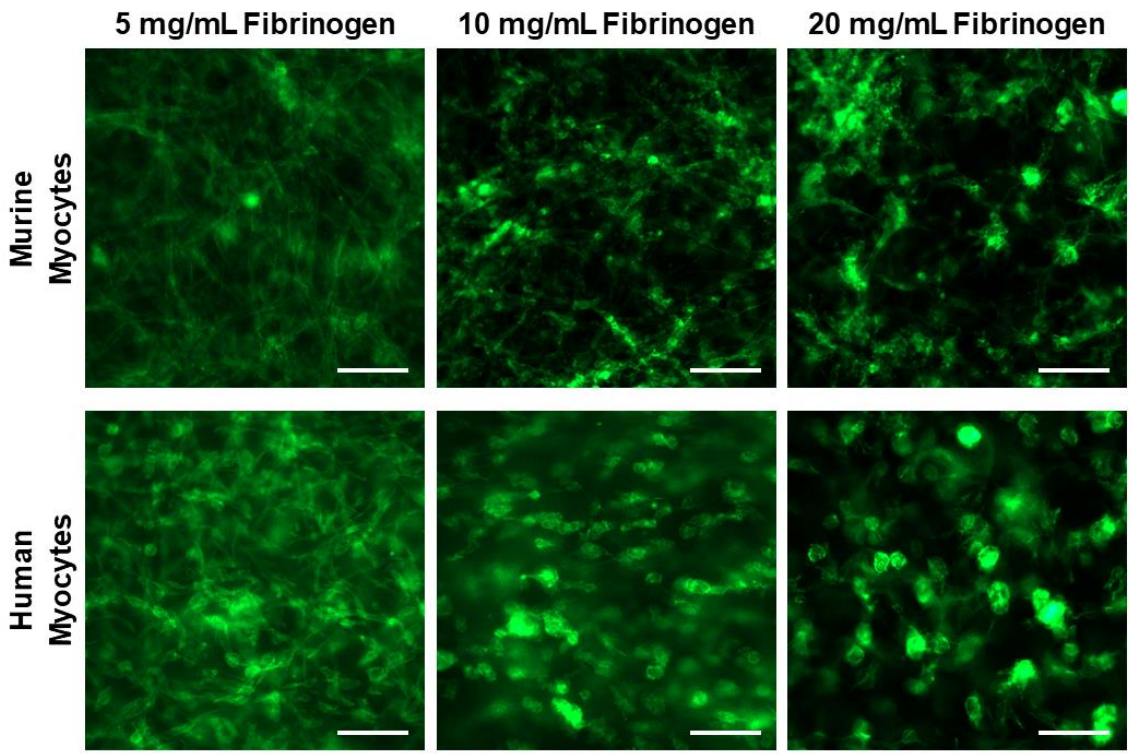

Supplementary figure 2: Myoblasts lose ability to spread when embedded in substrates with higher stiffness. Murine and human myoblasts were cultured embedded in 3D fibrin hydrogels with varying fibrinogen concentrations (5 mg/ml, 10 mg/mL and 20 mg/mL fibrinogen, which correspond to Young´s moduli of 5.1, 10.3 and 20.6 kPa, respectively) under proliferative conditions for 3 days. The cytoskeleton was visualized with phalloidin (green). A representative image is shown for each group (N = 2, n = 4; scale bar represents 100 µm).

Optimizing the surface structural and morphological properties of silk thin films via ultra-short laser texturing for creation of muscle cell matrix model

Liliya Angelova[1,*] , Albena Daskalova[1] , Emil Filipov[1] , Xavier Monforte Vila[2,3], **Janine Tomasch[2,3]**, Georgi Avdeev [4], Andreas H. Teuschl-Woller[2,3], Ivan Buchvarov[5]

[1]Institute of Electronics, Bulgarian Academy of Sciences, Sofia, Bulgaria

[2]Department Life Science Engineering, University of Applied Sciences Technikum Wien, Vienna, Austria;

[3] Austrian Cluster for Tissue Regeneration, 1200 Vienna, Austria

[4]Institute of Physical Chemistry, Bulgarian Academy of Sciences, Sofia, Bulgaria

[5]Faculty of Physics, St. Kliment Ohridski University of Sofia, Sofia, Bulgaria

*Corresponding author: Liliya Angelova, lily1986@abv.bg

Published in *Polymers* on June 25th, 2022

Abstract

Temporary scaffolds that mimic the extracellular matrix's structure and provide a stable substratum for the natural growth of cells are an innovative trend in the field of tissue engineering. The aim of this study is to obtain and design porous 2D fibroin-based cell matrices by femtosec- ond laser-induced microstructuring for future applications in muscle tissue engineering. Ultra-fast laser treatment is a non-contact method, which generates controlled porosity—the creation of mi- cro/nanostructures on the surface of the biopolymer that can strongly affect cell behavior, while the control over its surface characteristics has the potential of directing the growth of future muscle tissue in the desired direction. The laser structured 2D thin film matrices from silk were characterized by means of SEM, EDX, AFM, FTIR, Micro-Raman, XRD, and 3D-roughness analyses. A WCA evaluation and initial experiments with murine C2C12 myoblasts cells were also performed. The results show that by varying the laser parameters, a different structuring degree can be achieved through the initial lifting and ejection of the material around the area of laser interaction to generate porous channels with varying widths and depths. The proper optimization of the applied laser parameters can significantly improve the bioactive properties of the investigated 2D model of a muscle cell matrix.

Keywords: silk fibroin; biopolymers; femtosecond laser processing; muscle tissue engineering; muscle cell matrix 2D model

1. Introduction

Sports injuries, accidents, and other types of muscle trauma can lead to major muscle tears. As a result, the body is not capable of natural endogenous muscle regeneration, which may subsequently cause the permanent loss of muscle function and the deterioration of the quality of life of the injured person [175]–[177]. Severe burns, lacerations, or various muscle injuries often require tissue transplantation from either the patient's own body or from a donor [178]–[180]. Unfortunately, traditional treatment options have many negative consequences for the recipient, such as the creation of a new injury, whose normal healing may be disrupted, leading to a risk of additional infections and a high immune response [181]–[183]. Skeletal muscle tissue engineering, on the other hand, relies on temporary cellular scaffolds that mimic the extracellular matrix (ECM) and provide a stable structure for the natural growth of muscle cells – in certain types of muscle trauma in the body, the matrices can be implanted directly at the site of injury or pre-seeded *in vitro* with cells and implanted thereafter [60], [184], [185]. In their elaborate review, Carnes and Pins [186] explain in detail the complex nature of the muscular structure, endogenous regeneration phases, and the advantages and disadvantages of the different muscle tissue engineering approaches. The main purpose of the matrix is to create a biomimetic environment that stimulates cell adhesion, differentiation, and proliferation [187]–[190]. In this way, the cells can be reorganized into new three-dimensional tissues. In the process of tissue regeneration, the matrix degrades gradually leaving behind only the newly formed tissue [186], [190], [191]. Silk fibroin (SF) is one of the most preferred natural polymers for this purpose, as it satisfies all ECM requirements for the creation of a successful temporary cellular scaffold. This is due to SF's unique mechanical properties, controlled rate of biodegradability, and high biocompatibility [191]–[200]. All these qualities underlie its wide field of biomedical applications. The most used SF in medical applications is a fibrous protein derived mainly from Bombyx mori cocoons [201]–[205]. It is a fibrous protein showing a high content of the amino acid motif composed of the following aligned amino acid monomers (Gly-Ser-Gly-Ala-Gly-Ala)n, which are the molecular basis for its high toughness and strength [204], [206]–[209]. Detailed information on the bio-applications of SF is given in the comprehensive reviews of Thurber *et al.* [191] and Holland *et al.* [198].

In skeletal muscle tissue engineering, fibroin is used mainly in the form of hydrogels or 2D hydro-thin layers [197], [204], [206], [207], [210], [211]. The creation of "smart" biomimetic muscle tissue matrices based on extracted and purified silk fibroin requires improving their functionality through non-destructive structuring. The functional and physical properties of muscle as a tissue are orientation-dependent qualities [190] – *in vivo*, ECM structure, characterized by micro grooves between neighboring muscle fibers, guides myoblast alignment during the myotube formation process [186], [212], [213]. To mimic *in vivo* muscle organization, differ- ent methods have been applied to create biomimetic muscle scaffolds with an aligned structure, including electrospinning [134], [214]–[218], wet and dry spinning [134], [219]–[221], and 3D bioprinting [134], [222]–[224]. Ultra-short pulse laser treatment is a non-contact, non-

invasive, non-destructive, and fully biocompatible method, which generates controlled porosity in biopolymer-based cell matrices [225] – this type of modification leads to the creation of micro and nano structures on the surface of the material that can strongly affect cell adhesion, orientation, and differentiation [219], [226]. The method relies on control over the surface characteristics of biomaterials, and accordingly, the growth of future muscle tissue can be directed in the desired direction as microchannels/microgrooves with precisely controlled dimensions, and periodicity can be generated on the scaffold surface in a highly reproducible manner [227]–[231]. This is very important for muscle tissue engineering, as aligned surface structures are the key to obtaining natural muscle cells' morphology and orientation [93], [232]. The group of Jin *et al.* [232], for example, achieved uniform laser-ablated microchannels on a substrate that orientated the C2C12 myoblast cells along them, thus helping the natural regenerating process. Apart from that, femtosecond (fs) laser treatment successfully overcomes the limitations associated with the application of other traditional "structuring" methods such as sandblasting or chemical etching that might leave toxic residuals (e.g., from solvents) for the cells in the matrix after treating [204], [225]. The side effects (such as microcracking and the absence of molten zones) caused by the interaction of ultra-short laser pulses with biocompatible structures are also minimized [225].

The aim of the presented work is to obtain and design porous 2D fibroin-based cell matrices by femtosecond (fs) laser-induced microstructuring for future application in the engineering of muscle tissue. The surface functionalized samples were characterized by means of morphological (SEM and AFM) and qualitative (EDX, FTIR, micro-Raman, and XRD) analyses, as well as the surface roughness (Sa and Ra) evaluation of the material before and after laser treatment using an optical profilometer was performed. A WCA evaluation, an *in vitro* degradation test, and initial cellular experiments were also performed.

The analysis of the experimental results clearly shows that femtosecond laser structuring can be applied to assess the surface properties of SF-based cell matrices with a high level of accuracy. By varying the applied fs parameters, different degrees of structuring can be achieved from the initial lifting and ejection of the material around the area of laser interaction to porous channels with different controlled dimensions. Laser modification of the 2D model of muscle cell matrix can significantly improve the bioactive properties of this material, which after the laser parameters' proper optimization can make its biomedical applications even more successful.

2. Materials and methods

2.1. Silk fibroin bombyx mori cocoons extraction and sample preparation

Silk fibroin (SF) was extracted and purified from Bombyx mori cocoons (Institute of silkworm breeding, Vratsa, Bulgaria) according to the protocol described in detail in [233]. Briefly, the production of silk fibroin (approximately 7–9% in dH2O) consists of degumming with sodium carbonate and lithium bromide (Sigma-Aldrich®, Munich, Germany). The procedure includes three main steps: first – preparation of silk cocoons by removing the moth from the cocoon and peeling off the inner layer; second – degumming by boiling the cocoon material in 0.02M Na2CO3, washing, and drying the degummed silk obtained, a crucial step for sericin (a protein that shields the fibroin in silk fibers) removal, as it is toxic for the cells; and last – dissolving the sericin free silk in 9.3M LiBr solution for 3h at 60 ◦C. Afterward, the dissolved silk is dialyzed against water for 48h and centrifuged for 10 min at 4618×g. The obtained SF (7.26% w/v solution) was used for 2D thin layers' preparation (1 × 1 cm, 110 μm thickness) by spreading the solution on glass slides and removing the prepared thin films samples after drying.

2.2. Ultra-short laser texturing of the 2D fibroin-based cell matrices

The 2D thin layers' surface microstructuring was performed in air by means of a fs regeneratively amplified Ti:sapphire mode-locked Quantronix-Integra-C system (Hamden, CT, USA), precisely controlled by LabView software. All experiments were performed at λ = 800 nm, v = 500 Hz, and τ = 150 fs continuous raster surface scanning in XY direction, perpendicular to the SF sample surface, that is positioned on a high-precision XYZ translation stage. The fluence (F) and the scanning velocity (V) were varied as follows F = 0.4 ÷ 2.5 J/cm2 and V = 1.7 ÷ 32 mm/s to optimize the dimensions and morphology of the microgrooves created by the laser beam (table 4), in respect to myoblasts C2C12 cells dimensions, which will be seeded. To promote the natural regeneration process, the distance between the microchannels was also precisely controlled to be optimized with respect to cellular dimensions and orientation inside the channels. According to the literature, widths of grooves and ridges promoting C2C12 alignment and differentiation vary between 20 μm and 100 μm [93], [96], [186], [234]. All analyses of the fs structured samples that followed were averaged on ten separate measurements and performed in respect to the control, a laser non-treated SF scaffold. An illustrative scheme of the experimental setup is given elsewhere [231].

Table 4: Continuous fs XY raster scan: ƛ=800nm, ν=500 Hz, τ=150fs, F=0.4÷2.5 J/cm^2 and V=1.7÷32mm/s, given for each SF sample group (Group №) treated in respect to control, fs non-treated Group 17. The thickness and the Sa and Ra roughness parameters (in μm), measured for each group of scaffolds are also given

Group №	V mm/s	F J/cm^2	Sa (μm)	Ra (μm)	thickness (μm)
1	32	0.4	28.11	5.68	115
2	16	0.4	12.2	6.56	121
3	3.8	0.4	113.8	3.74	140
4	1.7	0.4	23.35	12.87	146
5	32	0.8	17.68	0.95	126
6	16	0.8	2.23	1.38	145
7	3.8	0.8	3.18	1.56	149
8	1.7	0.8	12.92	5.79	161
9	32	1.7	12.82	1.53	123
10	16	1.7	7.23	0.64	130
11	3.8	1.7	4.98	0.62	143
12	1.7	1.7	8.02	1.12	156
13	32	2.5	4.89	0.76	134
14	16	2.5	1.52	0.74	137
15	3.8	2.5	2.49	0.62	142
16	1.7	2.5	7.59	1.32	146
17 contr.	-	-	1.55	0.26	110

2.3. Methods for characterization of fs laser-modified SF samples

The obtained morphology of the SF 2D thin films after laser processing was investigated by means of Scanning Electron Microscopy (SEM) equipped with an Energy- Dispersive X-ray Spectroscopy module (EDX) – (SEM-TESCAN/LYRA/XMU, Fuveau, France). The samples were gold-sputtered (~20 nm Au layer) in vacuum and SEM images were taken at two different magnifications (500× and 3000×/5000×); EDX was performed on an area at higher magnification, the elemental composition was estimated in [wt.%] in respect to control surface. Atomic Force Microscopy (AFM) was also performed. For this purpose, an atomic force microscope MultiMode V (Veeco Instruments Inc., New York, NY, USA) and Controller NanoScope V (Bruker Ltd., Berlin, Germany) in dynamic tapping mode of operation were used. The 2D, 3D, and phase AFM images were taken over an area of 15 × 15 μm2 and 5 × 5 μm2 via Tap300Al-G (BudgetSensors, Switzerland) silicon AFM probe. Evaluation of samples' surface roughness profile was additionally performed by a 3D Optical profiler, Zeta-20 (Zeta Instruments, KLA, Milpitas, CA, USA) at 20× magnification. ProfilmOnline software

(https://www.profilmonline.com (accessed on 23 March 2022)) was used for better visualization of the 3D true color images obtained; roughness parameters Ra (the mean value of the deviations of the surface height from the median line, according to DIN4776 standards) and Sa (the extension of Ra to a surface area) were also estimated. The samples thickness was measured by a VA 8042 coating meter (Zhejiang, China). In addition to the EDX analysis conducted, the chemical composi- tion of laser treated and untreated surfaces was examined by Fourier-Transform Infrared (FTIR) and micro-Raman Spectroscopy. For this purpose, FTIR spectrophotometer (IR Affinity-1, Shimadzu, Kyoto, Japan), with a working range of 500–4500 cm−1, was used for obtaining the IR transmittance spectra [%], and a microRaman spectrometer (LabRAM HR Visible, HORIBA Jobin Yvon, Kyoto, Japan), working with a He-Ne laser (633 nm) and equipped with Olympus BX41 microscope, was used for obtaining the micro-Raman profile of the samples investigated (time of exposition-10s at 100× magnification). For the identification of the crystalline phase of silk fibroin scaffolds, X-ray crystallography analysis was performed within the range of 5–70° θ2 (step size of 0.065◦ θ2, at continuous scan mode and counting time of 195s) via Philips PW1050 X-ray diffractometer (XRD) system (Philips, Amsterdam, The Netherlands), equipped with a secondary monochromator of the diffraction beam and a copper anode. The phase identification was acquired via QualX2 software through the Crystallography Open Database. Contact Angle (CA) wettability measurements and surface free energy evaluation were performed in air by a video-based optical contact angle measurement device DSA100 Drop Shape Analyzer (KRÜSS GmbH, Hamburg, Germany). For this purpose, two different solutions were used: dH2O, and diiodo-methane (DM) in an average volume of 2 μL for a period of 3 min. Contact angles and surface energy were calculated by ADVANCE software (KRÜSS GmbH, Hamburg, Germany) fitting the drop profiles to the Young–Laplace equation and following the Owens–Wendt-Rable–Kaeble (OWRK) equation, respectively. *In vitro* degradation test performed in PBS buffer saline (pH 7.2, Sigma-Aldrich®, Munich, Germany) at 37°C for a period of two weeks was conducted to predict the stability and biodegradation rate of the fs treated/control SF muscle matrices for when the *in vitro* cell culture was to be performed. For this purpose, the relative percent weight loss of the scaffolds was calculated at the end of every week and the PBS was replaced with a fresh buffer solution. Comparison between laser microstructured and untreated SF samples was made in all analyses performed.

2.4. Cellular experiments for biological evaluation of laser-textured 2D model of muscle cell matrix

Four groups of fs treated samples were chosen for preliminary cellular experiments: groups G3, G4, G8, and G11 fs treated SF thin films with respect to control G17 (see table 4 for reference of the fs parameters used). Before seeding the myoblasts cell line C2C12, the samples were sterilized in ethanol for 1 h. Cells were seeded at a density of 5 × 104 cells/cm2 in a growth medium (Dulbecco's modified Eagle's medium-high Glucose (Life Technologies, Carlsbad, CA, USA), supplemented with 10% fetal calf serum (GE Healthcare, Buckinghamshire, UK), 1%

penicillin/streptomycin (Lonza, Basel, Switzerland), and 1% L-glutamine (Lonza, Basel, Switzerland). After 24 h, the medium was replaced by a differentiation medium (Dulbecco's modified Eagle's medium-high Glucose (Life Technologies, Carlsbad, CA, USA), supplemented with 3% horse serum (GE Healthcare, Buckinghamshire, United Kingdom), 1% penicillin/streptomycin (Lonza, Basel, Switzer- land), and 1% L-glutamine (Lonza, Basel, Switzerland) that was exchanged every second day. Cells were fixed with 4% paraformaldehyde (Roth, Karlsruhe, Germany) for 10 min at room temperature on days 3, 7, and 11 after seeding for analysis of myogenic differentiation by immunofluorescence staining. The staining was performed by washing with dH2O and permeabilizing with Tris-Buffered Saline/0.1% (v/v) Triton X-100 (TBS/T) for 15 min at room temperature, followed by blocking in PBS/T-1% (w/v) bovine serum albumin and 1% (v/v) goat serum at room temperature for one hour. The primary antibody targeting all MHC isoforms (MF 20, Developmental Studies Hybridoma Bank, Iowa, USA) was diluted at 1:300 in a blocking solution and incubated overnight at 4 ◦C. The secondary antibody labeled with Alexa Fluor 488 (Life Technologies, Lofer, Austria) was diluted at 1:400 in a blocking solution and incubated at 37 ◦C for one hour. Nuclei were labeled by staining with 4?,6-diamidino-2-phenylindole (DAPI) diluted 1:1000 in a blocking solution for 10 min at room temperature. All stainings were analyzed with a Leica DMI 6000b inverted microscope (Leica Microsystems GmbH, Wetzlar, Germany). The main steps for the preparation and characterization of fs surface functionalized fibroin-based cellular matrices for application in muscle tissue engineering performed in this work are summarized schematically in figure 17.

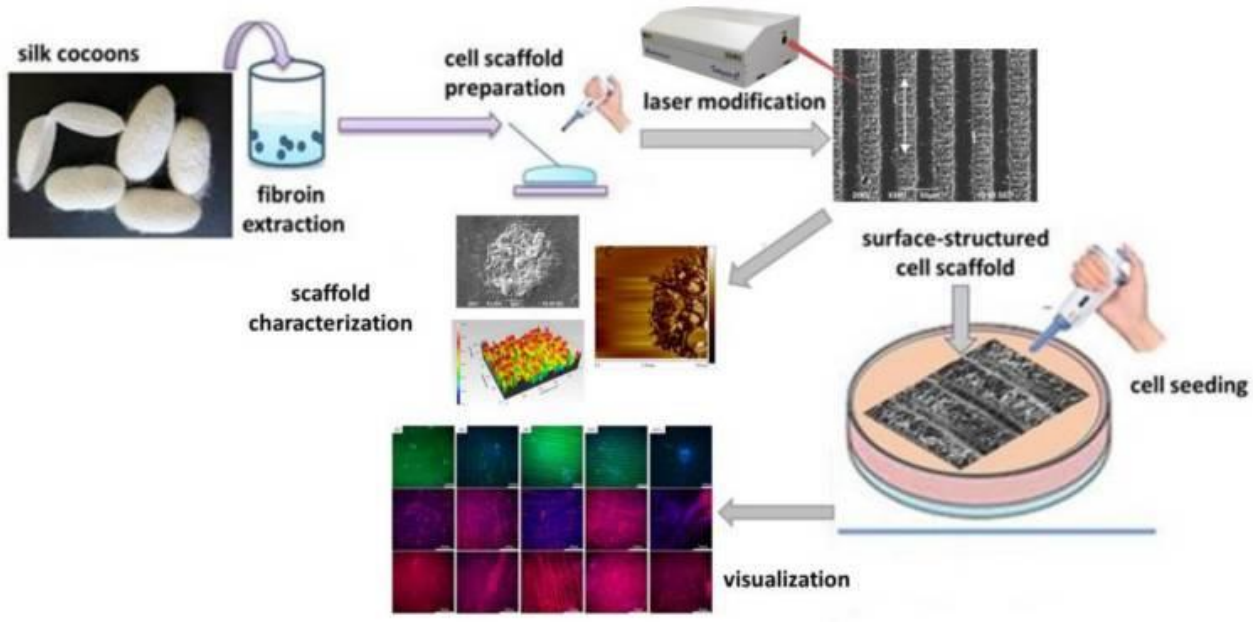

Figure 17: Schematic representation of the main steps for the preparation and characterization of surface-functionalized silk fibroin-based cellular matrices for application in muscle tissue engineering.

3. Results and discussion

3.1. SEM, EDX, AFM, and 3D optical profiler analysis of Fs laser created structuredness of SF based thin layers

Figure 18 contains SEM images of the SF layers, which were fs laser structured while simultaneously varying both the fluence and the scanning velocity in the diapason as follows: F = 0.4 ÷ 2.5 J/cm2 and V = 1.7 ÷ 32 mm/s. This process was followed to estimate the optimal laser parameters in order to create structures with the specific dimensions, which were appropriate for cultivating the muscle cells in an oriented manner.

As can be seen from the thickness measurements of the SF thin film samples presented in table 4 and the selection of the representative morphological SEM images, presented in figure 18, in all the cases of laser processing an ejection of the material above the basic surface line occurs, which leads to the formation of a thicker, inflated zone in the area of interaction (samples thickness = 115 ÷ 161 μm) in respect to the control group (thickness = 110 μm). At the “gentler” mode of structuring conditions, the laser created zones of interaction, in the form of circular spots, (at V = 32 mm/s and 16 mm/s) which were emerging above the surface baseline (group G1 and group G2), while at a higher applied energy, a material thrown outside of the edges of the created rims was detected, resulting in a hole-like structure (G5, G6, G9, G10, G13, and G14). The basic demand of structuring by the fs laser radiation for obtaining an orientated growth of muscle cells is associated with the formation of groove-like patterns [40,41]. In our experiment, the created grooves limits can be tuned to become narrower and deeper with the increase of F and the decrease of the scanning speed (V), while the highly porous nature of the created microstructures (G3, G4) becomes smoother and more homogenous, a rather granular as opposed to porous morphology. However, material ejection, whether or not it is accompanied by the introduction of additional porosity in the structure, does not lead to damage of the sample’s integrity, nor do cracks or unwanted melting side effects at the groove/spot boundary occur (figure 18). This fact could be explained by the ultra-fast nature of the processes taking place during fs laser–material interaction, which does not allow for the development of thermal damage effects in the scaffold’s structure, since the interaction ends long before these effects could appear [66–68]. In other words, one of the great achievements of ultra-short pulse ablation is the ability to produce a minimal heat-affected zone around the laser spot area. This is because significant accumulated energy is removed during the early stages of material removal and less heat is dissipated beneath the surface. Moreover, in this case, laser processing does not lead to a change in the elemental composition of the samples treated, but only to a slight deviation in the weight concentration [wt.%] of the elements, which can be clearly seen from the results of the EDX analysis performed simultaneously with the SEM (table 5).

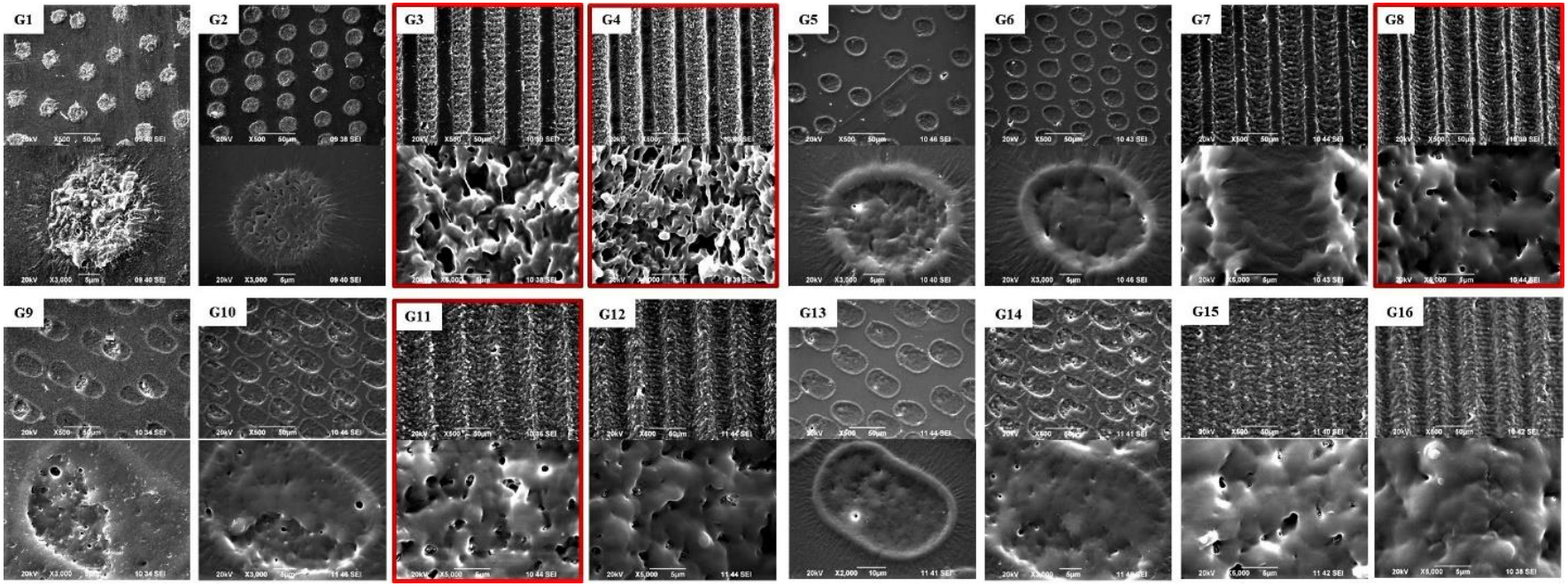

Figure 18: SEM images of G1 ÷ G16 silk fibroin-based cellular scaffolds taken at 500× and 3000×/5000× magnification. In red—SF samples chosen for cellular experiments, based on the results of the analyses performed.

Table 5: EDX elemental composition given in weight% [wt.%] of each fs treated SF sample group (G1-G16) in respect to control, fs non-treated Group 17.

EDX Spectrum	C [wt.%]	N [wt.%]	O [wt.%]	Total [wt.%]
G1 V=32mm/s, F=0.4J/cm^2	44.87	20.87	34.26	100
G2 V=16mm/s, F=0.4J/cm^2	46.08	18.96	34.97	100
G3 V=3.8mm/s, F=0.4J/cm^2	45.57	19.16	35.27	100
G4 V=1.7mm/s, F=0.4J/cm^2	44.21	21.89	33.9	100
G5 V=32mm/s, F=0.8J/cm^2	45.58	20.53	33.89	100
G6 V=16mm/s, F=0.8J/cm^2	43.07	23.63	33.3	100
G7 V=3.8mm/s, F=0.8J/cm^2	44.03	21.32	34.65	100
G8 V=1.7mm/s, F=0.8J/cm^2	42.74	20.23	37.03	100
G9 V=32mm/s, F=1.7J/cm^2	46.25	19.79	33.96	100
G10 V=16mm/s, F=1.7J/cm^2	43.65	22.92	33.43	100
G11 V=3.8mm/s, F=1.7J/cm^2	44.9	21.96	33.14	100
G12 V=1.7mm/s, F=1.7J/cm^2	44.59	21.62	33.79	100
G13 V=32mm/s, F=2.5J/cm^2	47.96	20.03	32.01	100
G14 V=16mm/s, F=2.5J/cm^2	46.52	18.36	35.12	100
G15 V=3.8mm/s, F=2.5J/cm^2	48.04	18.01	33.95	100
G16 V=1.7mm/s, F=2.5J/cm^2	46.15	19.78	34.07	100
G17-control	48.27	17.95	33.78	100

This slight increase in the elemental presence of oxygen [O] in respect to carbon [C] andnitrogen [N] could be explained by the surface oxidation, taking place during the fs laser structuring. Apart from that, the high intensity femtosecond laser–matter interaction, which occurs at higher values of F and lower values of V, leads to the subsequent appearance of O=C–NH bonds' fragmentation (*i.e.*, a very slight decrease in [C] and [N]), due to the increased material ejection [235].

A representative selection of 3D real-color images, obtained under variation of F and V in respect to a non-treated surface, is given in figure 19; the corresponding Ra and Sa rough- ness parameters of all the groups of samples, measured during the optical profilometer analysis, are presented in table 4. As already mentioned, the specific patterning conditions were chosen in relation to the optimal dimensions and morphology of the patterns created by the laser in respect to the myoblast cells' suitable seeding conditions [234].

The obtained results are in accordance with the morphological findings acquired from the SEM analysis. As can be seen from figure 19, the depth and width of the microchannels created by the ultrafast laser, as well as the roughness of the samples (table 4), can be varied by tuning the applied laser parameters (F and V). The created grooves have clear cuts with U or V-shaped

edges. There is no evidence of mechanical distortion of the biopolymer material. Based on a literature survey, the optimal dimensions for muscle cells vary between 20 μm and 100 μm, as during skeletal muscle formation or regeneration, myoblasts fuse into multi-nucleated tubes to form myofibers, the muscle's basic "building blocks", whose diameter ranges in this diapason, depending on the muscle location and function [96], [186], [234]. By tuning the applied laser parameters (F and V), the SF scaffolds morphology could maximally mimic the ECM of the muscle tissue and be "personally" designed in respect to the specific needs of the seeded cell line. For example, Jin *et al.* [93], who achieved uniform laser-ablated microgrooves that orientated the C2C12 myoblast cells along them, has varied the spacing between the groove patterns in the range of 0 ÷ 80 μm and have obtained up to 100 μm depth of the channels depending on the energy and number of pulses applied in their experimental work.

The results of the conducted AFM analysis complement those of the SEM and 3D profilometer images and even reveal additional structures at the nano- and micro-levels – nano-roughness, nano- and micro-pores, and sub-microgranulation were observed inside the laser-generated microstructures, which can be clearly seen from the AFM 2D and 3D images of the border zone between the laser-treated and surrounding surface (15 × 15 μm), and the 5 × 5 μm area images inside the laser-generated structures of the SF samples. Some representative AFM images are given in figure 20.

The AFM images of the control fibroin sample, G17 (figure 20 a), reveal the typical roughness of fibroin films at the nanometric scale. After a laser treatment, the SF films reveal remarkable morphological changes not only at the micro (which is confirmed by SEM and 3D roughness analyses) but also at the nano level: the presence of diverse micro and nanostructures, grains, and pores is clearly observed (figure 20 a,c). Figure 20 c visualizes the ejection of the material at the border area of the fs craters created at the four fluences used in this study, but at the highest scanning velocity applied (corresponding to N = 1 in the selection of single-pulse laser mode of operation).

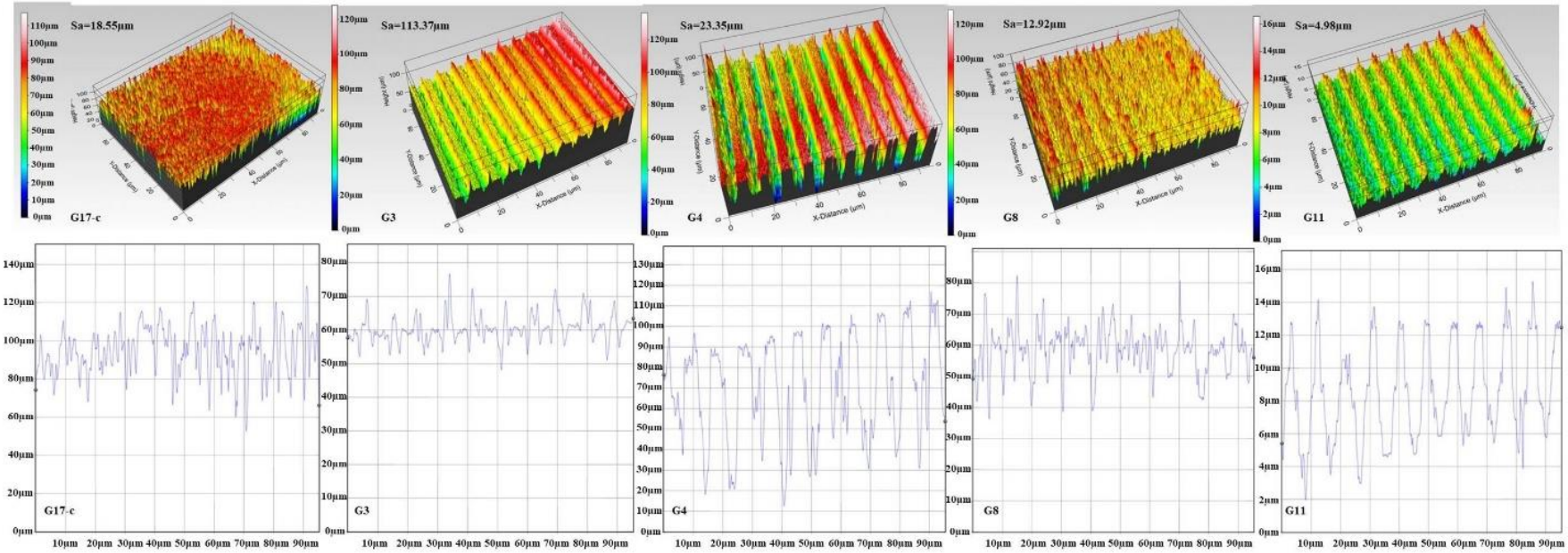

Figure 19: Representative selection of 3D real-color surface profile images of G3, G4, G8, and G11 silk fibroin-based cellular scaffolds in respect to G17-control sample (at 20× magnification); Sa-surface roughness (upper line) and Ra-line roughness cross-section profile (lower line)

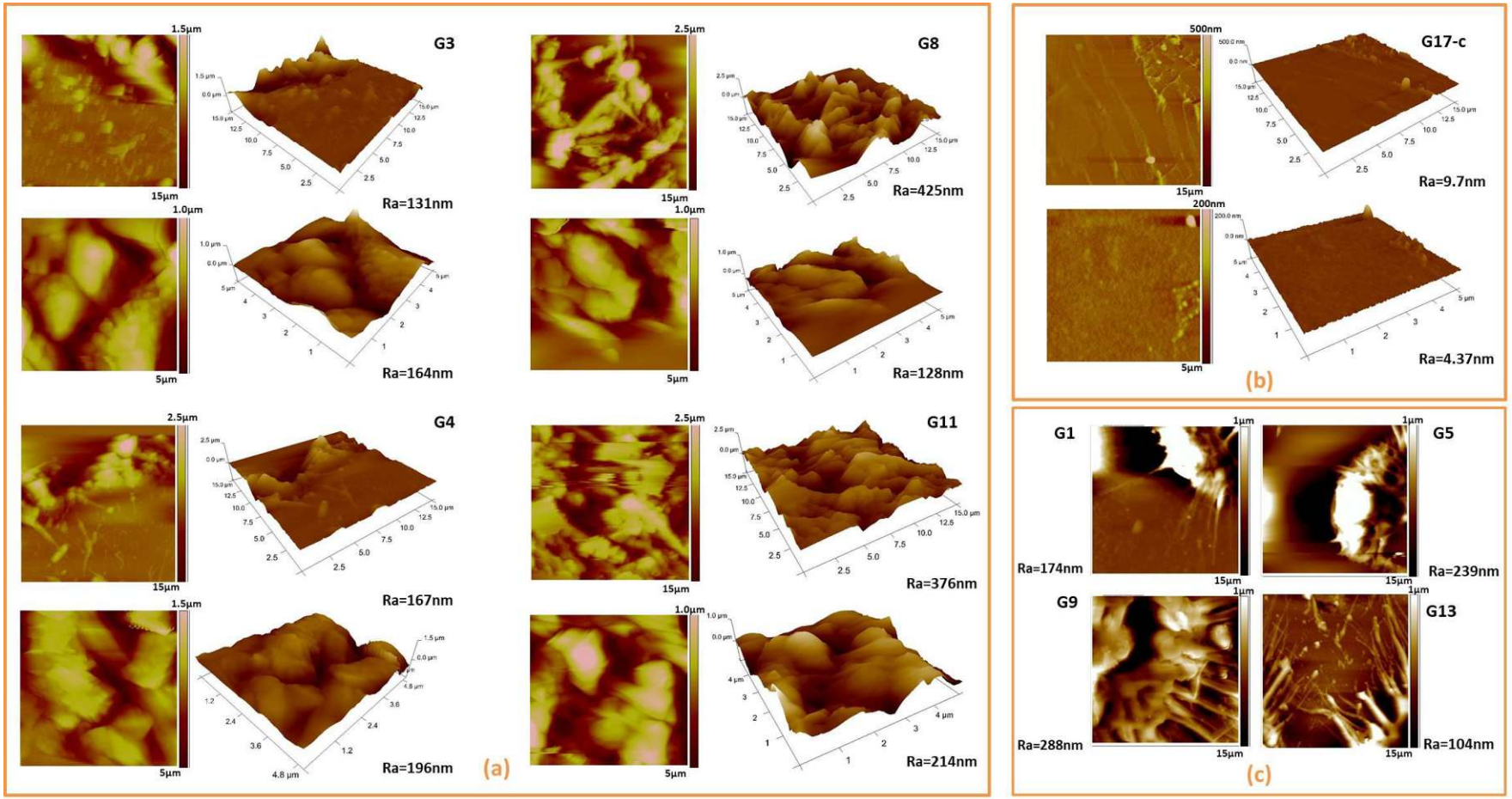

Figure 20: Representative selection of 2D and 3D AFM images at 15 × 15 µm of the border area and 5 × 5 µm inside the laser created structures: **(a)** G3, G4, G8, and G11 silk fibroin-based cellular scaffolds in respect to **(b)** G17-control sample; **(c)** visualizes the ejection of the material at the border area of the fs craters that were created. Local Ra of the areas examined is also given.

Comparing the data from the performed morphological analysis, no disturbance was observed in the surface integrity at the applied specific conditions of fs laser processing. Optimizing the laser induced micro-features (in respect to the roughness, porosity, and dimensions of the created structures) could subsequently affect muscle cells' behavior, such as their adhesion, morphology, direction of migration, and differentiation, and hopefully could favor the natural regeneration process of the muscle tissue *in vitro*, and potentially *in vivo* [186], [236]–[238]. In the last two decades, femtosecond laser processing of different biopolymers for tissue engineering applications have been intensively studied by many research groups; a detailed review of the subject has already been made by Terakawa [225]. Regarding the ultrafast laser structuring of silk fibroin, the information is scarce; there are almost no data on the fs laser modification of the silk protein for bioapplications, nor are there data specifically for muscle tissue engineering. The group of Santos *et al.* [239], for example, used fs-laser pulses to produce optical waveguides in SF by the direct laser writing of for a biosensor application. In another publication, the same group is further developing their previous results by fs-based printing of well-defined 2D micropatterns of pure and functionalized SF for optical and biomedical applications, such as lab-on-a-chip devices and microsensors [240]. A novel and simple platelet repellent surface was reported by Yang *et al.*, who achieved fabrication of micropattern films based on tannic acid that could be widely used in the clinical evaluation of antiplatelet therapies [241]. Kim *et al.*, on the other hand, proposed a one-step functionalization of a zwitterionic polymer surface by using a soft lithographic technique [242]. The applied TA-Fe-based coating converted the non-biofouling properties of the polymer to be protein- and diatom-adhesion friendly by a one-step procedure; the lithographic technique provided a regular micropattern for protein and marine diatoms' surface adhesion.

Based on all the data obtained (in respect to the dimensions and roughness of the microstructures created by the laser processing) and the performed literature survey, the following groups of patterned SF samples were chosen for cellular experiments (in respect to control group 17): F = 0.4 J/cm2 and V = 3.8 mm/s (group 3), F = 0.4 J/cm2 and V = 1.7 mm/s (group 4), F = 0.8 J/cm2 and V = 1.7 mm/s (group 8), and F = 1.7 J/cm2 and V = 3.8 mm/s (group 11) – marked in red on the corresponding SEM images of fgure 18 and presented in figure 19. All fs modifications in the form of individual spots or too "sharp", narrow, or deep microgrooves created by the laser were excluded as not optimal for directing guided muscle cell growth and the future establishment of functional tissue [186], [190], [212], [213].

The ablation thresholds of the applied fluences were also determined according to the diameter regression technique described in detail in [243]. After the diameter of the craters created on the surface of the SF samples for each scanning velocity used in our study (or the corresponding N-number of pulses) was determined, the corresponding threshold fluences (Fth) of the material were defined from the plot of squared crater diameters (d2) versus the laser fluence for different N (in our case, V as continuous scanning is performed) by extrapolating the curve to zero (figure 21). According to the logarithmic relationship between D2 and F, a linear dependence (well seen

from the graph) is evident [243]. Based on this method (by using the equations presented in [243]), for the applied in the current study fluences (F = 0.4 J/cm2, F = 0.8 J/cm2, F = 1.7 J/cm2 and F = 2.5 J/cm2), Fth were defined as follows: 0.22, 0.18, 0.14, and 0.08 J/cm2. As can be seen from the presented graph, the ablation threshold decreases with the decrease of V in the case of continuous scanning (or with increasing N in a single pulse laser mode of operation, respectively). Some representative optical microscope images of laser spots on the SF thin film sample irradiated at the lowest scanning velocity (V = 1.7 mm/s) at every F applied in the current study are also presented in figure 21; for better visualization of the spot size growth with increasing F at a constant V, the diameter of the spots is also provided.

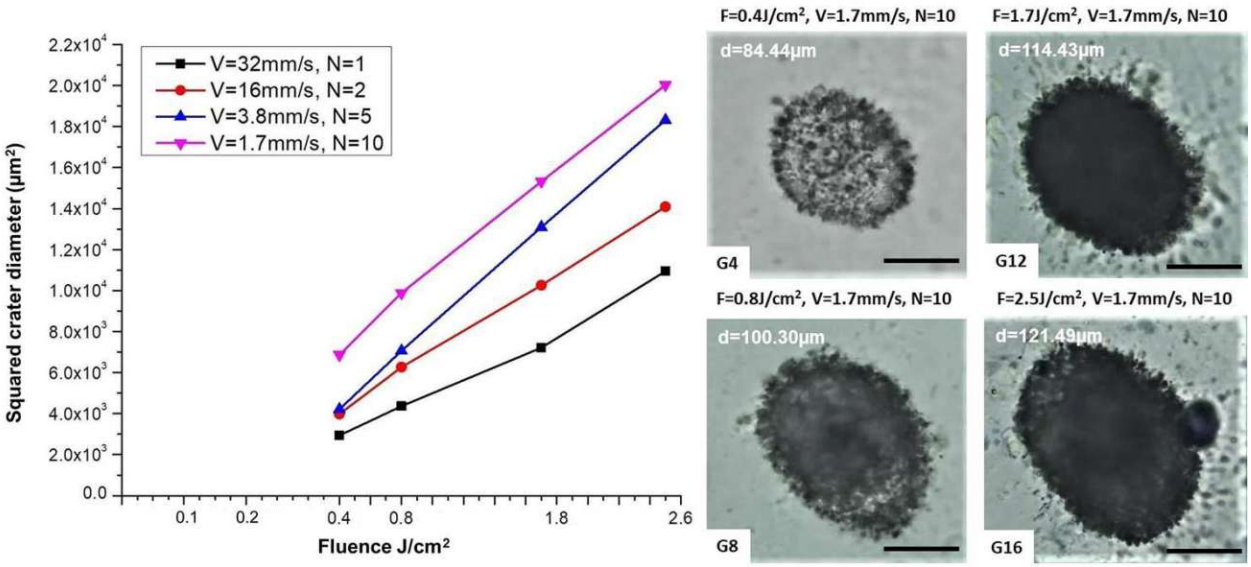

Figure 21: Squared crater diameters (μm2) versus the laser fluence for different V (corresponding N) applied on SF sample when irradiated in air (left); Optical microscope images of laser spots on SF thin film sample irradiated with N = 10 (at the corresponding lowest scanning velocity V = 1.7 mm/s used) at every F applied in the current study (right); scale bar = 50 μm.

3.2. FTIR, Micro-Raman, and XRD Analysis of SF scaffolds

Figure 22 summarizes the FTIR transmittance spectra [%] of all the SF laser-treated samples (group 1 ÷ 16) with respect to the control scaffold (group 17).

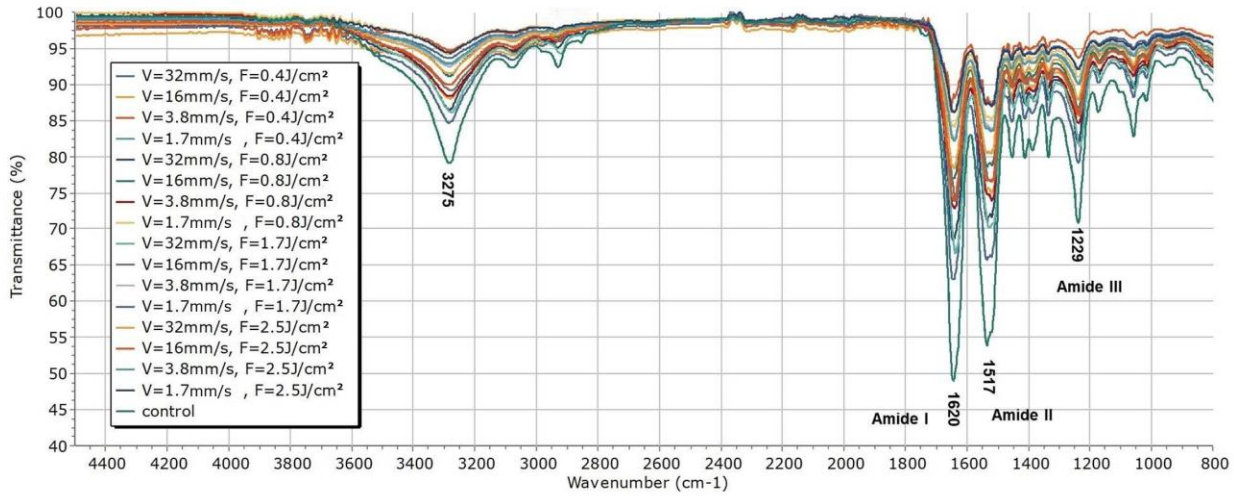

Figure 22: FTIIR Transmittance [%] spectra of G1 ÷ G17 silk fibroin-based cellular scaffolds.

As can be seen from the presented spectra, there are no deviations in the number, shape, or position of the peaks, while clearly a difference in their intensity is observed with respect to the spectrum taken from the control SF sample. The transmittance spectra exhibit all the characteristic peaks, arising from the peptide bond –CONH–, namely amide I, amide II, and amide III [244]–[246]. All the bands in the FTIR spectra in figure 22 correspond to C=O stretching (at 1620 cm−1) for amide I, N–H bending, and the in-phase combination of C=O bending and C–N stretching (at 1517 cm−1 and 1229 cm−1, respectively) for amide II and amide III [246]. The decrease in the intensity of the bands representing the data obtained from the laser processed samples can be attributed to the increase of the applied laser energy that causes a disturbance in the vibrations of the amide groups, resulting in a lower peak intensity. This result strongly correlates with the micro-Raman results. The Micro-Raman spectra of the laser-treated matrices (G1 ÷ 16) with respect to the control one (G17) are shown in figure 23 – all the bands characteristic of the amides are well defined, as follows: amide I at 1671 cm−1, amide II at 1463 cm−1, and amide III at 1274 cm−1 [247], [248]. The C–H bond at 2945 cm−1 and the polarization-dependent peak regarding the Tyr amino acid side-chain at 855 cm−1 are also very well pronounced. The polarization-dependent peaks typical for B. mori silk at 1401, 1369, 1083, 1001, and 881 cm−1 originate from β- sheets formed in the SF structure [249]. The main trend is related to a decrease in the signal intensity after laser treatment, but no change in the number or position of the peaks was observed. Even though some O=C-NH bond fragmentation was detected by the EDX analysis performed on fs processed SF scaffolds (table 5), the amide I, amide II, and amide III bands detected in all FTIR transmittance (figure 22) and micro-Raman spectra (figure 23) presented are in accordance with the native silk fibroin structure-β-turns (silk I) and β-sheet crystalline silk-II structure, which is a more compact characteristic form of the protein after spinning of the silk fiber by B. mori during cocoon formation [248], [250].

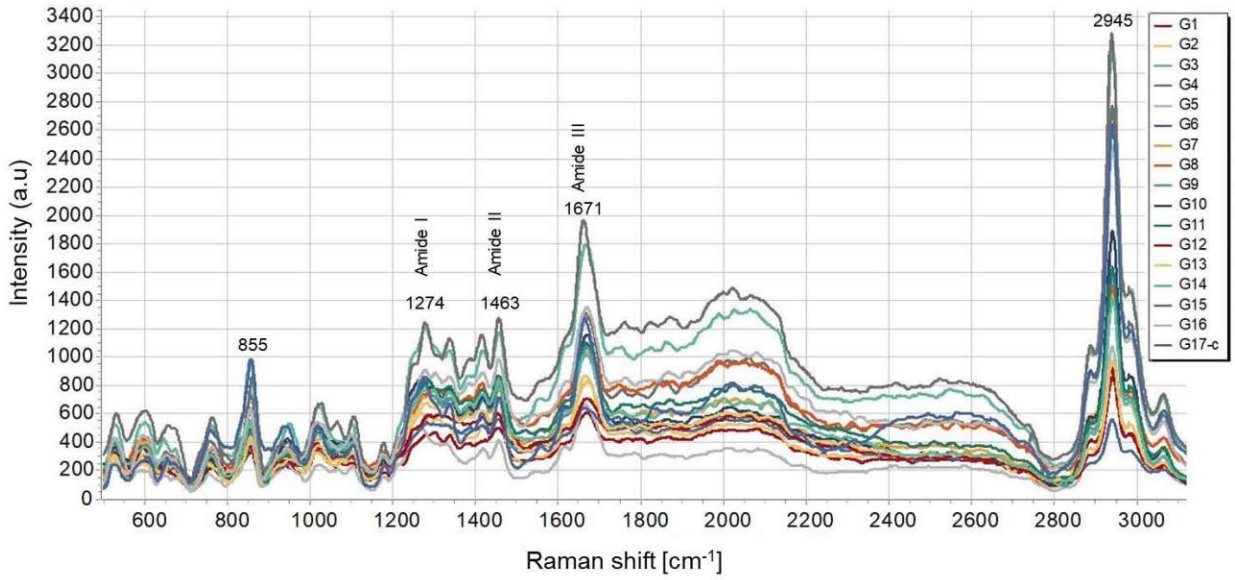

Figure 23: Micro-Raman spectra of G1 ÷ G17 silk fibroin-based cellular scaffolds.

As a rule, the natural silk fibroin and the degummed SF materials include crystalline and amorphous structures (less stable α-helices, turns, and random coils). The stability of silk fibers is dependent on their β-sheet composition. Crystalline structures have two forms: silk I, a dominant water-soluble helical structural conformation of β-turns, and a water-insoluble silk II structure formed by folded β-sheets [248]–[252]. The results obtained from the XRD analysis performed on the four groups of laser-processed SF scaffolds, chosen for the preliminary cellular experiments (G3, G4, G8, and G11 laser structured SF thin films in respect to control G17), are given in figure 24.

As can be seen from the figure, only the XRD spectrum of the G3 SF sample indicated an increased crystallization after laser-induced treatment with respect to the control group (G17) and other fs patterned SF scaffolds—obvious diffraction peaks at 2θ, namely 12.1◦, 19.8◦, and 24.4◦ which correspond to the silk I crystalline structure are well pronounced. A lack of well-defined diffraction peaks was observed for silk II in all G3, G4, G8, G11, and G17 XRD spectra (the typical diffraction peaks between 20◦ and 21◦, indicating that the corresponding silk II structures were not detected) [253]. From these findings, it could be concluded that the ultra-short laser processing does not significantly affect the crystal structure of the investigated SF thin films (G4, G8, and G11), as no substantial difference in the XRD spectra is evident when compared with the control SF scaffold (G17). An increased crystallization ability of silk fibroin was observed only after treatment with F = 0.4 J/cm2 and V = 1.7 mm/s (G3). Therefore, it is possible that fs laser treatment with the specific parameters leads to the maintenance of silk I's water-soluble crystalline structure, which could have a positive impact on the protection of the integrity of the fibroin thin films.

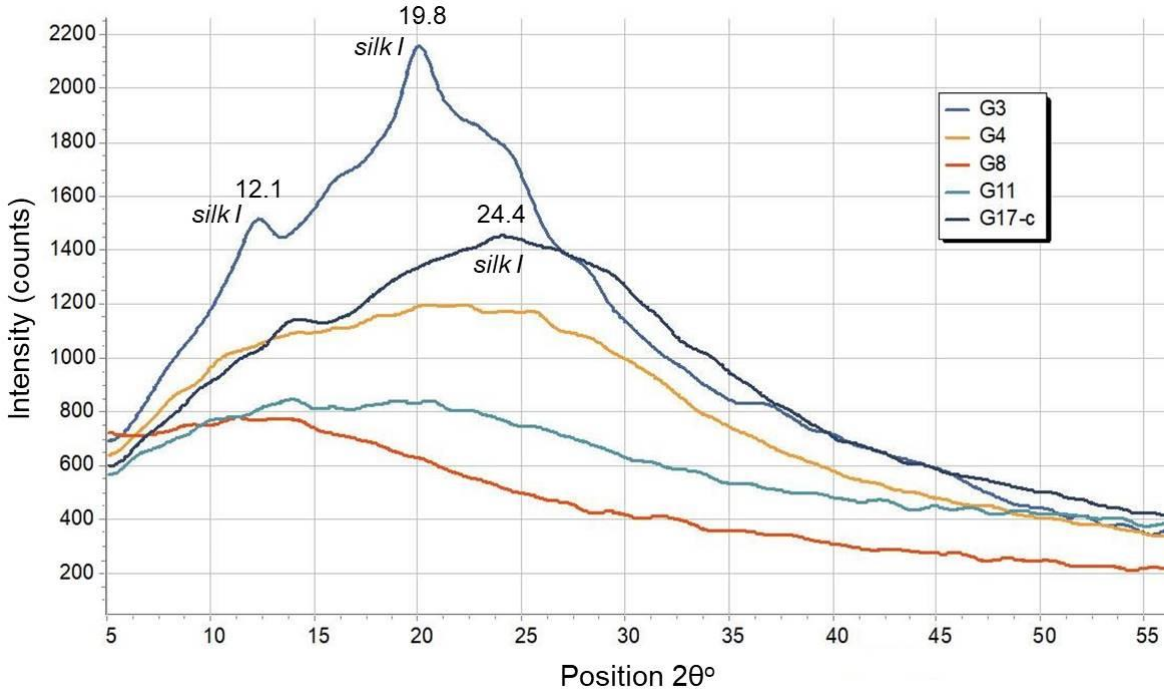

Figure 24: XRD spectra of G3, G4, G8, G11, and G17 SF-scaffolds.

3.3. Contact angle evaluation analysis

A wettability and total surface energy evaluation (table 6) of the control (G17) and the laser structured SF thin films, which were chosen for cell studies (G3, G4, G8 and G11), were performed via the sessile drop method using two liquids with different polarities: distilled water (highly polar) and diiodomethane (very low polarity). The obtained results of the Contact angle (CA) evaluation analysis are summarized in figure 25, where CA change in time is graphically presented; images of water and diiodomethane droplets on 0.00 s and 3 min of application for the SF examined can be also seen in the figure.

As a whole, the results of the both laser-processed and control SF thin films followed a similar trend over the 180s period of wettability evolution: the contact angle decreased in certain boundaries (much more narrow for DM than for dH2O), as a slight fluctuation in the total linear behavior was observed at the first 60 s of the droplet contact (for both liquids used) to the fs structured samples (which was not observed on the control SF surface). This could be attributed to a varying amount of entrapped air between the droplet and the surface formed by the laser microstructures, during the liquid's first contact with the rough surface underneath [254], and this could be explained by the irregular profile of the structures at a submicrometric scale (micro- and nano-pores, grains, etc.) and by a transition between the Cassie–Baxter and Wenzel wetting states [255]. The hydrophilic nature of the scaffolds, attributed to the hydrophilic carboxylic and amino groups in the SF structure [256], was additionally enhanced by the laser processing,

especially for the G11 group, where an almost superhydrophilic surface was achieved (WCA dropped from ~25 to ~20◦ after 3 min of dH2O application). In the case of DM CA evaluation, G3 and G4 were characterized with higher CA in respect to the control group G17. An exception in the droplet behavior was observed in the case of G4, where the CA increased even more after 60 sec. of application. The wettability and the total surface energy of G8 were not measured as DM spread over the entire modified surface at the first second of application and it was not possible for the system to measure the CA. As can be seen from the results presented in table 6, the surface free energy of the laser-treated surface was also enhanced in respect to the control G17 group.

Table 6: Total surface free energy (SFE) evaluation of G3, G4, G8, G11 and G17-c calculated on OWRK-SFE model based on water and diiodo-methane used as substances. The total SFE of G8 was not obtained, as CA of DM was not possible to measure.

Silk fibroin group sample	**Surface free energy [mN/m]**	**Disperse free energy [mN/m]**	**Polar free energy [mN/m]**
G3	47.89	35.91	11.98
G4	46.91	32.3	14.61
G8	-	-	-
G11	70.92	40.62	30.3
G17-c	37.71	31.85	5.86

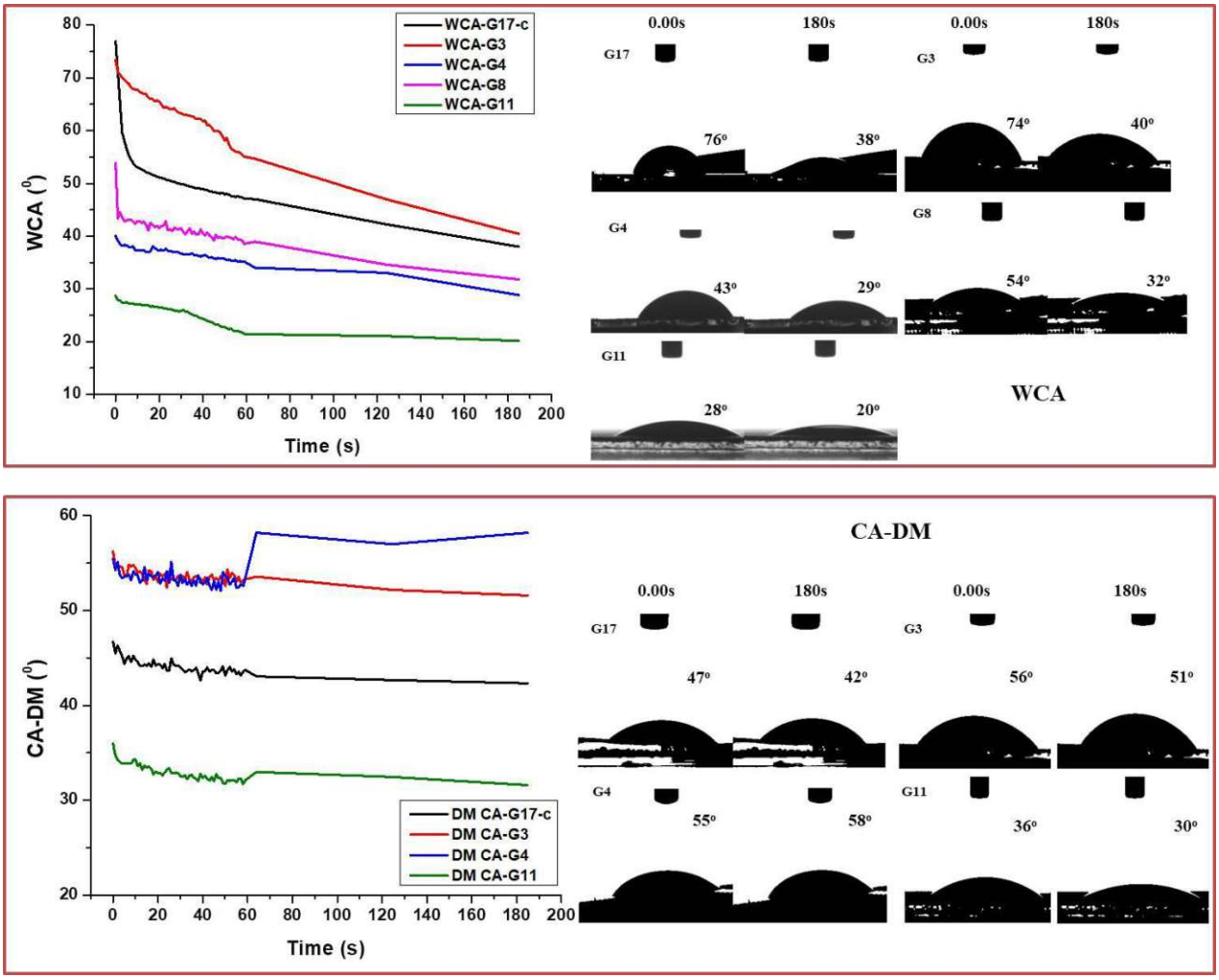

Figure 25: CA evaluation analysis of G3, G4, G8, and G11 silk fibroin-based cellular scaffolds in respect to G17-control sample performed with dH2O (upper graph) and DM (lower graph); images of the droplets taken at 0.00 s and 180 s of application and corresponding CA.

3.4. *In vitro* degradation test of the 2D model of muscle cell matrix

To evaluate the stability and biodegradability of the samples investigated, their percent weight losses during the *in vitro* degradation test performed in PBS (2 weeks at 37°C, 1 mL for each sample) was calculated according to: weight loss (%) = [(Wat the beginning– Wat the end of the week)/Wat the beginning] * 100. The results obtained which are important for evaluating the stability of the scaffolds for diverse cell culture periods, are given in the table below (table 7) and visualized by SEM images of the SF scaffolds taken at the end of each week (figure 26). The measured weight loss of the SF matrices indicates a considerably slow degradation for both the laser structured (G3, G4, G8, and G11) and the control samples (G17), which could be attributed to the already mentioned β-sheet structure of the silk fibroin [248]–[250]. This result is in accordance with the FTIR transmittance (figure 22) and micro-Raman spectra (figure 23) obtained and with the works of Wang *et al.* [197], Farokhi *et al.* [257], and Lee *et al.*, who

estimated a weight loss less than 5% for a period of 14 days during an *in vitro* degradation of silk-fibroin nanofibrous composite samples [258]. The mechanical properties of the cellular scaffold are a key parameter for *in vitro* and *in vivo* tissue regeneration. In the case of skeletal muscle injury, the repair phase, as a part of the regeneration process, takes between 1 and 4 weeks (most often around 2 weeks) for functional regeneration of the myotubes to take place [186]. This process is closely related to muscle satellite cells' alignment as a basic step for their subsequent differentiation into functional muscle tissue [259].

From the results of the *in vitro* degradation test and the SEM images, which visualized no appreciable change of the fs groove morphology of the G3, G4, G8, and G11 tested samples, it could be estimated that the fs structured and control SF scaffolds would be significantly stable during the cellular experiments performed afterwards. The ability of the microgrooved scaffold to sustain structural integrity is crucial not only for *in vitro* experiments but even more for maintaining mechanical stability after body implantation.

Table 7: *In vitro* degradation test in PBS of G3, G3, G4, and G11 and control SF scaffolds (G17) prior to preliminary cellular experiments. Weight loss (%) results on day 7 and day 14 are presented.

Group №	weight on day 1 (mg)	weight on day 7 (mg)	weight on day 14 (mg)	weight loss (%) on day 7	weight loss (%) on day 14
1	10.1	9.8	9.7	2.97	3.9
3	10.3	10.0	9.9	2.91	3.88
4	10.1	9.7	9.65	3.9	4.45
8	10.5	10.1	10.0	3.8	4.76
11	10.9	10.7	10.5	1.8	3.6
17 contr.	11.0	10.7	10.6	2.73	3.64

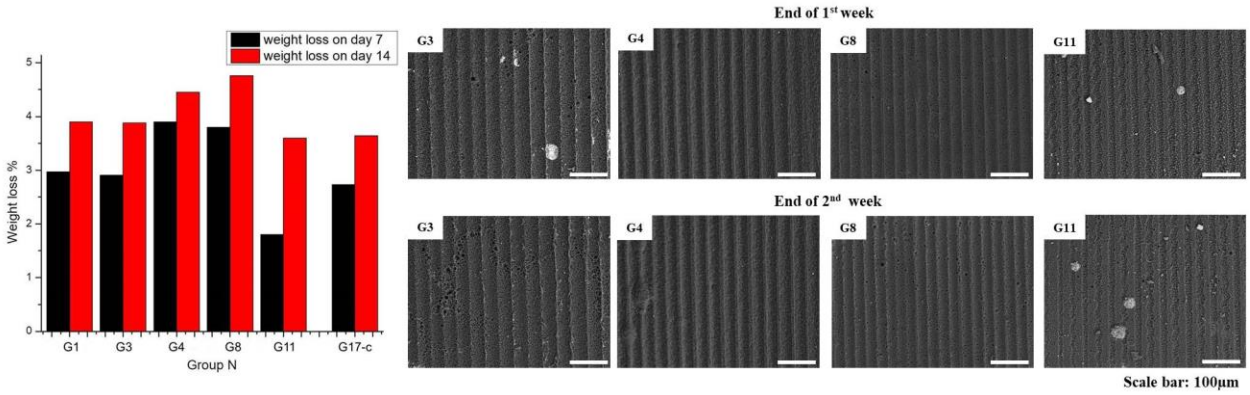

Figure 26: Graphical representation of the weight loss (%) during the 14-day *in vitro* degradation test and corresponding SEM images of G3, G4, G8, and G11 silk fibroin-based cellular scaffolds at the end of the first and second week of the test. Scale bar = 100 μm.

3.5. Differentiation of myoblasts on laser patterned silk fibroin based scaffolds

Murine C2C12 myoblasts were seeded on the 2D fibroin matrices with fs laser pre-treated surfaces and differentiated for 11 days. The staining of the nuclei confirmed the presence of C2C12 cells on the samples on days 3, 7, and 11 of the culturing (in blue) with no apparent differences between the fs laser-treated and control samples. The myogenic differentiation was evaluated by immunofluorescence staining of the myogenic marker myosin heavy chain (MHC) in respect to the control SF thin film (figure 27). Starting from day 3, signs of differentiation can be observed, as indicated by the positive staining for MHC and the elongation of cells. Myogenic development progressed further over the culture period, including the fusion of cells to myotubes at later time points. Fs laser treatment influenced the C2C12 morphology and the organization in the differentiating cells (days 7 and 11). They have a more elongated shape when cultivated on samples G4 and G8, while those seeded on G17-control group have a random organization. Furthermore, the myoblasts seeded on sample G4 align along the grooves from the earliest observed time point on.

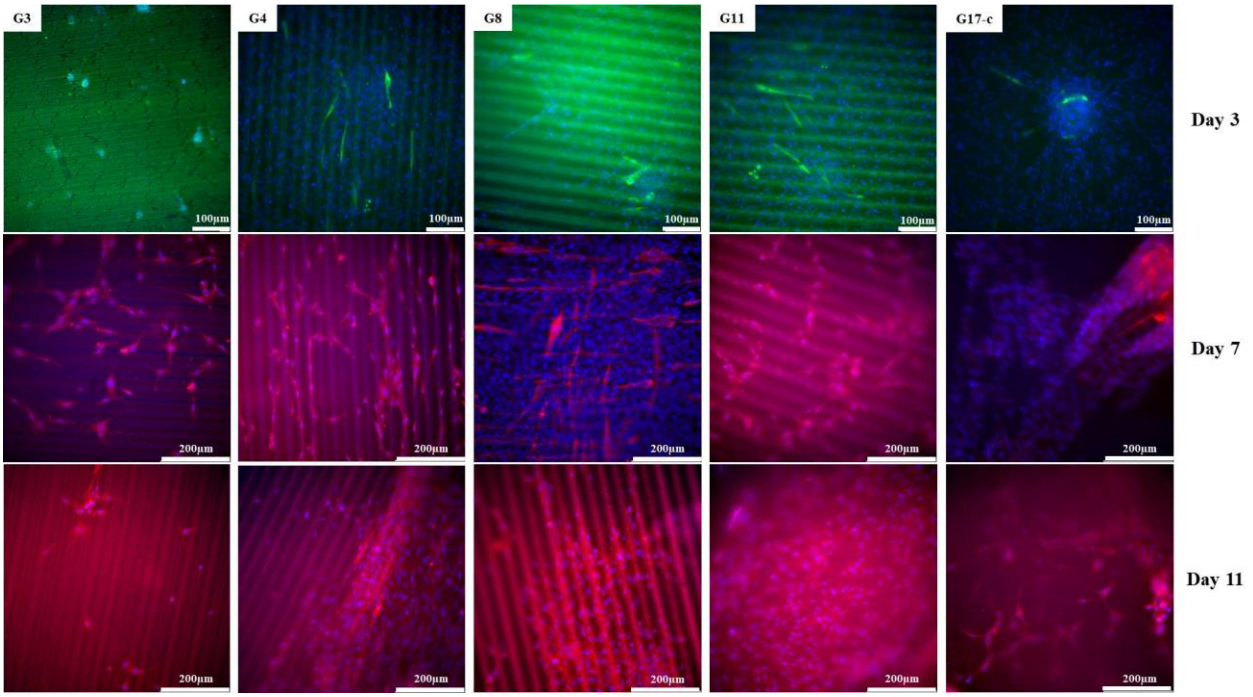

Figure 27: Fluorescence microscopy images (at 20× magnification) of viability (DAPI—nuclei in blue) and muscle differentiation (myosin heavy chain—muscle-specific marker in green on day 3 and in red on days 7 and 11) staining of C2C12 myoblasts cell line, cultured for 3, 7, and 11 days on G3, G4, G8, and G11 fs treated SF thin films in respect to control G17.

4. Conclusions

The proposed femtosecond laser induced surface modification method via a selection of different combinations of fluence and scanning velocities is an alternative, non-contact approach for the microstructuring of the SF-based 2D muscle matrices model as it can be successfully applied to the enhancement of scaffolds' surface properties with a high level of accuracy in respect to the specific cell line needs. By precisely combining the applied laser parameters, different degrees of structuring can be achieved, from the initial lifting and ejection of the material around the area of the laser's interaction to the generation of porous and granular microgrooves with varying dimensions. At the same time, no side effects such as damage of the sample's integrity, cracks, melting, or unwanted chemical alternations would could be observed due to the absence of thermal side effects. The ultra-short laser texturing did not affect the elemental composition, morphological integrity, or biodegradability of the SF thin layers; moreover, the hydrophilicity and the surface energy of the scaffolds were enhanced. The performed biological evaluation of the muscle cell compatibility of the laser processed SF matrices demonstrated without a doubt that the cells' orientation and differentiation were achievable. The analysis of the experimental results clearly shows that laser modification of the 2D model of a muscle cell matrix can significantly improve the surface properties of this material, which, after the optimization of laser parameters, can enhance its biomedical applications. The proposed technique is reliable for the establishment of a fs-microgrooved natural muscle environment model. Our next step is the fs structuring of 3D hydrogel scaffolds that will then be implanted into an animal model for an *in vivo* evaluation of the silk fibroin-based muscle matrix model.

Author contributions

Conceptualization, L.A. and A.D.; methodology, L.A. and A.D.; validation, A.D., L.A. and A.H.T.-W.; formal analysis, L.A., E.F., G.A., J.T. and X.M.V.; investigation, L.A. and E.F.; data curation, L.A. and A.D.; writing—original draft preparation, L.A.; writing—review and editing, A.D. and A.H.T.-W.; visualization, L.A. and E.F.; supervision, A.D. and I.B.; project administration, A.D. and A.H.T.-W. All authors have read and agreed to the published version of the manuscript.

Funding

The authors acknowledge the support from the Bulgarian national science fund (NSF) under grant number No. KP-06-Austria/5 (2021–2023), the OeAD (Austria's Agency for Education and Internationalization) under grant number BG 08/2021, the City of Vienna (MA 23 #30-11), and EUROPEAN UNION'S H2020 research and innovation program under the Marie Sklodowska-Curie Grant Agreement AIMed No. 861138.

Institutional review board statement

Not applicable.

Informed consent statement

Not applicable.

Data availability statement

Not applicable.

Conflicts of interest

The authors declare no conflict of interest

CHAPTER 2

CHOOSING APPROPRIATE SYSTEM COMPONENTS, PARTICULARLY BIOPHYSICAL AND BIOCHEMICAL STIMULI ALLOWS FOR THE CREATION OF OPTIMIZED SMTE STRATEGIES

The importance of biophysical and biochemical stimuli in dynamic skeletal muscle models

The importance of biophysical and biochemical stimuli in dynamic skeletal muscle models

Babette Maleiner[1,2], **Janine Tomasch**[1,2], Philipp Heher[2,3,4], Oliver Spadiut[5], Dominik Rünzler[1,2], Christiane Fuchs[1,2,*]

[1]Department of Biochemical Engineering, University of Applied Sciences Technikum Wien, Vienna, Austria

[2]The Austrian Cluster for Tissue Regeneration, Vienna, Austria

[3]Ludwig Boltzmann Institute for Experimental and Clinical Traumatology/AUVA Research Center, Vienna, Austria

[4]Trauma Care Consult GmbH, Vienna, Austria

[5]Institute of Chemical Engineering, Vienna University of Technology, Vienna, Austria

*Corresponding author: Christiane Fuchs, cfuchs1@mgh.harvard.edu

Published in *Frontiers in Physiology* on August 22nd, 2018

Abstract

Classical approaches to engineer skeletal muscle tissue based on current regenerative and surgical procedures still do not meet the desired outcome for patient applications. Besides the evident need to create functional skeletal muscle tissue for the repair of volumetric muscle defects, there is also growing demand for platforms to study muscle-related diseases, such as muscular dystrophies or sarcopenia. Currently, numerous studies exist that have employed a variety of biomaterials, cell types and strategies for maturation of skeletal muscle tissue in 2D and 3D environments. However, researchers are just at the beginning of understanding the impact of different culture settings and their biochemical (growth factors and chemical changes) and biophysical cues (mechanical properties) on myogenesis. With this review, we intend to emphasize the need for new *in vitro* skeletal muscle (disease) models to better recapitulate important structural and functional aspects of muscle development. We highlight the importance of choosing appropriate system components, e.g. cell and biomaterial type, structural and mechanical matrix properties or culture format, and how understanding their interplay will enable researchers to create optimized platforms to investigate myogenesis in healthy and diseased tissue. Thus, we aim to deliver guidelines for experimental designs to allow estimation of the potential influence of the selected skeletal muscle tissue engineering setup on the myogenic outcome prior to their implementation. Moreover, we offer a workflow to facilitate identifying and selecting different analytical tools to demonstrate the successful creation of functional skeletal muscle tissue. Ultimately, a refinement of existing strategies will lead to further progression in understanding important aspects of muscle diseases, muscle ageing and muscle regeneration to improve quality of life of patients and enable the establishment of new treatment options.

Keywords: skeletal muscle tissue engineering, stimulation strategies, bioreactors, myokines, skeletal muscle disease models, biomaterials, myogenesis

1. Introduction

The field of regenerative medicine and tissue engineering (TE) is still one of the fastest growing research areas in biomedical science. Previous TE efforts mostly focused on tissues and organs that are associated with diseases occurring at high frequencies in 1st world countries, such as the heart and the musculoskeletal apparatus with a strong emphasis on bone, cartilage and ligaments. Muscle tissue, which for long has been relatively neglected, has gained more attention in the TE community recently. The view on muscle evolved from being the tissue mainly responsible for locomotion, thermogenesis and postural support to an endocrine organ able to secrete cytokines (termed myokines) that exert beneficial effects on surrounding tissues [260].

Tissue-specific stem cells, termed satellite cells [101], [261]–[263] are responsible for maintaining the regenerative capacity of skeletal muscle. Upon injury, satellite cells can re-enter the cell cycle, proliferate and either fuse to existing myofibers or generate myofibers *de novo*. Since their discovery in 1961 [264], [265], extensive research has been conducted on the regulatory mechanisms guiding satellite cell activity and their role in healthy and diseased muscle [100], [101], [263], [266].

1.1. Pathologic muscle states and muscle loss

Skeletal muscle TE (SMTE) aims at the functional restoration of either lost, atrophic or impaired muscle tissue. Of late, the field has particularly emphasized using cellular and acellular therapeutic approaches for pathological muscle states such as muscular dystrophies, sarcopenia, or traumatic volumetric muscle loss. In the young, regeneration generally occurs efficiently as skeletal muscle can cope with slight injuries due to its high regenerative potential. However, regeneration is inefficient when trauma causes extensive damage or when the muscle is affected by a chronic pathology. This is especially severe in the elderly, where the regenerative capacity of muscle is diminished due to a decrease in the muscle stem cell pool. This leads to progressive replacement of muscle with scar and fat tissue, causing substantial deteriorations in muscle function and motility and thus quality of life. In addition, the loss of muscle associated with aging (sarcopenia) affects a growing number of patients as the global increase in life expectancy leads to population aging. Thus there is an unmet clinical need for approaches to restore or maintain muscle function, especially in the older population which is highly affected by muscle wasting and atrophy [8], [267]–[269]. In contrast to sarcopenia, genetic muscle diseases, such as muscular dystrophies (MDs), result in progressive muscle weakening and breakdown starting already in childhood or middle age. MDs are a group of more than 30 rare hereditary diseases caused by mutations leading to either a dysfunction in, or lack of

proteins essential for muscle stability [270], [271]. MDs greatly vary in the type of muscle affected (some forms of MD may affect cardiac muscle), extent of muscle weakness, the age of onset, the rate of progression and the pattern of inheritance [270].

Duchenne muscular dystrophy (DMD) is the most common MD affecting approximately 1 in 5000 males [272]–[276]. DMD is caused by the absence of functional dystrophin, either through deletion, point mutations, insertions or duplication. Dystrophin is a structural protein, which acts as a linker between the cytoskeleton (via the dystroglycan complex) and the surrounding extracellular matrix (ECM). Dystrophin stabilizes muscle cells under mechanical load and is essential for the maintenance of the intracellular structural organization of muscle cytoskeletal proteins in the contractile apparatus [277]–[279]. Thus, lack of dystrophin predisposes muscle fibers to fragility in response to mechanical forces, leading to continuous cycles of muscle de- and regeneration [280]. Recent evidence additionally suggests that dystrophin is directly involved in regulating satellite cell behavior and that satellite cells from dystrophin knock out animals show lower proliferation rates as well as functional impairment [281]–[284]. As a result, the muscle stem cell (satellite cell) pool is prematurely exhausted, a phenomenon somewhat analogous with aging [285], which eventually leads to muscle weakness, loss of motility and, in the worst case, premature death [286]. Other MD types include Becker MD, a less severe variant of DMD, Emery-Dreifuss MD, facioscapulohumeral MD, congenital MD, limb-girdle MD or myotonic MD [270].

To date, there is no cure for MDs. Although symptomatic treatments such as physical or drug therapies are used to delay disease progression, the prognosis for people with chronic muscle pathologies is poor. This creates a considerable world-wide socioeconomic burden for health systems, patients and caregivers alike. Sarcopenia accounts for roughly $18.5 billion per year in direct healthcare costs in the U.S. [31], [287]. A cross-sectional study in 2014 reported the mean annual direct costs per DMD patient to range from 23,920$ to 54,270$ in Europe and the U.S., which is 7 to 16 times higher than the mean annual per capita health expenditures in these countries [288]. A more recent study focusing on European DMD patients and their caregivers provided similar figures but identified direct non-healthcare costs as the main part of total annual costs [289].

In the past, research on regenerative therapies for diseased skeletal muscle mostly focused on methods to deliver healthy myogenic cells or to restore the endogenous myogenic potential of satellite cells [290]. Although satellite cell transplantation holds great therapeutic potential for MDs, the vast number of cells needed for treatment and their phenotypic changes after prolonged *in vitro* culture limit this approach. In addition to the restoration of the stem cell pool

and host myofiber repair, healthy myogenic donor cells can also act as vectors to (re)establish expression of normal (wild-type) alleles in the muscle fibers they fuse to [291]. However, the pathomechanisms leading to MD phenotypes, muscle wasting, and atrophy are still not fully understood. In addition, the fact that some MD animal models do not faithfully recapitulate the respective disease creates another burden for translation of novel therapies into clinics. Therefore, tissue engineered *in vitro* muscle (disease) model systems can serve as an alternate pre-clinical approach to gain further insight into the molecular causes and potential treatments of chronic pathological muscle states.

1.2 Skeletal muscle tissue engineering

Current clinical strategies to restore muscle function are limited to symptomatic treatments and, consequently, healthcare costs are progressively rising; e.g. healthcare costs of direct and indirect traumatic injury in the year 2000 was greater than $400 billion in the US [32]. SMTE constitutes a promising tool to lower this immense socioeconomic burden, as it enables the creation of new muscle to replace lost tissue without the need of donor tissue. Furthermore, SMTE can be used to study muscle development, and the impact of biomaterials and mechanical cues on myogenesis and muscular disorders in *in vitro* (disease) models [292]. Conducting traditional studies on muscle biology in 3D settings, which more closely mimic the physiological microenvironment of the whole organ [11], is the new state of the art in this rapidly growing field (figure 28). However, so far, TE only successfully entered clinics when it comes to skin, bone or cartilage replacement and regeneration [293]–[298].

Current clinical approaches to compensate for lost skeletal muscle tissue are to transfer skeletal muscle tissue from other sites of the body to the area of injury (free functional muscle transfer). However, this causes donor site morbidity and an extra surgical procedure resulting in additional stress for the patient [60]. The gold standard is the use of freestanding flaps which include functional vessels as tissue grafts. Although free functional muscle transfer is still considered the best option for restoring function in otherwise non-reconstructable muscles, a return to pre-injury levels of muscle strength and functionality does not usually occur. Thus, many research groups are now focusing on *in vitro* SMTE, providing new remarkable data for this field, some of which will be discussed in more detail in the subsequent sections [64], [85], [299]–[303]. To date, the majority of *in vitro* SMTE strategies aim at creating functional skeletal muscle tissue in the lab to offer new therapeutic possibilities for patients suffering from volumetric muscle loss, sarcopenia or genetic muscle disorders [304], [305]. Given the current clinical treatment limitations and the

rising prevalence of pathological muscle states (especially sarcopenia), these patients would greatly benefit from further research on alternative therapeutic approaches.

Another approach is *in vivo* SMTE which involves introducing cells with myogenic potential [61], either as bolus injections or in combination with a scaffold biomaterial, into the site of injury to form and regenerate new muscle tissue [306]. However, this strategy is limited by the vast amount of cells needed [61]. Alternatively, the cell-free approach of *in situ* SMTE has been introduced [307], [308], where instructive biomaterials are grafted into a muscle defect to trigger the endogenous regenerative potential and regenerate the diseased tissue via release of bioactive signaling molecules from the biomaterial implanted into the patient [60]. *Ex vivo* SMTE demonstrates an alternative strategy to *in vivo* approaches, where autologous cells are expanded in cell culture beforehand and eventually reintroduced into the defect site for regeneration [309], [310].

With this review, we would like to highlight the state of the art in SMTE, trigger ideas for refinements and provide the scientific community with putative strategies and criteria to increase the performance and maturity of tissue engineered muscle. Additionally, we give an outlook on future challenges and general considerations for SMTE applications in healthy and diseased muscle.

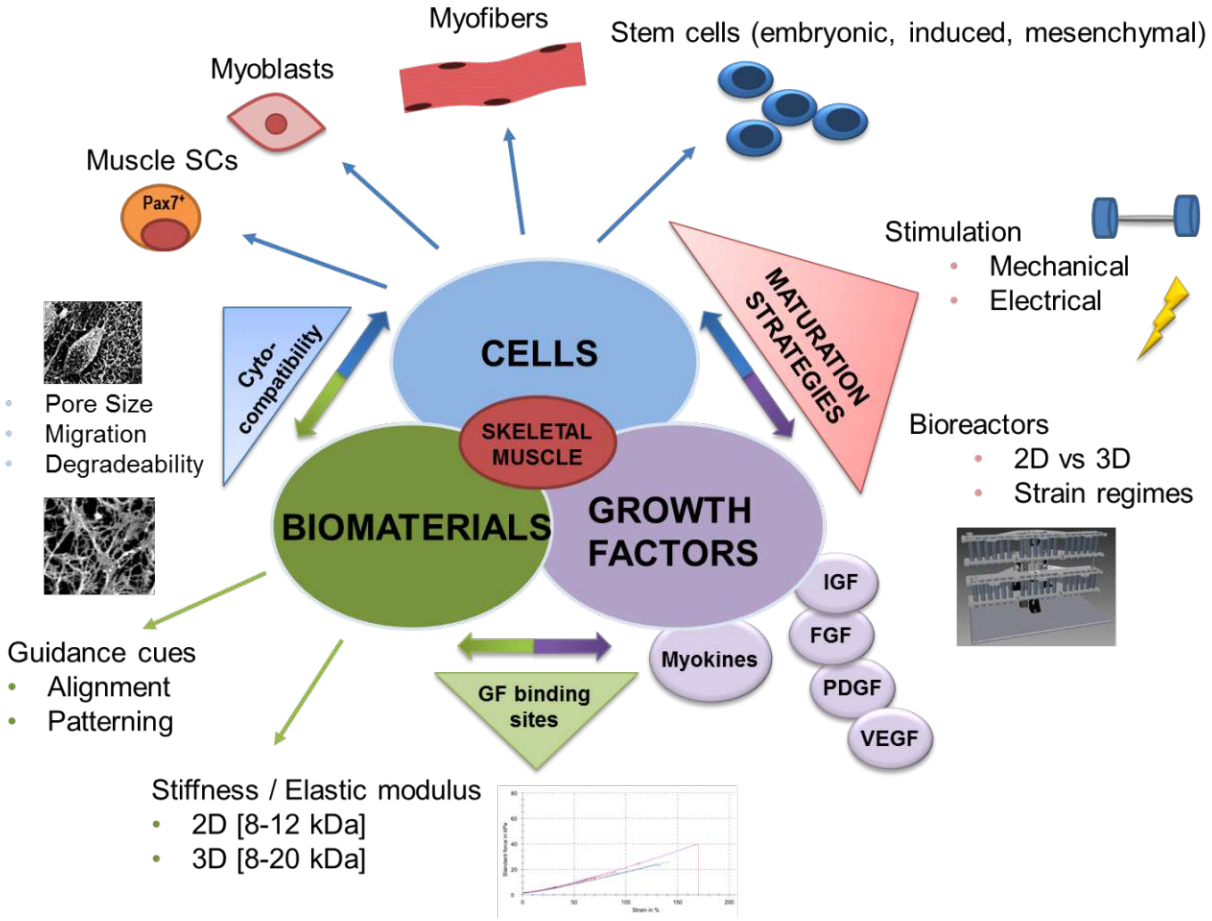

Figure 28: Advances in skeletal muscle tissue engineering – from classic to functional approaches. Until recently, the classic tissue engineering approach was the combination of the following components: biomaterials, cells, and growth factors. In recent years, this classic triad was combined with novel methodologies allowing for more biomimetic approaches. Advances in cross-linking chemistry made it possible to link growth factors to the biomaterial or to provide growth factor binding sites. In addition, guidance cues like patterning or alignment of the biomaterial, as well as the mechanical properties, have been demonstrated to significantly influence cell behavior such as adhesion, migration, and maturation. Likewise, the number of cell types that can potentially be used has increased ranging from cell lines and primary cells to muscle stem cells and cells with mesenchymal stem cells characteristics. One of the major advances in the past has been the incorporation of dynamic culture systems into existing SMTE approaches to improve tissue maturation. In this respect, the most commonly used techniques are electrical or mechanical stimulation via sophisticated bioreactor systems. These bioreactors allow controlled provision of different mechanical or electrical stimuli to drive both early myogenesis and functional maturation. GF, growth factor; 2D, 2-dimensional; 3D, 3-dimensional; SCs, stem cells; IGF, insulin growth factor; FGF, fibroblast growth factor; PDGF, platelet derived growth factor; VEGF, vascular endothelial growth factor.

2 Factors influencing the myogenic outcome (*in vitro and in vivo)*

In vitro SMTE relies on efficient maturation strategies to generate functional 3D skeletal muscle constructs, which firstly requires biomaterials as scaffolds. These scaffold matrices should offer adequate physicochemical properties as well as bioactive cues like incorporated growth factors to enhance myogenic differentiation or cell adhesion motives to improve cellular attachment. Additionally, potent myogenic cells that are able to differentiate into mature myotubes under appropriate environmental conditions are a prerequisite [11]. Finally, effective stimulation strategies in the form of mechanical, electrical or electromechanical stimulation are needed to trigger cell alignment, fusion and differentiation (figure 29). After densely packed arrays of aligned myotubes are generated, the ultimate goal is to implement methods to (pre)vascularize and innervate such muscle constructs before they can serve as functional transplants.

2.1 Biomaterials in skeletal muscle tissue engineering

Natural biomaterials are biocompatible and biodegradable, and thus constitute favorable biomaterials for SMTE. They possess tunable mechanical and structural properties such as porosity, topographical cues, and the option of functionalization with growth factors and/or cell adhesion motives. Furthermore, natural hydrogel materials can be molded into different shapes, which is advantageous for repairing volumetric muscle defects that usually have irregular shapes. However, natural biomaterials harbor potential immunogenicity and sometimes lack of mechanical strength [60], [311]. The most commonly used natural biomaterials in SMTE are **collagen** [81], [82], [319], [320], [125], [312]–[318], **fibrin** [64], [65], [325], [326], [81], [82], [299], [300], [321]–[324], **alginate** [308], [326]–[331], **Matrigel®** [80], [332], **hyaluronic acid (HA)** [333]–[335], **gelatin** [96], [336], **silk fibroin** [337], **chitosan** [307] and **decellularized tissues** (Borschel *et al.*, 2004; Conconi *et al.*, 2005; Coppi *et al.*, 2006; Corona *et al.*, 2014; DeQuach *et al.*, 2012; Machingal *et al.*, 2011; Mase *et al.*, 2010; Merritt *et al.*, 2010; Perniconi *et al.*, 2011; Sicari *et al.*, 2014; Wolf *et al.*, 2012). Common synthetic biomaterials are manufactured from biodegradable polyesters of **polyglycolic acid**, **polyethylene glycol (PEG)**, **polycaprolactone**, **poly(lactic-co-glycolic acid)** and **poly-l-lactic acid** [215], [218], [336], [348]–[353]. These synthetic biomaterials are versatile in use as they are degradable (over weeks to years, depending on the formulation and degree of cross-linking), allow for precise control over their physicochemical properties (e.g. degradation rate, stiffness/elasticity or the presence of topographical or biochemical cues) and usually are considerably cheaper than natural biomaterials. Additionally, they can be used in the form of hydrogels [354]. However, they do not always support cell attachment and adhesion, can potentially cause inflammatory responses (after degradation or through prolonged persistence at the injury site *in vivo*) and lack biomimicry of the native ECM [352]. Therefore, they are often combined or coated with natural biomaterials to present biological recognition cues e.g. integrin-binding motives like Arg-Gly-Asp

to increase cell attachment [60]. An overview of commonly used biomaterials for SMTE and their advantages and disadvantages is given in table 8.

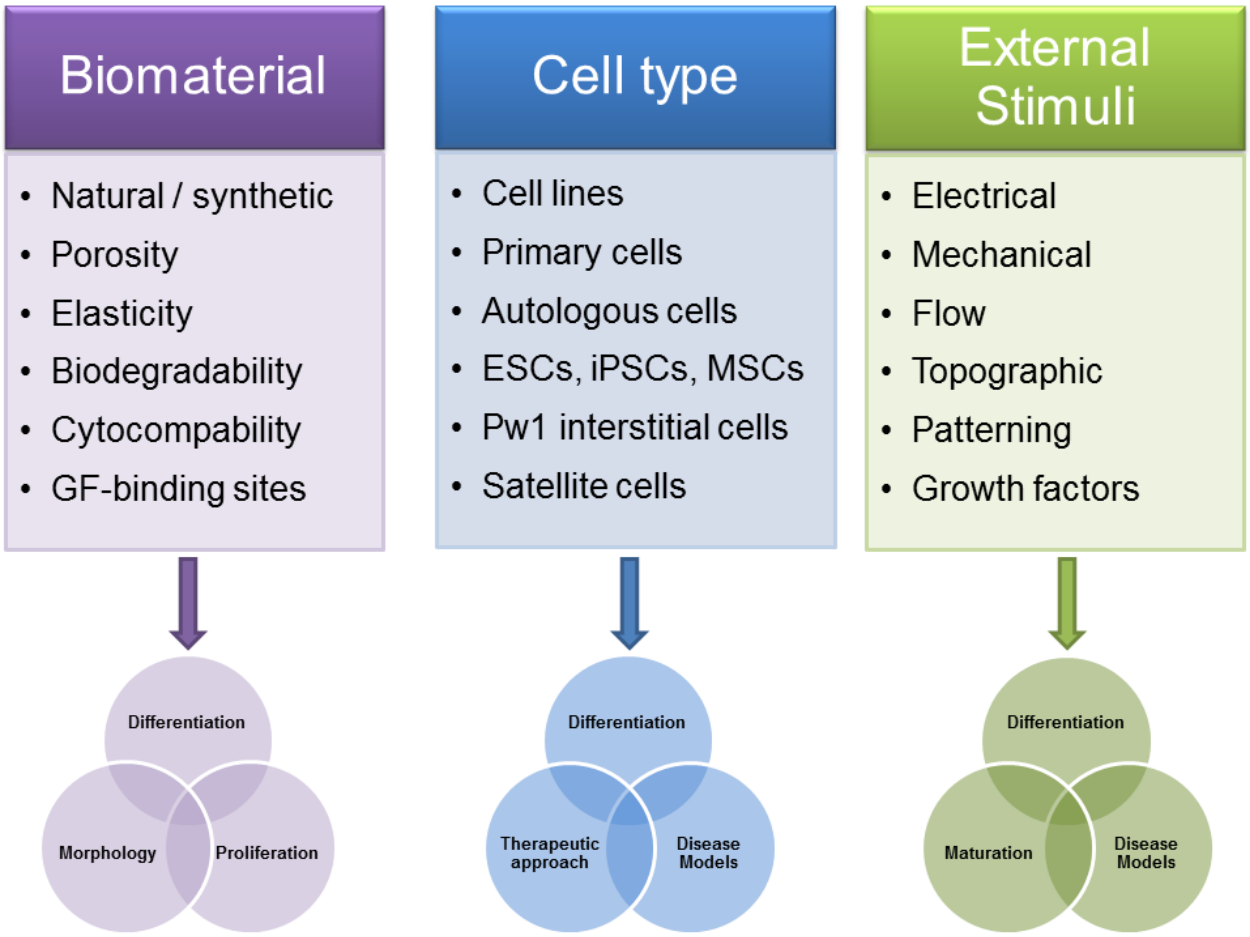

Figure 29: Differences in experimental design of skeletal muscle tissue engineering approaches influence outcome. The choice of the biomaterial and its biophysical properties influence the TE construct in terms of cell adhesion, migration, morphology, proliferation, and differentiation. Notably, differentiation of muscle cells into contractile myofibers is highly dependent on factors such as matrix elasticity, porosity or the availability of growth factors within the construct. The selection of the appropriate cell type is of equal importance as it partially predetermines which scientific questions can be answered using a given SMTE approach. Thus, changing cell types within the same SMTE setup can increase its application range, from studies on different stages in myogenesis or disease modeling to transplantation or cellular gene therapy. Finally, application of external stimuli to cells embedded in biomaterials greatly enhances myogenic maturation. Patterning of the biomaterial via provision of defined topographical cues can drive cell differentiation and further enables control over cell/myofiber arrangement. As engineered muscles are required to create sufficiently large contractile forces upon transplantation, the importance of dynamic culture systems using such stimulation strategies has been unambiguously shown. GF, growth factors; ESCs, embryonic stem cells; iPSCs, induced pluripotent stem cells; MSCs, mesenchymal stem cells; SM interstitial cells, skeletal muscle interstitial cells.

Table 8: Commonly used biomaterials and their useful properties for SMTE.

Biomaterial	Natural / Synthetic	ADVANTAGES	DISADVANAGES	Types of scaffolds	Studies
Fibrin	Natural	Biocompatible, biodegradable, combination of materials possible, functionalization with growth factors, cell encapsulation, injectable, cell adhesive cues, tunable porosity, can enhance myoblast differentiation	Potential immunogenicity, limitation in fabrication due to denaturation, lack of mechanical strength	Hydrogels (application as 3D scaffolds), 2D pattered surfaces, coatings,	[60], [64], [81], [299], [300], [311], [321]–[324]
Collagen	Natural	Biocompatible, biodegradable, combination of materials possible, interconnectivity, macroporous structure, topographical cues, cell adhesive cues, tunable porosity, can enhance myoblast differentiation, injectable	Potential immunogenicity, limitation in fabrication due to denaturation, lack of mechanical strength	Hydrogels (application as 3D scaffolds), 2D pattered surfaces, coatings	[60], [81], [316]–[320], [82], [125], [262], [311]–[315]
Gelatin	Natural	Biocompatible, biodegradable, combination of materials possible, topographical cues, can enhance myoblast differentiation	Potential immunogenicity, limitation in fabrication due to denaturation, lack of mechanical strength	Coatings	[60], [96], [311], [336]
Alginate	Natural	Biocompatible, biodegradable, high surface area, interconnectivity, functionalization with growth factors, cell encapsulation, injectable, cell adhesive cues, tunable porosity, macroporous structure, minimally invasive	Potential immunogenicity, limitation in fabrication due to denaturation, lack of mechanical strength, need for adhesive cues (RGD)	Hydrogels (application as 3D scaffolds)	[60], [262], [308], [311], [326], [328]–[330][353][353][353][349][349][349][346][346][346][345][344][344][343][342][342][341][337][336][335][335][334][335][333][333][333][333][332][332][332][329][335][335][335][335][335][335][335][335][335][335][338][338]
Chitin Chitosan	Natural	Biocompatible, biodegradable, topographical cues, varying mechanical properties, tunable porosity	Potential immunogenicity, limitation in fabrication due to denaturation, lack of mechanical strength	Grooved scaffolds, application as 3D scaffolds	[60], [307], [311]

Biomaterial	Natural / Synthetic	ADVANTAGES	DISADVANAGES	Types of scaffolds	Studies
Decellularized tissues/ECM	Natural	Tunable structural integrity, native structural & biochemical cues, matches host tissue, mechanical properties, bioactive	Potential immunogenicity, processing relies on chemical/biological agents which break down natural ECM structure, acquisition of material more complicated - especially for human tissue	Hydrogels (application as 3D scaffolds), full thickness *in vitro*	[60], [311], [346], [347], [355], [338]–[345]
Hyaluronic acid	Natural	Biocompatible, biodegradable, tunability, injectable, cell encapsulation, minimally invasive	Potential immunogenicity, limitation in fabrication due to denaturation	Hydrogels (application as 3D scaffolds)	[60], [262], [308], [311], [333]
PEG	Synthetic	Biocompatible, high tunability, injectable, cell encapsulation, minimally invasive	Recellularization is slow, poor support in remodeling, lack of adhesive sites for cell attachment	Hydrogels (application as 3D scaffolds)	[60], [262], [352], [356]
PLLA	Synthetic	Biocompatible, combination of materials possible, offer topographical cues, tunability (e.g. groove width and depth), electrically conductive, can enhance myoblast differentiation	Recellularization is slow, poor support in remodeling, lack of adhesive sites for cell attachment	2D patterned surfaces, electrospun fibers with tunable ridge width, alignment and variable composition of polymer material	[60], [215], [356], [357]
PLGA	Synthetic	Biocompatible, biodegradable, combination of materials possible, offer topographical cues, tunability (e.g. groove width and depth), electrically conductive, can enhance myoblast differentiation	Recellularization is slow, poor support in remodeling, lack of adhesive sites for cell attachment	2D patterned surfaces, electrospun fibers with tunable ridge width, alignment and variable composition of polymer material	[60], [218], [336], [356], [357]
PCL	Synthetic	Biocompatible, biodegradable, combination of materials possible, offer topographical cues, tunability (e.g. groove width and depth), electrically conductive, can enhance myoblast differentiation, can be used in drug delivery systems	Recellularization is slow, poor support in remodeling, lack of adhesive sites for cell attachment	2D patterned surfaces electrospun fibers with tunable ridge width, alignment and variable composition of polymer material	[60], [348], [350]–[352], [356], [357]

2.1.1 Hydrogels

Hydrogels are particularly popular in SMTE due to their tunability regarding structure, shape and mechanical stability as well as their amenability to incorporate contact guidance and biochemical cues. Additionally, hydrogels can be functionalized with growth factors or other bioactive molecules to enhance regeneration [60], [142], [330]. 3D hydrogels promote a spatially uniform cell distribution after encapsulation, enabling the generation of dense tissue constructs through high initial cell seeding densities and hydrogel compaction by the cells over time. The high amount of cell-cell contacts promotes and enhances myogenic fusion and increases myofiber length and thickness [322]. Furthermore, 3D environments mimic the physiological conditions of the tissue more closely than 2D cultures. The use of hydrogel-based biomaterials is a promising strategy to introduce therapeutic myogenic precursor cells into a defect for subsequent formation of new muscle tissue *in vivo* [262]. Notably, hydrogels can be injected in a minimally invasive manner to support or fill void spaces after muscle trauma or disease [60].

Collagen is the most abundant protein in the human body and the main constituent of natural ECM, which is why it has been used in a multitude of TE applications [358]. However, if muscle satellite cells (MuSCs) are used, laminin has to be added to match the specific integrin complex formed by α7 and β1 isoforms [359]. In a pioneering study, Vandenburgh et al used collagen gels to incorporate and differentiate avian myoblasts into contractile myotubes with structural characteristics similar to neonatal myofibers [318]. Since then, many other groups have used myogenic precursor cells combined with collagen hydrogels [314], [319], [320], [360]. Okano *et al* highlighted that C2C12 myoblasts combined with 3D collagen gels led to differentiation into multinucleated aligned myotubes, successful capillary infiltration *in vivo*, and remodeling after implantation [316].

Another natural biomaterial for hydrogel production is alginate, a polysaccharide found in seaweed, rendering it a feasible and cheap hydrogel source [361], [362]. An advantage of alginate hydrogels is the possibility to modify them, for example by introducing cell adhesive ligands or adjusting stiffness and degradability [326], [327], [329]–[331]. Alginate hydrogels are used in many medical applications, including wound healing management or the delivery of bioactive molecules due to their low toxicity and good biocompatibility [363].

The ECM component HA is also used for the fabrication of hydrogels by photo cross-linking via UV light treatment [262] or by chemical cross-linking [364]–[366]. HA enhances myoblast proliferation and differentiation. However, degradation by hyaluronidases *in vivo* is difficult to control, which may lead to apoptosis of the introduced cells due to loss of attachment to the material [262].

Fibrin is a favored biomaterial to produce hydrogels. It is the end-product of the blood clotting cascade, formed when fibrinogen is cleaved by thrombin [367]. As fibrin is a natural component of the human body like collagen and HA, it provides attractive features, including biocompatibility, biodegradability and non-toxicity. Encapsulating myogenic cells in fibrin hydrogels provides cues to trigger growth and differentiation into myotubes and eventually to myofibers [292]. Further advantageous features include tunability of its structural network, modifiable polymerization [262] and the potential for incorporating growth factors [71]. Some studies claim fibrin to be superior to other biomaterials (e.g. collagen I) due to the strong integrin binding (integrin α7 and α5) of myotubes to fibrin [368], [369]. This effect is more pronounced in fibrin, as myotubes do not have the collagen I specific integrin α2 receptor. Therefore, a fibrin environment is more conducive to distributing contractile forces from myocytes [292]. The major drawback of fibrin is finding an appropriate material density that balances the required material integrity to mimic natural stiffness and sufficient porosity for nutrient transport and cell migration [367], [370]. Fibrin hydrogels have been used successfully in numerous SMTE approaches using different stimuli to enhance differentiation [64], [299], [300], [321]–[323].

Injectable hydrogels derived from decellularized muscle ECM may offer a more flexible approach than whole decellularized muscles [342]. Although muscle ECM breakdown and subsequent processing into hydrogels destroys all existing architectural cues of the ECM (such as the vascular bed), the hydrogel formulation's composition in terms of proteins, growth factors and cytokines is preserved and can still instruct endogenous regenerative processes. Importantly, hydrogels can be produced from xenogeneic ECM sources, such as porcine dermis, submucosa or urinary bladder [347], [371], circumventing the need for autologous muscle ECM which would be inapplicable in clinics due to donor site morbidity.

Synthetic hydrogels based on PEG are cytocompatible and offer tremendous variability for chemical manipulation. For SMTE applications, PEG can be tailored to mimic the natural stiffness of skeletal muscle tissue [292] and seems to be a promising biomaterial for myogenic differentiation [262]. Laminin-coated PEG hydrogels, as an example of combined synthetic and natural materials, favored MuSC proliferation and differentiation *in vitro* [262]. PEG combined with fibrinogen constitutes a promising scaffold to embed skeletal muscle-derived pericytes [372] or mesoangioblasts [83], [373] and favors differentiation of cells and regeneration of muscle tissue. Moreover, PEG-based hydrogels can be functionalized with different growth factors to directly promote muscle regeneration *in situ*, recruit endogenous stem cells to the site of injury, or enhance differentiation of muscle progenitor cells on/in the gel [374], [375].

2.2 Cells for muscle tissue engineering

Another essential factor influencing the myogenic outcome is choosing appropriate cells when generating functional muscle tissue constructs. The pool of cell types scientists can choose from has grown enormously in recent years and a variety of cell populations that are able to differentiate along the myogenic lineage have been identified [97]. In addition, new techniques, such as the generation of patient-specific induced pluripotent stem cells (iPSCs) or gene editing via the CRISPR/Cas9 technology have opened new therapeutic possibilities, especially for the treatment of MDs.

The two main groups of cells potentially being used for SMTE are either freshly isolated and expanded primary cells or immortalized cell lines. The main application of immortalized cells is the establishment of model systems, whereas primary cells are used in clinical applications and for implant studies. Myoblasts, satellite cells and stem cells from various sources are employed in different therapeutic approaches to improve muscle regeneration and function [61]. The most prominent type of primary myogenic cells are MuSCs, which demonstrate a high proliferative capacity, have the ability to self-renew and differentiate into myotubes [60], [101]. Autologous MuSCs cultured with homologous acellular muscular matrices enhances their engraftment, and subsequently those matrices can be used as transplants to compensate for tissue loss [376]. A drawback is that they have poor survival and engraftment rates after injection into damaged tissue [377]. MuSCs can be isolated either via enzymatic digestion of muscle tissue or via cellular outgrowth by plating single muscle fibers onto protein-coated dishes, which serve as a niche for satellite cells [100], [292]. However, a drawback of satellite cells is that once activated and differentiated into myotubes they cannot be brought back to a self-renewing state. Thus, the pool of cells able to proliferate and build new myotubes is eventually exhausted [102].

Over the years, other tissue resident cells have been discovered, namely interstitial skeletal muscle progenitor cells, which constitute a heterogeneous cell pool and seem to derive from the interstitium near the blood vessels [102]. They offer a great regenerative potential and have already been used in studies of rodent and human SMTE. Pw1 interstitial cells, a fraction of interstitial skeletal muscle progenitor cells [103], originate upstream of MuSCs in the muscle precursor lineage and can induce the formation of MuSCs. Therefore, their presence is a key factor in the satellite cell niche [378]. In the murine model, Pw1 interstitial cells enhanced muscle regeneration by releasing paracrine growth factors. Other subsets of skeletal muscle interstitial cells that play important roles in inducing muscle differentiation are fibroadipogenic progenitors, pericytes and mesoangioblasts. All three cell populations are promising for SMTE approaches, since they are capable of ameliorating myogenic regeneration, offer high proliferative rates, and can be genetically modified [104]–[106], [108], [110], [379], [380]. These characteristics also increase their relevance for potential MD treatments [381]–[384]. Furthermore, these cells are suitable for regenerative medicine approaches due to their good survival rates and their ability to fuse to preexisting myofibers, thereby promoting muscle regeneration *in vivo* [104]–[106], [108], [381], [385].

Another cell type with great potential for regenerative medicine is mesenchymal stem cells (MSCs). MSCs are multipotent cells capable of migrating to the site of injury to promote tissue repair [112], [386] and reducing inflammation [113]. MSCs are able to differentiate into the myogenic lineage [112]. Furthermore, they enhance muscle fiber formation and regeneration *in vivo* [113], [114], [116], [386], [387]. This might be due to their support of functional satellite cells when implanted in murine muscle tissue [114] and through recovery of expressed mechano growth factor, which is crucial for skeletal muscle maintenance and repair [388]. This positive effect on muscle regeneration has been validated in *in vivo* disease models, where autologous MSCs were transplanted into crush trauma injuries in rats [60], [117]. MSCs' therapeutic effects may also stem from their ability to secrete soluble paracrine factors [113], [118] including Interleukin (IL)-6, IL-10, stromal cell-derived factor [389]–[392], vascular endothelial growth factor, fibroblast growth factor (FGF), IL-1, matrix metalloproteinases (MMPs), platelet derived growth factor, transforming growth factor ß, angiopoyetin [120], [393], hepatocyte growth factor, and adrenomedullin [394]–[396]. Via secretion of these factors, MSCs assert substantial anti-inflammatory effects by modulating the immune response [397]. However, a study by Ferrari et al reported that bone-marrow transplantation did not ameliorate the dystrophic phenotype in *mdx* mice, a widely used mouse model for DMD [398]. One suggested reason for the low regenerative potential of MSCs in this setting was that a vast number of cell types is present in the bone-marrow, which resulted in relatively low numbers of MSCs actually being transplanted in the course of a bone-marrow transplantation (reviewed by [399]). Alternative cells used for SMTE are L6 rat myoblasts, neonatal muscle-derived progenitor cells and xenogeneic cells derived from adult muscles from other species [301].

Human or murine embryonic stem cells represent another regularly used source for obtaining skeletal myoblasts. It is possible to obtain $CD73^{+}$ multipotent mesenchymal precursors, which can be differentiated into myoblasts by co-culturing them with C2C12 cells [400]. Since their generation by Yamanaka et al in 2006, iPSCs have been widely implemented in different research areas. This technique makes it possible to reprogram cells directly from patients for autologous cell therapy of MDs [401], [402]. Since iPSCs can be derived from healthy or diseased patients, they offer great potential in TE for disease modeling and drug testing [403]. Such autologous patient-derived cells are non-immunogenic and, in addition, genetic defects can be corrected during *ex vivo* culture using tools such as CRISPR/Cas9. Interestingly, iPSCs generated from mesoangioblasts were shown to fuse to existing muscle with higher efficiency than iPSCs generated from fibroblasts [401]. An important proof-of-concept study was performed by Tedesco et al, who used genetically corrected iPSCs derived from myoblasts or fibroblasts of limb-girdle MD patients, differentiated them into mesoangioblasts and grafted them into affected muscles in a humanized limb-girdle MD mouse model [404]. This not only ameliorated the dystrophic phenotype and restored the depleted satellite cell pool, but importantly also demonstrated that treatment with patient-specific iPSC-derived cells can be utilized for stem cell therapy in MDs. However, it has to be noted that there are still limitations regarding both the use

of embryonic stem cells, which raise ethical concerns [405], and iPSCs, which entail the risk of genetic recombination and tumor formation. To date, iPSC-based regenerative stem cell therapies have not entered clinics due to these safety considerations [10], [406].

Finally, one of the most widely used cell line in SMTE are C2C12 murine myoblasts, established in 1977 from MuSCs derived from a C3H mouse [407]. Many researchers start their initial experiments with these cells, as they are easy to cultivate, proliferate rapidly, and differentiate well upon serum deprivation. Thus, they represent an ideal tool to evaluate new biomaterials or bioreactor systems for the generation of skeletal muscle tissue. However, due to the immortalization of the cells, translation into clinical use is not feasible. Human cell lines, however, may still serve as attractive cells for *in vitro* studies. A recent transcriptomics analysis revealed that immortalization of C25 human myoblasts neither interferes with their myogenic potential, nor with any other aspect of cell physiology - apart from the elicited protection against senescence [99]. Biomimetic *in vitro* skeletal muscle disease models employing patient-derived human myoblast lines may therefore provide a higher predictive capability than rodent *in vivo* models.

2.3 Stimulation strategies for enhancing maturation of 3D bioengineered muscle constructs

Besides choosing the appropriate biomaterial and cell type, another key element that needs to be addressed is suitable stimulation strategies (either mechanical-, electrical-, or electromechanical stimulation), which are indispensable for enhanced muscle maturation *in vitro*. Cells are highly responsive to their microenvironment such as the surrounding ECM, mechanical forces, and biochemical signals. Furthermore, the mechanical properties of biomaterials, such as the material stiffness or the presence of distinct microarchitectural features, can influence cellular behavior tremendously [10], [86], [408]. The stiffness/elasticity of a material is usually assessed by measuring the Young´s modulus (elastic modulus) which is determined by a material's composition and capability for deformation.

One strategy to mimic the natural environment is the application of biochemical and/or biophysical stimulation to engineered constructs. Exercise can be simulated by the application of mechanical stimuli, such as cyclic and/or static strain. Exercise leads to the activation of satellite cells and subsequent fusion to already existing myofibers *in vitro* [409] through triggering the release of hepatocyte growth factor and nitric oxide (NO) radicals, which in turn activate the satellite cells. NO is produced by nitric oxide synthases which are up-regulated by exercised or injured muscle tissue *in vitro* and *in vivo* [410].

Regarding myogenesis, passive (e.g. bone elongation during development) as well as active (e.g. exercising during sport) mechanical stretching is essential for the development of skeletal muscle from embryonic to adult tissue [322], [411]. An appropriate stimulation protocol can exert a positive effect on gene regulation, protein expression and thus proliferation and differentiation

of cells [125], [411], [412]. Furthermore, exercise training improves fusion and alignment of myofibers [50], [322], [413], and enhances the generation of mature myofibers [412]. Morphologically, mature skeletal muscle tissue is characterized by widespread sarcomeric patterning, which is indispensable for contraction. Moreover, mechanical stimulation causes an increase in the cross-striations of the tissue and a switch of myosin heavy chain isoforms from embryonic to adult [292].

One of the first studies implementing mechanical stimulation was conducted by Goldberg et al in which hypertrophy was induced by overloading of synergistic muscle within just 24 hours [414], [415]. Further sophisticated mechanical stimulation protocols were conducted using bioreactors with mechanical stimuli to create dynamic 2D or 3D culture systems. These studies are listed in more detail in table 9 [49], [50], [132], [133], [320], [416], [60], [64], [66], [124]–[127], [129].

Muscle tissue can also be stimulated with electrical stimulation, which positively affects myogenic gene regulation as well as protein expression [125], [411], [412]. Motor neurons are responsible for innervating muscle fibers and the signal inducing contraction of the muscle tissue is distributed via branched axons [417]. Electrical stimulation aims to recapitulate the processes of innervation by fast and slow motor neurons, which are responsible for the switch of muscle fiber types [418], [419]. Electrical stimulation of mouse myoblasts improves myogenic differentiation [420] and enhances their contractile properties compared to unstimulated controls [421], [422]. In monolayer myogenic cultures, twitches happen spontaneously after the formation of myotubes, but electrical stimulation is needed for a controlled and sustained contraction. Chronic periods of electrical stimulation are relevant for the formation of mature phenotypes in muscle tissue constructs as well as to improve their contractile properties [423]. Many groups have applied sophisticated electrical stimulation protocols to muscle cells *in vitro* [421], [424]–[428] (table 10).

To the best of our knowledge, so far there is only one published study combining both electro- and mechanical stimulation for engineering mature muscle constructs [416] (table 10). In literature, there is only one bioreactor system reported, which combines the application of electrical and mechanical stimulation of 3D constructs. It is a commercially available system from EBERS Medical Technology, Spain, and allows for media perfusion under sterile conditions [423]. An overview of bioreactor systems used in SMTE with their used electrical stimulation protocols and the observed outcome is given in table 10.

Table 9: Summary of bioreactor systems with corresponding mechanical stimulation protocols

MECHANICAL STIMULATION

Cells	Biomaterial	Set-up	2D / 3D Culture	Stress regime, Frequency [Hz]	Strain [%]	Time span of stimulation	Outcome	Studies
Embryonic avian pectoralis muscle cells	Collagen constructs	Mechanical cell stimulator device (computerized)	3D	Cyclic ramp stretch at a rate of 0.35 mm/h	Up to 300%	3 days	Increase of proliferation, fusion and myotube length	[413]
C2C12 myoblasts	Collagen hydrogel	Stimulation of rod-shaped tissue via custom-designed stress chamber	3D	Cyclic, 60 Hz	5%	7 days	Dense, oriented myotubes	[124]
Myoblasts	Porous collagen scaffold	Stimulation via Bio-Stretch system	3D	Continuous or cyclic uniaxial rapid ramp stretch (RRS) or cyclical ramp strain (CRS)	7.5% and 15%	6 hours	MMP-2 expression, and hence extracellular matrix remodeling, is up-regulated in response to strain	[127]
Human skeletal muscle cells	Collagen / Matrigel ® Mix	Stimulation of hBAMs by custom-made mechanical cell stimulator	3D	5-pulse at 5 Hz bursts for 2 mins afterwards 28 mins resting phase	5% on day 8-10, 10% on day 10-12, 15% on day 12-16	8 days	Enhance myofiber diameter and area diminished tissue stiffness	[125]
Myoblasts	Fibrin	Use of custom-made device	3D	Tensile strain	25 or 50%	7 days	Fiber alignment along direction of strain	[64]
Primary muscle precursor cells	Collagen based acellular ECM scaffolds	Computerized bioreactor system	3D	Cyclic stretch	10%	5-21 days	Generation of fast twitch and tetanic force after implantation	[49]

MECHANICAL STIMULATION

Cells	Biomaterial	Set-up	2D / 3D Culture	Stress regime, Frequency [Hz]	Strain [%]	Time span of stimulation	Outcome	Authors
Adult rat Muscle progenitor cells (MPCs)	BAM scaffolds from acellular bladder ECM	Stimulation via computer-controlled bioreactor system	3D	Cyclic stretch 3x per min, for the first 5 mins every hour	10%	7 days	After implanting improved host recovery	[129], [429]
Rat primary cells	Collagen	Sliding chamber model	2D	Isometric tension	n/a	21 days	3D constructs made of aligned myotubes	[320]
C2C12 myoblasts	Collagen constructs	Mechanical loads applied by tensioning culture force monitor bioreactor	3D	Repetitive cyclic stretch ramp stretch	1% 10%	up to 12 hours	IGF-IEa > upregulated by single ramp stretch, reduced by repetitive cyclic stretch MGF > upregulated by single ramp stretch and cyclic stimulation	[133]
C2C12 myoblasts	Aligned electrospun polyurethane (PU) fibers	Tubular custom-made setup, computer program controlled	2D/3D	Repetitive cyclic stretch, 1 Hz for 1 h every 6 h	5 or 10% with or without pre-strain of 5% static	2-14 days	Alignment, contractile proteins	[416]
C2C12 myoblasts	Biodegradable microfibrous scaffold (DegraPol(R))	Stimulation of constructs via custom made bioreactor	3D	2 days ramp stretch (3.3%), afterwards cyclic stretch (5 pulse, 0.5 Hz, 3.4% burst stretches	6.7%	7-10 days	Enhanced MHC expression	[126]
C2C12 myoblasts	Fibrin hydrogels	Stimulation of constructs via MagneTissue bioreactor	3D	Static strain	10%	9 days	Increased gene expression, myotube diameter and length	[322]

Table 10: Summary of bioreactor systems with corresponding electrical and electro-mechanical stimulation protocols.

Cells	Biomaterial	Set-up	2D / 3D Culture	Stress regime, frequency (Hz), (V), pulse width, strain (%)	Time span of stimulation	Outcome	Studies
ELECTRICAL STIMULATION							
Primary rat myoblasts	Fibrin	Biphasic stimulation of culture slide chamber via platinum electrodes	3D	6.8 mA (4 ms duration), bursts at 250 ms > intervals every 4s	Up to 8 days	No evidence of differentiation and fusion	[424]
Rat primary cells (fast muscle)	Fibrin	Stimulation of myooid constructs via custom build force transducer	3D	5 pulses at 20 Hz / 4s at 5 V, 1.5 ms	After culturing of 14 days	Increase in contractility and an enhancement of 15 % in TPT and 14 % in ½ RT	[426]
90% C2C12, 10 % 3T3	Fibrin	Stimulation of myooid constructs via custom-made stimulation bioreactor	3D	4 pulses, periods at 1.25, 2.5 and 5 V/mm, 0.1 ms in a 400 ms train, recovery of 3.6 s	7 days	2.5 V/mm seemed to be the optimum as it demonstrated a stronger force production and excitability	[427]
90% C2C12, 10 % 3T3	Fibrin	Stimulation of constructs via custom-made electrical stimulator	2D/3D	0.7, 1, 1.4 V/mm, 0.25 to 1, 4, 9 and 16 ms pulse width	24 hours	Electrical field higher than 0.7 - 2.5 V/mm + pulse width of 1-4 ms > showed enhanced force productions, stronger force dynamics	[428]
C2C12	n/a	Electrical pulse stimulation of coverslips	2D	40 V/60mm, 1Hz	8 days after differentiation for 1 hour, 2 hours or 6 hours	Development of contractile activity by application of 2 hours stimulation at 1 Hz, decrease of contractility when applying electrical stimulus for more than 4 hours	[421]
C2C12, muscle progenitor cells (MPCs)	Collagen type I	Bipolar field stimulation of mBAMs via C-Pace Culture Pacer	2D/3D	4 V/cm, 6 ms pulses at 2 Hz	48 hours started on day 0, 1, 2 or 3	More mature cross-striations in MPC mBAMs than C2C12 and fast to slow MHC isoform switch in MPC mBAMs	[425]
ELECTROMECHANICAL STIMULATION							
C2C12 myoblasts	Electro spun polyurethane (PU)	Tubular custom-made set up, computer program controlled	2D/3D	Cyclic stretch, 4 V/mm, 1 Hz, 5%	1hour mechanical strain, resting time 5 hours + 7 days of electrical stimuli	Enhanced myotube formation, increase in alpha actinin + MHC	[416]

2.4 Myokines released by exercised muscle tissue and their effect on various tissue types

Myokines are another factor influencing muscle as well as other tissues and therefore might offer an interesting therapeutic option to treat patients in future. They are released by muscle tissue in response to exercise training. It is known that regular exercise has beneficial effects on overall health status. Accumulating epidemiologic evidence suggests that physical activity plays an independent role in preventing frequent chronic diseases like osteoporosis, diabetes, Alzheimer´s, osteoarthritis or degenerative muscle conditions, and that the beneficial effects of exercise training are partially due to secreted myokines [260], [430], [431].

Skeletal muscle has been recognized as an endocrine organ due to its ability to produce, store and secrete hormones and myokines. In particular, myokines are able to affect and regulate inflammatory and metabolic processes in muscle and in many other tissues in an endocrine or paracrine manner [432]–[435]. To date, there are 69 putative myokines, which are released via exercise training [436].

So far, the most prominently investigated myokines are IL-6 [433], IL-7 [437], IL-8 [438], IL-15 [439], leukemia inhibitory factor [440], FGF-21 [441], [442], insulin-like 6 [443], follistatin-like 1 [444], musculin [445], irisin [446], myonectin [447], secreted protein acidic rich in cysteine (SPARC) [448] and Meteorin-like 1 [449].

IL-6 is a pleiotropic myokine and acts on muscle tissue by influencing satellite cell activation and differentiation, which is usually triggered by stress due to injury or mechanical stimulation [450]. It is the first myokine to be released after acute exercise [451]. Besides primarily acting on muscle, other organs such as adipose tissue, the liver and the brain are responsive to secreted IL-6 [452]. Secondly, it negatively regulates pro-inflammatory cytokines [432], [453] such as tumor necrosis factor alpha and elevates levels of anti-inflammatory cytokines e.g. IL-10 and IL-1 receptor antagonist released from leukocytes [452]. On the other hand, IL-6 is also considered a pro-inflammatory cytokine. Therefore, further investigations are needed to identify the exact role of IL-6 in muscle and other influenced tissues [454].

Leukemia inhibitory factor belongs to the IL-6 superfamily [455] and is secreted by hypertrophic muscle [456]–[458]. It is also released upon resistance training in human muscle and in electrically stimulated cultured human myoblasts [440]. Studies in rodents demonstrated that production of IL-6 and leukemia inhibitory factor help to regenerate muscle tissue after injury by activating satellite cells [459]–[462].

Irisin is a hormone-like myokine secreted during exercise [446]. It plays an important role in bone-muscle cross talk, and supposedly influences both tissues [463]. This might explain why diseases like osteoporosis and sarcopenia are linked to each other [464]. Studies suggest that myokines like IL-6, IL-8 and IL-15 indirectly influence bone via acting on other tissues, while irisin affects bone tissue directly by increasing the differentiation of osteoblasts *in vitro* as well as enhancing cortical bone mass *in vivo* [463], [465]–[467]. Irisin also reduces body weight when

administered to obese patients [463]. Another study showed that irisin uptake reduces body weight due to increased adipocyte and glucose metabolism and even elevated oxygen intake levels in an animal model [446]. Irisin has the potential to transform white adipose tissue into brown adipose tissue, which is metabolically very active. This is supposed to ameliorate obesity and is called browning [468]. Furthermore, Colaianni et al conducted a study in which they analyzed conditioned media from muscle cells of mice performing exercise training. They found that Irisin levels in the media caused a stronger differentiation of bone marrow stromal cells into osteoblasts (Colaianni *et al.*, 2014).

Another myokine, Meteorin-like 1, also induces adipose tissue browning [449]. The myokines IL-8 and Fstl-1 both induce angiogenesis [438], the latter by inducing endothelial cell-mediated neovascularization in ischemic tissue [444].

IL-15 as well as IL-15 receptor alpha are involved in anabolic/catabolic regulation of skeletal muscle tissue (Busquets *et al.*, 2005; Furmanczyk and Quinn, 2003; Pistilli *et al.*, 2007; Quinn, 2002; Quinn *et al.*, 1995; Riechman *et al.*, 2004). IL-15 enhances the expression of myosin heavy chain in differentiating myocytes [473] and myotubes [470], [472]. One session of resistance exercise is sufficient to increase IL-15 levels in trained and untrained humans (Riechman *et al.*, 2004). Furthermore, Quinn et al found high levels of IL-15 to reduce fat mass and therefore lower adiposity in mice [439].

In 2012, Seldin et al identified another myokine called myonectin. Higher levels of myonectin were secreted into the media by differentiated C2C12 compared to non-differentiated cells. Furthermore, exercise elevated the expression of myonectin in muscle and it is putatively involved in the cross talk between muscle and other tissues like liver and adipose tissue [447].

Another exercise-induced myokine, musculin, is activated by calcium signaling via the AKT pathway [475]. Its function is to enhance mitochondrial biogenesis, which improves physical perseverance [445], [475].

SPARC is a myokine found in humans and mice and secreted during muscle contraction [448]. Catoire et al first identified SPARC to be released upon exercise training through secretome analysis [436]. SPARC affects many crucial mechanisms in the cell such as regulation of cell shape, differentiation and adhesion [476]. SPARC additionally affects insulin secretion in humans [477] and erythropoiesis in mice [478]. Interestingly, the duration of the exercise seems to be more important than the intensity of the exercise for its secretion [448].

3 Disease models

To this day, there are no effective cures for muscular dystrophies, hence there is an urgent need for models mimicking them. Novel biomimetic disease modeling platforms could offer a way to understand and study underlying mechanisms of such diseases and furthermore to test potential treatment options. Muscular dystrophy disease models have been used to study the underlying mechanisms, course of the disease over time, as well as therapeutic agents. Some of these will be discussed in the next sections. Animal models are the cornerstone of research on elucidating the mechanisms underlying dystrophies and on developing new treatment strategies. To date, there are around 50 *in vivo* animal models for studying muscular dystrophies in various species ranging from invertebrates (e.g. *Caenorhabditis elegans*), non-mammalian vertebrates, especially zebrafish [33], to mammals (e.g. mice, rats, dogs and pigs) [34]. The most commonly utilized mammalian DMD models are the mdx mouse model, the mdx utrophin double mutant mouse model (mdx:utrn$^{-/-}$) and the canine x-linked MD model (cxmd) [35]. A frequently used model system is the *mdx* mouse that carries a mutation in the dystrophin gene, resulting in a DMD phenotype. However, there are significant differences in the course of the disease in human DMD patients and *mdx* mice regarding characteristics, such as lifespan, severity, timeline, body weight, impact on other physiological functions and many more [479]. Canine DMD models offer a way to overcome these obstacles, as they present fewer differences to the human DMD pathology regarding the aforementioned characteristics. Furthermore, dystrophic dogs are more suitable for studies using gene therapy approaches than mice, since the former presents a closer simulation of the human immune response towards introduction of vectors for gene repair and replacement [34]. Thus, development of new strategies to introduce vectors evading the immune system is facilitated [480].

3.1 *In vitro* skeletal muscle disease models

Despite the immense amount of knowledge gained on the pathophysiology of skeletal muscle diseases, animal models entail certain disadvantages and ethical considerations. They cannot recapitulate the exact manifestation of the disease in regard of physiological, biochemical and clinical conditions as they appear in the human body. This has prompted research trying to find appropriate time and cost effective alternatives [35], [36]. Furthermore, results gained from *in vivo* drug testing setups frequently fail when translated to the clinics, due to major differences in underlying molecular mechanisms between different species. *In vitro* human disease models are a potential way to overcome these limitations. They can more closely mimic human pathological conditions concerning tissue and organ specific cell types [36] through the possibility of using patient-derived cells, which reflects the patient's individual skeletal muscle physiology and the disease progression in the dystrophic state [271]. Moreover, it is possible to change single parameters within these systems and study the resulting effects, which constitutes another advantage of *in vitro* disease modeling [303].

In general, miniaturizing disease models has gained attraction in the past years, as it allows reduction in cell number and reagents (and, thus, overall costs), while maintaining the quality of results. Additionally, the assessment of results and provision of external stimuli can be carried out in a precise and controlled manner. Thus, research on microfluidic devices for disease modeling has emerged in recent years [303]. One microfluidic system by Ferreira et al used a different approach in modeling dystrophy. Instead of using cells with a diseased phenotype, they established a device that mimicked the cellular environment of dystrophies. This was done by using different ECM compositions and applying a concentration gradient of basic FGF (bFGF), which is known to be released upon muscle injury. Thereby, it was possible to assess the influence of bFGF and different substrates on myoblast recruitment in normal or DMD simulating environments [481].

Another miniaturized 2D *in* vitro disease model was published by Serena et al, who created myotubes derived from primary myoblasts from healthy donors as well as patients suffering from DMD cultured on polyacrylamide hydrogels. This was achieved through adequate substrate design, including appropriate mechanical properties (*i.e.* a Young´s modulus of 15 kPa). Furthermore, micro-patterning the substrate in parallel lanes to enhance myotube alignment and coatings with the adhesion molecules laminin, fibronectin and Matrigel ® were utilized as well. Thereby, it was possible to generate myotubes positive for myosin heavy chain II and α-actinin that developed a highly ordered sarcomeric patterning. Furthermore, myotubes generated from healthy donors exhibited dystrophin expression. This is a key aspect for assessing the functionality of DMD therapies, as they often aim at restoring dystrophin expression [158]. The basic principle of this test system was recently used to study the potential of mesoangioblasts in DMD treatment as they ameliorated dystrophin distribution in DMD myoblasts [482].

The course of dystrophies varies widely from one patient to another, as the mutations causing the disease are very heterogeneous, ranging from severe forms completely lacking dystrophin to a partially functioning truncated form of the protein. This variance cannot be considered in animal or standard *in vitro* models. Creating iPSCs from patient-derived cells offers a solution to this problem, since it allows direct comparison of the pathological phenotype of the patient and the cultured cells. This makes drug screening results and the evaluation of specific genetic aberrations more reliable. Therefore, they present a promising tool for modeling a variety of diseases. Also, recent advances in the field of iPSC research have boosted the efficiency of reprogramming. Myogenic progenitor-derived iPSCs showed good engraftment after transplantation, were able to regenerate myofibers and could repopulate the stem cell niche [402], [483], [484]. Nevertheless, this approach also bears certain disadvantages such as the lengthy processes involved in generating iPSCs and inducing differentiation into iPSC-derived myogenic progenitors, or the need to integrate so-called reprogramming factors, which could have unknown implications on the phenotype of the disease [271]. Tanaka et al were able to create myotubes from human iPSCs derived from Miyoshi Myopathy patients through inducible MyoD1 expression. These myotubes exhibited hallmarks of the disease, such as the role of

Dysferlin during this disease. A lack of Dysferlin expression led to inefficient membrane repair, which could be overcome by an induced overexpression of Dysferlin, rescuing dystrophic myotubes and leading to a healthy phenotype. These results suggest that this model has the potential to shed light on the pathology of the disease, and may be applicable to other types of dystrophies [485]. Another study using human iPSCs from DMD and Becker MD patients was published by Abujarour *et al.* Human iPSCs were subjected to MyoD1 overexpression, inducing myogenic commitment and finally yielding myotubes. To investigate whether this model has the potential to be used for drug testing, dystrophic myotubes were subjected to IGF-1 and Wnt7a treatment, factors that elicit skeletal muscle hypertrophy. A treatment with these two factors resulted in significant increase in fiber diameter, suggesting usability of this model for drug testing [486]. Nevertheless, to date these models have not been used to test drugs or other therapies for DMD.

However, it is not possible to accurately mimic the complex organization of tissues *in vivo* using 2D disease models. Thus, drug-screening results gained from these systems cannot directly be translated for the use in clinical studies. To overcome the limitations of 2D cell-based systems, more recent research has focused on the development of 3D systems that more adequately reflect the *in vivo* situation [38], where cells can interact with the matrix they are embedded in and form 3D structures [303]. A 3D drug testing platform was established by Madden and colleagues using human primary myoblasts grown in so-called myobundles generated by incorporation in fibrinogen and Matrigel® frames using polydimethylsiloxane molds. The bundles differentiated into chemically and electrically responsive muscle-like constructs capable of contraction. To prove their suitability for drug screening, the myobundles were treated with three different drugs, namely statins that induce muscle weakness, chloroquine that induces autophagy and clenbuterol which increases hypertrophy in low doses but leads to apoptosis and necrosis at higher concentrations. Overall, treatment with these compounds resulted in the expected outcomes. Therefore, this model appears suitable for drug testing. However, its usability as a disease model to study the pathophysiology of dystrophies remains to be established, as it has only been examined with cells derived from healthy donors [487]. Thus, there is only one actual *in vitro* skeletal muscle disease model reported in 3D so far. This model used dystrophic myoblasts from *mdx* mice that were incorporated in natural hydrogels (collagen type I or fibrin) that were cast around posts. The resultant myotubes were electrically stimulated and contractile force generation was measured. In addition, 31 compounds that have the potential to serve as DMD drugs were screened by measuring changes in force generation upon treatment. Since this system works semi-automatically and in a 96-well culture format it is considered a potential high-throughput system for testing novel drugs for MD treatment. The major drawback of this model, however, is that it used murine cells. Thus, the results do not account for possible differences in drug response between humans and mice. Furthermore, the phenotype of the engineered constructs appeared to be closer to neonatal than adult according to the myosin heavy chain profiles [488].

In summary, there is still a great need for further research in the field of 3D skeletal muscle disease modeling. The creation of mature and functional *in vitro* muscle constructs could help enhance our fundamental understanding of the skeletal muscle physiology. Hence, the next step would be to create appropriate and translatable disease model systems to bring *in vitro* research one step closer to the *in homine* situation.

4 Future perspectives of skeletal muscle tissue engineering

When it comes to SMTE approaches, the fact that 2D culture systems behave fundamentally different from 3D systems has often been overlooked. Hence, results from 2D experiments may not be directly compared or even translated to 3D settings. Identifying applicable treatment options will require engineering of functional 3D muscle tissue constructs. In this respect, several questions need to be addressed: I) When does one look at gene expression levels or signaling pathways involved in muscle development or differentiation? II) What are representative time points for the evidence of mature and functional muscle tissue? III) Which analytical tools and methods can be applied for the morphological and functional assessment of skeletal muscle tissue constructs? IV) How can a given biomaterial recapitulate the physiological environment supporting the myogenic potential of the cells?

Therefore, there is urgent need for standardized dynamic 3D model systems to enable comparability of results. Additionally, careful deliberation of the choice of biomaterial, cell type and the external stimuli, prior to the start of the actual experimental SMTE approach, may help to improve the outcome and save valuable time (figure 29). The field of SMTE would greatly benefit from a workflow of criteria, factors, and analytical methods, which could be utilized by researchers globally. Here we provide a putative example of such a workflow that displays different experimental and developmental stages in *in vitro* SMTE culture systems, and produces results that are translatable to *in vivo* settings (figure 30). It suggests analytical tools for endpoint analysis and evaluation of requirements for achieving SMTE constructs with desirable properties (e.g. determination of elastic modulus, activation of involved signaling pathways and expression of myogenic markers and functional characteristics). Optimization of dynamic culture conditions comprises a thorough cell biological analysis including investigation of signaling pathways involved in myogenesis, muscle hypertrophy and proliferation, myogenic gene expression profiling, morphological analysis through immunofluorescence staining for contractile proteins, calculation of the fusion index and the quantification of sarcomeric striations – the latter indicating a certain degree of muscle maturity. Finally, environmental culture conditions should be fine-tuned, e.g. applying external stimuli including appropriate training. Such stimuli are commonly applied via bioreactor systems, which contribute to the desired outcome of engineering 3D skeletal muscle constructs by recapitulating physiological or pathophysiological muscle states. A unified SMTE approach following certain design criteria would render results between groups more comparable, possibly accelerating and streamlining new therapeutic discoveries and advancements in the field of SMTE.

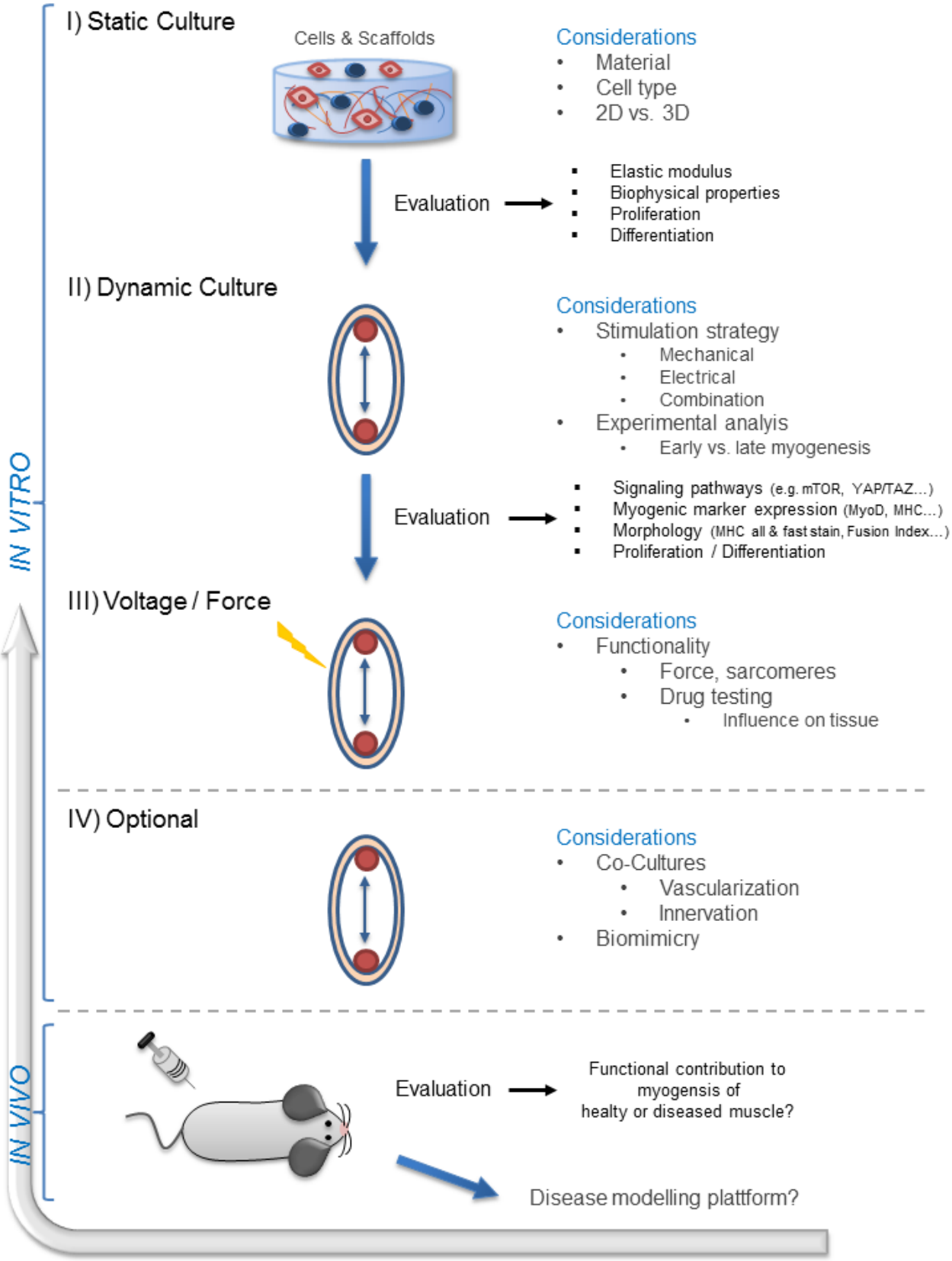

Figure 30: Envisioned future of skeletal muscle tissue engineering – a suggested workflow. This schematic presents a skeletal muscle tissue engineering workflow including stage-specific experimental considerations. Initially, the compatibility of biomaterials with potent myogenic cells has to be evaluated. This first step also involves the decision whether the cells will be cultured and grown in a 2D (monolayer on a pliant matrix) or 3D (encapsulation into a pliant matrix) environment. This still represents a static cell culture, where only the first steps in the SMTE approach are addressed. Evaluation of the biophysical matrix properties, biocompatibility and effects of the biomaterial on cell proliferation/differentiation can be evaluated via this process. The second step involves dynamic culture of the evaluated biomaterial and cells, where the main consideration is which stimulation strategy will be implemented into the culture system—ranging from mechanical to electrical stimulation or a combination of both. The third step addresses the functional analysis of the engineered muscle construct via twitch force measurements. At this point, contractile muscle constructs can furthermore be tested for their response to drugs with known effects, which is a prerequisite for later application of engineered muscle tissue in drug screening studies. An ideal setup would involve co-cultures to engineer muscle tissue with built-in vascular and neuronal structures to further enhance muscle maturity and contractility. After successful *in vitro* evaluation, the final step is the translation into animal models to test for the contribution of the engineered muscle to myogenesis and regeneration in healthy and/or diseased muscle. Ultimately, the knowledge gained from *in vivo* experiments can also be transferred back to *in vitro* setups for the generation of disease models.

5 Conclusion

Numerous sophisticated SMTE strategies exist, ranging from basic 2D to complex dynamic 3D setups, and researchers have a plethora of biomaterials and cell types to choose from. Nevertheless, to date the clear majority of SMTE approaches have failed to achieve broad clinical utility due to several reasons: I) Systemic elucidation of suitable cell types and biomaterials as well as stimulation protocols (to induce muscle maturation) are still ongoing. II) The pathomechanisms of a variety of MDs are still poorly understood which limits the clinical success of cell therapeutic approaches. Hence, model systems for developmental/mechanistic and pathophysiological studies (disease models) are urgently needed to perform drug screenings for potential new treatment options. Currently, the focus is on finding reliable physiological models to further understand and study the pathophysiological processes in MDs. III) Although acellular approaches bypass the general risks associated with (stem) cell therapy, many seemingly promising biomaterials have ultimately failed to meet the physical and native requirements to drive muscle regeneration.

ESC- and iPSC-derived myogenic precursors are increasingly used for drug screening purposes in disease models, while immortalized cell lines are used for initial testing of novel biomaterials and/or bioreactor systems. In an optimal scenario, autologous primary muscle (stem) cells directly derived from the patient would be used for personalized therapeutic approaches or disease models that involve the use of either undifferentiated or preconditioned cells. Although the current pool of applicable cells permits many different methodologies, each cell type has its limitations. However, advances in cell biology will establish adequate culture conditions in the future which will ideally diminish the phenotypic changes of cell types suitable for SMTE during *ex vivo* culture. Biomaterial systems that can serve as artificial satellite cell niches have already improved the efficiency of cell grafting in *in vivo* studies, and a more thorough evaluation of the satellite cell niche composition and microarchitecture will further improve current cell-based therapies. Finally, strategies for *in vitro* pre-vascularization and innervation will likely enhance the functional contribution of engineered muscle transplants to repair muscle *in vivo*. In addition, co-culture systems will allow studies on the interface between the different cell types in the muscle construct. Furthermore, myokines might offer novel therapeutic opportunities in the future, due to their positive effects on muscle as well as on other tissues. In *in vitro* culture systems, they might also be useful as supplements which can act as supportive factors for myogenesis, thereby improving the myogenic outcome of engineered muscle tissue constructs.

Therefore, elevating SMTE to the next level will require a thorough re-evaluation of biomaterial and cell sources as well as fine-tuning of stimulation techniques. Additionally, taking the above-mentioned criteria into account and implementing them into current research strategies will yield novel skeletal muscle (disease) model systems helping to improve therapeutic approaches to finally translate them into clinical setups.

Acknowledgements

We would like to acknowledge DI Dr. Andreas Teuschl, DI Dr. Karl H. Schneider, Carina Hromada and Prof. Dr. Heinz Redl for their valuable input.

CHAPTER 3

APPLICATION OF MECHANICAL OVERLOAD ON SKELETAL MUSCLE-LIKE CONSTRUCTS INDUCES HYPERTROPHY AND MYONUCLEAR ACCRETION

Cyclic tensile stress induces skeletal muscle hypertrophy and myonuclear accretion in a tissue-engineered model

Janine Tomasch[1,2*], Babette Maleiner[1,2], Carina Hromada[1,2], Dorota Szwarc-Hofbauer[1,2], Andreas H. Teuschl-Woller[1,2]

[1]Department Life Science Engineering, University of Applied Sciences Technikum Wien, Vienna, Austria

[2]The Austrian Cluster for Tissue Regeneration, Vienna, Austria

*Corresponding author: Janine Tomasch, tomasch@technikum-wien.at

Submitted to *Tissue Engineering Part A*

Abstract

Skeletal muscle is highly adaptive to mechanical stress due to its resident stem cells and the pronounced level of myotube plasticity. Herein, we study the adaptation to mechanical stress and its underlying molecular mechanisms in a tissue-engineered skeletal muscle model. We subjected differentiated 3D skeletal muscle-like constructs to cyclic tensile stress using a custom-made bioreactor system, which resulted in immediate activation of stress-related signal transducers (Erk1/2, p38). Cell cycle re-entry, increased proliferation and onset of myogenesis indicated subsequent myoblast activation. Furthermore, elevated focal adhesion kinase and β-catenin activity in mechanically stressed constructs suggested increased cell adhesion and migration. After three days of mechanical stress, gene expression of the fusogenic markers MyoMaker and MyoMixer, myotube diameter, myonuclear accretion as well as S6 activation were significantly increased. Our results highlight that we established a promising tool to study sustained adaptation to mechanical stress in healthy, hypertrophic, or regenerating skeletal muscle.

Keywords: skeletal muscle tissue engineering, fibrin, tensile stress bioreactor, hypertrophy, regeneration

1. Introduction

Skeletal muscle tissue is known for its particularly high capacity to regenerate after injury or trauma and to quickly adapt to mechanical stress. This high degree of plasticity and regenerative capacity is due to versatile alterations in intracellular regulatory mechanisms in myofibers as well as the presence of stem cells committed to the myogenic lineage, termed muscle satellite cells (MuSCs). MuSCs are the main muscle progenitor cell type and, under normal conditions, remain quiescent in their niche between the sarcolemma and the basal lamina in healthy adult tissue [489]. Upon injury or mechanical overload, they are activated to re-enter the cell cycle, which allows them to regenerate the tissue to a large extent despite their initial low cell count [410]. *In vivo*, MuSC activation is induced or supported by an inflammatory response upon mechanical overload that involves neutrophil invasion [490], a shift from an M1 to an M2 macrophage phenotype[491] and the release of a plethora of activating factors [492]. These events are followed by MuSC migration to the damaged site, where they undergo postnatal myogenesis to eventually produce new myofibers or fuse to already existing ones. Thereby, myonuclear accretion (*i.e.* the accumulation of several nuclei in one myotube), as well as myotube size increase [410]. In parallel to regenerating injured muscle, MuSCs undergo self-renewal to maintain a pool of stem cells available for future injuries [19], [493], [494].

In contrast to the role of MuSCs in skeletal muscle regeneration, their contribution to hypertrophy as an adaptive response after non-injurious mechanical loading is less clear. There are numerous studies describing that the increase in myofiber size upon mechanical stimulation depends on two processes: elevated levels of protein synthesis and increased myonuclear accretion [495], [496]. Upregulation of protein synthesis is predominantly mediated by insulin-like growth factor 1 (IGF1) [497] and calcium signaling [498], both resulting in the activation of mechanistic target of rapamycin (mTOR) activation. mTOR is known to be a crucial regulator of numerous components required for protein synthesis, such as initiation and elongation factors, and the biogenesis of ribosomes [499], [500]. The necessity of myonuclear accretion for successful hypertrophy, however, was uncertain for a long time. As Fukada *et al.* pointed out in their recent review [492], this can be partially attributed to the fact that MuSCs are mostly studied with regard to their crucial role in skeletal muscle regeneration, disregarding their involvement in hypertrophy. Nevertheless, in recent years, several studies showed that an increased number of myonuclei in hypertrophic myotubes is indispensable to sustain functional growth over longer timeframes [47], [501]–[503]. Interestingly, it was shown that the mechanisms underlying activation and myogenesis of MuSCs, as well as their fusogenic behavior differ between physiologically loaded and regenerating muscle [492].

The knowledge of how mechanical stimulation affects skeletal muscle fusion and hypertrophy *in vivo* is based predominantly on rodent animal models. This is due to the invasive nature of biopsy collection needed to study phenotype changes in muscle tissue. Surgical synergist ablation is the most common *in vivo* model used to study overload of muscle. However, since

this model exerts a high amount of overload on the muscle, it does not allow for discrimination between hypertrophy upon mechanical load and hypertrophy occurring in the course of regeneration [43], [44]. Voluntary wheel running presents a less invasive alternative but does not provoke hypertrophy to the same extent [45]. Currently, weighted wheel running [46] and high intensity interval training [47] are under investigation as intermediate forms of high-impact training that induce hypertrophy without causing tissue damage. Nonetheless, animal models entail inherent disadvantages, such as being costly and time-consuming and the fact that numerous parameters influence the outcome due to the complexity of the organism, in addition to obvious ethical considerations. Therefore, 2D *in vitro* models have contributed immensely to understanding the underlying mechanisms of myotube formation, regeneration, hypertrophy and myonuclear accretion. In the past, various systems were applied to study the impact of stretch on muscle hypertrophy and fusion using mechanical stimulation e.g., with magnetic beads [48] or various bioreactor systems [49]–[51], including the FlexCell® system [52]–[54]. Moreover, specific targeting of integrins was used to induce hypertrophy [55], [56]. While providing crucial insights into the intricate mechanisms of mechanobiology involved in these processes, only few approaches were successful in inducing significant hypertrophy comparable to the outcomes of successful *in vivo* models. Scott *et al.* presented an advancement of their established stretch bioreactor system by exposing myogenic cells to agrin, a proteoglycan required for the development of neuromuscular junctions. Thereby, they induced substantial hypertrophy in 3D tissue-engineered muscle constructs [57]. Furthermore, Terrie *et al.* recently reported a drastic increase in hypertrophy in 3D bioartificial muscles upon electromagnetic stimulation [58]. Nevertheless, these studies, focused on the morphological changes in the hypertrophic myotubes, while the present study includes analyses of intracellular activity during hypertrophy.

Previously, our group published a bioreactor system called MagneTissue used to generate 3D tissue-engineered skeletal muscle-like constructs (SMLCs) that resemble native muscle in terms of structure, gene expression profile and maturity through static mechanical stimulation of mouse myoblast cells for 9 days [66]. In the present study, we used an improved version of this bioreactor system to apply cyclic tensile stress to the pre-engineered SMLCs for 3 days to trigger myoblast activation and overload-induced hypertrophy. Besides analyses of morphological changes upon mechanical stress, we examined intracellular signaling pathways during these processes to characterize the model for skeletal muscle hypertrophy and myonuclear accretion.

2. Methods

2.1. Reagents

Unless indicated otherwise, all chemicals and reagents were purchased from Sigma Aldrich (Vienna, Austria) and were of analytical grade. Antibodies for phospho-p44/42 mitogen-activated protein kinase (MAPK) (Thr-202/Tyr-204) (phospho-Erk1/2), total p44/42 MAPK (total Erk1/2), phospho-p38 MAPK (Thr-180/Tyr-182), total p38 MAPK, phospho-focal adhesion kinase (Tyr397) (p-FAK), β-catenin, phospho-AKT (Ser-473), total AKT, phospho-S6 ribosomal protein (Ser-240/244), and total S6 ribosomal protein were obtained from Cell Signaling Technology (Danvers, Massachusetts, USA). The myosin heavy chain (MHC) antibody targeting all isoforms (MF-20c) was obtained from Developmental Studies Hybridoma Bank (Iowa City, Iowa, USA). The secondary antibodies for western blot detection IRDye® 680LT donkey anti-rabbit IgG, IRDye® 800CW goat anti-rabbit IgG, and IRDye® 800CW goat anti-mouse IgG were obtained from LI-COR Biosciences (Lincoln, NE, USA). The secondary antibody for immunofluorescence Goat anti-Mouse IgG (H+L) Cross-Adsorbed Secondary Antibody, Alexa Fluor™ 488 was purchased from Invitrogen (Waltham, Massachusetts, USA).

2.2. Cell culture

The murine myoblast cell line C2C12 (CLS, Eppelheim, Germany) was cultured in Dulbecco's modified Eagle's medium high glucose (DMEM-HG; Life Technologies, Carlsbad, CA, United States), supplemented with 10% fetal calf serum (v/v) (GE Healthcare, Buckinghamshire, United Kingdom), 1% penicillin/streptomycin (v/v) (Lonza, Basel, Switzerland) and 1% L-glutamine (v/v) (Lonza, Basel, Switzerland), referred to as growth medium (GM). For expansion, cells were cultured in standard cell culture dishes at 37°C and 5% CO_2 and sub-cultured at 70% confluence to avoid induction of differentiation. Differentiation media (DM) consisted of DMEM-HG, supplemented with 3% horse serum (v/v), 1% penicillin/streptomycin (v/v) and 1% L-glutamine (v/v).

2.3. Scaffold fabrication

Ring-shaped fibrin scaffolds with embedded cells were produced as previously described[66], [504] using the clinically approved Tissucol Duo 500 5.0 ml Fibrin Sealant (Baxter Healthcare Corp., Deerfield, USA). Briefly, fibrinogen was diluted in GM to a working solution of 40 mg/mL and thrombin was diluted in 40 mM $CaCl_2$ to a working solution of 4 U/mL. To create cell-laden scaffolds, the thrombin solution was further diluted with cell suspension (in GM) to a concentration of 1.25 U/mL. The thrombin-cell solution was mixed in a 1:1 ratio with the fibrinogen solution, injected into custom-made polyoxymethylene molds (figure 31 A) and allowed to polymerize at 37°C. The final volume of each scaffold was 500 µL with $4*10^6$ cells, a fibrinogen concentration of 20 mg/mL and 0.625 U/mL thrombin.

2.4. MagneTissue bioreactor system

The MagneTissue bioreactor is a custom-made bioreactor system that exerts uniaxial tensile strain onto ring-shaped scaffolds as previously described [66]. For mechanical stimulation, scaffolds were mounted between a spool and a hook that were fixed on inlays designed to fit in 14 mL Snap-Cap Falcon tubes (BD Biosciences, Bedford, USA) (figure 31 B). Magnets that were incorporated into the hooks interacted with magnets integrated into plates of the bioreactor (figure 31 C). Vertical movement of the plates led to a changed position of the hooks and therefore stretching of the scaffolds via magnetic force transmission (figure 31 D). A stepper motor that was controlled with a microcontroller enabled movement of the plates. We implemented an updated version of the bioreactor system from Heher *et al.* [66] that is capable of higher absolute velocities (up to 10 mm/s). Thereby, we could realize deformations of 10% (3 mm) at up to 1.2 Hz.

2.5. Experimental plan and mechanical stimulation protocol

After the casting of scaffolds, they were cultivated without mechanical stimulation for three days (until D3) to allow the cells to recover. Differentiation was induced on D3 by change to DM and start of moderate mechanical stimulation of 10% static strain for 6 hours per day for seven days according to our previously published study [66] (figure 31 E, F). On D10, SMLCs were stimulated with 10% cyclic strain at 1.2 Hz (“cyclic tensile stress”) for 6 hours per day for three more days, whereas control samples were continuously stimulated with 10% static strain (figure 31 E-G). Samples for analysis of signaling pathway activation, cell cycle and progression of myogenesis were collected after 15 minutes of cyclic tensile stress, after the first 6-hour session (on D10) or after three 6-hour sessions (on D12). Samples for analysis of morphological changes were collected after three 6-hour sessions (on D12).

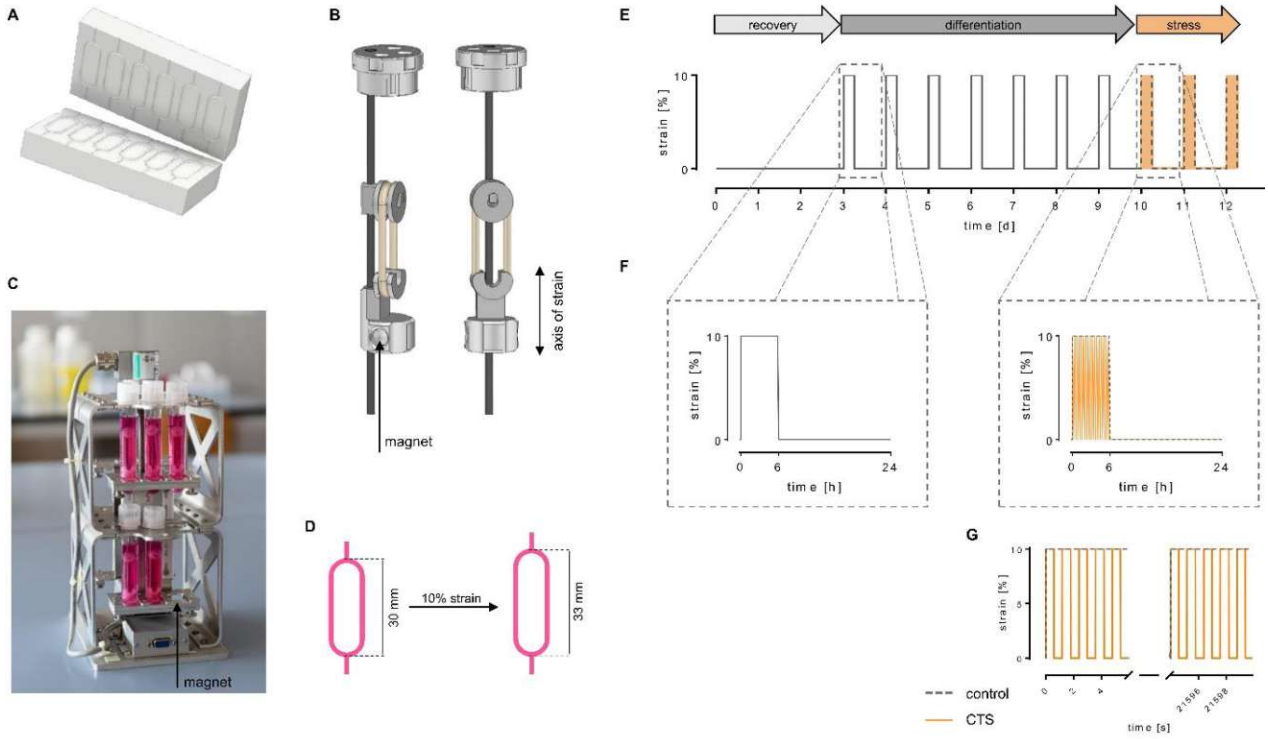

Figure 31: MagneTissue bioreactor system and mechanical stimulation protocol. (A) Polyoxymethylene molds for scaffold casting through injection molding. **(B)** Tube inlet with the spool-hook system the ring-shaped scaffolds are mounted on. The black arrow indicates the magnet incorporated into the hook that enables uniaxial stretching of the scaffold. **(C)** MagneTissue bioreactor unit. The black arrow indicates the fixed magnets that are connected to a stepper motor that is controlled through a microcontroller. Vertical movement of the magnets led to stretching of the ring-shaped scaffolds via magnetic force transmission. **(D)** Elongation of stretched rings from 30 mm to 33 mm after application of 10% strain. **(E)** Overview of the experimental plan. After casting of fibrin scaffolds, cells recovered for three days. Differentiation was induced on D3 by a change to differentiation medium and moderate mechanical stimulation of 6 hours of 10% static tensile strain per day (close up in the left panel in **(F)** and in **(G)**) for 7 days. On D10, differentiated skeletal muscle-like constructs were subjected to 6 hours of 10% cyclic tensile strain at 1.2 Hz per day (orange line) (“cyclic tensile stress (CTS)”). Control samples were continuously stimulated with 10% static tensile strain per day (dotted grey line) (close up in the right panel in **(F)** and in **(G)**).

2.6. Western blot

Fibrin scaffolds were washed in PBS, snap-frozen in liquid nitrogen and crunched with a tissue forceps. The resulting powder was dissolved in 200 µL protein isolation buffer (nonidet P-40 buffer containing 40 mM HEPES (pH 7.9), 120 mM NaCl, 1 mM EDTA (pH 8.0), 10 mM 2-glycerolphosphate, 50 mM NaF, 0.5 mM sodium orthovanadate, 10% nonidet P-40 substitute, and 1 mM Phenyl-Methyl-Sulfonyl Fluoride supplemented with 2 µg/mL aprotinin, 2 µg/mL leupeptin, 0.3 µg/mL benzamidine chloride, and 10 µg/mL trypsin inhibitor) per scaffold. The samples were lysed with motorized pellet pestles (DWK Life Sciences, Wertheim, Germany), incubated on ice for 1 hour and centrifuged at 22,000 × g for 20 minutes at 4°C. The supernatants were collected, mixed with 4x loading buffer (200 mM tris(hydroxymethyl)aminomethan (Tris) (pH 6.8), 400 mM dithiothreitol, 8% sodium dodecyl sulfate (SDS), 0.4% bromophenol blue and 40% glycerol) and denatured at 95°C for 5 minutes. Equal volumes of protein were loaded onto an SDS-polyacrylamide gel (10% running gel and 5% stacking gel) and transferred to a nitrocellulose membrane (GE Healthcare, Little Chalfont, UK) after separation. Membranes were blocked in 5% (w/v) nonfat milk powder in Tris-buffered Saline/0.1% Triton X-100 (TBS/T) (v/v) for 1 hour at room temperature. Primary antibody incubations were performed in 5% (w/v) bovine serum albumin (BSA) in TBS/T overnight at 4°C and secondary antibody incubations in 5% (w/v) nonfat milk powder in TBS/T. Signals were detected with the Odyssey® Fc Imaging System (LI-COR, Lincoln, NE, USA) and quantified with Image Studio Lite (LI-COR, Lincoln, NE, USA).

2.7. Quantitative reverse transcription polymerase chain reaction (RT- qPCR)

Fibrin scaffolds were washed in PBS and cells were retrieved by digestion with nattokinase (Japan Bioscience Lab, CA, United States). Each fibrin scaffold was incubated in 500 µL nattokinase at a concentration of 100 U/mL in PBS, pH 7.4 supplemented with 15 mM ethylenediaminetetraacetic acid (EDTA) for 20 minutes at 37°C. To facilitate digestion, samples were constantly agitated at 700 RPM. The cell suspension was centrifuged for 5 minutes at 300 × g, the cell pellet was washed with PBS and RNA was isolated with the peqGOLD total RNA Kit (VWR International GmbH, Erlangen, Germany), followed by reverse transcription into cDNA with the EasyScript PlusTM Reverse Transcriptase cDNA Synthesis Kit (ABM, Richmond, Canada) according to the manufacturers' protocols. Reverse transcription of 1 µg RNA was performed for 50 minutes at 42°C, followed by an inactivation step at 85°C for 5 minutes. Quantitative PCR was performed with the PerfeCTa® SYBR® Green FastMix® Low ROX (Quantabio, Beverly, MA, USAStratagene Mx3005P cycler (Agilent Technologies, Santa Clara, United States). Assays were performed in triplicates with 10 ng input cDNA per reaction and 200 nM forward and reverse primers. Thermal cycle conditions were 5 minutes at 95°C, followed by 40 cycles of either 10 s at 95°C and 30 s at 60°C ("fast-two-step"), 30 s at 95°C and 1 minute at 60°C ("normal-two-step"), or 15 s at 95°C, 15 s at 60°C and 15 s at 72°C ("fast-three-step"). Target cycle threshold (CT) values were normalized to the housekeeping gene *Ribosomal Protein Lateral Stalk Subunit P0* (*RPLP0*) (known to be stably expressed independent of

mechanical stress [148]) and compared to D3 values or to control samples of the respective time point using the comparative CT (ΔΔCT) method. Primer sequences and used thermal profiles are listed in table 11. Two primers for different myosin heavy chain genes were used. The primer referred to as “MHC I” is specific for the gene *Myh7* that encodes the slow-twitch myosin heavy chain found in type I fibers. The primer referred to as “*MHC II*” is specific for genes that encode all different fast-twitch myosin heavy chains.

Table 11: Primer sequences and thermal profiles used for qPCR.

target	*primer forward*	*primer reverse*	*thermal profile*
RPLP0	CTCCAACAGAGCAGCAGA	ATAGCCTTGCGCATCTGGT	fast-two-step
CCND1	TCAAGTGTGACCCGGACTG	ATGTCCACATCTCGCACGTC	fast-two-step
MyoD	ACTACAGTGGCGACTCAGAT	CCGCTGTAATCCATCATGCC	normal-two-step
MyoG	GGTCCCAACCCAGGAGATCAT	ACGTAAGGGAGTGCAGATTG	normal-two-step
Tnnt1	AAACCCAGCCGTCCTGTG	CCTCCTCCTTTTTCCGCTGT	fast-two-step
MHC I	CTCAAGCTGCTCAGCAATCTATTT	GGAGCGCAAGTTTGTCATAAGT	fast-three-step
MHC II	GAGGGACAGTTCATCGATAGCAA	GGGCCAACTTGTCATCTCTCAT	fast-three-step
MyoMaker	ATCGCTACCAAGAGGCGTT	CACAGCACAGACAAACCAGG	fast-two-step
MyoMixer	AAGAAGTTCAGGCTTCAGGTGC	GAGCCTCTCTCATGTCTTGGG	fast-two-step
p21	CCGTGGACAGTGAGCAGTTG	TGGGCACTTCAGGGTTTTCT	fast-three-step
cFOS	ATCTGTCCGTCTCTAGTG	GCTTGGAGTGTATCTGTC	fast-three-step

2.8. Immunofluorescence staining and analyses

Fibrin scaffolds were fixed with 4% paraformaldehyde (Roth, Karlsruhe, Germany) overnight at 4°C, washed with distilled water, permeabilized with Tris-buffered saline/0.1% Triton X-100 (TBS/T) (v/v) for 15 minutes at room temperature and blocked with phosphate-buffered saline/0.1% Triton X-100 (PBS/T) with 1% BSA (w/v) at room temperature for 1 hour. The primary MHC antibody was diluted 1:300 in PBS/T-1% BSA and incubated overnight at 4°C followed by washing in PBS/T. The secondary antibody was diluted 1:400 in PBS/T-1% BSA and incubated at 37°C for 1 h. Nuclei were visualized by staining with 4′,6-diamidino-2-phenylindole (DAPI) diluted 1:1000 in PBS/T-1% BSA for 10 minutes at room temperature. Whole scaffolds were mounted onto glass slides with Mowiol® and analyzed with the LSM 700 confocal microscope (Zeiss, Oberkochen, Germany) with solid-state lasers (405 nm with 5 mW and 488 nm with 10mW).

For assessment of myotube maturation, myotube alignment, myotube diameter and fusion index, MHC-stained samples were analyzed using the imaging analysis software Fiji. Myotube alignment was calculated as the deviation between the axis of orientation of single myotubes from the axis of strain. The mean diameter was calculated from three measurements per

myotube. The fusion index was calculated as the ratio of nuclei in fused myotubes (defined as myotubes with a minimum of three nuclei) to the total number of nuclei.

2.9. Statistical analyses

All statistical calculations and depictions of data were performed with GraphPad Prism Software (GraphPad Software Inc., SanDiego, CA, USA). Gene expression and protein activation and expression data is presented in box and whisker plots (minimum to maximum) or as time-lines relative to baseline (means + SD are shown). Myotube diameters and deviations from the main axis of strain are shown as histograms. The fusion indices are shown as scatter dot plots. All data sets were analyzed for normal distribution with the D'Agostino and Pearson omnibus normality test. Comparison between groups was performed with unpaired t-test (with Welch's correction in case of unequal variances) or 2way ANOVA with Sidak's multiple comparison test as indicated in the figure legends, with p values < 0.05 considered statistically significant.

3. Results

3.1. Mechanical stimulation with cyclic tensile stress activates intracellular signaling pathways in skeletal muscle-like constructs

To investigate the effect of cyclic tensile stress on skeletal muscle, we generated mature tissue-engineered SMLCs and subjected them to 10% cyclic strain at 1.2 Hz for 6 hours per day followed by 18 hours of rest without strain for up to three days (figure 31). To assess the immediate effects of the mechanical force on the muscle constructs, we analyzed activation of various signaling pathways known to be involved in stress response and processes required for myogenic regeneration and hypertrophy, such as migration, adhesion or protein synthesis. Activation of Erk1/2 and p38, which are both signal transducers of the MAPK pathway required for immediate response to stress, was significantly increased (1.8-fold and 1.3-fold, respectively) after 15 minutes of cyclic stress compared to the control condition (10% static strain) (figure 32 A, B). Furthermore, we assessed changes in signaling molecules involved in cell adhesion and migration, as those processes are prerequisites for myonuclear fusion, and observed an increased activation of FAK and expression of β-catenin after 6 hours of cyclic tensile stress compared to statically strained control samples (figure 32 C, D). Since the mTOR signaling network has a pivotal role in control of protein synthesis required for muscle hypertrophy, we analyzed activation of two of its members, AKT and S6. Interestingly, there were no differences in activation of AKT between control and cyclically stimulated samples, while activation of its downstream target S6 was higher in the cyclic tensile stress samples throughout the three days of overstimulation (figure 32 E, F).

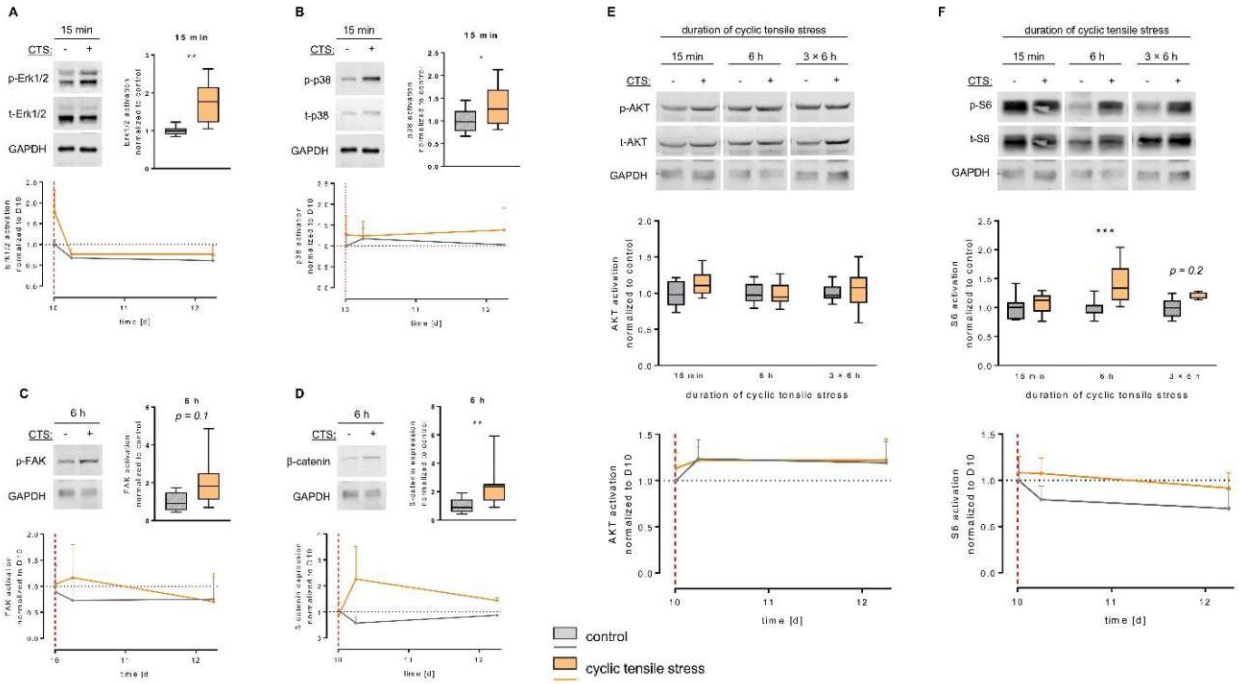

Figure 32: Cyclic tensile stress (CTS) induces activation of intracellular signaling pathways. Skeletal muscle-like constructs were stimulated with cyclic tensile stress (10% strain at 1.2 Hz) for 15 minutes, 6 hours or 3 times 6 hours (with 18-hour breaks in between) compared to moderately stimulated controls (static tensile stress of 10%) after 9 days of differentiation induced by moderate mechanical stimulation. Erk1/2 **(A)** and p38 **(B)** activation were assessed after 15 minutes of stimulation (ratio of phosphorylated protein to total protein); focal adhesion kinase (FAK) activation **(C)** and β-catenin expression **(D)** after 6 hours of stimulation (normalized to the loading control GAPDH); AKT **(E)** and S6 **(F)** activation throughout the whole stimulation period (ratio of phosphorylated protein to total protein). Representative western blots of three independent experiments (N = 3, n ≥ 8) are shown. Box plots show the protein activation/expression of cyclically stressed samples normalized to moderately stimulated control samples; data is shown as box and whiskers (min to max). Timelines show the protein activation/expression normalized to the start of cyclic tensile stress (D10 of the experiment, indicated by the dotted red line). Data is shown as mean + SD. Unpaired t-test (A, B, C, D) or 2way ANOVA (E, F) comparing the cyclically stressed samples to control at the respective timepoints were performed; *p < 0.05, **p < 0.01, ***p < 0.001.

3.2. Changes in cell cycle stage after cyclic tensile stress leads to increased proliferation

Myoblast transition from quiescence to a proliferative state constitutes the first step of most adaptive processes in skeletal muscle, such as regeneration or hypertrophy [15], [492]. To evaluate changes in cell cycle progression after stimulation with cyclic tensile stress, we performed gene expression analysis of cell cycle markers and quantified the amount of total DNA in the scaffolds. Gene expression of the cell cycle regulator *cyclin D1* (*CCND1*) increased 1.5-fold after 6 hours of cyclic tensile stress compared to control (figure 33 A). Moreover, scaffolds subjected to mechanical stress for 3 days contained 1.4-times more DNA than statically stimulated samples (figure 33 C). Interestingly, cyclically stressed muscle constructs also showed a slight (1.2-fold), but not significant ($p = 0.43$) increase in *p21* gene expression, which is linked to cell cycle arrest (figure 33 B).

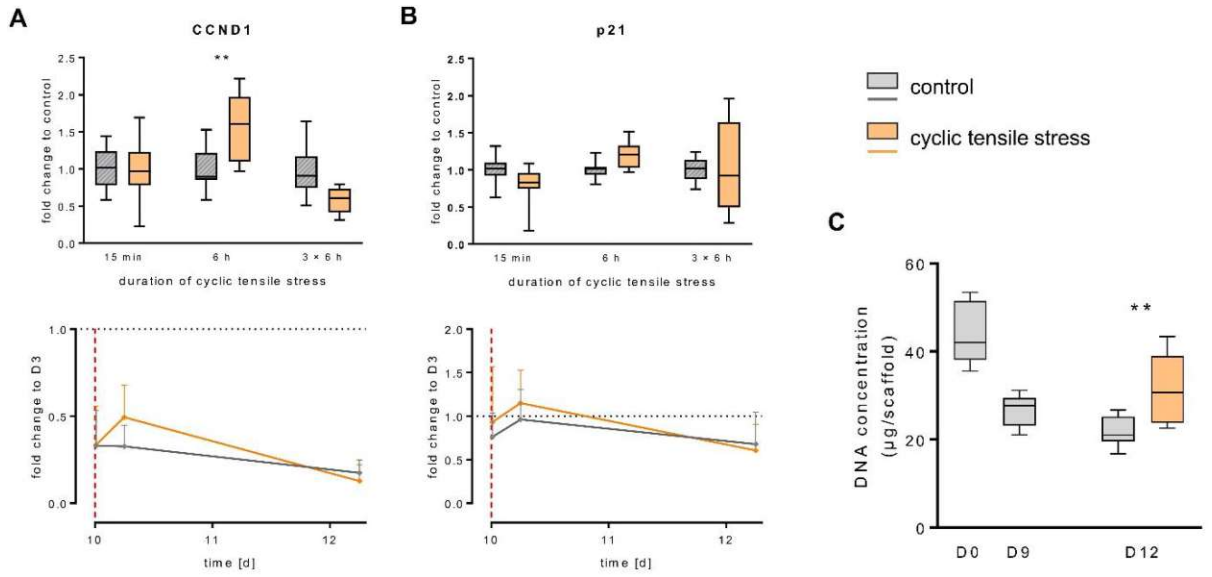

Figure 33: Effects of cyclic tensile stress on myoblast proliferation. Skeletal muscle-like constructs were stimulated with cyclic tensile stress (10% strain at 1.2 Hz) for 15 minutes, 6 hours or 3 times 6 hours (with 18-hour breaks in between) compared to moderately stimulated controls (static tensile stress of 10%) after 9 days of differentiation induced by moderate mechanical stimulation. mRNA expression levels of *cyclin D 1* (*CCND1*) (A) and *p21* (B) were assessed by RT-qPCR. Box plots show the fold change expression levels of cyclically stressed samples normalized to moderately stimulated control samples; data is shown as box and whiskers (min to max). Timelines show the fold change expression levels normalized to the baseline (timepoint of the induction of differentiation, D3 of the experiment). The start of cyclic tensile stress (D10 of the experiment) is indicated by the dotted red line; data is shown as mean + SD. N = 3, n ≥ 8; 2way ANOVA comparing the cyclically stressed samples to control at the respective timepoints was performed; **$p < 0.01$. (C) DNA content of scaffolds was quantified after scaffold production (D0), after 9 days of differentiation induced by moderate mechanical stimulation (D9) and after three more days of cyclic tensile stress (D12). Data is shown as box and whiskers (min to max). N ≥ 3, n ≥ 8; unpaired t-test comparing the cyclically stressed samples to control on D12 was performed; **$p < 0.01$.

3.3. Cyclic tensile stress induces further myogenic differentiation in skeletal muscle-like constructs

Since we observed increased activation of myoblasts, we further aimed to assess their development along the myogenic lineage upon cyclic tensile stress. We observed that cyclic stimulation of pre-engineered SMLCs with 10% tensile stress at 1.2 Hz led to upregulated expression of marker genes for different stages of myogenic development. Gene expression of the myogenic regulatory factors myogenic differentiation 1 (MyoD) and myogenin (MyoG) were increased 2.4-fold and 1.9-fold, respectively, after 6 hours of cyclic tensile stress compared to static strain (figure 34 A, B). While expression of MyoD and MyoG decreased and reached the same levels as in control samples at day three of cyclic stimulation, late-stage myogenesis markers troponin T 1 (Tnnt1) and Myozenin 1 (Myoz1) were higher (up to 1.3- fold and 1.9-fold, respectively) than in control samples throughout the culture period ($p = 0.084$ for Tnnt1 and $p = 0.09$ for Myoz1 comparing cyclic tensile stress to control over time) (figure 34 C, D). Furthermore, genes encoding the different isotypes of the major protein required for muscle contraction, myosin heavy chain (MHC), were upregulated after 6 hours of cyclic tensile stress compared to static strain (figure 34 E, F). This was followed by a 7-fold increased MHC protein expression after three days of cyclic stress (figure 34 G).

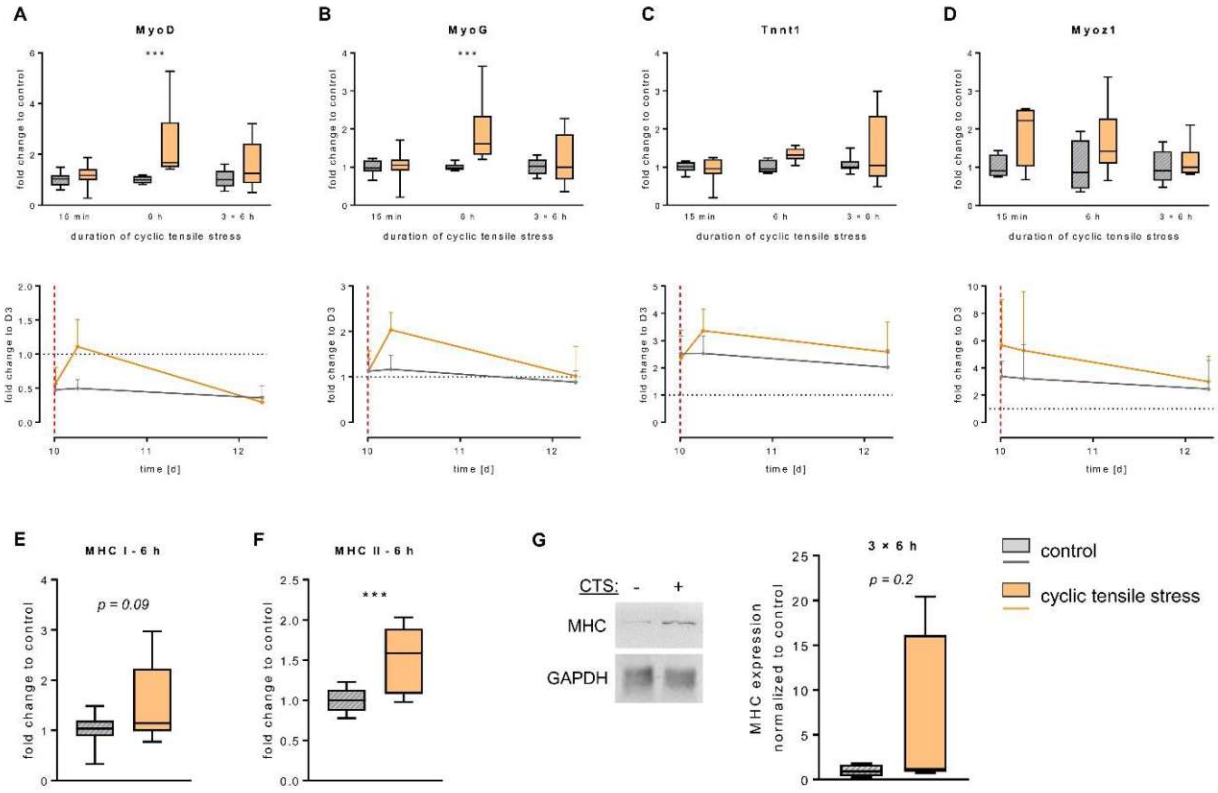

Figure 34: Cyclic tensile stress (CTS) triggers the myogenic differentiation cascade. Skeletal muscle-like constructs were stimulated with CTS (10% strain at 1.2 Hz) for 15 minutes, 6 hours or 3 times 6 hours (with 18-hour breaks in between) compared to moderately stimulated controls (static tensile stress of 10%) after 9 days of differentiation induced by moderate mechanical stimulation. mRNA expression levels of myogenic regulatory factors *MyoD* **(A)**, *myogenin* (*MyoG*) **(B)**, *troponin T 1* (*Tnnt1*) **(C)** and *Myozenin 1* (*Myoz1*) **(D)** were assessed by RT-qPCR. Box plots show the fold change expression levels of cyclically stressed samples normalized to moderately stimulated control samples. Data is shown as box and whiskers (min to max). Timelines show the fold change expression levels normalized to the baseline (timepoint of the induction of differentiation, D3 of the experiment). The dotted red line indicates the start of CTS (D10 of the experiment). Data is shown as mean + SD. N = 3, n ≥ 8; 2way ANOVA comparing the cyclically stressed samples to control at the respective timepoints was performed; ***p < 0.001. **(E, F)** Gene expression level of the myogenic markers *myosin heavy chain I* and *II* (*MHC I* and *MHC II*) were assessed after 6 hours of cyclic tensile stress and normalized to control. N = 3, n ≥ 8; unpaired t-test comparing the cyclically stressed samples to control was performed; ***p < 0.001. (**G**) MHC protein expression was investigated after three times 6 hours of CTS and normalized to control. Representative western blots of two independent experiments (N = 2, n ≥ 4) are shown. Box plots show the protein expression of stressed samples normalized to control samples. Data is shown as box and whiskers (min to max). Unpaired t-test comparing the cyclically stressed samples to control was performed.

3.4. Cyclic tensile stress causes increased myonuclear fusion

To elucidate whether the intracellular effects of cyclic tensile mechanical stress on SMLCs also affected their development on a structural level, we performed immunofluorescence stainings for the motor protein MHC. The effects of cyclic tensile stress on the morphology of SMLCs were in accordance with the observations concerning gene expression of myogenic markers. Myotubes in samples subjected to cyclic tensile stress displayed a more mature morphology, including larger myotube diameters (figure 35 B) and a higher fusion index, with 31% of all nuclei fused into myotubes compared to 19% in control samples stimulated with static strain (figure 36 C). However, the SMLCs subjected to cyclic tensile stress showed a higher variance in myotube morphology, while myotubes in control samples displayed a uniform morphology over all regions of interest (ROIs). Nuclei in almost all the myotubes of control samples were aligned along the axis of the myotube, whereas only some of myotubes in cyclically stimulated samples displayed this morphology. In contrast, these samples exhibited much thicker myotubes with large clusters of nuclei (figure 35 A). Increased variance in morphological characteristics was also seen concerning differences in myotube diameter and myotube alignment (figure 35 B, C) and in scanning electron microscope images (supplementary figure 3).

Overall, fusion of myogenic cells was significantly increased in SMLCs subjected to cyclic tensile stress. The observations from the immunofluorescence stainings (figure 35 A) were confirmed in the quantification of the fusion index (figure 36 C). Furthermore, expression of genes encoding the fusogenic proteins MyoMaker and MyoMixer was significantly increased (2.1-fold and 1.8-fold, respectively) after three days of cyclic stimulation (figure 36 A, B). Quantification of immunofluorescence stainings furthermore showed that samples subjected to cyclic tensile stress had a higher total number of nuclei per ROI (figure 36 D), which is in accordance with the findings on increased proliferation (figure 33).

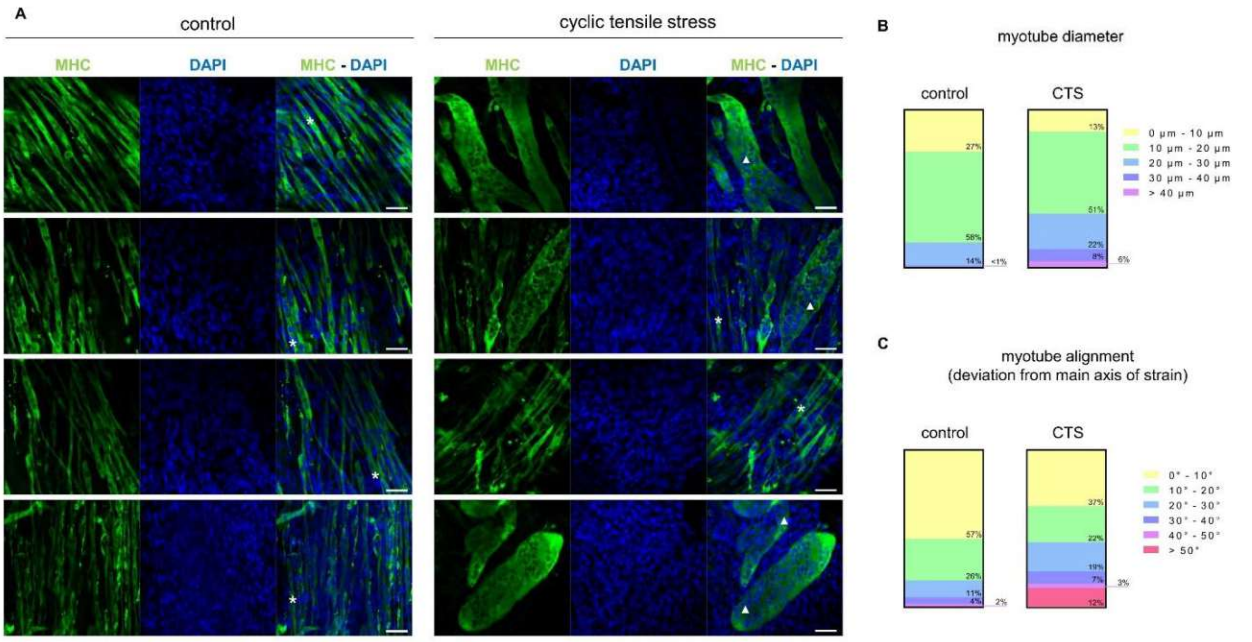

Figure 35: Effect of cyclic tensile stress (CTS) on myotube morphology. Skeletal muscle-like constructs were stimulated with CTS (10% strain at 1.2 Hz) for 3 days (6 hours of stimulation per day, followed by an 18-hour break) compared to moderately stimulated controls (static tensile stress of 10%) after 9 days of differentiation induced by moderate mechanical stimulation. **(A)** Representative images of immunofluorescence stainings for MHC (green) with nuclei stained with DAPI (blue) of three independent experiments (N = 3, n ≥ 6) are shown. Scale bars represent 50 µm; white asterisks indicate myotubes with nuclei aligned along the axis of the myotube and white triangles indicate myotubes with clusters of nuclei. **(B)** Myotube diameters were measured at three different spots of 447 myotubes in control samples and 392 myotubes in cyclically stressed samples. Data is presented as a histogram of myotube diameters. N = 3, n ≥ 6 with four regions of interest (ROIs) per sample. **(C)** Myotube alignment score was analyzed as the deviation of single myotubes from the axis of strain and is represented as a histogram of the percentage of myotubes deviating in the respective interval of 10° angles. N = 3, n ≥ 6 with at least 180 myotubes per experimental group analyzed in four ROIs per sample.

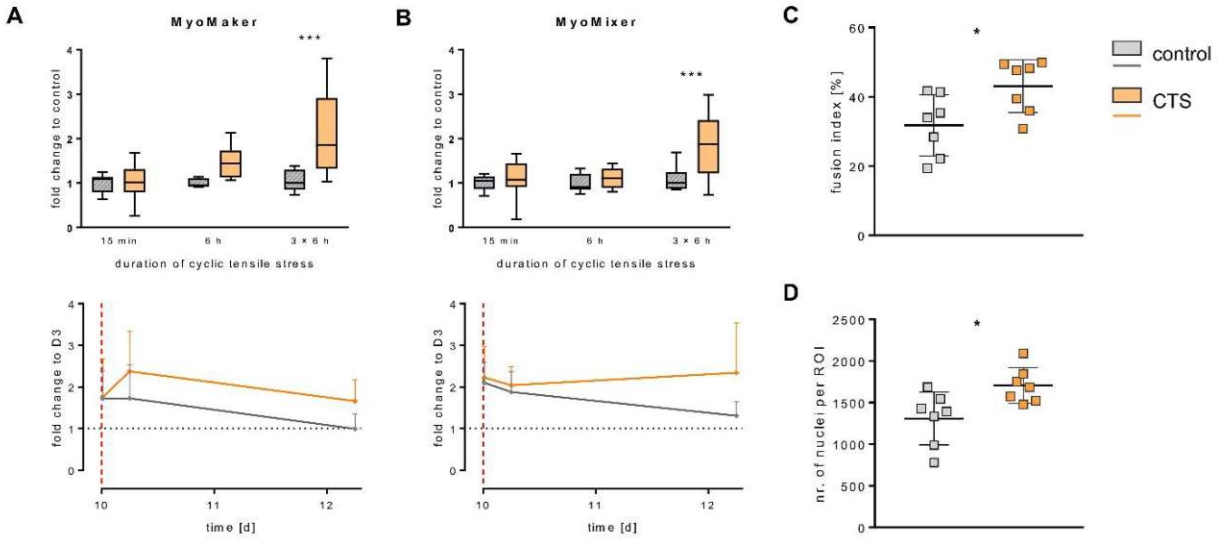

Figure 36: Cyclic tensile stress (CTS) increases myotube fusion. Skeletal muscle-like constructs were stimulated with CTS (10% strain at 1.2 Hz) for 3 days (6 hours of stimulation per day, followed by an 18-hour break) compared to moderately stimulated controls (static tensile stress of 10%) after 9 days of differentiation induced by moderate mechanical stimulation. mRNA expression levels of genes encoding fusogenic proteins MyoMaker **(A)** and MyoMixer **(B)** were assessed by RT-qPCR. Box plots show the fold change expression levels of cyclically stressed samples normalized to moderately stimulated control samples. Data is shown as box and whiskers (min to max). Timelines show the fold change expression levels normalized to the baseline (timepoint of the induction of differentiation, D3 of the experiment). The dotted red line indicates the start of cyclic tensile stress (D10 of the experiment). Data is shown as mean + SD. N = 3, n ≥ 8; 2way ANOVA comparing the cyclically stressed samples to control at the respective timepoints was performed; ***p < 0.001. **(C)** Myotube fusion index of IF stainings (MHC and DAPI); analyzed as the ratio of fused nuclei to total nuclei per visual field (N = 3, n = 7 with four regions of interest (ROIs), at least 250 nuclei per sample and 9000 nuclei per experimental group analyzed). Data is shown as a scatter dot plot with mean ± SD. Unpaired t-test comparing the cyclically stressed samples to control was performed; *p < 0.05. **(D)** Nuclei per ROI of immunofluorescence stainings (MHC and DAPI). Data is shown as a scatter dot plot with mean ± SD. N = 3, n = 7; Unpaired t-test comparing the cyclically stressed samples to control was performed; *p < 0.05.

4. Discussion

In the past years, the field of skeletal muscle tissue engineering mainly focused on the creation of biomimetic muscle constructs that resemble *in vivo* muscle tissue concerning structure and functionality. Contributing to these advances, our group established a bioreactor system (MagneTissue) that applies mechanical stimulation to myogenic cells embedded in fibrin scaffolds through magnetic force transmission [66]. While we were able to create skeletal muscle-like constructs (SMLCs) displaying key characteristics of mature skeletal muscle (such as alignment, sarcomeric patterning, expression of myogenic markers), the applied static mechanical strain did not lead to substantial hypertrophy. In the present study, we created SMLCs according to our previously published protocol (9 days of static strain) and subsequently subjected them to cyclic tensile stress (1.2 Hz, 10% relative deformation, 6 hours a day with 18 hours of rest in between) for up to 3 days, and then analyzed its influence on muscle hypertrophy and myonuclear accretion.

The constructs were generated using the cell line C2C12 that is widely accepted and used as a model system for muscle satellite cells (MuSCs), since it demonstrates similar behavior concerning the course of myogenesis and expresses characteristic markers crucial for MuSCs development [48], [54], [505] (most importantly Pax7 [506]). We clearly observed transduction of the mechanical stress to intracellular signals, shown by the activation of Erk1/2 and p38 MAPK after only 15 minutes of stimulation (figure 32 A, B). Both kinases are known to be involved in crucial mechanotransduction pathways [29], but also hypertrophy [507]. Moreover, C2C12 cells were activated immediately after onset of cyclic tensile stress, as indicated by the upregulation of MyoD gene expression compared to controls stimulated with our standard static loading regime (figure 34 A). We also observed increased gene expression of the cell cycle regulator CCND1 after 6 hours (figure 33 A), followed by higher amounts of DNA (figure 33 C) and higher number of nuclei after 3 days of mechanical stress (figure 36 D). This suggests that C2C12 activation also resulted in increased proliferation, which presents another analogue to MuSC activation [15], [19]. Furthermore, MyoD expression was followed by myogenic development, finally resulting in increased gene and protein expression of markers for myogenic maturation, such as Tnnt1 and MHC (figure 34).

Moreover, the mechanical stimulation clearly led to hypertrophy, as evidenced by the increased myotube size (figure 35). One cornerstone of skeletal muscle hypertrophy is increased protein synthesis, which is associated with the activation of distinct signaling mechanisms. In this regard, the IGF-AKT-mTOR pathway is considered as one of the most important ones [497]. Interestingly, we did not observe any changes in AKT activity upon cyclic tensile stress, whereas activation of the mTOR target S6 was significantly increased by the end of the first 6 hours training session (figure 32 E, F). It has been shown, however, that in the context of skeletal muscle hypertrophy, IGF activity on a systemic level (e.g., produced by the liver) is more important than on a paracrine level [508]. A study by Spangenburg *et al.* showed that lacking the

IGF1 receptor in skeletal muscle does not interfere with hypertrophy in mice subjected to mechanical overload [509]. These findings highlight the important role of signal transduction through mechanosensors in the plasma membrane or cytoskeleton, such as the dystrophin glycoprotein complex or integrins [508], that potentially caused S6 activation in our model as well. This hypothesis is supported by the increased phosphorylation of FAK, a cytoplasmic tyrosine kinase well-known as a key mediator of intracellular signaling by integrins [510], that we observed upon mechanical stress (figure 32 C).

Beside increased protein synthesis, myonuclear accretion presents the second prerequisite for functional hypertrophy. As shown by the immunofluorescence stainings for MHC, calculations of the fusion index and gene expression analysis of genes encoding the fusogenic regulators MyoMaker and MyoMixer, the application of cyclic tensile stress induced significant myoblast fusion. In this regard, the large clusters of nuclei observed in cyclically stimulated constructs that do not conform with the lateral alignment in statically stimulated ones are particularly noteworthy (figure 35 and figure 36). The extent of fusion and changed morphology we observed in our model exceeds the usual observations in *in vitro* studies using both, cell lines and primary cells. Particularly, we observed high myotube diameters of up to 40 µm, while others reported myotubes with diameters of only 20 µm to 30 µm [50], [55], [125]. This might be attributed to improved possibility for cellular migration, a known prerequisite for fusion as it increases the probability of cell-cell contacts[17], that might have been enabled due to the constant structural change of the fibrin network upon cyclic stretch. Increased expression of β-catenin and activation of FAK substantiate this theory, since their signaling activities are involved in cell recognition and adhesion prior to fusion [511], [512]. In this regard, our findings are in accordance with Grossi *et al.*, who showed that mechanical stimulation of C2C12 cells led to phosphorylation of FAK [48]. Furthermore, Murphy *et al.* showed that Wnt/β-catenin signaling was transiently activated in early stages of muscle regeneration [513].

Interestingly, myotubes in samples stimulated with cyclic tensile stress showed an increased diversity in morphology (myotube diameter, alignment of myotubes and myoblast fusion). Throughout the whole study, the phenotypic variances between samples were higher in this group than in the statically stimulated group. The morphological differences might be a further result of the dynamically changing structure of the fibrin network, since it is known that myotube alignment benefits from uniformly aligned substrates [51], [514]. The application of static tensile stress to the fibrin scaffolds in the first 9 days of the experiment generated alignment of both, fibrin fibrils as well as myotubes [66]; however, it was lost due to the cyclic stretch, as shown in scanning electron microscope images (supplementary figure 3). Nevertheless, a positive side effect of these rapid structural changes might lie in the increased medium supply that potentially supported the high extent of myoblast activation and increased myotube growth.

Whether the reason for the increased myoblast activation, myonuclear accretion and myotube diameter is based on regeneration or on merely overload-induced hypertrophy cannot be clearly

distinguished at this point. Differentiation between these two processes *in vivo* depends on systemic events (such as factors released by inflammatory cells) and structural characteristics (such as leaving the MuSC niche) [492] that cannot be recapitulated with our simplified tissue-engineered *in vitro* model. We did not observe any visual signs of myotube injury, such as ruptures or myotube dissociation, indicating that the observed effects were triggered exclusively by the mechanical stimulation. It must be noted, however, that we did not perform specific assays to detect membrane damage, such as measuring released lactate dehydrogenase. On the other hand, a study by Fukada *et al.* showed that MuSCs in overloaded muscle did not express *MyoD* in the course of their activation, in contrast to MuSCs in regenerating muscle [515]. The increased gene expression of *MyoD* that we observed after 6 hours of cyclic tensile stress therefore suggests that regeneration, and not overload-induced hypertrophy, caused the cascade that followed.

In follow-up studies based on this model, we will aim to provide evidence of potential myotube damage to substantiate the observations on ongoing regeneration. Furthermore, we will focus on the long-term effects of phases of cyclic tensile stress on regeneration and hypertrophy, including read-outs determining skeletal muscle functionality. In summary, independently of the cause of myoblast activation, subjecting tissue-engineered SMLCs to cyclic tensile stress induced both, hypertrophy and myonuclear accretion. On an intracellular level, we also observed characteristic behavior of myoblasts activated by mechanical stimulation. Therefore, we conclude that with this approach we established a model of sustained skeletal muscle growth that presents a promising tool to further study adaptation to mechanical stimulation or recovery from overload in the future.

Acknowledgement

The authors want to thank the imaging core facility of the Medical University of Vienna for assistance in confocal microscopy and Bendegúz Nagy for creating images of the bioreactor equipment. Furthermore, we gratefully acknowledge Andreas Graupe and Johannes Schachner (TGM, Vienna, Austria) for designing, optimizing and building the MagneTissue bioreactor and programming the software.

Author contributions

JT: Performed all cell-based experiments, analysis of results, preparation of the manuscript, design of figures and tables; BM: establishment of methods; CH, DS-H: critical discussion of results and preparation of the manuscript; AT-W: development of study design, revising manuscript.

Funding

This study was supported by the DOC scholarship of the Austrian Academy of Sciences and the projects Aging Tissue (MA23#29-07), Histocytometrie (MA23#30-06) and ImmunTissue (MA23#30-11).

Data

All data presented herein are available from the corresponding author on request.

Declaration of conflicting interests

The authors declare no potential conflicts of interest with respect to the research, authorship, and/or publication of this article.

Informed consent, ethical approval and human rights – n/a

This study involved no human or animal subjects.

5. Supplemental information

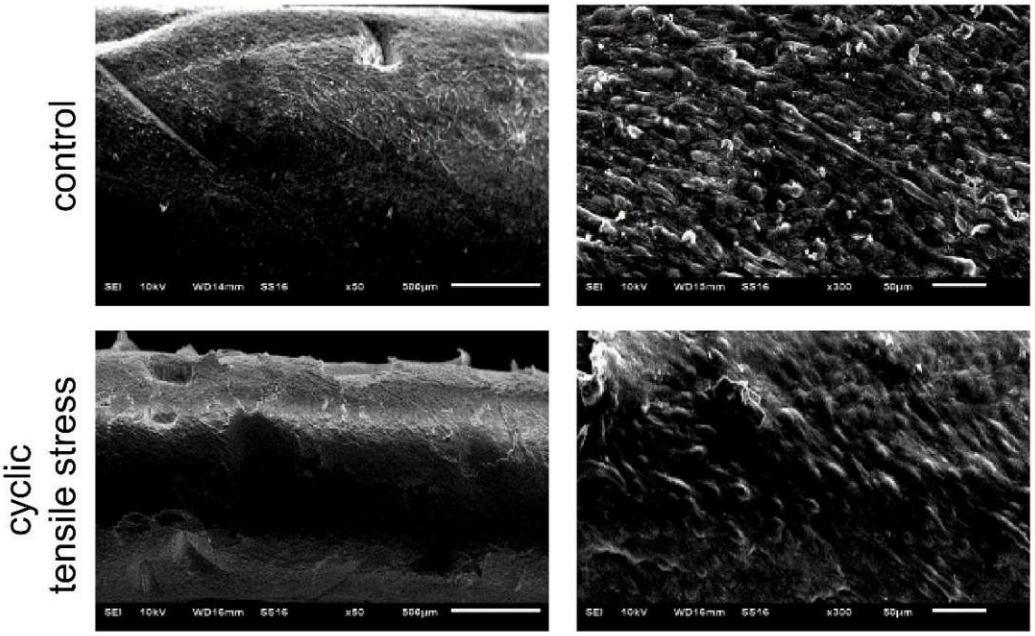

Supplementary figure 3: Effect of cyclic tensile stress on fibrin and myotube alignment. Skeletal muscle-like constructs were stimulated with cyclic tensile stress (10% strain at 1.2 Hz) for 3 days (6 h of stimulation per day, followed by an 18 h break) compared to moderately stimulated controls (static tensile stress of 10%) after 9 days of differentiation induced by moderate mechanical stimulation. Representative images of scanning electron microscope images (n = 3) are shown. Scale bars represent 500 µm (left panels) and 50 µm (right panels).

Contribution to the scientific field

There are numerous sophisticated SMTE strategies, ranging from basic 2D to complex dynamic 3D setups that employ a plethora of biomaterials and cell types. Nevertheless, the vast majority of SMTE approaches have failed to achieve broad clinical application. As described in chapter 2, there are three main reasons for this gap: I) Systemic analyses of suitable cell types, biomaterials, and stimulation protocols to induce muscle maturation are still ongoing. II) The mechanisms underlying many muscle pathologies are still poorly understood, which limits the clinical success of therapeutic approaches. One way to overcome this is the development of reliable physiological models to further understand and study the pathophysiological processes and to perform drug screenings for potential new treatment options. III) Although acellular approaches bypass the general risks associated with cell therapy, many seemingly promising biomaterials have ultimately failed to meet the physical and native requirements to drive muscle regeneration and therefore need to be optimized further.

Within this thesis, we contributed to the development of SMTE approaches by assessing the effect of the properties of a material on its ability to promote and foster myogenic differentiation. From a practical perspective, we made the particularly evident and relevant observation that cellular behavior in 2D setups cannot be translated to more complex 3D structures. The same holds true for translation of findings from a frequently used murine myoblast line to a cell line of human origin. These findings contribute to answering the questions of comparability of different approaches in SMTE, which will facilitate their translation to *in vivo* settings. Furthermore, we developed porous 2D fibroin-based cell matrices by femtosecond laser-induced microstructuring that served as a suitable matrix for culture of myogenic cells. Cells cultivated on microgrooved scaffolds benefitted from the parallel alignment and displayed a more elongated morphology. As the proposed technique presents a suitable environment for myogenic cells, further development of the process will yield promising scaffolds for *in vivo* testing in muscle injury models.

The second main focus of this thesis lay in the improvement of culture settings in SMTE approaches in terms of exerting mechanical stimulation on cells to improve their ability to recapitulate the *in vivo* environment. Hereby, we concentrated on the fact that skeletal muscle is known for its high capacity to adapt to mechanical stress and to regenerate after injuries and the underlying mechanisms enabling its plasticity. Since there is a lack of *in vitro* models that study these processes, we aimed to create a tissue-engineered model for skeletal muscle adaptation to mechanical stress. We created differentiated 3D skeletal muscle-like constructs using a strain-bioreactor and subjected them to cyclic tensile stress to trigger myoblast activation and overload-induced hypertrophy. Besides analyses of morphological changes upon mechanical stress, we examined intracellular signaling pathways during these processes to characterize the model for skeletal muscle hypertrophy and myonuclear accretion.

In summary, this thesis contributes to the field of SMTE by critically assessing current research strategies and introducing new insights in biomaterial optimization and stimulation techniques. Thereby, the myogenic outcome of future SMTE approaches, as well as the relevance of *in vitro* models of skeletal muscle mechanisms and pathologies will be improved.

References

[1] W. R. Frontera and J. Ochala, “Skeletal muscle: a brief review of structure and function,” *Calcif. Tissue Int.*, vol. 96, no. 3, pp. 183–195, 2015.

[2] A. Pratesi, F. Tarantini, and M. Di Bari, “Skeletal muscle: an endocrine organ.,” *Clin. Cases Miner. Bone Metab.*, vol. 10, no. 1, pp. 11–14, 2013.

[3] J.-Y. Reginster, C. Beaudart, F. Buckinx, and O. Bruyère, “Osteoporosis and sarcopenia: two diseases or one?,” *Curr. Opin. Clin. Nutr. Metab. Care*, vol. 19, no. 1, pp. 31–6, Jan. 2016.

[4] C. Laske *et al.*, “Stage-dependent BDNF serum concentrations in Alzheimer’s disease,” *J. Neural Transm.*, vol. 113, no. 9, pp. 1217–1224, Sep. 2006.

[5] A. L. Carey *et al.*, “Interleukin-6 Increases Insulin-Stimulated Glucose Disposal in Humans and Glucose Uptake and Fatty Acid Oxidation In Vitro via AMP-Activated Protein Kinase,” *Diabetes*, vol. 55, no. 10, pp. 2688–2697, Oct. 2006.

[6] B. F. DiCosmo, D. Picarella, and R. A. Flavell, “Local production of human IL-6 promotes insulitis but retards the onset of insulin-dependent diabetes mellitus in non-obese diabetic mice.,” *Int. Immunol.*, vol. 6, no. 12, pp. 1829–37, Dec. 1994.

[7] B. K. Pedersen, “The diseasome of physical inactivity--and the role of myokines in muscle--fat cross talk.,” *J. Physiol.*, vol. 587, no. Pt 23, pp. 5559–68, Dec. 2009.

[8] J. G. Ryall, J. D. Schertzer, and G. S. Lynch, “Cellular and molecular mechanisms underlying age-related skeletal muscle wasting and weakness,” *Biogerontology*, vol. 9, no. 4. pp. 213–228, 2008.

[9] E. Landfeldt *et al.*, “The burden of Duchenne muscular dystrophy: an international, cross-sectional study.,” *Neurology*, vol. 83, no. 6, pp. 529–536, Aug. 2014.

[10] G. Cittadella Vigodarzere and S. Mantero, “Skeletal muscle tissue engineering: strategies for volumetric constructs.,” *Front. Physiol.*, vol. 5, p. 362, 2014.

[11] N. Bursac, M. Juhas, and T. A. Rando, “Synergizing Engineering and Biology to Treat and Model Skeletal Muscle Injury and Disease,” *Annu. Rev. Biomed. Eng.*, vol. 17, no. 1, pp. 217–242, 2015.

[12] T. Endo, “Molecular mechanisms of skeletal muscle development, regeneration, and osteogenic conversion,” *Bone*, vol. 80, pp. 2–13, 2015.

[13] P. Bailey, T. Holowacz, and A. B. Lassar, “The origin of skeletal muscle stem cells in the embryo and the adult,” *Curr. Opin. Cell Biol.*, vol. 13, no. 6, pp. 679–689, 2001.

[14] A. G. Borycki and C. P. Emerson, “Multiple tissue interactions and signal transduction pathways control somite myogenesis.,” *Curr. Top. Dev. Biol.*, vol. 48, pp. 165–224, 2000.

[15] C. F. Bentzinger, Y. X. Wang, M. A. Rudnicki, C. F. Bentzinger, Y. X. Wang, and M. A. Rudnicki, “Building Muscle : Molecular Regulation of Myogenesis Building Muscle : Molecular Regulation of Myogenesis,” pp. 1–16, 2012.

[16] M. J. Petrany and D. P. Millay, “Cell Fusion: Merging Membranes and Making Muscle,” *Trends Cell Biol.*, vol. 29, no. 12, pp. 964–973, Dec. 2019.

[17] S. M. Abmayr and G. K. Pavlath, “Myoblast fusion: lessons from flies and mice,” *Development*, vol. 139, no. 4, pp. 641–656, Feb. 2012.

[18] K. J. M. Boonen, K. Y. Rosaria-Chak, F. P. T. Baaijens, D. W. J. van der Schaft, and M. J. Post, “Essential environmental cues from the satellite cell niche: optimizing proliferation and differentiation,” *Am. J. Physiol. - Cell Physiol.*, vol. 296, no. 6, 2009.

[19] S. Kuang, K. Kuroda, F. Le Grand, and M. A. Rudnicki, “Asymmetric self-renewal and commitment

of satellite stem cells in muscle.," *Cell*, vol. 129, no. 5, pp. 999–1010, Jun. 2007.

[20] L. B. Verdijk, R. Koopman, G. Schaart, K. Meijer, H. H. C. M. Savelberg, and L. J. C. van Loon, "Satellite cell content is specifically reduced in type II skeletal muscle fibers in the elderly," *Am. J. Physiol. Metab.*, vol. 292, no. 1, pp. E151–E157, Jan. 2007.

[21] J. D. Walston, "Sarcopenia in older adults.," *Curr. Opin. Rheumatol.*, vol. 24, no. 6, pp. 623–7, Nov. 2012.

[22] A. M. Pearson and R. B. Young, "Diseases and disorders of muscle.," *Adv. Food Nutr. Res.*, vol. 37, pp. 339–423, 1993.

[23] B. Alberts, A. Johnson, J. Lewis, M. Raff, K. Roberts, and P. Walter, "Molecular Biology of the Cell." Garland Science, 2002.

[24] A. J. Galpin *et al.*, "Human skeletal muscle fiber type specific protein content.," *Anal. Biochem.*, vol. 425, no. 2, pp. 175–82, Jun. 2012.

[25] J. HANSON and H. E. HUXLEY, "Structural Basis of the Cross-Striations in Muscle," *Nature*, vol. 172, no. 4377, pp. 530–532, Sep. 1953.

[26] F. Martino, A. R. Perestrelo, V. Vinarský, S. Pagliari, and G. Forte, "Cellular mechanotransduction: From tension to function," *Front. Physiol.*, vol. 9, no. JUL, p. 824, Jul. 2018.

[27] G. Cittadella Vigodarzere and S. Mantero, "Skeletal muscle tissue engineering: strategies for volumetric constructs.," *Front. Physiol.*, vol. 5, p. 362, 2014.

[28] J. B. Morrissey, R. Y. Cheng, S. Davoudi, and P. M. Gilbert, "Biomechanical Origins of Muscle Stem Cell Signal Transduction," *J. Mol. Biol.*, vol. 428, no. 7, pp. 1441–1454, Apr. 2016.

[29] T. J. Burkholder, "Mechanotransduction in skeletal muscle," *Front. Biosci.*, vol. 12, no. 1, pp. 174–191, 2007.

[30] T. a Hornberger, "Mechanotransduction and the regulation of mTORC1 signaling in skeletal muscle.," *Int. J. Biochem. {\&} cell Biol.*, vol. 43, no. 9, pp. 1267–1276, 2011.

[31] I. Janssen, D. S. Shepard, P. T. Katzmarzyk, and R. Roubenoff, "The healthcare costs of sarcopenia in the United States.," *J. Am. Geriatr. Soc.*, vol. 52, no. 1, pp. 80–5, Jan. 2004.

[32] P. Corso, E. Finkelstein, T. Miller, I. Fiebelkorn, and E. Zaloshnja, "Incidence and lifetime costs of injuries in the United States," *Inj Prev*, vol. 12, no. 4, pp. 212–218, Aug. 2006.

[33] J. R. Guyon, L. S. Steffen, M. H. Howell, T. J. Pusack, C. Lawrence, and L. M. Kunkel, "Modeling human muscle disease in zebrafish.," *Biochim. Biophys. Acta*, vol. 1772, pp. 205–215, 2007.

[34] J. W. McGreevy, C. H. Hakim, M. A. McIntosh, and D. Duan, "Animal models of Duchenne muscular dystrophy: from basic mechanisms to gene therapy," *Dis Model Mech*, vol. 8, no. 3, pp. 195–213, 2015.

[35] G. B. Banks and J. S. Chamberlain, *Chapter 9 The Value of Mammalian Models for Duchenne Muscular Dystrophy in Developing Therapeutic Strategies*, 1st ed., vol. 84, no. 08. Elesvier Inc., 2008.

[36] K. H. Benam *et al.*, "Engineered In Vitro Disease Models.," *Annu. Rev. Pathol.*, vol. 10, pp. 195–262, 2015.

[37] S. Bersini, C. Arrigoni, S. Lopa, M. Bongio, I. Martin, and M. Moretti, "Engineered miniaturized models of musculoskeletal diseases," *Drug Discov. Today*, vol. 21, no. 9, pp. 1429–1436, Sep. 2016.

[38] K.-H. Nam, A. S. T. Smith, S. Lone, S. Kwon, and D.-H. Kim, "Biomimetic 3D Tissue Models for Advanced High-Throughput Drug Screening.," *J. Lab. Autom.*, vol. 20, no. 3, pp. 201–215, 2015.

[39] S. K. Tsivitse, E. Mylona, J. M. Peterson, W. T. Gunning, and F. X. Pizza, “Mechanical loading and injury induce human myotubes to release neutrophil chemoattractants,” *Am. J. Physiol. - Cell Physiol.*, vol. 288, no. 3, 2005.

[40] G. Agrawal, A. Aung, and S. Varghese, “Skeletal muscle-on-a-chip: an in vitro model to evaluate tissue formation and injury.,” *Lab Chip*, vol. 17, no. 20, pp. 3447–3461, Oct. 2017.

[41] D. Gawlitta and C. Bouten, “In Vitro Muscle Model Studies,” in *Pressure Ulcer Research*, Berlin/Heidelberg: Springer-Verlag, 2005, pp. 287–300.

[42] D. Hardy *et al.*, “Comparative Study of Injury Models for Studying Muscle Regeneration in Mice,” *PLoS One*, vol. 11, no. 1, p. e0147198, Jan. 2016.

[43] J. J. McCarthy, E. E. Dupont-Versteegden, C. S. Fry, K. A. Murach, and C. A. Peterson, “Methodological issues limit interpretation of negative effects of satellite cell depletion on adult muscle hypertrophy,” *Development*, vol. 144, no. 8, pp. 1363–1365, Apr. 2017.

[44] I. M. Egner, J. C. Bruusgaard, and K. Gundersen, “An apparent lack of effect of satellite cell depletion on hypertrophy could be due to methodological limitations. Response to ‘Methodological issues limit interpretation of negative effects of satellite cell depletion on adult muscle hypertrophy,’” *Development*, vol. 144, no. 8, pp. 1365–1367, Apr. 2017.

[45] E. Masschelein *et al.*, “Exercise promotes satellite cell contribution to myofibers in a load-dependent manner,” *Skelet. Muscle*, vol. 10, no. 1, Jul. 2020.

[46] C. M. Dungan *et al.*, “Elevated myonuclear density during skeletal muscle hypertrophy in response to training is reversed during detraining,” *Am. J. Physiol. Cell Physiol.*, vol. 316, no. 5, pp. C649–C654, 2019.

[47] Q. Goh *et al.*, “Myonuclear accretion is a determinant of exercise-induced remodeling in skeletal muscle,” *Elife*, vol. 8, Apr. 2019.

[48] A. Grossi, A. H. Karlsson, and M. A. Lawson, “Mechanical stimulation of C2C12 cells increases m-calpain expression, focal adhesion plaque protein degradation,” *Cell Biol. Int.*, vol. 32, no. 6, pp. 615–622, Jun. 2011.

[49] D. G. Moon, G. Christ, J. D. Stitzel, A. Atala, and J. J. Yoo, “Cyclic Mechanical Preconditioning Improves Engineered Muscle Contraction,” *Tissue Eng. Part A*, vol. 14, no. 4, pp. 473–482, Apr. 2008.

[50] B. T. Corona *et al.*, “Further development of a tissue engineered muscle repair construct in vitro for enhanced functional recovery following implantation in vivo in a murine model of volumetric muscle loss injury.,” *Tissue Eng. Part A*, vol. 18, no. 11–12, pp. 1213–1228, Jun. 2012.

[51] B. Maleiner, J. Tomasch, P. Heher, O. Spadiut, D. Rünzler, and C. Fuchs, “The importance of biophysical and biochemical stimuli in dynamic skeletal muscle models,” *Front. Physiol.*, vol. 9, no. AUG, pp. 1–24, 2018.

[52] A. Baccam *et al.*, “The mechanical stimulation of myotubes counteracts the effects of tumor-derived factors through the modulation of the activin/follistatin ratio,” *Front. Physiol.*, vol. 10, no. APR, 2019.

[53] S. J. Zhang, G. A. Truskey, and W. E. Kraus, “Effect of cyclic stretch on β1D-integrin expression and activation of FAK and RhoA,” *Am. J. Physiol. - Cell Physiol.*, vol. 292, no. 6, Jun. 2007.

[54] S.-H. Kook, H.-J. Lee, W.-T. Chung, I.-H. Hwang, S.-A. Lee, and B.-S. K. and J.-C. Lee, “Cyclic Mechanical Stretch Stimulates the Proliferation of C2C12 Myoblasts and Inhibits Their Differentiation via Prolonged Activation of p38 MAPK,” *Mol. Cells*, vol. 25, no. 4, pp. 479–486.

[55] R. Ding *et al.*, “Effect of cell-extracellular matrix interaction on myogenic characteristics and artificial skeletal muscle tissue,” *J. Biosci. Bioeng.*, vol. 130, no. 1, pp. 98–105, Jul. 2020.

[56] A. N. Ramey-Ward, H. Su, and K. Salaita, “Mechanical Stimulation of Adhesion Receptors Using Light-Responsive Nanoparticle Actuators Enhances Myogenesis,” *ACS Appl. Mater. Interfaces*, vol. 12, no. 32, pp. 35903–35917, Aug. 2020.

[57] J. B. Scott *et al.*, “Achieving acetylcholine receptor clustering in tissue-engineered skeletal muscle constructs in vitro through a materials-directed agrin delivery approach,” *Front. Pharmacol.*, vol. 7, no. JAN, Jan. 2017.

[58] L. Terrie, M. Burattini, S. Van Vlierberghe, L. Fassina, and L. Thorrez, “Enhancing Myoblast Fusion and Myotube Diameter in Human 3D Skeletal Muscle Constructs by Electromagnetic Stimulation,” *Front. Bioeng. Biotechnol.*, vol. 10, p. 1, Jun. 2022.

[59] J. P. Mertens, K. B. Sugg, J. D. Lee, and L. M. Larkin, “Engineering muscle constructs for the creation of functional engineered musculoskeletal tissue,” *http://dx.doi.org/10.2217/rme.13.81*, vol. 9, no. 1, pp. 89–100, Dec. 2013.

[60] T. H. Qazi, D. J. Mooney, M. Pumberger, S. Geißler, and G. N. Duda, “Biomaterials based strategies for skeletal muscle tissue engineering: Existing technologies and future trends,” *Biomaterials*, vol. 53, pp. 502–521, Jun. 2015.

[61] A. D. Bach, J. P. Beier, J. Stern-Staeter, and R. E. Horch, “Skeletal muscle tissue engineering.,” *J. Cell. Mol. Med.*, vol. 8, no. 4, pp. 413–422, 2004.

[62] M. Juhas, J. Ye, and N. Bursac, “Design, evaluation, and application of engineered skeletal muscle,” *Methods*, vol. 99, pp. 81–90, Apr. 2015.

[63] Y.-C. Y. C. Huang, R. G. R. G. R. G. R. G. Dennis, L. Larkin, and K. Baar, “Rapid formation of functional muscle in vitro using fibrin gels,” *J. Appl. Physiol.*, vol. 98, no. 2, pp. 706–713, 2005.

[64] T. Matsumoto, J. I. Sasaki, E. Alsberg, H. Egusa, H. Yatani, and T. Sohmura, “Three-dimensional cell and tissue patterning in a strained fibrin gel system,” *PLoS One*, vol. 2, no. 11, pp. 1–6, Nov. 2007.

[65] J. P. Beier, J. Stern-Straeter, V. T. Foerster, U. Kneser, G. B. Stark, and A. D. Bach, “Tissue Engineering of Injectable Muscle: Three-Dimensional Myoblast-Fibrin Injection in the Syngeneic Rat Animal Model,” *Plast. Reconstr. Surg.*, vol. 118, no. 5, pp. 1113–1121, Oct. 2006.

[66] P. Heher *et al.*, “A novel bioreactor for the generation of highly aligned 3D skeletal muscle-like constructs through orientation of fibrin via application of static strain,” *Acta Biomater.*, vol. 24, pp. 251–265, Sep. 2015.

[67] J. W. Weisel and R. I. Litvinov, “Mechanisms of fibrin polymerization and clinical implications.,” *Blood*, vol. 121, no. 10, pp. 1712–9, Mar. 2013.

[68] P. A. Janmey, J. P. Winer, and J. W. Weisel, “Fibrin gels and their clinical and bioengineering applications.,” *J. R. Soc. Interface*, vol. 6, no. 30, pp. 1–10, Jan. 2009.

[69] J. W. Weisel, “The mechanical properties of fibrin for basic scientists and clinicians,” *Biophys. Chem.*, vol. 112, no. 2, pp. 267–276, Dec. 2004.

[70] W. M. Han, Y. C. Jang, and A. J. García, “Engineered matrices for skeletal muscle satellite cell engraftment and function,” *Matrix Biol.*, vol. 60–61, pp. 1–14, Jul. 2016.

[71] T. A. E. E. Ahmed, E. V. Dare, and M. Hincke, “Fibrin: a versatile scaffold for tissue engineering applications.,” *Tissue Eng. Part B. Rev.*, vol. 14, no. 2, pp. 199–215, Jun. 2008.

[72] J. Liu, H. H. K. Xu, H. Zhou, M. D. Weir, Q. Chen, and C. A. Trotman, “Human umbilical cord stem cell encapsulation in novel macroporous and injectable fibrin for muscle tissue engineering,” *Acta Biomater.*, vol. 9, no. 1, pp. 4688–4697, 2013.

[73] A. C. M. Sinanan, J. R. A. Machell, G. T. Wynne-Hughes, N. P. Hunt, and M. P. Lewis, “αvβ3 and αvβ5 integrins and their role in muscle precursor cell adhesion,” *Biol. Cell*, vol. 100, no. 8, pp. 465–

477, Aug. 2008.

[74] K. Yokoyama, X.-P. Zhang, L. Medved, and Y. Takada, “Specific Binding of Integrin αvβ3 to the Fibrinogen γ and α E Chain C-Terminal Domains †,” *Biochemistry*, vol. 38, no. 18, pp. 5872–5877, May 1999.

[75] M. Buckingham, “How the community effect orchestrates muscle differentiation,” no. 7, pp. 13–16, 2002.

[76] J. W. Weisel and R. I. Litvinov, “Fibrin formation, structure and properties,” *Subcell. Biochem.*, vol. 82, pp. 405–456, Jan. 2017.

[77] L. Hecker, K. Baar, R. G. Dennis, and K. N. Bitar, “Development of a three-dimensional physiological model of the internal anal sphincter bioengineered in vitro from isolated smooth muscle cells,” *Am. J. Physiol. - Gastrointest. Liver Physiol.*, vol. 289, no. 2, 2005.

[78] M. T. Lam, Y.-C. C. Huang, R. K. Birla, and S. Takayama, “Microfeature guided skeletal muscle tissue engineering for highly organized 3-dimensional free-standing constructs,” *Biomaterials*, vol. 30, no. 6, pp. 1150–1155, Feb. 2009.

[79] L. Wang, J. Shansky, and H. Vandenburgh, “Induced formation and maturation of acetylcholine receptor clusters in a defined 3D bio-artificial muscle.,” *Mol. Neurobiol.*, vol. 48, no. 3, pp. 397–403, Dec. 2013.

[80] M. Juhas and N. Bursac, “Roles of adherent myogenic cells and dynamic culture in engineered muscle function and maintenance of satellite cells,” *Biomaterials*, vol. 35, no. 35, pp. 9438–9446, Nov. 2014.

[81] W. Bian and N. Bursac, “Engineered skeletal muscle tissue networks with controllable architecture.,” *Biomaterials*, vol. 30, no. 7, pp. 1401–12, Mar. 2009.

[82] S. Hinds, W. Bian, R. G. Dennis, and N. Bursac, “The role of extracellular matrix composition in structure and function of bioengineered skeletal muscle,” *Biomaterials*, vol. 32, no. 14, pp. 3575–3583, May 2011.

[83] C. Fuoco *et al.*, “Injectable polyethylene glycol-fibrinogen hydrogel adjuvant improves survival and differentiation of transplanted mesoangioblasts in acute and chronic skeletal-muscle degeneration.,” *Skelet. Muscle*, vol. 2, no. 1, p. 24, Nov. 2012.

[84] P. M. Gilbert *et al.*, “Substrate elasticity regulates skeletal muscle stem cell self-renewal in culture.,” *Science*, vol. 329, no. 5995, pp. 1078–81, Aug. 2010.

[85] A. J. Engler, M. A. Griffin, S. Sen, C. G. Bönnemann, H. L. Sweeney, and D. E. Discher, “Myotubes differentiate optimally on substrates with tissue-like stiffness: pathological implications for soft or stiff microenvironments.,” *J. Cell Biol.*, vol. 166, no. 6, pp. 877–887, Sep. 2004.

[86] A. J. Engler, S. Sen, H. L. Sweeney, and D. E. Discher, “Matrix Elasticity Directs Stem Cell Lineage Specification,” *Cell*, vol. 126, no. 4, pp. 677–689, Aug. 2006.

[87] X. Hu, S.-H. Park, E. S. Gil, X.-X. Xia, A. S. Weiss, and D. L. Kaplan, “The influence of elasticity and surface roughness on myogenic and osteogenic-differentiation of cells on silk-elastin biomaterials.,” *Biomaterials*, vol. 32, no. 34, pp. 8979–89, Dec. 2011.

[88] S. Romanazzo *et al.*, “Substrate stiffness affects skeletal myoblast differentiation in vitro.,” *Sci. Technol. Adv. Mater.*, vol. 13, no. 6, p. 064211, Dec. 2012.

[89] V. Gribova, C. Gauthier-Rouvière, C. Albigès-Rizo, R. Auzely-Velty, and C. Picart, “Effect of RGD functionalization and stiffness modulation of polyelectrolyte multilayer films on muscle cell differentiation.,” *Acta Biomater.*, vol. 9, no. 5, pp. 6468–80, May 2013.

[90] A. M. Noonan, N. Mazara, D. P. Zwambag, E. Weersink, G. A. Power, and S. H. M. Brown, “Age-related changes in human single muscle fibre passive elastic properties are sarcomere length

dependent," *Exp. Gerontol.*, vol. 137, Aug. 2020.

[91] R. L. Lieber, E. Runesson, F. Einarsson, and J. Fridén, "Inferior mechanical properties of spastic muscle bundles due to hypertrophic but compromised extracellular matrix material," *Muscle and Nerve*, vol. 28, no. 4, pp. 464–471, Oct. 2003.

[92] S. Agyapong-Badu, M. Warner, D. Samuel, and M. Stokes, "Measurement of ageing effects on muscle tone and mechanical properties of rectus femoris and biceps brachii in healthy males and females using a novel hand-held myometric device," *Arch. Gerontol. Geriatr.*, vol. 62, pp. 59–67, Jan. 2016.

[93] I. Jun *et al.*, "Creating Hierarchical Topographies on Fibrous Platforms Using Femtosecond Laser Ablation for Directing Myoblasts Behavior," vol. 8, no. 5, pp. 3407–3417, Feb. 2016.

[94] O. V. Pham-Nguyen *et al.*, "Preparation of Stretchable Nanofibrous Sheets with Sacrificial Coaxial Electrospinning for Treatment of Traumatic Muscle Injury," *Adv. Healthc. Mater.*, vol. 10, no. 8, Apr. 2021.

[95] R. Shah, J. C. Knowles, N. P. Hunt, and M. P. Lewis, "Development of a novel smart scaffold for human skeletal muscle regeneration," *J. Tissue Eng. Regen. Med.*, vol. 10, no. 2, pp. 162–171, Feb. 2016.

[96] V. Hosseini *et al.*, "Engineered contractile skeletal muscle tissue on a microgrooved methacrylated gelatin substrate," *Tissue Eng. - Part A*, vol. 18, no. 23–24, pp. 2453–2465, Dec. 2012.

[97] J. M. Fishman *et al.*, "Skeletal muscle tissue engineering: which cell to use?," *Tissue Eng. Part B. Rev.*, vol. 19, no. 6, pp. 503–515, Dec. 2013.

[98] D. Yaffe and O. Saxel, "Serial passaging and differentiation of myogenic cells isolated from dystrophic mouse muscle," *Nature*, vol. 270, no. 5639, pp. 725–727, 1977.

[99] M. Thorley *et al.*, "Skeletal muscle characteristics are preserved in hTERT/cdk4 human myogenic cell lines," *Skelet. Muscle*, vol. 6, no. 1, p. 43, Dec. 2016.

[100] P. S. Zammit, T. A. Partridge, and Z. Yablonka-Reuveni, "The skeletal muscle satellite cell: the stem cell that came in from the cold," *J. Histochem. Cytochem.*, vol. 54, no. 11, pp. 1177–1191, Nov. 2006.

[101] P. S. Zammit, J. P. Golding, Y. Nagata, V. Hudon, T. A. Partridge, and J. R. Beauchamp, "Muscle satellite cells adopt divergent fates: a mechanism for self-renewal?," *J. Cell Biol.*, vol. 166, no. 3, pp. 347–357, Aug. 2004.

[102] I. Y. Shadrin, A. Khodabukus, and N. Bursac, "Striated Muscle Function, Regeneration, and Repair," *Cell. Mol. Life Sci.*, vol. 73, no. 22, p. 4175, Jun. 2016.

[103] F. Relaix *et al.*, "Pw1, a Novel Zinc Finger Gene Implicated in the Myogenic and Neuronal Lineages," *Dev. Biol.*, vol. 177, no. 2, pp. 383–396, Aug. 1996.

[104] M. G. Minasi *et al.*, "The meso-angioblast: a multipotent, self-renewing cell that originates from the dorsal aorta and differentiates into most mesodermal tissues," *Development*, vol. 129, no. 11, pp. 2773–2783, 2002.

[105] A. Dellavalle *et al.*, "Pericytes of human skeletal muscle are myogenic precursors distinct from satellite cells," *Nat. Cell Biol.*, vol. 9, no. 3, pp. 255–267, Mar. 2007.

[106] R. Tonlorenzi, A. Dellavalle, E. Schnapp, G. Cossu, and M. Sampaolesi, "Isolation and Characterization of Mesoangioblasts from Mouse, Dog, and Human Tissues," in *Current Protocols in Stem Cell Biology*, Hoboken, NJ, USA: John Wiley & Sons, Inc., 2007.

[107] M. Crisan *et al.*, "A Perivascular Origin for Mesenchymal Stem Cells in Multiple Human Organs," *Cell Stem Cell*, vol. 3, no. 3, pp. 301–313, Sep. 2008.

[108] A. W. B. B. Joe *et al.*, “Muscle injury activates resident fibro/adipogenic progenitors that facilitate myogenesis,” vol. 12, no. 2, pp. 153–163, 2010.

[109] A. Birbrair *et al.*, “Skeletal muscle pericyte subtypes differ in their differentiation potential,” *Stem Cell Res.*, vol. 10, no. 1, pp. 67–84, Jan. 2013.

[110] S. Ostrovidov *et al.*, “Stem Cell Differentiation Toward the Myogenic Lineage for Muscle Tissue Regeneration: A Focus on Muscular Dystrophy,” *Stem Cell Reviews and Reports*, vol. 11, no. 6. Humana Press Inc., pp. 866–884, 01-Dec-2015.

[111] G. Ferrari *et al.*, “Muscle regeneration by bone marrow-derived myogenic progenitors.,” *Science*, vol. 279, no. 5356, pp. 1528–1530, Mar. 1998.

[112] M. Dezawa *et al.*, “Bone marrow stromal cells generate muscle cells and repair muscle degeneration,” *Science*, vol. 309, no. 5732, pp. 314–317, Jul. 2005.

[113] C. Sassoli, S. Zecchi-Orlandini, and L. Formigli, “Trophic Actions of Bone Marrow-Derived Mesenchymal Stromal Cells for Muscle Repair/Regeneration,” *Cells*, vol. 1, no. 4, pp. 832–850, Oct. 2012.

[114] C. De Bari, F. Dell’Accio, F. Vandenabeele, J. R. Vermeesch, J. M. Raymackers, and F. P. Luyten, “Skeletal muscle repair by adult human mesenchymal stem cells from synovial membrane,” *J. Cell Biol.*, vol. 160, no. 6, p. 909, Mar. 2003.

[115] J. K. Koponen *et al.*, “Umbilical Cord Blood–derived Progenitor Cells Enhance Muscle Regeneration in Mouse Hindlimb Ischemia Model,” *Mol. Ther.*, vol. 15, no. 12, pp. 2172–2177, 2007.

[116] J. W. Lee, X. Fang, A. Krasnodembskaya, J. P. Howard, and M. A. Matthay, “Concise review: Mesenchymal stem cells for acute lung injury: Role of paracrine soluble factors,” *Stem Cells*, vol. 29, no. 6, pp. 913–919, Jun. 2011.

[117] P. von Roth *et al.*, “Intra-Arterial MSC Transplantation Restores Functional Capacity After Skeletal Muscle Trauma.,” *Open Orthop. J.*, vol. 6, pp. 352–356, 2012.

[118] M. Gnecchi, Z. Zhang, A. Ni, and V. J. Dzau, “Paracrine mechanisms in adult stem cell signaling and therapy,” *Circ. Res.*, vol. 103, no. 11, pp. 1204–1219, Nov. 2008.

[119] K. Le Blanc and D. Mougiakakos, “Multipotent mesenchymal stromal cells and the innate immune system,” *Nat. Rev. Immunol. 2012 125*, vol. 12, no. 5, pp. 383–396, Apr. 2012.

[120] T. Kinnaird *et al.*, “Marrow-Derived Stromal Cells Express Genes Encoding a Broad Spectrum of Arteriogenic Cytokines and Promote In Vitro and In Vivo Arteriogenesis Through Paracrine Mechanisms,” *Circ. Res.*, vol. 94, no. 5, pp. 678–685, Mar. 2004.

[121] F. S. Tedesco *et al.*, “Transplantation of genetically corrected human iPSC-derived progenitors in mice with limb-girdle muscular dystrophy.,” *Sci. Transl. Med.*, vol. 4, no. 140, pp. 140ra89-140ra89, Jun. 2012.

[122] S. M. Maffioletti *et al.*, “Three-Dimensional Human iPSC-Derived Artificial Skeletal Muscles Model Muscular Dystrophies and Enable Multilineage Tissue Engineering.,” *Cell Rep.*, vol. 23, no. 3, pp. 899–908, Apr. 2018.

[123] S. Rangarajan, L. Madden, and N. Bursac, “Use of Flow, Electrical, and Mechanical Stimulation to Promote Engineering of Striated Muscles.,” *Ann. Biomed. Eng.*, vol. 42, no. 7, pp. 1391–1405, Jul. 2014.

[124] T. Okano and T. Matsuda, “Tissue engineered skeletal muscle: preparation of highly dense, highly oriented hybrid muscular tissues.,” *Cell Transplant.*, vol. 7, no. 1, pp. 71–82, 1998.

[125] C. A. Powell, B. L. Smiley, J. Mills, and H. H. Vandenburgh, “Mechanical stimulation improves tissue-engineered human skeletal muscle,” *AJP Cell Physiol.*, vol. 283, no. 5, pp. C1557--C1565,

2002.

[126] G. Candiani *et al.*, “Cyclic mechanical stimulation favors myosin heavy chain accumulation in engineered skeletal muscle constructs.,” *J. Appl. Biomater. {\&} Biomech. JABB*, vol. 8, no. 2, pp. 68–75, 2010.

[127] A. Auluck, V. Mudera, N. P. Hunt, and M. P. Lewis, “A three-dimensional in vitro model system to study the adaptation of craniofacial skeletal muscle following mechanostimulation,” *Eur. J. Oral Sci.*, vol. 113, no. 3, pp. 218–224, Jun. 2005.

[128] S. R. Chowdhury *et al.*, “One-Step Purification of Human Skeletal Muscle Myoblasts and Subsequent Expansion Using Laminin-Coated Surface.,” *Tissue Eng. Part C. Methods*, vol. 21, no. 11, pp. 1135–42, Nov. 2015.

[129] M. A. Machingal *et al.*, “A tissue-engineered muscle repair construct for functional restoration of an irrecoverable muscle injury in a murine model.,” *Tissue Eng. Part A*, vol. 17, no. 17–18, pp. 2291–303, Sep. 2011.

[130] H. Vandenburgh and S. Kaufman, “In vitro model for stretch-induced hypertrophy of skeletal muscle,” *Science (80-.).*, vol. 203, no. 4377, pp. 265–268, 1979.

[131] H. H. Vandenburgh, S. Hatfaludy, P. Karlisch, and J. Shansky, “Skeletal muscle growth is stimulated by intermittent stretch-relaxation in tissue culture,” *Am. J. Physiol. - Cell Physiol.*, vol. 256, no. 3, 1989.

[132] H. H. Vandenburgh and P. Karlisch, “Longitudinal growth of skeletal myotubes in vitro in a new horizontal mechanical cell stimulator.,” *Vitr. Cell. {\&} Dev. Biol. J. Tissue Cult. Assoc.*, vol. 25, no. 7, pp. 607–616, Jul. 1989.

[133] U. Cheema, R. Brown, V. Mudera, Y. Y. Shi, G. Mcgrouther, and G. Goldspink, “Mechanical signals and IGF-I gene splicing in vitro in relation to development of skeletal muscle,” *J. Cell. Physiol.*, vol. 202, no. 1, pp. 67–75, 2005.

[134] S. Jana, S. K. L. L. Levengood, and M. Zhang, “Anisotropic Materials for Skeletal-Muscle-Tissue Engineering,” *Adv. Mater.*, vol. 28, no. 48, pp. 10588–10612, Dec. 2016.

[135] J. M. Grasman, M. J. Zayas, R. L. Page, and G. D. Pins, “Biomimetic scaffolds for regeneration of volumetric muscle loss in skeletal muscle injuries,” *Acta Biomater.*, vol. 25, pp. 2–15, 2015.

[136] H. Manring, E. Abreu, L. Brotto, N. Weisleder, and M. Brotto, “Novel excitation-contraction coupling related genes reveal aspects of muscle weakness beyond atrophy-new hopes for treatment of musculoskeletal diseases,” *Frontiers in Physiology*, vol. 5 FEB. Frontiers Media SA, 2014.

[137] O. Chaudhuri, J. Cooper-White, P. A. Janmey, D. J. Mooney, and V. B. Shenoy, “Effects of extracellular matrix viscoelasticity on cellular behaviour,” *Nature*, vol. 584, no. 7822, pp. 535–546, Aug. 2020.

[138] S. Werner, H. T. K. Vu, and J. C. Rink, “Self-organization in development, regeneration and organoids,” *Current Opinion in Cell Biology*, vol. 44. Elsevier Ltd, pp. 102–109, 01-Feb-2017.

[139] M. M. J. P. E. Sthijns, V. L. S. Lapointe, and C. A. Van Blitterswijk, “Building Complex Life through Self-Organization,” *Tissue Eng. - Part A*, vol. 25, no. 19–20, pp. 1341–1346, Oct. 2019.

[140] R. Rizzi, C. Bearzi, A. Mauretti, S. Bernardini, S. Cannata, and C. Gargioli, “Tissue engineering for skeletal muscle regeneration,” *Muscles, Ligaments and Tendons Journal*, vol. 2, no. 3. CIC Edizioni Internazionali, pp. 230–234, Jul-2012.

[141] P. Bajaj *et al.*, “Patterning the differentiation of C2C12 skel1. Bajaj P, Reddy B, Millet L, et al. Patterning the differentiation of C2C12 skeletal myoblasts. Integr Biol 2011; 3: 897–909.etal myoblasts,” *Integr. Biol.*, vol. 3, no. 9, pp. 897–909, Sep. 2011.

[142] S. Ostrovidov *et al.*, “Skeletal Muscle Tissue Engineering : Methods to Form Skeletal Myotubes,”

Tissue Eng. Part B. Rev., vol. 00, no. 00, pp. 1–34, Oct. 2014.

[143] S. L. Hume *et al.*, “Alignment of multi-layered muscle cells within three-dimensional hydrogel macrochannels,” *Acta Biomater.*, vol. 8, no. 6, pp. 2193–2202, Jul. 2012.

[144] L. Rao, Y. Qian, A. Khodabukus, T. Ribar, and N. Bursac, “Engineering human pluripotent stem cells into a functional skeletal muscle tissue,” *Nat. Commun.*, vol. 9, no. 1, Dec. 2018.

[145] L. Kain *et al.*, “Calibration of colloidal probes with atomic force microscopy for micromechanical assessment,” *J. Mech. Behav. Biomed. Mater.*, vol. 85, pp. 225–236, Sep. 2018.

[146] O. G. Andriotis *et al.*, “Nanomechanical assessment of human and murine collagen fibrils via atomic force microscopy cantilever-based nanoindentation,” *J. Mech. Behav. Biomed. Mater.*, vol. 39, pp. 9–26, Nov. 2014.

[147] W. C. Oliver and G. M. Pharr, “An improved technique for determining hardness and elastic modulus using load and displacement sensing indentation experiments,” *J. Mater. Res.*, vol. 7, no. 6, pp. 1564–1583, Jun. 1992.

[148] M. L. Bayer *et al.*, “Release of tensile strain on engineered human tendon tissue disturbs cell adhesions, changes matrix architecture, and induces an inflammatory phenotype.,” *PLoS One*, vol. 9, no. 1, p. e86078, 2014.

[149] C. J. Sherr and J. M. Roberts, “CDK inhibitors: Positive and negative regulators of G1-phase progression,” *Genes and Development*, vol. 13, no. 12. Cold Spring Harbor Laboratory Press, pp. 1501–1512, 15-Jun-1999.

[150] C. F. Bentzinger, Y. X. Wang, and M. A. Rudnicki, “Building muscle: molecular regulation of myogenesis.,” *Cold Spring Harb. Perspect. Biol.*, vol. 4, no. 2, Feb. 2012.

[151] S. Yokoyama and H. Asahara, “The myogenic transcriptional network,” *Cellular and Molecular Life Sciences*, vol. 68, no. 11. Cell Mol Life Sci, pp. 1843–1849, Jun-2011.

[152] M. A. Rudnicki, P. N. J. Schnegelsberg, R. H. Stead, T. Braun, H. H. Arnold, and R. Jaenisch, “MyoD or Myf-5 is required for the formation of skeletal muscle,” *Cell*, vol. 75, no. 7, pp. 1351–1359, Dec. 1993.

[153] P. Londhe and J. K. Davie, “Sequential association of myogenic regulatory factors and E proteins at muscle-specific genes,” *Skelet. Muscle*, vol. 1, no. 1, Apr. 2011.

[154] R. L. Lieber and J. Fridén, “Functional and clinical significance of skeletal muscle architecture,” *Muscle and Nerve*, vol. 23, no. 11. Muscle Nerve, pp. 1647–1666, 2000.

[155] B. Wei and J. P. Jin, “Troponin T isoforms and posttranscriptional modifications: Evolution, regulation and function,” *Archives of Biochemistry and Biophysics*, vol. 505, no. 2. Arch Biochem Biophys, pp. 144–154, 15-Jan-2011.

[156] D. M. Brown, T. Parr, and J. M. Brameld, “Myosin heavy chain mRNA isoforms are expressed in two distinct cohorts during C2C12 myogenesis,” *J. Muscle Res. Cell Motil.*, vol. 32, no. 6, pp. 383–390, Mar. 2012.

[157] A. Birgersdotter, R. Sandberg, and I. Ernberg, “Gene expression perturbation in vitro - A growing case for three-dimensional (3D) culture systems,” *Seminars in Cancer Biology*, vol. 15, no. 5 SPEC. ISS. Academic Press, pp. 405–412, 2005.

[158] E. Serena, S. Zatti, E. Reghelin, A. Pasut, E. Cimetta, and N. Elvassore, “Soft substrates drive optimal differentiation of human healthy and dystrophic myotubes.,” *Integr. Biol. (Camb).*, vol. 2, no. 4, pp. 193–201, Apr. 2010.

[159] R. N. Palchesko, L. Zhang, Y. Sun, and A. W. Feinberg, “Development of Polydimethylsiloxane Substrates with Tunable Elastic Modulus to Study Cell Mechanobiology in Muscle and Nerve,” *PLoS One*, vol. 7, no. 12, p. e51499, Dec. 2012.

[160] C. T. McKee, J. A. Last, P. Russell, and C. J. Murphy, “Indentation versus tensile measurements of young’s modulus for soft biological tissues,” *Tissue Eng. - Part B Rev.*, vol. 17, no. 3, pp. 155–164, Jun. 2011.

[161] T. Boontheekul, E. E. Hill, H. J. Kong, and D. J. Mooney, “Regulating myoblast phenotype through controlled gel stiffness and degradation,” *Tissue Eng.*, vol. 13, no. 7, pp. 1431–1442, Jul. 2007.

[162] F. Trensz *et al.*, “Increased microenvironment stiffness in damaged myofibers promotes myogenic progenitor cell proliferation.,” *Skelet. Muscle*, vol. 5, p. 5, 2015.

[163] Baxter Deutschland GmbH, . “BEZEICHNUNG DES ARZNEIMITTELS.” [Online]. Available: http://www.synovislife.com/de/resources/pdfs/tissucol/TISSUCOL_IFU.pdf. [Accessed: 21-Jul-2017].

[164] C. Buchta, H. C. Hedrich, M. Macher, P. Höcker, and H. Redl, “Biochemical characterization of autologous fibrin sealants produced by CryoSeal® and Vivostat® in comparison to the homologous fibrin sealant product Tissucol/Tisseel®,” *Biomaterials*, vol. 26, no. 31, pp. 6233–6241, Nov. 2005.

[165] P. Danielsen, B. Jørgensen, T. Karlsmark, L. N. Jorgensen, and M. S. Agren, “Effect of topical autologous platelet-rich fibrin versus no intervention on epithelialization of donor sites and meshed split-thickness skin autografts: a randomized clinical trial.,” *Plast. Reconstr. Surg.*, vol. 122, no. 5, pp. 1431–1440, 2008.

[166] B. L. Eppley, J. E. Woodell, and J. Higgins, “Platelet quantification and growth factor analysis from platelet-rich plasma: implications for wound healing.,” *Plast. Reconstr. Surg.*, vol. 114, no. 6, pp. 1502–8, Nov. 2004.

[167] M. W. Oswald, H. H. Hunt, and J. Lazarchick, “Normal range of plasma fibrinogen.,” *Am. J. Med. Technol.*, vol. 49, no. 1, pp. 57–9, Jan. 1983.

[168] N. R. W. Martin *et al.*, “Factors affecting the structure and maturation of human tissue engineered skeletal muscle,” *Biomaterials*, vol. 34, no. 23, pp. 5759–5765, 2013.

[169] J. Stern-Straeter, G. Bran, F. Riedel, A. Sauter, K. Hörmann, and U. R. Goessler, “Characterization of human myoblast cultures for tissue engineering,” *Int. J. Mol. Med.*, vol. 21, no. 1, pp. 49–56, 2008.

[170] J.-F. Chen *et al.*, “The role of microRNA-1 and microRNA-133 in skeletal muscle proliferation and differentiation.,” *Nat. Genet.*, vol. 38, no. 2, pp. 228–33, 2006.

[171] A. Rangarajan and R. A. Weinberg, “Opinion: Comparative biology of mouse versus human cells: modelling human cancer in mice,” *Nat. Rev. Cancer*, vol. 3, no. 12, pp. 952–959, Dec. 2003.

[172] P. Muñoz-Cánoves, F. Miralles, M. Baiget, and J. Félez, “Inhibition of urokinase-type plasminogen activator (uPA) abrogates myogenesis in vitro,” *Thromb. Haemost.*, vol. 77, no. 3, pp. 526–534, 1997.

[173] M. Suelves *et al.*, “Plasmin activity is required for myogenesis in vitro and skeletal muscle regeneration in vivo,” *Blood*, vol. 99, no. 8, pp. 2835–2844, Apr. 2002.

[174] A. Khodabukus and K. Baar, “Regulating fibrinolysis to engineer skeletal muscle from the C2C12 cell line,” *Tissue Eng. - Part C Methods*, vol. 15, no. 3, pp. 501–511, Sep. 2009.

[175] B. T. Corona, J. C. Rivera, J. G. Owens, J. C. Wenke, and C. R. Rathbone, “Volumetric muscle loss leads to permanent disability following extremity trauma,” *J. Rehabil. Res. Dev.*, vol. 52, no. 7, pp. 785–792, 2015.

[176] J. D. Cross, J. R. Ficke, J. R. Hsu, B. D. Masini, and J. C. Wenke, “Battlefield orthopaedic injuries cause the majority of long-term disabilities,” *J. Am. Acad. Orthop. Surg.*, vol. 19, no. SUPPL.1, 2011.

[177] D. I. Devore *et al.*, “For Combat Wounded: Extremity Trauma Therapies from the USAISR,” *Mil.*

Med., vol. 176, no. 6, pp. 660–663, 2011.

[178] A. De Castro Pochini *et al.*, “Clinical considerations for the surgical treatment of pectoralis major muscle ruptures based on 60 cases: A prospective study and literature review,” *Am. J. Sports Med.*, vol. 42, no. 1, pp. 95–102, Jan. 2014.

[179] K. Doi, Y. Hattori, S. H. Tan, and V. Dhawan, “Basic science behind functioning free muscle transplantation,” *Clinics in Plastic Surgery*, vol. 29, no. 4. Clin Plast Surg, pp. 483–495, 2002.

[180] C. H. Lin, Y. Te Lin, J. T. Yeh, and C. T. Chen, “Free functioning muscle transfer for lower extremity posttraumatic composite structure and functional defect,” *Plast. Reconstr. Surg.*, vol. 119, no. 7, pp. 2118–2126, Jun. 2007.

[181] R. Lawson and L. Scott Lcvin, “Principles of free tissue transfer in orthopaedic practice,” *J. Am. Acad. Orthop. Surg.*, vol. 15, no. 5, pp. 290–299, 2007.

[182] A. Diwan, K. R. Eberlin, and R. M. Smith, “The principles and practice of open fracture care, 2018,” *Chinese J. Traumatol. - English Ed.*, vol. 21, no. 4, pp. 187–192, Aug. 2018.

[183] B. Bianchi, C. Copelli, S. Ferrari, A. Ferri, and E. Sesenna, “Free flaps: Outcomes and complications in head and neck reconstructions,” *J. Cranio-Maxillofacial Surg.*, vol. 37, no. 8, pp. 438–442, Dec. 2009.

[184] J. STERN-STRAETER, F. RIEDEL, G. BRAN, K. HÖRMANN, and U. R. GOESSLER, “Advances in Skeletal Muscle Tissue Engineering,” *In Vivo (Brooklyn).*, vol. 21, no. 3, 2007.

[185] D. Sengupta, S. D. Waldman, and S. Li, “From in vitro to in situ tissue engineering,” *Ann. Biomed. Eng.*, vol. 42, no. 7, pp. 1537–1545, 2014.

[186] M. E. Carnes and G. D. Pins, “Skeletal muscle tissue engineering: Biomaterials-based strategies for the treatment of volumetric muscle loss,” *Bioengineering*, vol. 7, no. 3. MDPI AG, pp. 1–39, 01-Sep-2020.

[187] M. D. Grounds, “Towards Understanding Skeletal Muscle Regeneration,” *Pathol. Res. Pract.*, vol. 187, no. 1, pp. 1–22, 1991.

[188] W. Bian and N. Bursac, “Tissue engineering of functional skeletal muscle: Challenges and recent advances,” *IEEE Engineering in Medicine and Biology Magazine*, vol. 27, no. 5. IEEE Eng Med Biol Mag, pp. 109–113, Sep-2008.

[189] N. J. Turner and S. F. Badylak, “Regeneration of skeletal muscle,” *Cell and Tissue Research*, vol. 347, no. 3. Cell Tissue Res, pp. 759–774, Mar-2012.

[190] A. Quigley *et al.*, “Towards bioengineered skeletal muscle: Recent developments in vitro and in vivo,” *Essays in Biochemistry*, vol. 65, no. 3. Portland Press Ltd, pp. 555–567, 01-Aug-2021.

[191] A. E. Thurber, F. G. Omenetto, and D. L. Kaplan, “In vivo bioresponses to silk proteins,” *Biomaterials*, vol. 71. Elsevier Ltd, pp. 145–157, 01-Dec-2015.

[192] S. Manchineella, G. Thrivikraman, K. K. Khanum, P. C. Ramamurthy, B. Basu, and T. Govindaraju, “Pigmented Silk Nanofibrous Composite for Skeletal Muscle Tissue Engineering,” *Adv. Healthc. Mater.*, vol. 5, no. 10, pp. 1222–1232, May 2016.

[193] V. Chaturvedi *et al.*, “Silk fibroin scaffolds with muscle-like elasticity support in vitro differentiation of human skeletal muscle cells,” *J. Tissue Eng. Regen. Med.*, vol. 11, no. 11, pp. 3178–3192, Nov. 2017.

[194] O. Tokareva, M. Jacobsen, M. Buehler, J. Wong, and D. L. Kaplan, “Structure-function-property-design interplay in biopolymers: Spider silk,” *Acta Biomaterialia*, vol. 10, no. 4. Elsevier Ltd, pp. 1612–1626, 2014.

[195] K. Jastrzebska, K. Kucharczyk, A. Florczak, E. Dondajewska, A. Mackiewicz, and H. Dams-

Kozlowska, “Silk as an innovative biomaterial for cancer therapy,” *Reports of Practical Oncology and Radiotherapy*, vol. 20, no. 2. Urban and Partner, pp. 87–98, 01-Mar-2015.

[196] J. Rnjak-Kovacina, T. M. Desrochers, K. A. Burke, and D. L. Kaplan, “The effect of sterilization on silk fibroin biomaterial properties,” *Macromol. Biosci.*, vol. 15, no. 6, pp. 861–874, Jun. 2015.

[197] Y. Wang *et al.*, “In vivo degradation of three-dimensional silk fibroin scaffolds,” *Biomaterials*, vol. 29, no. 24–25, pp. 3415–3428, Aug. 2008.

[198] C. Holland, K. Numata, J. Rnjak-Kovacina, and F. P. Seib, “The Biomedical Use of Silk: Past, Present, Future,” *Advanced Healthcare Materials*, vol. 8, no. 1. Wiley-VCH Verlag, 10-Jan-2019.

[199] S. U. Din Wani and G. H. Veerabhadrappa, “Silk Fibroin Based Drug Delivery Applications: Promises and Challenges,” *Curr. Drug Targets*, vol. 19, no. 10, pp. 1177–1190, Dec. 2017.

[200] P. Dubey, S. Murab, S. Karmakar, P. K. Chowdhury, and S. Ghosh, “Modulation of Self-Assembly Process of Fibroin: An Insight for Regulating the Conformation of Silk Biomaterials,” *Biomacromolecules*, vol. 16, no. 12, pp. 3936–3944, Nov. 2015.

[201] M. A. Tomeh, R. Hadianamrei, and X. Zhao, “Silk fibroin as a functional biomaterial for drug and gene delivery,” *Pharmaceutics*, vol. 11, no. 10. MDPI AG, 01-Oct-2019.

[202] V. Pandey, T. Haider, P. Jain, P. N. Gupta, and V. Soni, “Silk as a leading-edge biological macromolecule for improved drug delivery - ScienceDirect,” *J. Drug Deliv. Sci. Technol.*, vol. 55:101294, 2020.

[203] O. Gianak, E. Pavlidou, C. Sarafidis, V. Karageorgiou, and E. Deliyanni, “Silk Fibroin Nanoparticles for Drug Delivery: Effect of Bovine Serum Albumin and Magnetic Nanoparticles Addition on Drug Encapsulation and Release,” *Separations*, vol. 5, no. 2, p. 25, Apr. 2018.

[204] D. N. Rockwood, R. C. Preda, T. Yücel, X. Wang, M. L. Lovett, and D. L. Kaplan, “Materials fabrication from Bombyx mori silk fibroin.,” *Nat. Protoc.*, vol. 6, no. 10, pp. 1612–31, Oct. 2011.

[205] W. Guo *et al.*, “Sericin nanomicelles with enhanced cellular uptake and ph-triggered release of doxorubicin reverse cancer drug resistance,” *Drug Deliv.*, vol. 25, no. 1, pp. 1103–1116, 2018.

[206] O. Shchepelina, I. Drachuk, M. K. Gupta, J. Lin, and V. V. Tsukruk, “Silk-on-Silk Layer-by-Layer Microcapsules,” *Adv. Mater.*, vol. 23, no. 40, pp. 4655–4660, Oct. 2011.

[207] U. J. Kim, J. Park, H. Joo Kim, M. Wada, and D. L. Kaplan, “Three-dimensional aqueous-derived biomaterial scaffolds from silk fibroin,” *Biomaterials*, vol. 26, no. 15, pp. 2775–2785, May 2005.

[208] T. Arai, G. Freddi, R. Innocenti, and M. Tsukada, “Biodegradation ofBombyx mori silk fibroin fibers and films,” *J. Appl. Polym. Sci.*, vol. 91, no. 4, pp. 2383–2390, Feb. 2004.

[209] T. Giesa, M. Arslan, N. M. Pugno, and M. J. Buehler, “Nanoconfinement of spider silk fibrils begets superior strength, extensibility, and toughness,” *Nano Lett.*, vol. 11, no. 11, pp. 5038–5046, Nov. 2011.

[210] M. Saric and T. Scheibel, “Engineering of silk proteins for materials applications,” *Current Opinion in Biotechnology*, vol. 60. Elsevier Ltd, pp. 213–220, 01-Dec-2019.

[211] S. Salehi, K. Koeck, and T. Scheibel, “Spider silk for tissue engineering applications,” *Molecules*, vol. 25, no. 3. MDPI AG, 08-Feb-2020.

[212] A. R. Gillies and R. L. Lieber, “Structure and function of the skeletal muscle extracellular matrix,” *Muscle and Nerve*, vol. 44, no. 3. pp. 318–331, Sep-2011.

[213] T. A. H. Järvinen, T. L. N. Järvinen, M. Kääriäinen, H. Kalimo, and M. Järvinen, “Muscle injuries: Biology and treatment,” *American Journal of Sports Medicine*, vol. 33, no. 5. Am J Sports Med, pp. 745–764, May-2005.

[214] M. C. Chen, Y. C. Sun, and Y. H. Chen, “Electrically conductive nanofibers with highly oriented

structures and their potential application in skeletal muscle tissue engineering," *Acta Biomater.*, vol. 9, no. 3, pp. 5562–5572, 2013.

[215] N. F. Huang *et al.*, "Myotube assembly on nanofibrous and micropatterned polymers," *Nano Lett.*, vol. 6, no. 3, pp. 537–542, Mar. 2006.

[216] W. J. Li, R. L. Mauck, J. A. Cooper, X. Yuan, and R. S. Tuan, "Engineering controllable anisotropy in electrospun biodegradable nanofibrous scaffolds for musculoskeletal tissue engineering," *J. Biomech.*, vol. 40, no. 8, pp. 1686–1693, 2007.

[217] S. Zhang *et al.*, "Creating polymer hydrogel microfibres with internal alignment via electrical and mechanical stretching," *Biomaterials*, vol. 35, no. 10, pp. 3243–3251, Mar. 2014.

[218] K. J. Aviss, J. E. Gough, and S. Downes, "Aligned electrospun polymer fibres for skeletal muscle regeneration.," *Eur. cells {\&} Mater.*, vol. 19, pp. 193–204, 2010.

[219] J. M. Razal *et al.*, "Wet-Spun Biodegradable Fibers on Conducting Platforms: Novel Architectures for Muscle Regeneration," *Adv. Funct. Mater.*, vol. 19, no. 21, pp. 3381–3388, Nov. 2009.

[220] L. A. MacQueen *et al.*, "Muscle tissue engineering in fibrous gelatin: implications for meat analogs," *npj Sci. Food*, vol. 3, no. 1, Dec. 2019.

[221] A. F. Quigley *et al.*, "Wet-Spun Trojan Horse Cell Constructs for Engineering Muscle," *Front. Chem.*, vol. 8, Feb. 2020.

[222] Y. J. Choi *et al.*, "3D Cell Printing of Functional Skeletal Muscle Constructs Using Skeletal Muscle-Derived Bioink," *Adv. Healthc. Mater.*, vol. 5, no. 20, pp. 2636–2645, Oct. 2016.

[223] J. Groll *et al.*, "Biofabrication: Reappraising the definition of an evolving field," *Biofabrication*, vol. 8, no. 1. Institute of Physics Publishing, 08-Jan-2016.

[224] J. H. Kim *et al.*, "Pelvic floor muscle function recovery using biofabricated tissue constructs with neuromuscular junctions," *Acta Biomater.*, vol. 121, pp. 237–249, Feb. 2021.

[225] M. Terakawa, "Femtosecond Laser Processing of Biodegradable Polymers," *Appl. Sci.*, vol. 8, no. 7, p. 1123, Jul. 2018.

[226] A. F. Quigley *et al.*, "Electrical Stimulation of Myoblast Proliferation and Differentiation on Aligned Nanostructured Conductive Polymer Platforms," *Adv. Healthc. Mater.*, vol. 1, no. 6, pp. 801–808, 2012.

[227] R. Srinivasan, E. Sutcliffe, and B. Braren, "Ablation and etching of polymethylmethacrylate by very short (160 fs) ultraviolet (308 nm) laser pulses," *Appl. Phys. Lett.*, vol. 51, no. 16, pp. 1285–1287, Oct. 1987.

[228] W. Y. Yeong *et al.*, "Multiscale topological guidance for cell alignment via direct laser writing on biodegradable polymer," *Tissue Eng. - Part C Methods*, vol. 16, no. 5, pp. 1011–1021, Oct. 2010.

[229] C. H. Lee, Y. C. Lim, D. F. Farson, H. M. Powell, and J. J. Lannutti, "Vascular wall engineering via femtosecond laser ablation: Scaffolds with self-containing smooth muscle cell populations," *Ann. Biomed. Eng.*, vol. 39, no. 12, pp. 3031–3041, Dec. 2011.

[230] H. W. Wang, C. W. Cheng, C. W. Li, H. W. Chang, P. H. Wu, and G. J. Wang, "Fabrication of pillared PLGA microvessel scaffold using femtosecond laser ablation," *Int. J. Nanomedicine*, vol. 7, pp. 1865–1873, 2012.

[231] A. Daskalova *et al.*, "Biomimetic hierarchical structuring of pla by ultra-short laser pulses for processing of tissue engineered matrices: Study of cellular and antibacterial behavior," *Polymers (Basel).*, vol. 13, no. 15, Aug. 2021.

[232] C. A. Cezar and D. J. Mooney, "Biomaterial-based delivery for skeletal muscle repair.," *Adv. Drug Deliv. Rev.*, vol. 84, pp. 188–97, Apr. 2015.

[233] H. Amani *et al.*, “Controlling Cell Behavior through the Design of Biomaterial Surfaces: A Focus on Surface Modification Techniques,” *Adv. Mater. Interfaces*, vol. 6, no. 13, p. 1900572, Jul. 2019.

[234] F. Dessauge, C. Schleder, M. H. Perruchot, and K. Rouger, “3D in vitro models of skeletal muscle: myopshere, myobundle and bioprinted muscle construct,” *Veterinary Research*, vol. 52, no. 1. BioMed Central Ltd, 01-Dec-2021.

[235] D. A. Zayarny, A. A. Ionin, S. I. Kudryashov, I. N. Saraeva, E. D. Startseva, and R. A. Khmelnitskii, “Nonlinear absorption mechanisms during femtosecond laser surface ablation of silica glass,” *JETP Lett.*, vol. 103, no. 5, pp. 309–312, Mar. 2016.

[236] T. Ogawa, Ishizaki, Minamikawa, Ueno, Yamada, and Suzuki, “Nanometer-thin TiO2 enhances skeletal muscle cell phenotype and behavior,” *Int. J. Nanomedicine*, vol. 6, p. 2191, Oct. 2011.

[237] L. Ricotti *et al.*, “Proliferation and skeletal myotube formation capability of C2C12 and H9c2 cells on isotropic and anisotropic electrospun nanofibrous PHB scaffolds,” *Biomed. Mater.*, vol. 7, no. 3, 2012.

[238] K. Shimizu, H. Fujita, and E. Nagamori, “Alignment of skeletal muscle myoblasts and myotubes using linear micropatterned surfaces ground with abrasives,” *Biotechnol. Bioeng.*, vol. 103, no. 3, pp. 631–638, Jun. 2009.

[239] M. V. Santos *et al.*, “Femtosecond direct laser writing of silk fibroin optical waveguides,” *J. Mater. Sci. Mater. Electron.*, vol. 30, no. 18, pp. 16843–16848, Sep. 2019.

[240] M. V. Santos *et al.*, “Direct Femtosecond Laser Printing of Silk Fibroin Microstructures,” *ACS Appl. Mater. Interfaces*, vol. 12, no. 44, pp. 50033–50038, Nov. 2020.

[241] L. Yang, L. Han, and L. Jia, “A Novel Platelet-Repellent Polyphenolic Surface and Its Micropattern for Platelet Adhesion Detection,” *ACS Appl. Mater. Interfaces*, vol. 8, no. 40, pp. 26570–26577, Oct. 2016.

[242] S. Kim, S. Kwak, S. Lee, W. K. Cho, J. K. Lee, and S. M. Kang, “One-step functionalization of zwitterionic poly[(3-(methacryloylamino)propyl)dimethyl(3-sulfopropyl)ammonium hydroxide] surfaces by metal-polyphenol coating,” *Chem. Commun.*, vol. 51, no. 25, pp. 5340–5342, Mar. 2015.

[243] C. S. R. Nathala *et al.*, “Ultrashort laser pulse ablation of copper, silicon and gelatin: effect of the pulse duration on the ablation thresholds and the incubation coefficients,” *Appl. Phys. A Mater. Sci. Process.*, vol. 122, no. 2, pp. 1–8, Feb. 2016.

[244] N. Bhardwaj and S. C. Kundu, “Silk fibroin protein and chitosan polyelectrolyte complex porous scaffolds for tissue engineering applications,” *Carbohydr. Polym.*, vol. 85, no. 2, pp. 325–333, May 2011.

[245] N. Bhardwaj, R. Rajkhowa, X. Wang, and D. Devi, “Milled non-mulberry silk fibroin microparticles as biomaterial for biomedical applications,” *Int. J. Biol. Macromol.*, vol. 81, pp. 31–40, Nov. 2015.

[246] N. Bhardwaj, W. T. Sow, D. Devi, K. W. Ng, B. B. Mandal, and N. J. Cho, “Silk fibroin-keratin based 3D scaffolds as a dermal substitute for skin tissue engineering,” *Integr. Biol. (United Kingdom)*, vol. 7, no. 1, pp. 53–63, Jan. 2015.

[247] O. K. Gasymov *et al.*, “IR ellipsometry of silk fibroin films on Al nanoislands,” *Phys. status solidi c*, vol. 12, no. 6, pp. 628–630, Jun. 2015.

[248] Y. Q. Zhang, W. De Shen, R. L. Xiang, L. J. Zhuge, W. J. Gao, and W. B. Wang, “Formation of silk fibroin nanoparticles in water-miscible organic solvent and their characterization,” *J. Nanoparticle Res.*, vol. 9, no. 5, pp. 885–900, Oct. 2007.

[249] T. Lefèvre, F. Paquet-Mercier, J. F. Rioux-Dubé, and M. Pézolet, “Review: Structure of silk by Raman spectromicroscopy: From the spinning glands to the fibers,” *Biopolymers*, vol. 97, no. 6. Biopolymers, pp. 322–336, Jun-2012.

[250] N. Bhardwaj, Y. P. Singh, D. Devi, R. Kandimalla, J. Kotoky, and B. B. Mandal, “Potential of silk fibroin/chondrocyte constructs of muga silkworm Antheraea assamensis for cartilage tissue engineering,” *J. Mater. Chem. B*, vol. 4, no. 21, pp. 3670–3684, 2016.

[251] S. J. He, R. Valluzzi, and S. P. Gido, “Silk I structure in Bombyx mori silk foams,” in *International Journal of Biological Macromolecules*, 1999, vol. 24, no. 2–3, pp. 187–195.

[252] Q. Lu *et al.*, “Water-insoluble silk films with silk I structure,” *Acta Biomater.*, vol. 6, no. 4, pp. 1380–1387, 2010.

[253] C. Narita, Y. Okahisa, I. Wataoka, and K. Yamada, “Characterization of ground silk fibroin through comparison of nanofibroin and higher order structures,” *ACS Omega*, vol. 5, no. 36, pp. 22786–22792, Sep. 2020.

[254] J. Yong, F. Chen, Q. Yang, and X. Hou, “Femtosecond laser controlled wettability of solid surfaces,” *Soft Matter*, vol. 11, no. 46, pp. 8897–8906, Sep. 2015.

[255] D. Murakami, H. Jinnai, and A. Takahara, “Wetting transition from the cassie-baxter state to the wenzel state on textured polymer surfaces,” *Langmuir*, vol. 30, no. 8, pp. 2061–2067, Mar. 2014.

[256] L. Li *et al.*, “Electrospun poly (ε-caprolactone)/silk fibroin core-sheath nanofibers and their potential applications in tissue engineering and drug release,” *Int. J. Biol. Macromol.*, vol. 49, no. 2, pp. 223–232, 2011.

[257] M. Farokhi *et al.*, “Structural and functional changes of silk fibroin scaffold due to hydrolytic degradation,” *J. Appl. Polym. Sci.*, vol. 131, no. 6, p. n/a-n/a, Mar. 2014.

[258] H. Lee, C. H. Jang, and G. H. Kim, “A polycaprolactone/silk-fibroin nanofibrous composite combined with human umbilical cord serum for subacute tympanic membrane perforation; An in vitro and in vivo study,” *J. Mater. Chem. B*, vol. 2, no. 18, pp. 2703–2713, May 2014.

[259] J. Huard, A. Lu, X. Mu, P. Guo, and Y. Li, “Muscle injuries and repair: What’s new on the horizon!,” *Cells Tissues Organs*, vol. 202, no. 3–4. S. Karger AG, pp. 227–236, 01-Nov-2016.

[260] B. K. Pedersen, “Muscles and their myokines.,” *J. Exp. Biol.*, vol. 214, no. Pt 2, pp. 337–346, Jan. 2011.

[261] J. R. Beauchamp *et al.*, “Expression of Cd34 and Myf5 Defines the Majority of Quiescent Adult Skeletal Muscle Satellite Cells,” *J. Cell Biol.*, vol. 151, no. 6, 2000.

[262] W. M. Han, Y. C. Jang, and A. J. García, “Engineered matrices for skeletal muscle satellite cell engraftment and function,” *Matrix Biol.*, pp. 1–14, 2016.

[263] H. Yin, F. Price, and M. A. Rudnicki, “Satellite cells and the muscle stem cell niche.,” *Physiol. Rev.*, vol. 93, no. 1, pp. 23–67, Jan. 2013.

[264] B. Katz, “The termination of the afferent nerve fibre in the muscle spindle of the frog,” *Biol. Sci.*, 1961.

[265] A. Mauro, “Satellite cell of skeletal muscle fibers.,” *J. Biophys. Biochem. Cytol.*, vol. 9, pp. 493–495, 1961.

[266] P. Seale and M. A. Rudnicki, “A New Look at the Origin, Function, and ‘Stem-Cell’ Status of Muscle Satellite Cells,” *Dev. Biol.*, vol. 218, no. 2, pp. 115–124, 2000.

[267] H. M. Blau, B. D. Cosgrove, and A. T. V Ho, “The central role of muscle stem cells in regenerative failure with aging.,” *Nat. Med.*, vol. 21, no. 8, pp. 854–862, 2015.

[268] S. Carosio, M. G. Berardinelli, M. Aucello, and A. Musarò, “Impact of ageing on muscle cell regeneration,” *Ageing Research Reviews*, vol. 10, no. 1. pp. 35–42, 2011.

[269] S. B. P. Chargé and M. a Rudnicki, “Cellular and molecular regulation of muscle regeneration.,” *Physiol. Rev.*, vol. 84, no. 1, pp. 209–238, 2004.

[270] A. Theadom *et al.*, “Prevalence of muscular dystrophies: a systematic literature review,” *Neuroepidemiology*, vol. 43, no. 3–4, pp. 259–268, 2014.

[271] A. S. T. Smith, J. Davis, G. Lee, D. L. Mack, and D.-H. H. Kim, “Muscular dystrophy in a dish: engineered human skeletal muscle mimetics for disease modeling and drug discovery,” *Drug Discov. Today*, vol. 21, no. 9, pp. 1387–1398, Sep. 2016.

[272] J. K. Mah, L. Korngut, J. Dykeman, L. Day, T. Pringsheim, and N. Jette, “A systematic review and meta-analysis on the epidemiology of Duchenne and Becker muscular dystrophy,” *Neuromuscul Disord*, 2014.

[273] A. Goyenvalle, J. T. Seto, K. E. Davies, and J. Chamberlain, “Therapeutic approaches to muscular dystrophy,” *Hum. Mol. Genet.*, vol. 20, 2011.

[274] E. M. Yiu and A. J. Kornberg, “Duchenne muscular dystrophy,” *J. Paediatr. Child Health*, vol. 51, no. 8, pp. 759–764, Aug. 2015.

[275] A. E. Stark, “Determinants of the incidence of Duchenne muscular dystrophy.,” *Ann. Transl. Med.*, vol. 3, no. 19, p. 287, Nov. 2015.

[276] P. A. Romitti *et al.*, “Prevalence of Duchenne and Becker Muscular Dystrophies in the United States,” *Pediatrics*, vol. 135, no. 3, pp. 513–521, 2015.

[277] J. M. Ervasti and K. J. Sonnemann, “Biology of the Striated Muscle Dystrophin-Glycoprotein Complex,” *International Review of Cytology*, vol. 265. pp. 191–225, 2008.

[278] K. I. Gawlik, J. Holmberg, and M. Durbeej, “Loss of dystrophin and ??-sarcoglycan significantly exacerbates the phenotype of laminin ??2 chain-deficient animals,” *Am. J. Pathol.*, vol. 184, no. 3, pp. 740–752, 2014.

[279] B. Constantin, “Dystrophin complex functions as a scaffold for signalling proteins,” *Biochimica et Biophysica Acta - Biomembranes*, vol. 1838, no. 2. pp. 635–642, 2014.

[280] A. L. Serrano, C. J. Mann, B. Vidal, E. Ardite, E. Perdiguero, and P. Muñoz-Cánoves, *Cellular and molecular mechanisms regulating fibrosis in skeletal muscle repair and disease*, vol. 96. 2011.

[281] A. E. Almada and A. J. Wagers, “Molecular circuitry of stem cell fate in skeletal muscle regeneration, ageing and disease,” *Nat. Rev. Mol. Cell Biol.*, vol. 17, no. 5, pp. 267–279, 2016.

[282] A. Sacco *et al.*, “Short Telomeres and Stem Cell Exhaustion Model Duchenne Muscular Dystrophy in mdx/mTR Mice,” *Cell*, vol. 143, no. 7, pp. 1059–1071, 2010.

[283] N. A. Dumont *et al.*, “Dystrophin expression in muscle stem cells regulates their polarity and asymmetric division,” *Nat. Med.*, vol. 21, no. 12, pp. 1455–1463, 2015.

[284] N. A. Dumont and M. A. Rudnicki, “Targeting muscle stem cell intrinsic defects to treat Duchenne muscular dystrophy,” *npj Regen. Med.*, vol. 1, no. 1, p. 16006, 2016.

[285] C. Webster and H. M. Blau, “Accelerated age-related decline in replicative life-span of Duchenne muscular dystrophy myoblasts: Implications for cell and gene therapy,” *Somat. Cell Mol. Genet.*, vol. 16, no. 6, pp. 557–565, 1990.

[286] A. E. H. Emery, “Duchenne muscular dystrophy-Meryon’s disease,” *Neuromuscul. Disord.*, vol. 3, no. 4, pp. 263–266, 1993.

[287] C. Beaudart, R. Rizzoli, O. Bruyère, J.-Y. Reginster, and E. Biver, “Sarcopenia: burden and challenges for public health.,” *Arch. Public Health*, vol. 72, no. 1, p. 45, 2014.

[288] E. Landfeldt *et al.*, “The burden of Duchenne muscular dystrophy: an international, cross-sectional study.,” *Neurology*, vol. 83, no. 6, pp. 529–36, Aug. 2014.

[289] M. Cavazza *et al.*, “Social/economic costs and health-related quality of life in patients with Duchenne muscular dystrophy in Europe,” *Eur. J. Heal. Econ.*, vol. 17, no. S1, pp. 19–29, Apr.

2016.

[290] N. A. Dumont, C. F. Bentzinger, M.-C. Sincennes, and M. A. Rudnicki, “Satellite Cells and Skeletal Muscle Regeneration.,” *Compr. Physiol.*, vol. 5, no. 3, pp. 1027–1059, 2015.

[291] T. A. Partridge, J. E. Morgan, G. R. Coulton, E. P. Hoffman, and L. M. Kunkel, “Conversion of mdx myofibres from dystrophin-negative to -positive by injection of normal myoblasts,” *Nature*, vol. 337, no. 6203. pp. 176–179, 1989.

[292] M. Juhas, J. Ye, and N. Bursac, “Design, evaluation, and application of engineered skeletal muscle,” *Methods*, 2015.

[293] C. T. Vangsness, P. R. Kurzweil, and J. R. Lieberman, “Restoring articular cartilage in the knee.,” *Am. J. Orthop. (Belle Mead. NJ).*, vol. 33, no. 2 Suppl, pp. 29–34, Feb. 2004.

[294] B. W. Oakes, “Orthopaedic tissue engineering: from laboratory to the clinic,” *BONE Jt. Disord. Prev. Control*, 2004.

[295] J. Kopp, M. G. Jeschke, A. D. Bach, U. Kneser, and R. E. Horch, “Applied tissue engineering in the closure of severe burns and chronic wounds using cultured human autologous keratinocytes in a natural fibrin matrix,” *Cell Tissue Bank.*, vol. 5, no. 2, pp. 81–87, 2004.

[296] K. Kojima, L. J. Bonassar, R. A. Ignotz, K. Syed, J. Cortiella, and C. A. Vacanti, “Comparison of tracheal and nasal chondrocytes for tissue engineering of the trachea.,” *Ann. Thorac. Surg.*, vol. 76, no. 6, pp. 1884–1888, 2003.

[297] S. C. N. Chang, G. Tobias, A. K. Roy, C. A. Vacanti, and L. J. Bonassar, “Tissue Engineering of Autologous Cartilage for Craniofacial Reconstruction by Injection Molding,” *Plast. Reconstr. Surg.*, vol. 112, no. 3, pp. 793–799, Sep. 2003.

[298] R. E. Horch, M. Debus, G. Wagner, and G. B. Stark, “Cultured Human Keratinocytes on Type I Collagen Membranes to Reconstitute the Epidermis,” *Tissue Eng.*, vol. 6, no. 1, pp. 53–67, Feb. 2000.

[299] Y.-C. Huang, “Rapid formation of functional muscle in vitro using fibrin gels,” *J. Appl. Physiol.*, vol. 98, no. 2, pp. 706–713, 2004.

[300] M. T. Lam, Y. C. Huang, R. K. Birla, and S. Takayama, “Microfeature guided skeletal muscle tissue engineering for highly organized 3-dimensional free-standing constructs,” *Biomaterials*, vol. 30, no. 6, pp. 1150–1155, Feb. 2009.

[301] D. W. J. van der Schaft, A. C. C. van Spreeuwel, K. J. M. Boonen, M. L. P. Langelaan, C. V. C. Bouten, and F. P. T. Baaijens, “Engineering Skeletal Muscle Tissues from Murine Myoblast Progenitor Cells and Application of Electrical Stimulation,” *J. Vis. Exp.*, no. 73, p. e4267, 2013.

[302] F. Kurth, A. Franco-Obregon, M. Casarosa, S. K. Kuster, K. Wuertz-Kozak, and P. S. Dittrich, “Transient receptor potential vanilloid 2-mediated shear-stress responses in C2C12 myoblasts are regulated by serum and extracellular matrix,” *FASEB J.*, vol. 29, no. 11, pp. 4726–4737, Nov. 2015.

[303] S. Bersini, C. Arrigoni, S. Lopa, M. Bongio, I. Martin, and M. Moretti, “Engineered miniaturized models of musculoskeletal diseases,” *Drug Discov. Today*, vol. 00, no. 00, pp. 6–13, 2016.

[304] P. K. Law *et al.*, “Cell transplantation as an experimental treatment for Duchenne muscular dystrophy.,” *Cell Transplant.*, vol. 2, no. 6, pp. 485–505, 1993.

[305] S. Guettier-Sigrist, G. Coupin, S. Braun, J.-M. Warter, and P. Poindron, “Muscle could be the therapeutic target in SMA treatment,” *J. Neurosci. Res.*, vol. 53, no. 6, pp. 663–669, Sep. 1998.

[306] S. D. McCullen, A. G. Y. Chow, and M. M. Stevens, “In vivo tissue engineering of musculoskeletal tissues,” *Curr. Opin. Biotechnol.*, vol. 22, no. 5, pp. 715–720, 2011.

[307] S. Jana, A. Cooper, and M. Zhang, “Chitosan Scaffolds with Unidirectional Microtubular Pores for Large Skeletal Myotube Generation,” *Adv. Healthc. Mater.*, vol. 2, no. 4, pp. 557–561, Apr. 2013.

[308] L. Wang, L. Cao, J. Shansky, Z. Wang, D. Mooney, and H. Vandenburgh, “Minimally Invasive Approach to the Repair of Injured Skeletal Muscle With a Shape-memory Scaffold,” *Mol. Ther.*, vol. 22, no. 8, pp. 1441–1449, Aug. 2014.

[309] B. Barrilleaux, D. G. Phinney, D. J. Prockop, and K. C. O’Connor, “Review: ex vivo engineering of living tissues with adult stem cells,” *Tissue Eng.*, vol. 12, no. 11, pp. 3007–3019, 2006.

[310] M. M. Stern *et al.*, “The influence of extracellular matrix derived from skeletal muscle tissue on the proliferation and differentiation of myogenic progenitor cells ex vivo,” *Biomaterials*, vol. 30, no. 12, pp. 2393–2399, 2009.

[311] ASM International, “Overview of Biomaterials and Their Use in Medical Devices,” *ASM Int.*, pp. 1–11, 2003.

[312] C. Rhim, C. S. Cheng, W. E. Kraus, and G. A. Truskey, “Effect of MicroRNA Modulation on Bioartificial Muscle Function,” *Tissue Eng. Part A*, vol. 16, no. 12, pp. 3589–3597, Dec. 2010.

[313] J. Shansky, J. Chromiak, M. Del Tatto, and H. Vandenburgh, “A simplified method for tissue engineering skeletal muscle organoids in vitro,” *Vitr. Cell. {\&} Dev. Biol. - Anim.*, vol. 33, no. 9, pp. 659–661, Sep. 1997.

[314] J. Ma, K. Holden, J. Zhu, H. Pan, and Y. Li, “The application of three-dimensional collagen-scaffolds seeded with myoblasts to repair skeletal muscle defects.,” *J. Biomed. {\&} Biotechnol.*, vol. 2011, p. 812135, 2011.

[315] V. Kroehne, I. Heschel, F. Schügner, D. Lasrich, J. W. Bartsch, and H. Jockusch, “Use of a novel collagen matrix with oriented pore structure for muscle cell differentiation in cell culture and in grafts.,” *J. Cell. Mol. Med.*, vol. 12, no. 5A, pp. 1640–1648, 2008.

[316] T. Okano and T. Matsuda, “Tissue engineered skeletal muscle: Preparation of Highly Dense, Highly Oriented Hybrid Muscular Tissues,” *Cell Transplant.*, vol. 7, no. 1, pp. 71–82, 1998.

[317] T. Okano and T. Matsuda, “Muscular tissue engineering: capillary-incorporated hybrid muscular tissues in vivo tissue culture,” *Cell Transplant.*, vol. 7, no. 5, pp. 435–442, 1998.

[318] H. H. Vandenburgh, P. Karlisch, and L. Farr, “Maintenance of highly contractile tissue-cultured avian skeletal myotubes in collagen gel.,” *Vitr. Cell. {\&} Dev. Biol. J. Tissue Cult. Assoc.*, vol. 24, no. 3, pp. 166–174, 1988.

[319] U. Cheema, S.-Y. Yang, V. Mudera, G. G. Goldspink, and R. A. Brown, “3-D in vitro model of early skeletal muscle development,” *Cell Motil. Cytoskeleton*, vol. 54, no. 3, pp. 226–236, 2003.

[320] A. S. T. Smith, S. Passey, L. Greensmith, V. Mudera, and M. P. Lewis, “Characterization and optimization of a simple, repeatable system for the long term in vitro culture of aligned myotubes in 3D,” *J. Cell. Biochem.*, vol. 113, no. 3, pp. 1044–1053, 2012.

[321] G. H. Borschel, D. E. Dow, R. G. Dennis, and D. L. Brown, “Tissue-Engineered Axially Vascularized Contractile Skeletal Muscle,” *Plast. Reconstr. Surg.*, vol. 117, no. 7, pp. 2235–2242, Jun. 2006.

[322] P. Heher *et al.*, “A novel bioreactor for the generation of highly aligned 3D skeletal muscle-like constructs through orientation of fibrin via application of static strain,” *Acta Biomater.*, vol. 24, pp. 251–265, 2015.

[323] J. Liu, H. H. K. Xu, H. Zhou, M. D. Weir, Q. Chen, and C. A. Trotman, “Human umbilical cord stem cell encapsulation in novel macroporous and injectable fibrin for muscle tissue engineering.,” *Acta Biomater.*, vol. 9, no. 1, pp. 4688–4697, 2013.

[324] W. Bian and N. Bursac, “Soluble miniagrin enhances contractile function of engineered skeletal

muscle.," *FASEB J.*, vol. 26, no. 2, pp. 955–965, Feb. 2012.

[325] R. L. Page *et al.*, "Restoration of skeletal muscle defects with adult human cells delivered on fibrin microthreads.," *Tissue Eng. Part A*, vol. 17, no. 21–22, pp. 2629–2640, Nov. 2011.

[326] J. Liu, H. Zhou, M. D. Weir, H. H. K. Xu, Q. Chen, and C. A. Trotman, "Fast-degradable microbeads encapsulating human umbilical cord stem cells in alginate for muscle tissue engineering.," *Tissue Eng. Part A*, vol. 18, no. 21–22, pp. 2303–2314, 2012.

[327] C. Borselli *et al.*, "Functional muscle regeneration with combined delivery of angiogenesis and myogenesis factors.," *Proc. Natl. Acad. Sci. U. S. A.*, vol. 107, no. 8, pp. 3287–3292, Feb. 2010.

[328] C. Borselli, C. A. Cezar, D. Shvartsman, H. H. Vandenburgh, and D. J. Mooney, "The role of multifunctional delivery scaffold in the ability of cultured myoblasts to promote muscle regeneration," *Biomaterials*, vol. 32, no. 34, pp. 8905–8914, 2011.

[329] E. Hill, T. Boontheekul, and D. J. Mooney, "Regulating activation of transplanted cells controls tissue regeneration.," *Proc. Natl. Acad. Sci. U. S. A.*, vol. 103, no. 8, pp. 2494–2499, Feb. 2006.

[330] E. Hill, T. Boontheekul, and D. J. Mooney, "Designing Scaffolds to Enhance Transplanted Myoblast Survival and Migration," *Tissue Eng.*, vol. 12, no. 5, pp. 1295–1304, 2006.

[331] L. Shapiro and S. Cohen, "Novel alginate sponges for cell culture and transplantation," *Biomaterials*, vol. 18, no. 8, pp. 583–590, Apr. 1997.

[332] S. Grefte, S. Vullinghs, A. M. Kuijpers-Jagtman, R. Torensma, and J. W. Von den Hoff, "Matrigel, but not collagen I, maintains the differentiation capacity of muscle derived cells *in vitro*," *Biomed. Mater.*, vol. 7, no. 5, p. 055004, Oct. 2012.

[333] C. A. Rossi *et al.*, "In vivo tissue engineering of functional skeletal muscle by freshly isolated satellite cells embedded in a photopolymerizable hydrogel.," *FASEB J.*, vol. 25, no. 7, pp. 2296–2304, Jul. 2011.

[334] W. Wang, M. Fan, L. Zhang, S. Liu, L. Sun, and C. Wang, "Compatibility of hyaluronic acid hydrogel and skeletal muscle myoblasts," *Biomed. Mater.*, vol. 4, no. 2, p. 25011, Apr. 2009.

[335] C. Monge, K. Ren, K. Berton, R. Guillot, D. Peyrade, and C. Picart, "Engineering muscle tissues on microstructured polyelectrolyte multilayer films.," *Tissue Eng. Part A*, vol. 18, no. 15–16, pp. 1664–76, Aug. 2012.

[336] H. S. Yang *et al.*, "Nanopatterned muscle cell patches for enhanced myogenesis and dystrophin expression in a mouse model of muscular dystrophy.," *Biomaterials*, vol. 35, no. 5, pp. 1478–1486, Feb. 2014.

[337] B. B. Mandal and S. C. Kundu, "Cell proliferation and migration in silk fibroin 3D scaffolds," *Biomaterials*, vol. 30, no. 15, pp. 2956–2965, 2009.

[338] G. H. Borschel, R. G. Dennis, and W. M. Kuzon, "Contractile Skeletal Muscle Tissue-Engineered on an Acellular Scaffold," *Plast. Reconstr. Surg.*, vol. 113, no. 2, pp. 595–602, Feb. 2004.

[339] M. T. Conconi *et al.*, "Homologous muscle acellular matrix seeded with autologous myoblasts as a tissue-engineering approach to abdominal wall-defect repair," *Biomaterials*, vol. 26, no. 15, pp. 2567–2574, 2005.

[340] P. De Coppi *et al.*, "Myoblast–Acellular Skeletal Muscle Matrix Constructs Guarantee a Long-Term Repair of Experimental Full-Thickness Abdominal Wall Defects," *Tissue Eng.*, vol. 12, no. 7, pp. 1929–1936, Jul. 2006.

[341] B. T. Corona, C. L. Ward, H. B. Baker, T. J. Walters, and G. J. Christ, "Implantation of in vitro tissue engineered muscle repair constructs and bladder acellular matrices partially restore in vivo skeletal muscle function in a rat model of volumetric muscle loss injury.," *Tissue Eng. Part A*, vol. 20, no. 3–4, pp. 705–715, Feb. 2014.

[342] J. A. DeQuach *et al.*, “Injectable skeletal muscle matrix hydrogel promotes neovascularization and muscle cell infiltration in a hindlimb ischemia model.,” *Eur. cells {\&} Mater.*, vol. 23, pp. 400--12; discussion 412, Jun. 2012.

[343] V. J. Mase *et al.*, “Clinical Application of an Acellular Biologic Scaffold for Surgical Repair of a Large, Traumatic Quadriceps Femoris Muscle Defect,” *Orthopedics*, vol. 33, no. 7, p. 511, Jul. 2010.

[344] E. K. Merritt *et al.*, “Repair of traumatic skeletal muscle injury with bone-marrow-derived mesenchymal stem cells seeded on extracellular matrix.,” *Tissue Eng. Part A*, vol. 16, no. 9, pp. 2871–2881, Sep. 2010.

[345] B. Perniconi, A. Costa, P. Aulino, L. Teodori, S. Adamo, and D. Coletti, “The pro-myogenic environment provided by whole organ scale acellular scaffolds from skeletal muscle,” *Biomaterials*, vol. 32, no. 31, pp. 7870–7882, 2011.

[346] B. M. Sicari *et al.*, “An Acellular Biologic Scaffold Promotes Skeletal Muscle Formation in Mice and Humans with Volumetric Muscle Loss,” *Sci. Transl. Med.*, vol. 6, no. 234, pp. 234ra58--234ra58, Apr. 2014.

[347] M. T. Wolf, K. A. Daly, J. E. Reing, and S. F. Badylak, “Biologic scaffold composed of skeletal muscle extracellular matrix,” *Biomaterials*, vol. 33, no. 10, pp. 2916–2925, Apr. 2012.

[348] J. S. Choi, S. J. Lee, G. J. Christ, A. Atala, and J. J. Yoo, “The influence of electrospun aligned poly(ε-caprolactone)/collagen nanofiber meshes on the formation of self-aligned skeletal muscle myotubes,” *Biomaterials*, vol. 29, no. 19, pp. 2899–2906, Jul. 2008.

[349] I. Jun, S. Jeong, and H. Shin, “The stimulation of myoblast differentiation by electrically conductive sub-micron fibers,” *Biomaterials*, vol. 30, no. 11, pp. 2038–2047, Apr. 2009.

[350] M.-C. Chen, Y.-C. Sun, and Y.-H. Chen, “Electrically conductive nanofibers with highly oriented structures and their potential application in skeletal muscle tissue engineering,” *Acta Biomater.*, vol. 9, no. 3, pp. 5562–5572, 2013.

[351] S. H. Ku, S. H. Lee, and C. B. Park, “Synergic effects of nanofiber alignment and electroactivity on myoblast differentiation,” *Biomaterials*, vol. 33, no. 26, pp. 6098–6104, Sep. 2012.

[352] M. S. Kim, I. Jun, Y. M. Shin, W. Jang, S. I. Kim, and H. Shin, “The Development of Genipin-Crosslinked Poly(caprolactone) (PCL)/Gelatin Nanofibers for Tissue Engineering Applications,” *Macromol. Biosci.*, vol. 10, no. 1, pp. 91–100, Jan. 2010.

[353] M. H. Kim *et al.*, “The effect of VEGF on the myogenic differentiation of adipose tissue derived stem cells within thermosensitive hydrogel matrices,” *Biomaterials*, vol. 31, no. 6, pp. 1213–1218, Feb. 2010.

[354] I. Grizzi, H. Garreau, S. Li, and M. Vert, “Hydrolytic degradation of devices based on poly(DL-lactic acid) size-dependence.,” *Biomaterials*, vol. 16, no. 4, pp. 305–311, 1995.

[355] M. a Machingal *et al.*, “A Tissue Engineered Muscle Repair (TE-MR) Construct for Functional Restoration of an Irrecoverable Muscle Injury in a Murine Model.,” *Tissue Eng. Part A*, pp. 1–37, 2011.

[356] T. Le Bao Ha, T. Minh, D. Nguyen, and D. Minh, “Naturally Derived Biomaterials: Preparation and Application,” *Regen. Med. Tissue Eng.*, 2013.

[357] P. A. Gunatillake, R. Adhikari, and N. Gadegaard, “Biodegradable synthetic polymers for tissue engineering,” *Eur. Cells Mater.*, vol. 5, pp. 1–16, 2003.

[358] C. H. Lee, A. Singla, and Y. Lee, “Biomedical applications of collagen.,” *Int. J. Pharm.*, vol. 221, no. 1–2, pp. 1–22, Jun. 2001.

[359] W. E. Blanco-Bose, C.-C. Yao, R. H. Kramer, and H. M. Blau, “Purification of Mouse Primary

Myoblasts Based on $α$7 Integrin Expression," *Exp. Cell Res.*, vol. 265, no. 2, pp. 212–220, 2001.

[360] C. Rhim *et al.*, "Morphology and ultrastructure of differentiating three-dimensional mammalian skeletal muscle in a collagen gel," *Muscle {\&} Nerve*, vol. 36, no. 1, pp. 71–80, Jul. 2007.

[361] T. Boontheekul, H.-J. Kong, and D. J. Mooney, "Controlling alginate gel degradation utilizing partial oxidation and bimodal molecular weight distribution," *Biomaterials*, vol. 26, no. 15, pp. 2455–2465, 2005.

[362] J. W. Andrejecsk, J. Cui, W. G. Chang, J. Devalliere, J. S. Pober, and W. M. Saltzman, "Paracrine exchanges of molecular signals between alginate-encapsulated pericytes and freely suspended endothelial cells within a 3D protein gel," *Biomaterials*, vol. 34, no. 35, pp. 8899–8908, Nov. 2013.

[363] K. Y. Lee and D. J. Mooney, "Alginate: Properties and biomedical applications," *Prog. Polym. Sci.*, vol. 37, no. 1, pp. 106–126, 2012.

[364] Y. Zhang, P. Heher, J. Hilborn, H. Redl, and D. A. Ossipov, "Hyaluronic acid-fibrin interpenetrating double network hydrogel prepared in situ by orthogonal disulfide cross-linking reaction for biomedical applications," *Acta Biomater.*, vol. 38, pp. 23–32, Jul. 2016.

[365] A. M. Collinsworth, S. Zhang, W. E. Kraus, and G. a Truskey, "Apparent elastic modulus and hysteresis of skeletal muscle cells throughout differentiation," *AJP Cell Physiol.*, vol. 283, no. 4, pp. C1219--C1227, 2002.

[366] Y. Luo, K. R. Kirker, and G. D. Prestwich, "Cross-linked hyaluronic acid hydrogel films: New biomaterials for drug delivery," *J. Control. Release*, vol. 69, no. 1, pp. 169–184, 2000.

[367] Helgerson S. L., Seelich T., J. DiOrio, B. Tawil J., K. Bittner, and R. Spaethe, "Helgerson 2004 Fibrin.pdf." 2004.

[368] M. Morishima-Kawashima *et al.*, "Proline-directed and non-proline-directed phosphorylation of PHF-tau.," *J. Biol. Chem.*, vol. 270, no. 2, pp. 823–829, Jan. 1995.

[369] J. B. C. Papers and U. Mayer, "Integrins: redundant or important players in skeletal muscle?," *J. Biol. Chem.*, vol. 278, no. 17, pp. 14587–14590, Apr. 2003.

[370] A. C. Brown and T. H. Barker, "Fibrin-based biomaterials: Modulation of macroscopic properties through rational design at the molecular level," *Acta Biomater.*, vol. 10, no. 4, pp. 1502–1514, Apr. 2014.

[371] S. F. Badylak, J. L. Dziki, B. M. Sicari, F. Ambrosio, and M. L. Boninger, "Mechanisms by which acellular biologic scaffolds promote functional skeletal muscle restoration," *Biomaterials*, vol. 103, pp. 128–136, Oct. 2016.

[372] C. Fuoco *et al.*, "3D hydrogel environment rejuvenates aged pericytes for skeletal muscle tissue engineering," *Front. Physiol.*, vol. 5, p. 203, 2014.

[373] C. Fuoco *et al.*, "In vivo generation of a mature and functional artificial skeletal muscle," *EMBO Mol. Med.*, vol. 7, no. 4, pp. 411–422, Apr. 2015.

[374] D. W. Hammers, A. Sarathy, C. B. Pham, C. T. Drinnan, R. P. Farrar, and L. J. Suggs, "Controlled release of IGF-I from a biodegradable matrix improves functional recovery of skeletal muscle from ischemia/reperfusion," *Biotechnol. Bioeng.*, vol. 109, no. 4, pp. 1051–1059, Apr. 2012.

[375] V. Y. Rybalko *et al.*, "Controlled delivery of SDF-1α and IGF-1: CXCR4(+) cell recruitment and functional skeletal muscle recovery.," *Biomater. Sci.*, vol. 3, no. 11, pp. 1475–86, Nov. 2015.

[376] M. Marzaro *et al.*, "Autologous satellite cell seeding improves in vivo biocompatibility of homologous muscle acellular matrix implants," 2002.

[377] V. Mouly *et al.*, "Myoblast transfer therapy: Is there any light at the end of the tunnel?," *Acta Myol.*, vol. 24, no. 2, pp. 128–133, 2005.

[378] B. Malecova and P. L. Puri, "'Mix of Mics'- Phenotypic and Biological Heterogeneity of 'Multipotent' Muscle Interstitial Cells (MICs)," *J. stem cell Res. {\&} Ther.*, no. Suppl 11, 2012.

[379] M. Crisan *et al.*, "A Perivascular Origin for Mesenchymal Stem Cells in Multiple Human Organs," *Cell Stem Cell*, vol. 3, no. 3, pp. 301–313, Sep. 2008.

[380] A. Birbrair *et al.*, "Role of pericytes in skeletal muscle regeneration and fat accumulation," *Stem Cells Dev.*, vol. 22, no. 16, pp. 2298–2314, Aug. 2013.

[381] F. S. Tedesco and G. Cossu, "Stem cell therapies for muscle disorders," *Curr. Opin. Neurol.*, vol. 25, no. 5, pp. 597–603, 2012.

[382] M. Sampaolesi *et al.*, "Cell Therapy of -Sarcoglycan Null Dystrophic Mice Through Intra-Arterial Delivery of Mesoangioblasts," *Science (80-.).*, vol. 301, no. 5632, pp. 487–492, Jul. 2003.

[383] M. Sampaolesi *et al.*, "Mesoangioblast stem cells ameliorate muscle function in dystrophic dogs," *Nature*, vol. 444, no. 7119, pp. 574–579, Nov. 2006.

[384] M. Meregalli *et al.*, "Perspectives of stem cell therapy in Duchenne muscular dystrophy," *FEBS J.*, vol. 280, no. 17, pp. 4251–4262, Sep. 2013.

[385] L. De Angelis *et al.*, "Skeletal myogenic progenitors originating from embryonic dorsal aorta coexpress endothelial and myogenic markers and contribute to postnatal muscle growth and regeneration.," *J. Cell Biol.*, vol. 147, no. 4, pp. 869–878, Nov. 1999.

[386] G. Ferrari *et al.*, "Muscle regeneration by bone marrow-derived myogenic progenitors.," *Science*, vol. 279, no. 5356, pp. 1528–1530, 1998.

[387] J. K. Koponen *et al.*, "Umbilical Cord Blood–derived Progenitor Cells Enhance Muscle Regeneration in Mouse Hindlimb Ischemia Model," *Mol. Ther.*, vol. 15, no. 12, pp. 2172–2177, 2007.

[388] G. Goldspink, "Changes in muscle mass and phenotype and the expression of autocrine and systemic growth factors by muscle in response to stretch and overload.," *J. Anat.*, vol. 194 (Pt 3, no. Pt 3, pp. 323–34, Apr. 1999.

[389] A. Kortesidis, A. Zannettino, S. Isenmann, S. Shi, T. Lapidot, and S. Gronthos, "Stromal-derived factor-1 promotes the growth, survival, and development of human bone marrow stromal stem cells," *Blood*, vol. 105, no. 10, pp. 3793–3801, 2005.

[390] M. Gnecchi *et al.*, "Paracrine action accounts for marked protection of ischemic heart by Akt-modified mesenchymal stem cells," *Nat. Med.*, vol. 11, no. 4, pp. 367–368, Apr. 2005.

[391] M. Zhang *et al.*, "SDF-1 expression by mesenchymal stem cells results in trophic support of cardiac myocytes after myocardial infarction," *FASEB J.*, vol. 21, no. 12, pp. 3197–3207, 2007.

[392] Q. Yin *et al.*, "SDF-1α inhibits hypoxia and serum deprivation-induced apoptosis in mesenchymal stem cells through PI3K/Akt and ERK1/2 signaling pathways," *Mol. Biol. Rep.*, vol. 38, no. 1, pp. 9–16, Jan. 2011.

[393] T. Kinnaird, E. Stabile, M. S. Burnett, and S. E. Epstein, "This Review is part of a thematic series on Angiogenesis, which includes the following articles: Endothelial Progenitor Cells: Characterization and Role in Vascular Biology Bone Marrow–Derived Cells for Enhancing Collateral Development: Mechanisms, Animal."

[394] S. Ohnishi, H. Sumiyoshi, S. Kitamura, and N. Nagaya, "Mesenchymal stem cells attenuate cardiac fibroblast proliferation and collagen synthesis through paracrine actions," *FEBS Lett.*, vol. 581, no. 21, pp. 3961–3966, Aug. 2007.

[395] T. A. Wynn, "Cellular and molecular mechanisms of fibrosis," *J. Pathol.*, vol. 214, no. 2, pp. 199–210, Jan. 2008.

[396] J. Tang *et al.*, “Mesenchymal stem cells modified with stromal cell-derived factor 1$α$ improve cardiac remodeling via paracrine activation of hepatocyte growth factor in a rat model of myocardial infarction,” *Mol. Cells*, vol. 29, no. 1, pp. 9–19, Jan. 2010.

[397] K. Le Blanc and D. Mougiakakos, “Multipotent mesenchymal stromal cells and the innate immune system,” *Nat. Rev. Immunol.*, vol. 12, no. 5, pp. 383–396, 2012.

[398] G. Ferrari, A. Stornaiuolo, and F. Mavilio, “Bone-marrow transplantation: Failure to correct murine muscular dystrophy,” *Nature*, vol. 411, no. 6841, pp. 1014–1015, Jun. 2001.

[399] S.-V. Forcales, “Potential of adipose-derived stem cells in muscular regenerative therapies,” *Front. Aging Neurosci.*, vol. 7, p. 123, Jul. 2015.

[400] T. Barberi, L. M. Willis, N. D. Socci, and L. Studer, “Derivation of multipotent mesenchymal precursors from human embryonic stem cells.,” *PLoS Med.*, vol. 2, no. 6, p. e161, Jun. 2005.

[401] M. Quattrocelli *et al.*, “Mesodermal iPSC – derived progenitor cells functionally regenerate cardiac and skeletal muscle,” vol. 125, no. 12, pp. 4463–4482, 2015.

[402] M. Meregalli, A. Farini, C. Sitzia, and Y. Torrente, “Advancements in stem cells treatment of skeletal muscle wasting.,” *Front. Physiol.*, vol. 5, p. 48, 2014.

[403] Wobma Holly and Gordana Vunjak-Novakovic, “Tissue Engineering and Regenerative Medicine 2015: A Year in Review,” *Tissue Eng. Part B*, vol. 20, no. 1, pp. 1–16, 2016.

[404] F. S. Tedesco *et al.*, “Transplantation of Genetically Corrected Human iPSC-Derived Progenitors in Mice with Limb-Girdle Muscular Dystrophy,” *Sci. Transl. Med.*, vol. 4, no. 140, pp. 140ra89-140ra89, Jun. 2012.

[405] Y. An and D. Li, “Engineering skeletal muscle tissue in bioreactor systems,” *Chin. Med. J. (Engl).*, vol. 127, no. 23, pp. 4130–4139, 2014.

[406] H. Lee, J. Park, B. G. Forget, and P. Gaines, “Induced pluripotent stem cells in regenerative medicine: an argument for continued research on human embryonic stem cells.,” *Regen. Med.*, vol. 4, no. 5, pp. 759–769, 2009.

[407] D. Yaffe and O. Saxel, “Serial passaging and differentiation of myogenic cells isolated from dystrophic mouse muscle.,” *Nature*, vol. 270, no. 5639, pp. 725–7, 1977.

[408] A. J. Engler, H. L. Sweeney, D. E. Discher, and J. E. Schwarzbauer, “Extracellular matrix elasticity directs stem cell differentiation.,” *J. Musculoskelet. {\&} neuronal Interact.*, vol. 7, no. 4, p. 335, 2007.

[409] R. Tatsumi, S. M. Sheehan, H. Iwasaki, A. Hattori, and R. E. Allen, “Mechanical Stretch Induces Activation of Skeletal Muscle Satellite Cells in Vitro,” *Exp. Cell Res.*, vol. 267, no. 1, pp. 107–114, 2001.

[410] R. TATSUMI, “Mechano-biology of skeletal muscle hypertrophy and regeneration: Possible mechanism of stretch-induced activation of resident myogenic stem cells,” *Anim. Sci. J.*, vol. 81, no. 1, pp. 11–20, Feb. 2010.

[411] G. Goldspink, A. Scutt, P. T. Loughna, D. J. Wells, T. Jaenicke, and G. F. Gerlach, “Gene expression in skeletal muscle in response to stretch and force generation.,” *Am. J. Physiol.*, vol. 262, no. 3 Pt 2, pp. R356--63, 1992.

[412] G. Goldspink, “Gene expression in muscle in response to exercise.,” *J. Muscle Res. Cell Motil.*, vol. 24, no. 2–3, pp. 121–126, 2003.

[413] H. H. Vandenburgh and P. Karlisch, “Longitudinal growth of skeletal myotubes in vitro in a new horizontal mechanical cell stimulator.,” *Vitr. Cell. {\&} Dev. Biol. J. Tissue Cult. Assoc.*, vol. 25, no. 7, pp. 607–616, Jul. 1989.

[414] A. L. Goldberg, “Work-induced growth of skeletal muscle in normal and hypophysectomized rats,” *Am. J. Physiol. -- Leg. Content*, vol. 213, no. 5, 1967.

[415] R. B. Armstrong, P. Marum, P. Tullson, and C. W. Saubert, “Acute hypertrophic response of skeletal muscle to removal of synergists,” *J. Appl. Physiol.*, vol. 46, no. 4, 1979.

[416] I.-C. Liao, J. B. Liu, N. Bursac, and K. W. Leong, “Effect of Electromechanical Stimulation on the Maturation of Myotubes on Aligned Electrospun Fibers,” *Cell. Mol. Bioeng.*, vol. 1, no. 2–3, pp. 133–145, Sep. 2008.

[417] et al Purves D, Augustine GJ, Fitzpatrick D, “The Motor Unit,” in *Neuroscience. 2nd edition*, 2001.

[418] A. Khodabukus, L. M. Baehr, S. C. Bodine, and K. Baar, “Role of contraction duration in inducing fast-to-slow contractile and metabolic protein and functional changes in engineered muscle,” *J. Cell. Physiol.*, vol. 230, no. 10, pp. 2489–2497, 2015.

[419] U. Wehrle, S. Düsterhöft, and D. Pette, “Effects of chronic electrical stimulation on myosin heavy chain expression in satellite cell cultures derived from rat muscles of different fiber-type composition,” *Differentiation*, vol. 58, no. 1, pp. 37–46, Nov. 1994.

[420] H. Park *et al.*, “Effects of electrical stimulation in C2C12 muscle constructs,” *J. Tissue Eng. Regen. Med.*, vol. 2, no. 5, pp. 279–287, Jul. 2008.

[421] H. Fujita, T. Nedachi, and M. Kanzaki, “Accelerated de novo sarcomere assembly by electric pulse stimulation in C2C12 myotubes,” *Exp. Cell Res.*, vol. 313, no. 9, pp. 1853–1865, 2007.

[422] S. Salmons, Z. Ashley, H. Sutherland, M. F. Russold, F. Li, and J. C. Jarvis, “Functional Electrical Stimulation of Denervated Muscles: Basic Issues,” *Artif. Organs*, vol. 29, no. 3, pp. 199–202, 2005.

[423] A. M. Kasper, D. C. Turner, N. R. W. Martin, and A. P. Sharples, “Mimicking Exercise in Three-Dimensional Bioengineered Skeletal Muscle to Investigate Cellular and Molecular Mechanisms of Physiological Adaptation,” *J. Cell. Physiol.*, no. February, pp. 1–14, 2017.

[424] J. Stern-Straeter *et al.*, “Impact of electrical stimulation on three-dimensional myoblast cultures - a real-time RT-PCR study.,” *J. Cell. Mol. Med.*, vol. 9, no. 4, pp. 883–892, 2005.

[425] M. L. P. Langelaan, K. J. M. Boonen, K. Y. Rosaria-Chak, D. W. J. van der Schaft, M. J. Post, and F. P. T. Baaijens, “Advanced maturation by electrical stimulation: Differences in response between C2C12 and primary muscle progenitor cells,” *J. Tissue Eng. Regen. Med.*, vol. 5, no. 7, pp. 529–539, 2011.

[426] Y.-C. Huang, R. G. Dennis, and K. Baar, “Cultured slow vs. fast skeletal muscle cells differ in physiology and responsiveness to stimulation,” *AJP Cell Physiol.*, vol. 291, no. 1, pp. C11--C17, Jan. 2006.

[427] K. Donnelly *et al.*, “A Novel Bioreactor for Stimulating Skeletal Muscle In Vitro,” vol. 16, no. 4, pp. 3–10, 2010.

[428] A. Khodabukus and K. Baar, “Defined Electrical Stimulation Emphasizing Excitability for the Development and Testing of Engineered Skeletal Muscle,” *Tissue Eng. Part C Methods*, vol. 18, no. 5, pp. 349–357, 2012.

[429] B. T. Corona *et al.*, “Further development of a tissue engineered muscle repair construct in vitro for enhanced functional recovery following implantation in vivo in a murine model of volumetric muscle loss injury,” *Tissue Eng Part A*, vol. 18, no. 11–12, pp. 1213–1228, 2012.

[430] D. Dunstan, “Diabetes: Exercise and T2DM—move muscles more often!,” *Nat. Rev. Endocrinol.*, vol. 7, no. 4, pp. 189–190, 2011.

[431] B. Egan and J. R. Zierath, “Exercise metabolism and the molecular regulation of skeletal muscle adaptation,” *Cell Metab.*, vol. 17, no. 2, pp. 162–184, 2013.

[432] B. K. Pedersen and M. A. Febbraio, “Muscle as an Endocrine Organ.pdf,” *Physiol. Rev.*, vol. 88, no. 4, pp. 1379–1406, 2008.

[433] B. K. Pedersen, “Edward F. Adolph Distinguished Lecture: Muscle as an endocrine organ: IL-6 and other myokines,” *J. Appl. Physiol.*, vol. 107, no. 4, pp. 1006–1014, 2009.

[434] C. M. Girgis, N. Mokbel, and D. J. DiGirolamo, “Therapies for musculoskeletal disease: Can we treat two birds with one stone?,” *Current Osteoporosis Reports*, vol. 12, no. 2. pp. 142–153, 2014.

[435] C. Tagliaferri, Y. Wittrant, M. J. Davicco, S. Walrand, and V. Coxam, “Muscle and bone, two interconnected tissues,” *Ageing Research Reviews*, vol. 21. pp. 55–70, 2015.

[436] M. Catoire, M. Mensink, E. Kalkhoven, P. Schrauwen, and S. Kersten, “Identification of human exercise-induced myokines using secretome analysis,” *Physiol. Genomics*, vol. 46, no. 7, pp. 256–267, 2014.

[437] F. Haugen *et al.*, “IL-7 is expressed and secreted by human skeletal muscle cells.,” *Am. J. Physiol. Cell Physiol.*, vol. 298, no. 4, pp. C807--C816, 2010.

[438] A. R. Nielsen and B. K. Pedersen, “The biological roles of exercise-induced cytokines: IL-6, IL-8, and IL-15,” *Appl. Physiol. Nutr. Metab.*, vol. 32, no. 5, pp. 833–839, 2007.

[439] L. S. Quinn, B. G. Anderson, L. Strait-Bodey, A. M. Stroud, and J. M. Argiles, “Oversecretion of interleukin-15 from skeletal muscle reduces adiposity,” *AJP Endocrinol. Metab.*, vol. 296, no. 1, pp. E191--E202, 2008.

[440] C. Broholm *et al.*, “LIF is a contraction-induced myokine stimulating human myocyte proliferation,” *J. Appl. Physiol.*, vol. 111, no. 1, pp. 251–259, 2011.

[441] P. Hojman *et al.*, “Fibroblast growth factor-21 is induced in human skeletal muscles by hyperinsulinemia,” *Diabetes*, vol. 58, no. 12, pp. 2797–2801, 2009.

[442] Y. Izumiya, H. A. Bina, N. Ouchi, Y. Akasaki, A. Kharitonenkov, and K. Walsh, “FGF21 is an Akt-regulated myokine,” *FEBS Lett.*, vol. 582, no. 27, pp. 3805–3810, 2008.

[443] L. Zeng, Y. Akasaki, K. Sato, N. Ouchi, Y. Izumiya, and K. Walsh, “Insulin-like 6 is induced by muscle injury and functions as a regenerative factor,” *J. Biol. Chem.*, vol. 285, no. 46, pp. 36060–36069, 2010.

[444] N. Ouchi *et al.*, “Follistatin-like 1, a secreted muscle protein, promotes endothelial cell function and revascularization in ischemic tissue through a nitric-oxide synthase-dependent mechanism,” *J. Biol. Chem.*, vol. 283, no. 47, pp. 32802–32811, 2008.

[445] H. Nishizawa *et al.*, “Musclin, a Novel Skeletal Muscle-derived Secretory Factor,” *J. Biol. Chem.*, vol. 279, no. 19, pp. 19391–19395, 2004.

[446] P. Bostrom *et al.*, “A PGC1 alpha dependent myokine that drives brown fat like development of white fat and thermogenesis,” *Nature*, vol. 481, pp. 463–468, 2012.

[447] M. M. Seldin, J. M. Peterson, M. S. Byerly, Z. Wei, and G. W. Wong, “Myonectin (CTRP15), a novel myokine that links skeletal muscle to systemic lipid homeostasis,” *J. Biol. Chem.*, vol. 287, no. 15, pp. 11968–11980, 2012.

[448] P. Songsorn, J. Ruffino, and N. B. J. Vollaard, “No effect of acute and chronic supramaximal exercise on circulating levels of the myokine SPARC,” *Eur. J. Sport Sci.*, vol. 0, no. 0, pp. 1–6, 2016.

[449] R. R. Rao *et al.*, “Meteorin-like is a hormone that regulates immune-adipose interactions to increase beige fat thermogenesis,” *Cell*, vol. 157, no. 6, pp. 1279–1291, 2014.

[450] P. Muñoz-Cánoves, C. Scheele, B. K. Pedersen, and A. L. Serrano, “Interleukin-6 myokine signaling in skeletal muscle: A double-edged sword?,” *FEBS J.*, vol. 280, no. 17, pp. 4131–4148,

2013.

[451] M. Agarwal, “Cardiovascular Response and Serum Interleukin-6 Level in Concentric Vs. Eccentric Exercise,” *J. Clin. Diagnostic Res.*, vol. 11, no. 4, pp. 4–8, 2017.

[452] B. K. Pedersen, A. Steensberg, and P. Schjerling, “Muscle-derived interleukin-6: Possible biological effects,” *Journal of Physiology*, vol. 536, no. 2. pp. 329–337, 2001.

[453] F. B. Benatti and B. K. Pedersen, “Exercise as an anti-inflammatory therapy for rheumatic diseases—myokine regulation,” *Nat. Rev. Rheumatol.*, vol. 11, no. 2, pp. 86–97, 2014.

[454] M. Abeywardena, W. Leifert, K. Warnes, J. Varghese, and R. Head, “Cardiovascular Biology of Interleukin-6,” *Curr. Pharm. Des.*, vol. 15, no. 15, pp. 1809–1821, 2009.

[455] S. Rose-John, J. Scheller, G. Elson, and S. A. Jones, “Interleukin-6 biology is coordinated by membrane-bound and soluble receptors: role in inflammation and cancer,” *J. Leukoc. Biol.*, vol. 80, no. 2, pp. 227–236, 2006.

[456] E. E. Spangenburg and F. W. Booth, “Leukemia inhibitory factor restores the hypertrophic response to increased loading in the LIF(−/−) mouse,” *Cytokine*, vol. 34, no. 3–4, pp. 125–130, 2006.

[457] A. L. Serrano, B. Baeza-Raja, E. Perdiguero, M. Jardí, and P. Muñoz-Cánoves, “Interleukin-6 Is an Essential Regulator of Satellite Cell-Mediated Skeletal Muscle Hypertrophy,” *Cell Metab.*, vol. 7, no. 1, pp. 33–44, 2008.

[458] A. Guerci *et al.*, “Srf-dependent paracrine signals produced by myofibers control satellite cell-mediated skeletal muscle hypertrophy,” *Cell Metab.*, vol. 15, no. 1, pp. 25–37, 2012.

[459] J. B. Kurek, J. J. Bower, M. Romanella, F. Koentgen, M. Murphy, and L. Austin, “The role of leukemia inhibitory factor in skeletal muscle regeneration.,” *Muscle {\&} nerve*, vol. 20, no. 7, pp. 815–822, 1997.

[460] W. Barnard, J. Bower, M. A. Brown, M. Murphy, and L. Austin, “Leukemia inhibitory factor (LIF) infusion stimulates skeletal muscle regeneration after injury: Injured muscle expresses lif mRNA,” *J. Neurol. Sci.*, vol. 123, no. 1–2, pp. 108–113, 1994.

[461] J. B. Kurek, S. Nouri, G. Kannourakis, M. Murphy, and L. Austin, “Leukemia inhibitory factor and interleukin-6 are produced by diseased and regenerating skeletal muscle,” *Muscle and Nerve*, vol. 19, no. 10, pp. 1291–1301, 1996.

[462] C. Zhang, Y. Li, Y. Wu, L. Wang, X. Wang, and J. Du, “Interleukin-6/signal transducer and activator of transcription 3 (STAT3) pathway is essential for macrophage infiltration and myoblast proliferation during muscle regeneration,” *J. Biol. Chem.*, vol. 288, no. 3, pp. 1489–1499, 2013.

[463] G. Colaianni, S. Cinti, S. Colucci, and M. Grano, “Irisin and musculoskeletal health,” *Ann. N. Y. Acad. Sci.*, pp. 1–5, 2017.

[464] J.-Y. Reginster, C. Beaudart, F. Buckinx, and O. Bruyère, “Osteoporosis and sarcopenia,” *Curr. Opin. Clin. Nutr. Metab. Care*, p. 1, 2015.

[465] G. Colaianni *et al.*, “Irisin enhances osteoblast differentiation in vitro,” *Int. J. Endocrinol.*, vol. 2014, 2014.

[466] G. Colaianni *et al.*, “The myokine irisin increases cortical bone mass,” *Proc. Natl. Acad. Sci.*, vol. 112, no. 39, pp. 12157–12162, 2015.

[467] G. Colaianni and M. Grano, “Role of Irisin on the bone – muscle functional unit,” *Bonekey Rep.*, vol. 4, no. October, pp. 1–4, 2015.

[468] A. Bartelt and J. Heeren, “Adipose tissue browning and metabolic health,” *Nat. Rev. Endocrinol.*, vol. 10, no. 1, pp. 24–36, 2013.

[469] S. Busquets *et al.*, “Interleukin-15 decreases proteolysis in skeletal muscle: a direct effect.,” *Int. J. Mol. Med.*, vol. 16, no. 3, pp. 471–476, 2005.

[470] P. S. Furmanczyk and L. S. Quinn, “Interleukin-15 increases myosin accretion in human skeletal myogenic cultures,” *Cell Biol. Int.*, vol. 27, no. 10, pp. 845–851, 2003.

[471] E. E. Pistilli, P. M. Siu, and S. E. Alway, “Interleukin-15 responses to aging and unloading-induced skeletal muscle atrophy.,” *Am. J. Physiol. Cell Physiol.*, vol. 292, no. 4, pp. C1298--304, 2007.

[472] L. Quinn, “Overexpression of Interleukin-15 Induces Skeletal Muscle Hypertrophy in Vitro: Implications for Treatment of Muscle Wasting Disorders,” *Exp. Cell Res.*, vol. 280, no. 1, pp. 55–63, 2002.

[473] L. S. Quinn, K. L. Haugk, and K. H. Grabstein, “Interleukin-15: A novel anabolic cytokine for skeletal muscle,” *Endocrinology*, vol. 136, no. 8, pp. 3669–3672, 1995.

[474] S. E. Riechman, G. Balasekaran, S. M. Roth, and R. E. Ferrell, “Association of interleukin-15 protein and interleukin-15 receptor genetic variation with resistance exercise training responses,” *J. Appl. Physiol.*, vol. 97, no. 6, pp. 2214–2219, 2004.

[475] E. Subbotina *et al.*, “Musclin is an activity-stimulated myokine that enhances physical endurance,” *Proc. Natl. Acad. Sci.*, vol. 112, no. 52, pp. 16042–16047, 2015.

[476] J. E. Murphy-Ullrich and E. H. Sage, “Revisiting the matricellular concept,” *Matrix Biol.*, vol. 37, pp. 1–14, 2014.

[477] L. W. Harries, L. J. McCulloch, J. E. Holley, T. J. Rawling, H. J. Welters, and K. Kos, “A Role for SPARC in the Moderation of Human Insulin Secretion,” *PLoS One*, vol. 8, no. 6, 2013.

[478] Z. Luo, P. Luo, Y. Yu, Q. Zhao, X. Zhao, and L. Cheng, “SPARC promotes the development of erythroid progenitors,” *Exp. Hematol.*, vol. 40, no. 10, pp. 828–836, 2012.

[479] T. Partridge, “The Potential of Exon Skipping for Treatment for Duchenne Muscular Dystrophy,” *J. Child Neurol.*, vol. 25, no. 9, pp. 1165–1170, Sep. 2010.

[480] D. Duan, “Duchenne muscular dystrophy gene therapy in the canine model.,” *Hum. Gene Ther. Clin. Dev.*, vol. 26, no. 1, pp. 57–69, Mar. 2015.

[481] M. M. Ferreira, R. E. Dewi, and S. C. Heilshorn, “Microfluidic analysis of extracellular matrix-bFGF crosstalk on primary human myoblast chemoproliferation, chemokinesis, and chemotaxis.,” *Integr. Biol. (Camb).*, vol. 7, no. 5, pp. 569–579, 2015.

[482] E. Serena *et al.*, “Skeletal Muscle Differentiation on a Chip Shows Human Donor Mesoangioblasts’ Efficiency in Restoring Dystrophin in a Duchenne Muscular Dystrophy Model,” *Stem Cells Transl. Med.*, vol. 5, no. 12, pp. 1676–1683, Dec. 2016.

[483] R. Darabi *et al.*, “Human ES- and iPS-Derived Myogenic Progenitors Restore DYSTROPHIN and Improve Contractility upon Transplantation in Dystrophic Mice,” *Cell Stem Cell*, vol. 10, no. 5, pp. 610–619, 2012.

[484] Y. Kodaka, G. Rabu, and A. Asakura, “Skeletal Muscle Cell Induction from Pluripotent Stem Cells,” *Stem Cells Int.*, vol. 2017, pp. 1–16, Apr. 2017.

[485] A. Tanaka *et al.*, “Efficient and Reproducible Myogenic Differentiation from Human iPS Cells: Prospects for Modeling Miyoshi Myopathy In Vitro,” *PLoS One*, vol. 8, no. 4, 2013.

[486] R. Abujarour *et al.*, “Myogenic Differentiation of Muscular Dystrophy-Specific Induced Pluripotent Stem Cells for Use in Drug Discovery,” *Stem Cells Transl. Med.*, vol. 3, no. 2, pp. 149–160, Feb. 2014.

[487] L. Madden, M. Juhas, W. E. Kraus, G. A. Truskey, and N. Bursac, “Bioengineered human myobundles mimic clinical responses of skeletal muscle to drugs.,” *Elife*, vol. 4, no. January, p.

e04885, 2015.

[488] H. Vandenburgh *et al.*, “Drug-screening platform based on the contractility of tissue-engineered muscle,” *Muscle and Nerve*, vol. 37, no. 4, pp. 438–447, 2008.

[489] L. Boldrin and J. E. Morgan, “Human satellite cells : identification on human muscle fibres,” pp. 1–9, 2012.

[490] S. Orimo, E. Hiyamuta, K. Arahata, and H. Sugita, “Analysis of inflammatory cells and complement C3 in bupivacaine-induced myonecrosis,” *Muscle Nerve*, vol. 14, no. 6, pp. 515–520, 1991.

[491] R. Mounier *et al.*, “AMPKα1 regulates macrophage skewing at the time of resolution of inflammation during skeletal muscle regeneration,” *Cell Metab.*, vol. 18, no. 2, pp. 251–264, Aug. 2013.

[492] S. Fukada, T. Higashimoto, and A. Kaneshige, “Differences in muscle satellite cell dynamics during muscle hypertrophy and regeneration,” *Skelet. Muscle*, vol. 12, no. 1, p. 17, Dec. 2022.

[493] P. S. Zammit and J. R. Beauchamp, “The skeletal muscle satellite cell: stem cell or son of stem cell?,” *Differentiation.*, vol. 68, no. 4–5, pp. 193–204, 2001.

[494] B. Evano, S. Khalilian, G. Le Carrou, G. Almouzni, and S. Tajbakhsh, “Dynamics of Asymmetric and Symmetric Divisions of Muscle Stem Cells In Vivo and on Artificial Niches,” *Cell Rep.*, vol. 30, no. 10, pp. 3195-3206.e7, Mar. 2020.

[495] M. M. Bamman, B. M. Roberts, and G. R. Adams, “Molecular Regulation of Exercise-Induced Muscle Fiber Hypertrophy,” *Cold Spring Harb. Perspect. Med.*, vol. 8, no. 6, Jun. 2018.

[496] S. ichiro Fukada and N. Ito, “Regulation of muscle hypertrophy: Involvement of the Akt-independent pathway and satellite cells in muscle hypertrophy,” *Exp. Cell Res.*, vol. 409, no. 2, Dec. 2021.

[497] M. Cassano, M. Quattrocelli, S. Crippa, I. Perini, F. Ronzoni, and M. Sampaolesi, “Cellular mechanisms and local progenitor activation to regulate skeletal muscle mass,” *Journal of Muscle Research and Cell Motility*, vol. 30, no. 7–8. J Muscle Res Cell Motil, pp. 243–253, Dec-2009.

[498] N. Ito, U. T. Ruegg, A. Kudo, Y. Miyagoe-Suzuki, and S. Takeda, “Activation of calcium signaling through Trpv1 by nNOS and peroxynitrite as a key trigger of skeletal muscle hypertrophy,” *Nat. Med.*, vol. 19, no. 1, pp. 101–106, Jan. 2013.

[499] X. Wang and C. G. Proud, “The mTOR pathway in the control of protein synthesis,” *Physiology*, vol. 21, no. 5. Physiology (Bethesda), pp. 362–369, Oct-2006.

[500] S. J. Mahoney, J. M. Dempsey, and J. Blenis, “Chapter 2 Cell Signaling in Protein Synthesis. Ribosome Biogenesis and Translation Initiation and Elongation,” *Progress in Molecular Biology and Translational Science*, vol. 90, no. C. Prog Mol Biol Transl Sci, pp. 53–107, 2009.

[501] Q. Goh and D. P. Millay, “Requirement of myomaker-mediated stem cell fusion for skeletal muscle hypertrophy,” *Elife*, vol. 6, Oct. 2017.

[502] C. S. Fry *et al.*, “Regulation of the muscle fiber microenvironment by activated satellite cells during hypertrophy,” *FASEB J.*, vol. 28, no. 4, pp. 1654–1665, 2014.

[503] I. M. Egner, J. C. Bruusgaard, and K. Gundersen, “Satellite cell depletion prevents fiber hypertrophy in skeletal muscle,” *Development*, vol. 143, no. 16, pp. 2898–2906, Aug. 2016.

[504] J. Tomasch *et al.*, “Changes in Elastic Moduli of Fibrin Hydrogels Within the Myogenic Range Alter Behavior of Murine C2C12 and Human C25 Myoblasts Differently,” *Front. Bioeng. Biotechnol.*, vol. 10, May 2022.

[505] A. Kneppers *et al.*, “A novel in vitro model for the assessment of postnatal myonuclear accretion,” *Skelet. Muscle*, vol. 8, no. 1, pp. 1–13, Feb. 2018.

[506] P. Seale, L. A. Sabourin, A. Girgis-Gabardo, A. Mansouri, P. Gruss, and M. A. Rudnicki, “Pax7 Is Required for the Specification of Myogenic Satellite Cells skeletal muscle are mitotically quiescent and are acti- vated in response to diverse stimuli, including stretch- ing, exercise, injury, and electrical stimulation (Schultz,” *Cell*, vol. 102, pp. 777–786, 2000.

[507] F. Haddad and G. R. Adams, “Inhibition of MAP/ERK kinase prevents IGF-I-induced hypertrophy in rat muscles,” *J. Appl. Physiol.*, vol. 96, no. 1, pp. 203–210, Jan. 2004.

[508] S. Schiaffino, C. Reggiani, T. Akimoto, and B. Blaauw, “Molecular Mechanisms of Skeletal Muscle Hypertrophy,” *Journal of Neuromuscular Diseases*, vol. 8, no. 2. IOS Press BV, pp. 169–183, 2021.

[509] E. E. Spangenburg, D. Le Roith, C. W. Ward, and S. C. Bodine, “A functional insulin-like growth factor receptor is not necessary for load-induced skeletal muscle hypertrophy,” *J. Physiol.*, vol. 586, no. Pt 1, p. 283, Jan. 2008.

[510] A. C. Durieux, D. Desplanches, O. Freyssenet, and M. Flück, “Mechanotransduction in striated muscle via focal adhesion kinase,” *Biochem. Soc. Trans.*, vol. 35, no. Pt 5, pp. 1312–1313, Nov. 2007.

[511] E. Vasyutina, B. Martarelli, C. Brakebusch, H. Wende, and C. Birchmeier, “The small G-proteins Rac1 and Cdc42 are essential for myoblast fusion in the mouse,” *Proc. Natl. Acad. Sci. U. S. A.*, vol. 106, no. 22, p. 8935, Jun. 2009.

[512] N. L. Quach, S. Biressi, L. F. Reichardt, C. Keller, and T. A. Rando, “Focal Adhesion Kinase Signaling Regulates the Expression of Caveolin 3 and β1 Integrin, Genes Essential for Normal Myoblast Fusion,” *Mol. Biol. Cell*, vol. 20, no. 14, p. 3422, Jul. 2009.

[513] M. M. Murphy, A. C. Keefe, J. A. Lawson, S. D. Flygare, M. Yandell, and G. Kardon, “Transiently active wnt/β-catenin signaling is not required but must be silenced for stem cell function during muscle regeneration,” *Stem Cell Reports*, vol. 3, no. 3, pp. 475–488, Sep. 2014.

[514] L. Angelova *et al.*, “Optimizing the Surface Structural and Morphological Properties of Silk Thin Films via Ultra-Short Laser Texturing for Creation of Muscle Cell Matrix Model,” *Polymers (Basel).*, vol. 14, no. 13, p. 2584, Jun. 2022.

[515] S. Fukuda *et al.*, “Sustained expression of HeyL is critical for the proliferation of muscle stem cells in overloaded muscle,” *Elife*, vol. 8, Sep. 2019.

Abbreviations

ACTN	actinin
AFM	atomic force microscopy
AMPK	5´-adenosine mono-phosphate-activated protein kinase
ATP	adenosine triphosphate
bFGF	basic fibroblast growth factor
BMP	bone morphogenic proteins
CA	contact angle
CBFα1	core-Binding Factor Alpha 1
CCND1	cyclin D1
CT	cycle threshold
CTS	cyclic tensile stress
DAPI	4′,6-Diamidin-2-phenylindol
DM	differentiation medium
DMD	Duchenne muscular dystrophy
DMEM-HG	Dulbecco's modified Eagle's medium - high glucose
DTPA	diethylenetriaminepentaacetic acid
ECM	extracellular matrix
EDTA	ethylenediaminetetraacetic acid
EDX	energy-dispersive X-ray spectroscopy
EPR	electron paramagnetic resonance
FAK	focal adhesion kinase
Fbg	fibrinogen
FTIR	fourier-transform infrared
GM	growth medium
GPR	gly-pro-arg
HA	hyaluronic acid
HBAM	human bioartificial muscles
IF	immunofluorescence
IGF 1	insulin-like growth factor 1
IL	interleukin
iPSC	induced pluripotent stem cell
IT	integrin
LDH	lactate dehydrogenase
MAPK	mitogen-activated protein kinase
MD	muscular dystrophy
MHC	myosin heavy chain
MHC	myosin heavy chain
MMP	matrix metalloproteinase
MRF	myogenic regulatory factor
MSC	mesenchymal stem cell
MSX	Homeobox protein
mTOR	mechanistic target of rapamycin
MTT	3-(4,5-dimethylthiazol-2-yl)-2,5-diphenyltetrazolium bromide
MuSC	muscle satellite cell
MyoD	myogenic differentiation 1
MyoG	myogenin
PANI	polyaniline
Pax	paired box
PAX	paxilin
PBS	phosphate-buffered Saline
PCL	polycaprolactone
PDMS	polydimethylsiloxane
PEG	polyethylene glycol
PLCL	poly(L-lactide-co-ε-caprolactone)
PLGA	poly(lactic-co-glycolic acid)
PLLA	poly-L-lactic acid
POM	polyoxymethylene
Ppase	protein phosphatase
RGD	arg-gly-asp
ROI	region of interest
RPLP0	ribosomal protein lateral stalk subunit P0
RT-qPCR	reverse transcription polymerase chain reaction
SD	standard deviation
SDS	sodium dodecyl sulfate
SEM	scanning electron microscopy
SF	silk fibroin
Shh	Sonic Hedgehog
SM	standard medium without cells
SMLC	skeletal muscle-like construct
SMTE	skeletal muscle tissue engineering
TBS	Tris-buffered Saline
TE	tissue engineering
Thr	thrombin
TLN	talin
TnnT1	troponin T 1
Tris	tris(hydroxymethyl)aminomethan
VASP	vasodilator-stimulated phosphoprotein
VCL	vinculin
Wnt	wingless-Int proteins
XRD	X-ray diffractometer
ZYX	zyxin
ΔΔCT	comparative CT

Curriculum Vitae

Janine Tomasch, MSc.

[redacted]

Education

03/2018 – Present	**Doctoral Program in Engineering Sciences – Technical Chemistry** Technical University Vienna, Vienna (Austria) Faculty of technical chemistry
09/2015 – 09/2017	**Master of Science in Engineering** UAS Technikum Vienna, Vienna (Austria) Master Tissue Engineering and Regenerative Medicine Graduated with distinctions as *Master of Science in Engineering*
09/2012 – 06/2015	**Bachelor of Science in Engineering** UAS Technikum Vienna, Vienna (Austria) Bachelor Biomedical Engineering Focus on cell and tissue engineering Graduated with distinctions as *Bachelor of Science in Engineering*

Work Experience

09/2019 – Present	**Junior Researcher and Lecturer; DOC Scholarship** Establishment of a model for skeletal muscle injury via mechanical and oxidative stress and elucidating the role of reactive oxygen species in repair and regeneration

UAS Technikum Vienna, Vienna (Austria)

- Planning of research projects and performing laboratory work
- Development of cooperations with other research projects and/or other laboratories
- Teaching assignments:
  - Supervising students' laboratory-based research projects
  - Supervising bachelor's theses students
  - Holding seminars on cell culture methods

09/2017 – 09/2019 **Junior Researcher and Lecturer; FFG Project *DiseaseTissue***

Research project aiming at development of tissue engineered disease models using bioreactors

UAS Technikum Vienna, Vienna (Austria)

- Planning of research projects and performing laboratory work
- Teaching assignments:
  - Supervising students' laboratory-based research projects
  - Holding seminars on cell culture methods

09/2016 – 08/2017 **Research Internship**

Influence of Mechanical Stimulation and Substrate Stiffness on Myoblasts and its Implications for Skeletal Muscle Tissue Engineering

UAS Technikum Vienna, Vienna (Austria)

01/2015 – 05/2015 **Research Internship**

Characterization of EGFR in the Murine Mammary Carcinoma Cell Line 4T1 and Development of a Breast Cancer Mouse Model

Laboratory of Macromolecular Cancer Therapeutics, University of Vienna, Vienna (Austria)

09/2014 – 07/2016 **Tutoress / Learning Guide and Mentor**

Supporting teenagers with learning disabilities to graduate from their vocational training

Jugend am Werk, Vienna (Austria)

Professional Skills

- Cell culture with a special focus on 3D culture for the creation of artificial tissue
- Various biochemical and molecular biological analytical techniques (RT-qPCR, Western blotting, immunofluorescence stainings, flow cytometry, histology, etc.)
- Microscopy (fluorescence microscopy, scanning electron microscopy)
- Teaching in different settings, including one-to-one lessons, small project groups and larger theoretical seminars, partly applying the principles of problem-based learning

Publications and Awards

Publications

J. Tomasch, B. Maleiner, C. Hromada, D. Szwarc-Hofbauer, A. Teuschl-Woller, Cyclic tensile stress induces skeletal muscle hypertrophy and myonuclear accretion in a tissue-engineered model, Submitted to Tissue Engineering Part A (2022) (*original research*)

L. Angelova, A. Daskalova, E. Filipov, X. Monforte Vila, **J. Tomasch**, G. Avdeev, AH. Teuschl-Woller, I. Buchvarov, Optimizing the Surface Structural and Morphological Properties of Silk Thin Films via Ultra-Short Laser Texturing for Creation of Muscle Cell Matrix Model. Polymers (2022) *(original research)*

J. Tomasch, B. Maleiner, P. Heher, M. Rufin, O. Andriotis, P. Thurner, H. Redl, C. Fuchs, A. Teuschl, Changes in elastic moduli of fibrin hydrogels within the myogenic range alter behavior of murine C2C12 and human C25 myoblasts differently, Front. Bioeng. Biotechnol. (2022) *(original research)*

B. Maleiner, **J. Tomasch**, P. Heher, O. Spadiut, D. Rünzler, C. Fuchs, The Importance of Biophysical and Biochemical Stimuli in Dynamic Skeletal Muscle Models, Front. Physiol. (2018) *(review article)*

Podium / poster presentations – selection

"Tissue-engineered models for mechanical and oxidative stress", 3rd Padua Days of Muscle Mobility, 2022 (*podium presentation*)

"A tissue-engineered model for skeletal muscle pathologies", 6th world congress of the Tissue Engineering and Regenerative Medicine Society (*podium presentation*)

"Differential effects of substrate stiffness and architecture on proliferation and differentiation of human and murine myoblasts", 6th world congress of the Tissue Engineering and Regenerative Medicine Society (*poster presentation*)

"Effects of type, duration and time point of mechanical stimulation in myogenesis", European Meeting of the Tissue Engineering and Regenerative Medicine Society (*poster presentation*)

Awards

DOC Fellowship of the Austrian Academy of Sciences (09/2019)

Kapsch Award (Award for best master's theses at the UAS Technikum Wien) (11/2018)